THE UNIVERSITY OF HULL

New pre-catalysts for ring opening of lactides/lactones based on earth abundant metals

Being a thesis submitted for the degree of
Doctor of Philosophy at the University of Hull

Supervised by: Professor Carl Redshaw

By

Yahya AL-Khafaji

(December- 2016)

Abstract

In this study, a number of Nb, Ta, Mo, V, Al, Li and Zn complexes have been synthesised and fully characterised. The catalytic behavior of these pre-catalysts towards the ring opening polymerization (ROP) of the cyclic esters is discussed.

Chapter 1 Presents an introduction to the history of polymers (from polyethylene to biodegradable polymers from cyclic esters), early discovery, mechanism of ring opening polymerisation and the use of vanadium, niobium, tantalum and molybdenum, aluiminium, lithium and zinc complexes as polymerization catalysts.

Chpter 2 This chapter discussed results when the pre-ligands α,α,α',α'-tetra(3,5-di-*tert*-butyl-2-hydroxyphenyl-*p*-)xylene-*para*-tetraphenol(*p*-L^{1}H$_4$) and α,α,α',α'tetra (3,5-di-*tert*-butyl-2-hydroxyphenyl-*m*-)xylene-*meta*-tetraphenol (*m*-L^{2}H$_4$) are reacted with a number of niobium and tantalum precursors such as [NbCl$_5$], [TaCl$_5$] or [Nb(O)Cl$_3$(NCMe)$_2$]. The resulting products {[NbCl$_3$(NCMe)]$_2$(μ-*p*-L^1)}·6MeCN (**1**·6MeCN), {[NbCl$_2$(OEt)(NCMe)]$_2$(μ-*p*-L^1)}·3½MeCN·0.614 toluene (**2**·3½MeCN·0.614 toluene), {[TaCl$_2$(OEt)(NCMe)]$_2$(μ-*p*-L^1)}.5MeCN (**3**·5MeCN), {[Nb(NCMe)Cl(*m*-L^{2}H$_2$)$_2$]}·3½MeCN(**4**·3½MeCN) and {[Nb(NCMe)Cl(*m*-L^{2}H$_2$)$_2$]}·5MeCN (**4**·5MeCN) were structurally characterized. Complexes **1**–**4** were screened as pre-catalysts for the ROP of ε-caprolactone, both with and without benzyl alcohol or solvent present, and at various temperatures.

Chapter 3 In this chapter, the reaction of the bulky bi-phenols 2,2′-RCH[4,6-(t-Bu)$_2$C$_6$H$_2$OH]$_2$ (R = Me L^{3Me}H$_2$, Ph L^{4Ph}H$_2$) with the bis(imido) molybdenum(VI) *tert*-butoxides [Mo(NR^1)(NR^2)(Ot-Bu)$_2$] (R^1 = R^2 = 2,6-C$_6$H$_3$-i-Pr$_2$; R^1 = t-Bu, R^2 = C$_6$F$_5$) has been studied. The complexes [Mo(NC$_6$H$_3$$i$-Pr$_2$-2,6)$_2$L^{3Me}] (**5**), [Mo(NC$_6H_3$$i$-Pr$_2$-2,6)$_2$L^{4Ph}] (**6**) and [Mo(Nt-Bu)(μ-NC$_6$F$_5$)(L^{3Me})]$_2$ (**7**) were isolated. Similar use of the tri-phenol 2,6-bis(3,5-di-*tert*-butyl-2-hydroxybenzyl)-4-methylphenol (L^{5}H$_3$) with [Mo(NC$_6$H$_3$$i$-Pr$_2$-2,6)$_2$(O$t$-Bu)$_2$] afforded the oxo-bridged product [Mo(NC$_6$H$_3$$i$-Pr$_2$-2,6)(NCMe)(μ-O)L^{5}H]$_2$ (**8**), whilst use of the tetra-phenols L^{1p}H$_4$/L^{2m}H$_4$ led to {[Mo(NC$_6$H$_3$$i$-Pr$_2$-2,6)$_2$]$_2$(μ-L^{1p})} (**9**) or {[Mo(NC$_6$H$_3$$i$-Pr$_2$-2,6)$_2$]$_2$(μ-L^{2m})}(**10**), respectively. Similar use of [Mo(NC$_6$F$_5$)$_2$(Ot-Bu)$_2$] with L^{1p}H$_4$ afforded {[Mo(NC$_6$F$_5$)(Ot-Bu)$_2$]$_2$(μ-L^{1p})}·6MeCN (**11·6MeCN**). The molecular structures of **5**, **6·CH$_2$Cl$_2$**, **7**, **8·6MeCN**, **10·2C$_6$H$_{14}$**, and **11·6MeCN** are reported. These complexes have been screened for their ability to act as catalysts for the ROP of ε-caprolactone; for comparative studies the complex [Mo(NC$_6$H$_3$$i$-Pr$_2$ 2,6)$_2$Cl$_2$(DME) (**12**) has also been screened.

Chpter 4 This chapter focuses on the use of the vanadyl complexes. The new complexes [VO(Ot-Bu)L^3] (**13**), {[VO(Oi-Pr)]$_2$(μ-p-L^{1p})} (**14**) {[VO(OR)]$_2$(μ-p-L^{2m})} (R = i-Pr **15**, t-Bu **16** have been prepared from [VO(OR)$_3$] (R = n-Pr, i-Pr or t-Bu) and the respective phenol, namely 2,2$^/$-ethylidenebis(4,6-di-*tert*-butylphenol) (L^{3}H$_2$) or L$^{p/m}$H$_4$. For comparative studies, the known complexes [VO(μ-On-Pr)L^3]$_2$ (**18**), [VOL^6]$_2$ (**19**) (L^{6}H$_3$ = 2,6-bis(3,5-di-*tert*-butyl-2-hydroxybenzyl)-4-*tert*-butylphenol) were prepared. An imido complex {[VCl(Np-

tolyl)(NCMe)]$_2$(μ-p-L^{1p})} (**17**) has also been prepared. The molecular structures of complexes **13 – 19** are reported, and these complexes **13 – 19** have been screened for their ability to ring open polymerise ε-caprolactone, *L*-lactide or *rac*-lactide with and without solvent present. The co-polymerization of ε-caprolactone with *L*-lactide or *rac*-lactide was also studied.

Chapter 5 describes the reaction of R^{1}R^{2}CHN=CH(3,5-*t*-Bu$_2$C$_6$H$_2$-OH-2) (R^1 = R^2 = Me L^{7}H; R^1 = Me, R^2 = Ph L^{8}H; R^1 = R^2 = Ph L^{9}H) with slightly greater than one equivalent of R^3$_3$Al (R^3 = Me, Et), which afforded the complexes [(L$^{7-9}$)AlR^3$_2$] (L^7, R^3 = Me **20**, R^3 = Et **21**; L^8, R^3 = Me **22**, R^3 = Et **23**; L^3, R^3 = Me **24**, R^3 = Et **25**); complex **20** has been previously reported. Use of the *N,O*-ligand derived from 2,2/-diphenylglycine afforded either **24** or an amine by-product [Ph$_2$NCH$_2$(3,5-*t*-Bu$_2$C$_6$H$_2$-O-2)AlMe$_2$] (**26**). The known Schiff base complex [2-Ph$_2$PC$_6$H$_4$CH$_2$(3,5-*t*-Bu$_2$C$_6$H$_2$-O-2)AlMe$_2$] (**27**) and the product of the reaction of 2-diphenylphosphinoaniline 1-NH$_2$,2-PPh$_2$C$_6$H$_4$ with Me$_3$Al, namely {Ph$_2$PC$_6$H$_4$N[(Me$_2$Al)$_2$$\mu$-Me]($\mu$-Me$_2$Al)} (**28**) were also isolated. For structural and catalytic comparisons, complexes resulting from interaction of Me$_3$Al with diphenylamine or benzhydrylamine, namely {Ph$_2$N[(Me$_2$Al)$_2$$\mu$-Me]} (**29**) and [Ph$_2$CHNH($\mu$-Me$_2$Al)]$_2$·MeCN (**30**), were prepared. The molecular structures of the Schiff pro-ligands derived from Ph$_2$CHNH$_2$ and 2,2/-Ph$_2$C(CO$_2$H)(NH$_2$), together with complexes **24**, **26** and **28** - **30**·MeCN were determined. All complexes were screened for their ability to ROP ε-caprolactone, δ-valerolactone or *rac*-lactide, in the presence of benzyl alcohol, with or without solvent present.

Chapter 6 describes the reaction of lithium alkoxides LiOR (R = t-Bu, Ph) with the acids $2,2'$-$Ph_2C(X)(CO_2H)$, where X = OH, NH_2, *i.e.* benzilic acid ($2,2'$-diphenylglycolic acid, benzH) or $2,2'$-diphenylglycine (dpgH). In the case of benzH, reaction with one equivalent of LiOt-Bu in THF afforded the complex [Li(benz)(THF)]$_2$·2THF (**31**·2THF), which adopts a 1D chain structure. If acetonitrile is employed in the work-up under mild conditions, another solvate of **31** is isolated; use of LiOPh also lead to **31**. Use of more robust work-up conditions afforded the complex [Li_7(benz)$_7$(MeCN)] (**32**·2MeCN·THF). Increasing the amount of LiOt-Bu (2 equivalents) led to the isolation of the complex {Li_8(Ot-Bu)$_2$[(benz)](OCPh$_2$CO$_2$-CPh$_2$CO$_2t$-Bu)$_2$(THF)$_4$} (**33**). In the case of dpgH, use of two equivalents of LiOt-Bu in THF afforded [Li_6(Ot-Bu)$_2$(dpg)$_2$(THF)$_2$] (**34**), which contains an Li_2O_2 6-step ladder. Similar reaction of lithium phenoxide with dpg afforded the complex [Li_8(PhO)$_4$(dpg)$_4$(MeCN)$_4$] (**35**). The molecular structures of complexes **31 - 35** are reported; all were screened for their potential to act as pre-catalysts for ROP of ε-caprolactone (ε-CL), *rac*-lactide (*r*-LA) and δ-valerolactone (δ-VL).

Chapter 7 describes the reaction of the dialkylzinc reagents R_2Zn with the acids $2,2$-$Ph_2C(X)(CO_2H)$, where X = NH_2, OH, *ie* $2,2'$-diphenylglycine (dpgH) or benzilic acid (benzH$_2$). With dpgH, the tetra-nuclear ring complexes [RZn(dpg)]$_4$, where R = Me (**36**), Et (**37**), 2-$CF_3C_6H_4$ (**38**), $2,4,6$-$F_3C_6H_2$ (**39**) were isolated; complex **37** has been previously reported. The crystal structures of **36**·2MeCN, **37** and **38**·4(C_7H_8) ·1.59(H_2O) are reported, along with that of the intermediate compound (2-$CF_3C_6H_4$)$_3$B·MeCN and the known compound [$ZnCl_2$(NCMe)$_2$].

Complexes **36– 39**, together with the known [(ZnEt)$_3$(ZnL)$_3$(benz)$_3$] (**40**; L = MeCN), have been screened, in the presence and absence of benzyl alcohol, for their potential to act as catalysts for the ROP of ε-caprolactone (ε-CL), δ-valerolactone (δ-VL) and *rac*-lactide (*rac*-LA); the co-polymerization of ε-CL with *rac*-LA was also studied.

Chapter 8 This chapter presents the experimental section.

Chapter 9 Appendix.

Abbreviations

Å	angstrom
Ar	aryl
t-Bu	$tert$- butyl
TEA	triethylaluminium
MAO	methylaluminoxane
LDPE	low-density polyethylene
HDPE	high-density polyethylene
PP	polypropylene
TMA	trimethylaluminium
DEAC	diethylaluminium chloride
DMAC	dimethylaluminium chloride
DSC	differential scanning calorimetry
GPC	gel permeation chromatography
h	hour
MeCN	acetonitrile
Me	methyl
min	minute
M_n	number average molecular weight
M_w	weight average molecular weight
PDI	polydispersity index
n-Pr	n- propyl
THF	tetrahydrofuran

$^\circ C$	degree Celsius
NMR	nuclear magnetic resonance
br	broad
δ	chemical shift
d	doublet
J	coupling constant
ppm	parts per million
s	singlet
t	triplet
MS	mass spectrometry
EI	electron impact
MALDI	matrix-assisted laser desorption ionization
IR	infra-red
m	medium
s	strong
DME	1,2-dimethoxyethane
VSEPR	Valence shell electron pair repulsion
DMSO	Dimethyl sulfoxide
APCI	Atmospheric pressure chemical ionization
L_p effects	Lorenz and polarization eddects
i-Pr	i- propyl
PCL	polycaprolactone
PLA	polylactide

Contents

Acknowledgements

Chapter 1

General Introduction

1. Introduction

1.1 History of plastics

Plastic is one of the oldest types of polymer, dating back to work in 1909 by Baekeland, when he developed polyoxybenzylmethylenglycolanhydride (Bakelite). This substance has been associated with many different uses, for instance, in electrical apparatus, in cookware handles and general household gear. Three years later came a patent by Colette for the manufacturing process of polyvinyl chloride (PVC). A wide range of polymers were developed by early 1920s, for instance urea formaldehyde (electrical tools), cellulose acetate (combs and toothbrushes) as well as nylon (surgical sutures and stockings).[1]

As of 1925-1950, the idea of polymer properties was adequately comprehensible. In addition, a large number of commercial polymers were produced. There was a significant increase in the production of polymers subsequent to the Second World War, while in 1950s the establishment of novel plastics families, carbonates and acetals was achieved.[1] Owing to the fact that the significance of plastics escalated in modern society after the Second World War, the era from 1970 onwards has experienced growth in diverse forms and kinds of plastics, these can be identified as high-tech plastics, typically employed in diverse fields, such as technology and healthcare sectors. (**Figure1)** shows that the global production of plastics in 2014 rose to approximately 311 million tonnes, compared with the 225 million tonnes produced in 2004.[2]
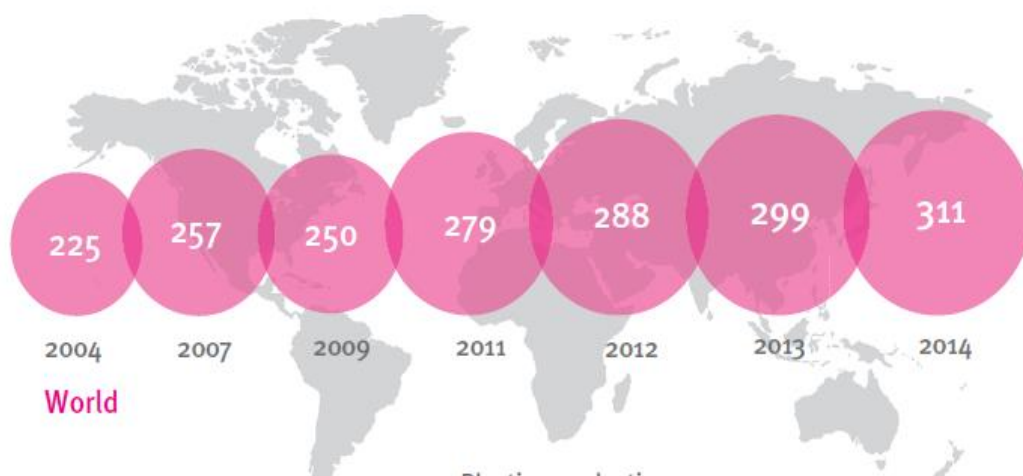
Figure 1. World plastic production 2004-2014 in million tonnes units.

Polymers are large molecules formed by linking large numbers of smaller units called monomers (subunit). These monomers typically have atoms joined by double bonds, and these bonds are broken to create the long chain molecules of the polymer via polymerization. Polymerization is the connecting of monomers by the reaction of unsaturated reactants, commonly a carbon-carbon double bond (**Scheme 1**).[3]
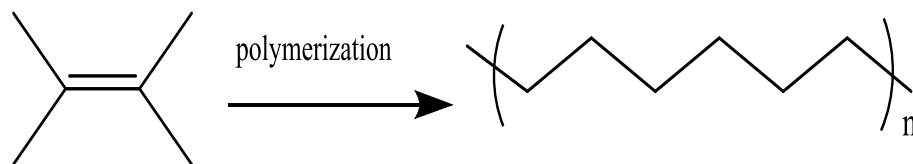
Scheme 1. General polymerization scheme.

1.2 Early discoveries of polymerization catalysts.

During the mid-twentieth century, Karl Ziegler was able to discover a new catalyst based on $TiCl_4$ and using $(C_2H_5)_2AlCl$ as an initiator for the polymerization of ethylene into polyethylene at room temperature. He used the equipment shown in (**Figure 2**).[4] Later, Guilio Natta developed these catalysts to polymerize propylene into polypropylene.[5] Their discoveries created a new

dimension in the field of polymers leading to both Ziegler and Natta sharing the Noble prize in chemistry in 1963.[6]

Figure 2. The original equipment used by Karl Ziegler for discovering his catalyst and co-catalyst systems for the polymerization of ethylene to HDPE.

Presently, Ziegler-Natta catalysts have been utilized globally in the generation of a significant number of diverse α-olefins polymers. Linear low-density and high-density polyethylenes are examples of such polymers.[7] At around the same time, Hogan and Banks, working for the Philips Petroleum Firm discovered silica-sustained nickel/cobalt oxide heterogeneous catalysis systems. They were able to co-polymerize olefins to generate polymers with increased molecular weight.[8] Later on, Field and Feller discovered increased activities among group-six oxide catalysts, identical to Hogan and Banks systems.[9] Nonetheless, the results revealed no control over the generated polymer. This types of catalyst possesses different reaction sites enabling the growth of the polymer at many sites. It is this research that resulted ultimately in the invention of olefin polymerization catalysis based on metallocenes.

1.3 Metallocene catalysts

In 1953, Natta reported the use of metallocene catalysts to polymerize ethylene to polyethylene using titanocene catalysts and triethylaluminium (TEA) as a co-catalyst,[10] which was first used by the Ziegler-Natta olefin system. Breslow has also reported similar work.[11] Natta and Breslow noted that the titanocene catalyst was an active complex towards the polymerization of ethylene, but it was less active than the titanium tetrachloride/TEA system. Twenty three years later, Sinn and Kaminsky reported that the resulting water from the reaction led to highly active ethylene polymerization, due to hydrolysis of trimethylaluminium (TMA), resulting in the formation of the co-catalyst methylaluminoxane (MAO).[12] Kaminsky extended this work to the synthesis of methylaluminoxane and used it to activate a bis-(cyclopentadienyl) zirconium(IV) complex, a system which showed high polymerization activity (**Scheme 2**).[13] Therfore increased desire towards metallocene type catalysts, both academic and industrial researchers have avoided the conventional metallocenes as an approach of seeking inexpensive, uncertified ligand technology/system.[14] Having either a single or two of the cyclopentadienyl ligands replaced with other ligand systems has been thoroughly examined both industrially and academically of late.
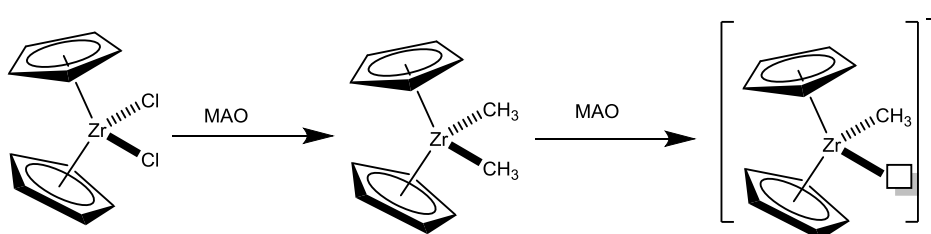
Scheme 2. Zirconocenes used by Kaminsky.

1.4 The problems with plastics

Polymers are very important due to their applications in all aspects of human life. However, the majority of polymers are based on polyolefins, polyethylene (LDPE and HDPE) and polypropylene (PP) (**Figure 3**).[15] These suffer from a severe lack of biodegradability,[16] and are derived from depleted sources.[17] For example, polyethylene plastic bags can take up to 400 years in landfill sites to degrade.[16] A global push towards environmentally friendly plastics has led to further improvement, including alloying plastics to form many usable materials from what was considered waste. For these reasons, much research has been done to develop new ways to synthesise polymers derived from renewable, biodegradable and natural resources.
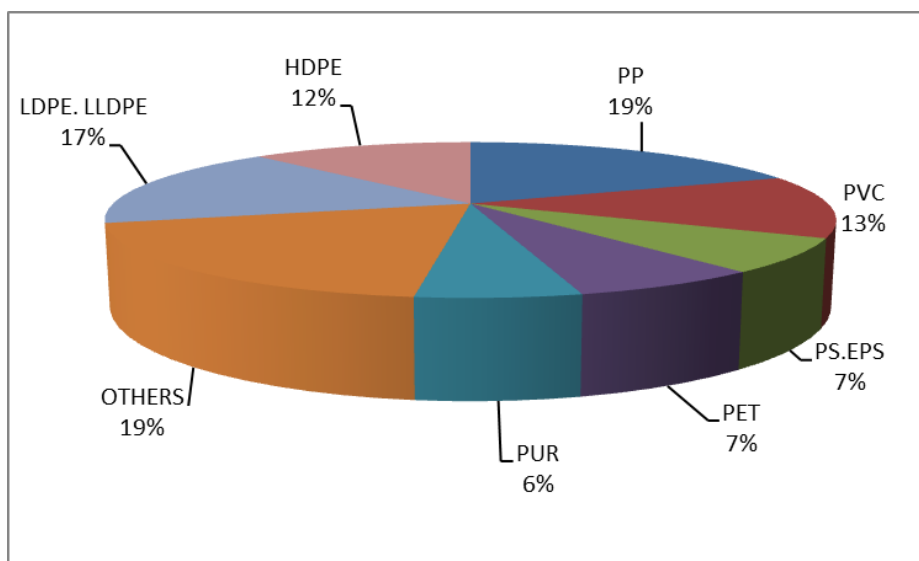
Figure 3. A pie chart showing that poly(olefin)s are the most widely used polymer worldwide.

2. Polylactide and Polylactones

Polylactide, polylactones and related co-polymers are the most widely studied class of biodegradable polymers, because they are ideal for different applications these include medical applications as scaffolds in tissue engineering and drug delivery systems, due to their biocompatibility.[18] In addition, they can be used in industrial applications, for example manufacturing plastic bags and food packaging.[19] In terms of availability, they are produced from renewable and natural resources, such as lactide from corn starch. Another important feature of poly(lactide) and polylactone is that there is no toxicity observed for these polymers, so for this reason they can be used in food packaging.[20] Polylactide, poly(ε-caprolactone) and poly(δ-valerolactone) can be synthesized by polymerization of lactides and lactones monomers (**Scheme 3**).
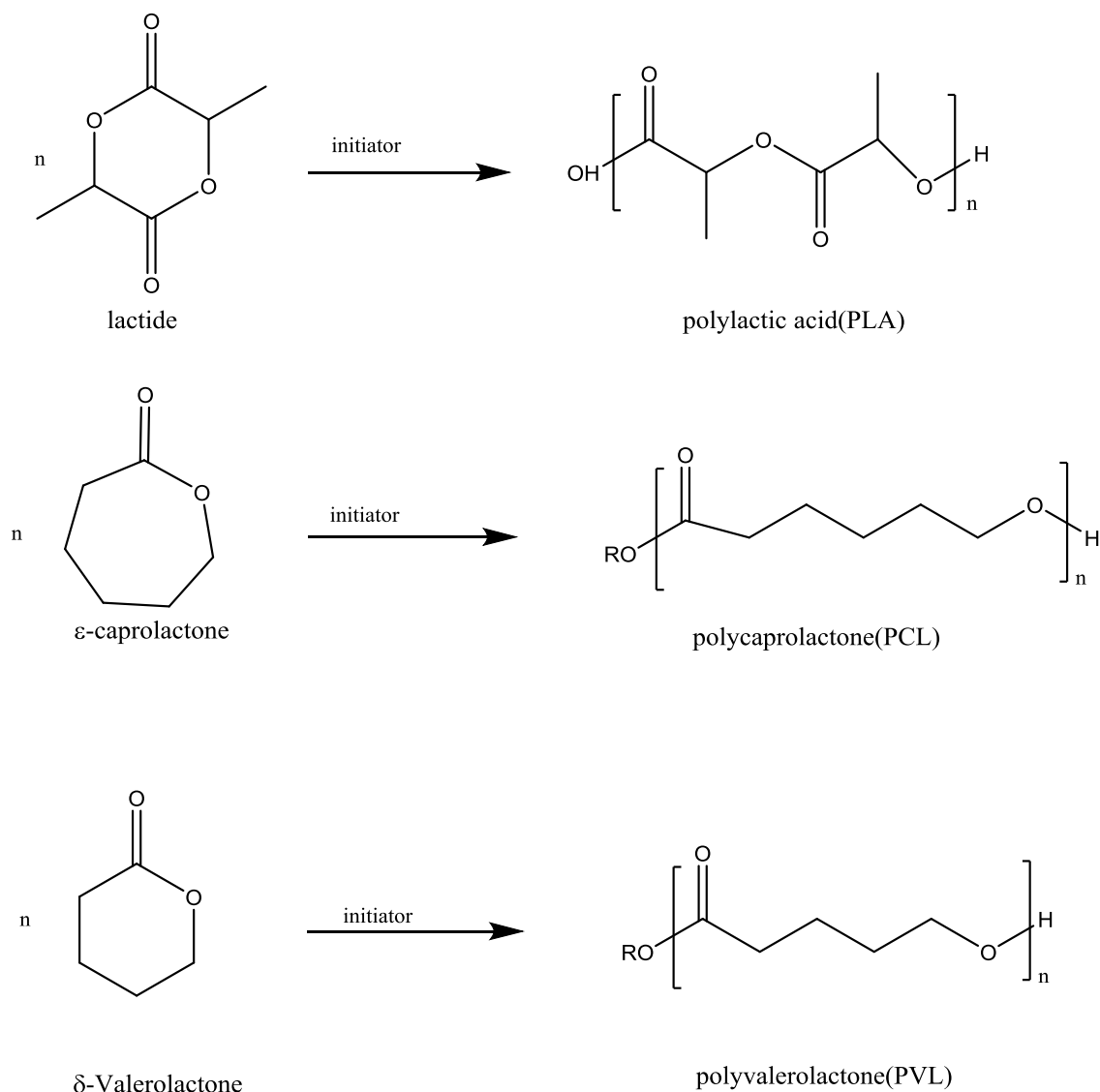
Scheme 3. Polymerization of lactide, ε-caprolactone and δ-valerolactone.

3. Co-polymers

The co-polymerization of monomers such as lactide and ε-caprolactone gives a useful way of mixing the properties of the individual homopolymers. For example, the drug permeability of polycaprolactone is higher compared to that of polylactide. Also the thermal properties and the flexibility of the resulting co-polymer are other beneficial features.[21] There are two different types of co-polymer a random co-polymer or block co-polymer. A random co-polymer makes

it possible for the behaviour to be continuous while a block structure will make it possible for the polymer to possess properties that are more similar to those of the separate homopolymers.[22],[23] Previous work presented by Feng and co-workers revealed that polylactide block co-polymer with polycaprolactone was capable of yielding a material with PCL permeability and more rapid PLA degradation.[24]

4. Polymerization of cyclic esters

Cyclic esters can be polymerized in a variety of ways, including polycondensation or ring-opening polymerization.

4.1 Polycondensation

A reaction between a diol with a diacidic or hydroxyl acid forms a polyester; this reaction involves losing water from the reaction medium (**Scheme 4**).[25]
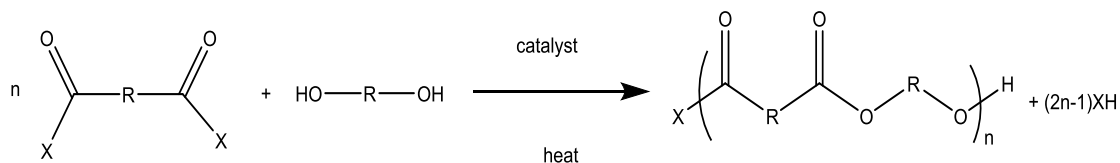
Scheme 4. Polycondensation reaction

Braud *et al*. used hydroxycarboxylic acid to prepare PCL oligomers in a vacuum. This reaction is completed without a catalyst in six hours at a temperature that was gradually increased from 80 ^{o}C to 150 ^{o}C.[26]

The polycondensation is less expensive than other techniques, but it is difficult to get high molecular weight, control of end group and to get well-defined co-polymers.

4.2 Ring opening polymerization of cyclic esters

Ring opening polymerization is the usual method to prepare polyesters from cyclic monomers. Carothers *et al.* reported the synthesis of poly(ε-caprolactone) by ring-opening polymerization in 1934.[27] The reaction between a catalyst and cyclic esters formed polyesters (**Scheme 5**).
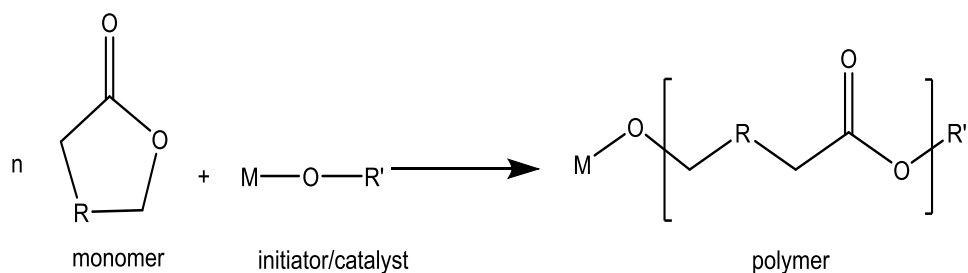
Scheme 5. Schematic representation of the polymerization of a cyclic ester.

It is therefore clear that the polymer chain ends contain two different functional groups, one of them originating from the monomer and the other originating from the catalyst or initiator. In the ordinary cyclic esters polymerization catalyzed by metal complexes, a hydroxyl compound (alcohol) is added as the real initiator. The alcohol initiator first reacts with metal complexes to generate a metal alkoxide bond by ligand exchange. By using different catalysts and initiators the nature of the end groups can be varied to change the nature of the polymer to fit the application.[28]

4.3 Mechanism of ring opening polymerization

In general, there are three major reaction mechanisms for ROP, depending on whether the initiation occurs by anionic, cationic or coordination-insertion mechanisms.

4.3.1 Cationic ring opening polymerization (CROP)

Polyesters are formed upon having cationic catalysts reacted with 4-, 6- and 7-membered rings (of the cyclic esters). Creation of positively charged species defines the cationic ring-opening polymerization, and which is subsequently attacked by a monomer. Due to this attack, the positively charged species ring-opening occur via SN2-process.[29,30]

Two different mechanisms can occur in cationic ring-opening polymerization (CROP) either *active chain end* or *activated monomer*. However, using CROP to polymerize lactide and lactone remains rare, due to the possibility of side reactions such as transesterification, and proton and hydride transfer reactions (**Scheme 6**). [25],[31]
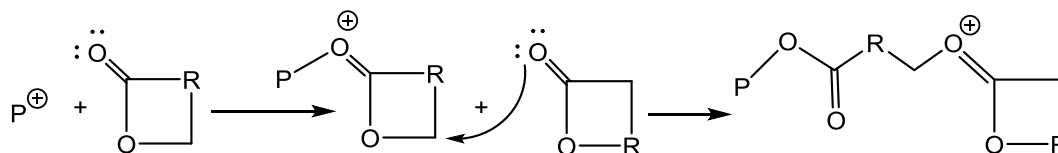
Scheme 6. CROP mechnism of a cyclic ester.

CROP of lactide in solution was first reported by Kleine *et al.*[32] Kricheldorf *et al.* reported the synthesis of co-polymers by CROP of glycolide and ε-caprolactone using different catalysts.[33] Also, many researcher reported the CROP of lactone, for example, Endo and co-worker reported the polymerization of ε-thionocaprolactone via CROP by using $BF_3.OEt_2$ as an intiator in CH_2Cl_2.[34] It is difficult to control the structures of the polymers formed by CROP. In addition, polymerization of monomers by this mechanism produces polymers with low molecular weight.

4.3.2 Anionic ring opening polymerization (AROP)

A linear polyester is formed in the AROP mechanism via the nucleophilic attack of a negative charge (anionic species) on the carbonyl carbon or the carbon atom next to the acyl-oxygen of the monomer. This mean there are two possibilities for (AROP): acyl-oxygen cleavage or alkyl-oxygen cleavage **Scheme 7**.[35]
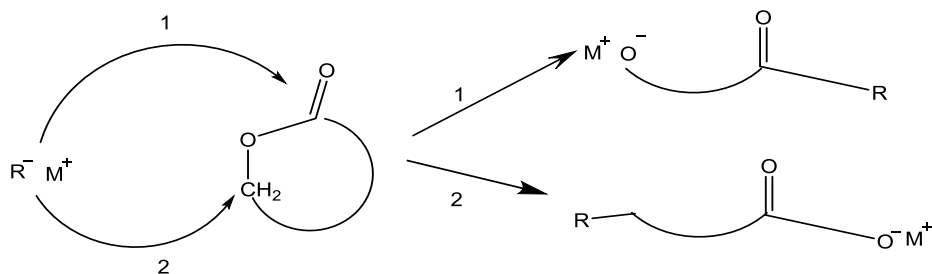
Scheme 7. AROP mechanism of a cyclic ester.

Anionic polymerization is one of the best controlled techniques resulting in high molecular weight polymers conducted in a polar solvent. The Jedlinski group established living anionic ROP approaches of 4- and 5-membered ring lactones and has reported high molecular weight co-polymers and homopolymers.[36] The 4-membered rings' anionic ring-opening (lactones) happens via acyl-oxygen or alkyl-oxygen cleavage resulting in alkoxide or carboxylate.[37],[38] Lactones with large membered rings (6 or more), like lactide or ε-caprolactone tend to react only by attacking the carbonyl carbon atom with acyloxygen scission and the generation of an alkoxide as the growing species.[39]

4.3.3 Coordination-insertion ring opening polymerization

The coordination-insertion mechanism involves alkoxides of metals such as Mg, Zn and Al (metals with free p, d or f orbitals) initiating the polymerization of lactone and lactide. If we take the polymerization of lactide as an example

(**Scheme 8**), we find it involves two steps: the metal centre coordinates with the monomer, then nucleophilic attack of the alkoxide on the acyl-carbon atom and insertion of the lactide into the metal alkoxide species. This leads to the formation of a new negative charge which is then capable of extra insertion reactions.[40]
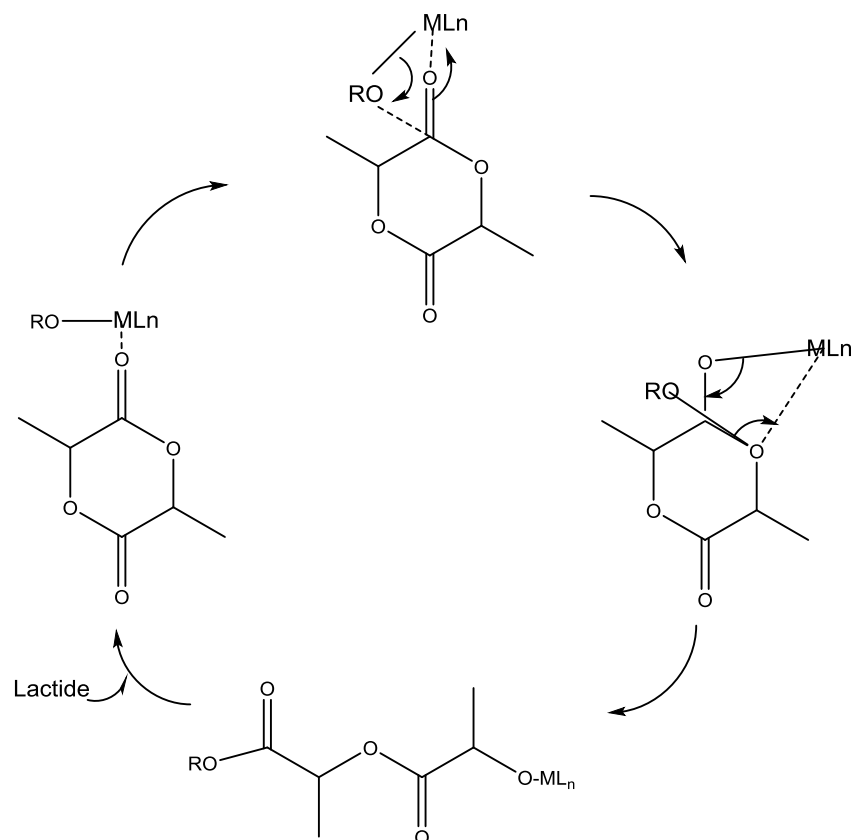
Scheme 8. Coordination-insertion mechanism of acyclic ester.

5. Coordination complexes as catalysts.

Complexes are investigated in a number of studies as catalysts for ROP of cyclic esters, *i.e.* metal carboxylates and alkoxides. A significant number of the reactions catalyzed by metal complexes are very specific, as well as, through alteration of metals and ligands, reactions tend to produce a preferred polymer structure.

5.1 Group IV complexes.

A variety of metal complexes have been investigated as catalysts for the ROP of cyclic ester. However, examples for group V metal compounds for such polymerization remain rare.

5.1.1 Vanadium complexes pre-catalysts to polymerize ethylene and cyclic esters.

In 1960, Natta *et al*. published a paper in which they described the ability of vanadium tetrachloride and vanadium triacetyacetonate with aluminium dialkylmonohalide as the co-catalyst for the polymerization of propylene to give stereo polymers.[41] Later, there were many examples of vanadium complexes which are used commercially to polymerize ethylene and propylene, but the problem with such a system is that it is necessary to add an excess of organoaluminium compounds to get high activities. However, the use of excess co-catalyst needs to be removed from the resulting polymers. In 2004, Fujita *et al.* described the first example of a highly active catalyst system based on Zr, Ti and V complexes for polymerization of olefin (**Figure 4**, **1**).[42] Redshaw and *et al* reported using bi- and tri-phenolate ligands with a vanadium metal which showed high activity towards homo-polymerization of ethylene (**Figure 4**, **2-5**).[43] In the 2006, Redshaw *et al*. also published new highly active catalysts for ethylene polymerization with *N, O* donor atom ligands (**Figure4**, **6**) .[44]

R₁=Me, R₂= R₃= ᵗBu   (2)

R₁=H, R₂= ᵗBu, R₃= Me (3)

R₁= ᵗBu, R₂= R₃= Me (4)

R₁= R₂= ᵗBu, R₃= Me (5)

6
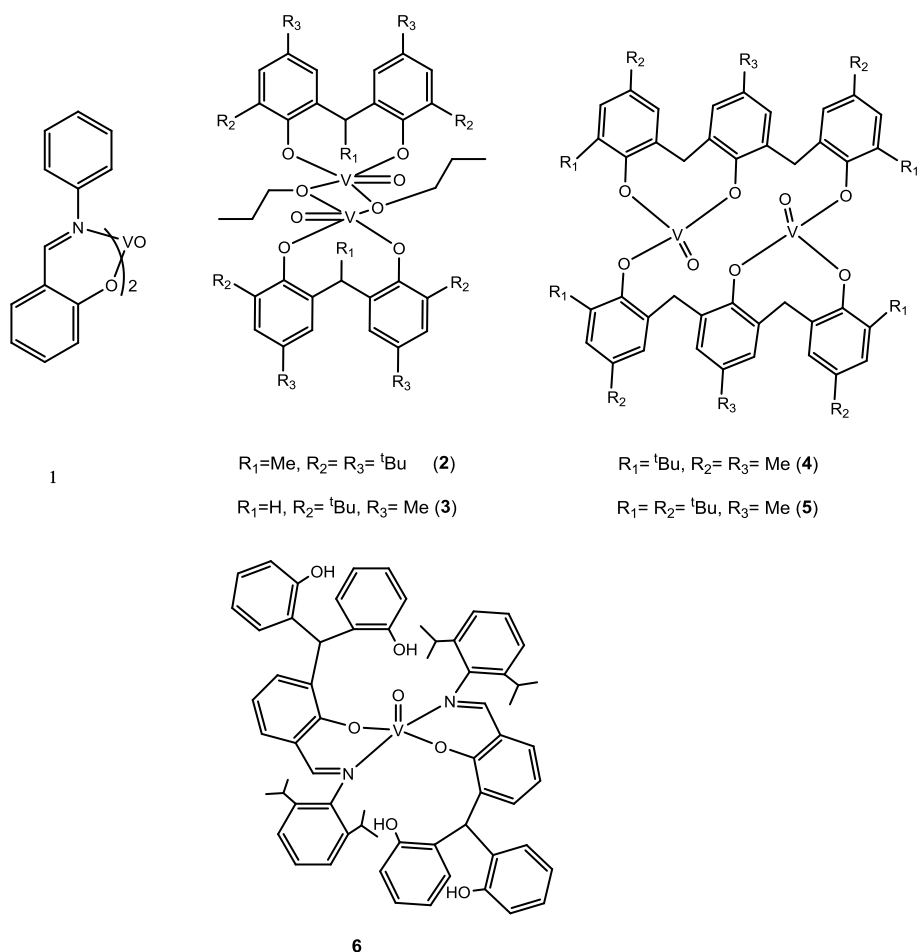
Figure 4. Literature examples of vanadium pre-catalysts for ethylene polymerization.

Vanadium complexes have received less attention for the ring opening polymerzation of cyclic esters.[16]

In 2005, Atlamsan and co-workers demonstrated that oligomerization of ε-caprolactone and δ-valerolactone using vanadium or molybdenum catalysts with heteropolyacid as co-catalyst. Vanadium heteropolyacid and $VOSO_4$ were both found to be active.[45] Later, Redshaw *et al*. reported a range of vanadium complexes that can polymerse cyclic esters (**Figure 5**, **7-9**).[46]

7 = (R= n-Pr, R'= H, Me)   **8**(Ar= p-tolyl, p-C(C$_6$H$_4$) R= ^{t}Bu, C(CF$_3$)$_2$Me   **9**(Ar= *p*-tolyl, *p*-C(C$_6$H$_4$), *p*-(MeO)C$_6$H$_4$, *p*-CF$_3$C$_6$H$_4$; R= *i*-Pr, *n*-Pr, Et)
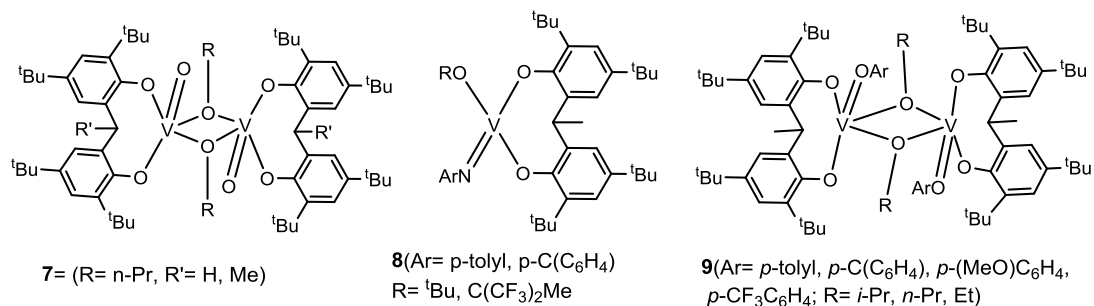
Figure 5. Vanadium complexes used by Redshaw *et al*.

5. 1. 2 Niobium and tantalum catalysts

Niobium and tantalum elements share many properties such as non toxicity, which has motivated many research groups to study niobium and tantalum complexes as catalysts. However, until recently, using such a system was rare and they exhibited low activities towards ethylene polymerization. Chen *et al*. reported a series of niobium-benzamidinato complexes; they found these complexes exhibited low activities toward ethylene polymerization (**Figure 6**, **10**).[47] Other research groups, such as Hubert-Pfalzgraf and co-workers have observed no activity of niobium(V) and tantalum(V) complexes toward polymerization of ethylene (**Figure 6**, **11** and **12**).[48] Redshaw *et al*. reported various niobium complexes systems and tested their ability toward polymerization of ethylene.[49] An example of these complexes is shown in (**Figure 6**, **13**).
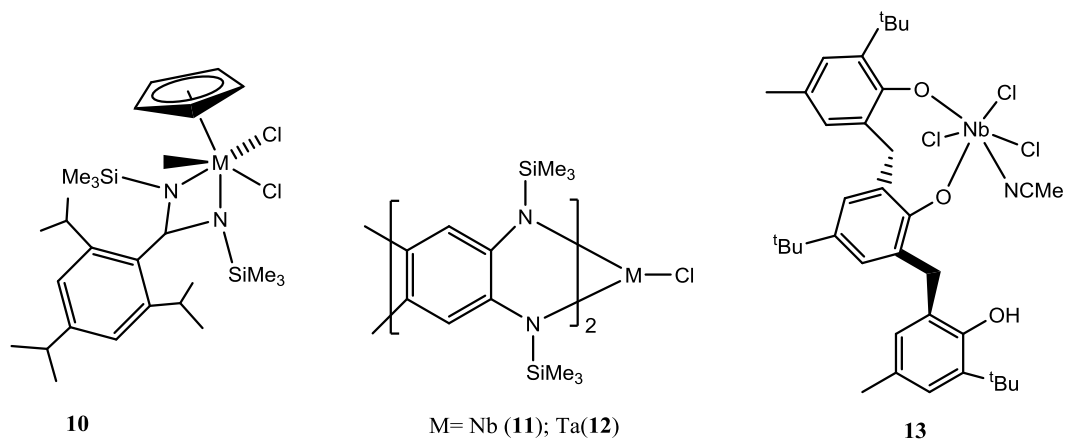
Figure 6. Literature examples of Nb and Ta catalysts.

5. 2 Molybdenum complexes.

Molybdenum compounds as a catalysts have been studied over the latest few decades because molybdenum is a versatile element existing in many catalytic systems used for polymerization, for example polymerization of norbornenes (1)[50] (**Figure 7**, **14**) and ethylene polymerization(**Figure 7**, **15**).[51] Molybdenum is also a biologically essential metal. It is the heaviest atomic number element to have a wide range of functions in living organisms. Over the past few decades, there have been many studies of high oxidation state molybdenum-imido complexes, due to their participation in the catalysis of olefin metathesis and olefin polymerization of the Ziegler-Natta system.[52] There have been few studies in the literature using molybdenum complexes as catalysts in the ROP of cyclic esters for examples Martınes-Richa *et al*. reported using ammonium decamolybdate $(NH_4)_8[Mo_{10}O_{34}]$ in the ROP of ε-CL and δ-VL.[53] Redshaw and co-worker also investigated using molybdenum complexes derived from the oxydianiline $[(2-NH_2C_6H_4)_2O]$ (**Figure 7**, **16**).[54]
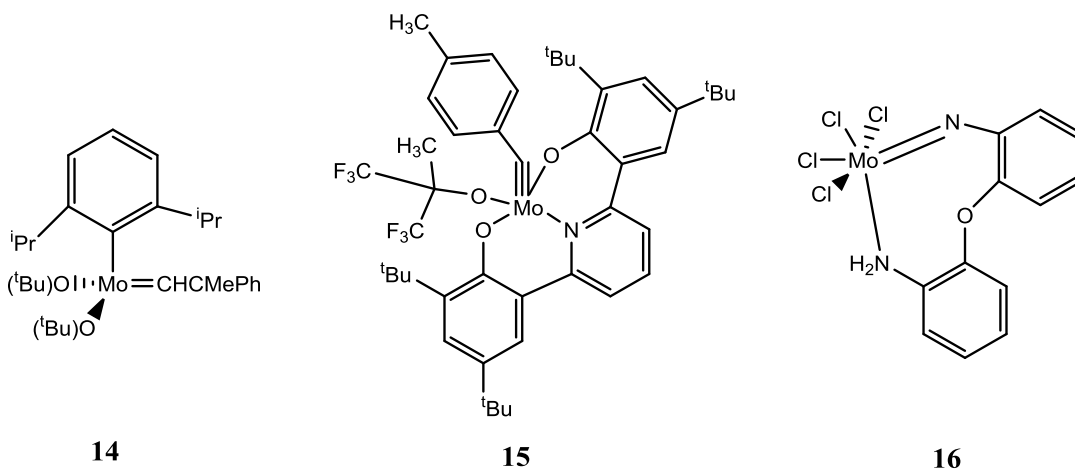
Figure 7. Literature examples of molybdenum catalysts.

5. 3 *Aluminium complexes*

Aluminum-based catalysts are investigated by many research groups, due to their ability to produce narrow PDI and high molecular weight with well-defined end groups.[55-56] An examples for these studies, Duda *et al.* reported the polymerization of LLA using two aluminum isopropoxide ($Al(O^iPr)_3$) aggregates that show high monomer conversions (> 90 %) (**17** and **18**).[57-58] Yu Liu and co-worker also, reported β ketiminato aluminium complexes in polymerization of ε-caprolactone and *L*-lactide(**19** and **20**) (**Figure 8**).[59]
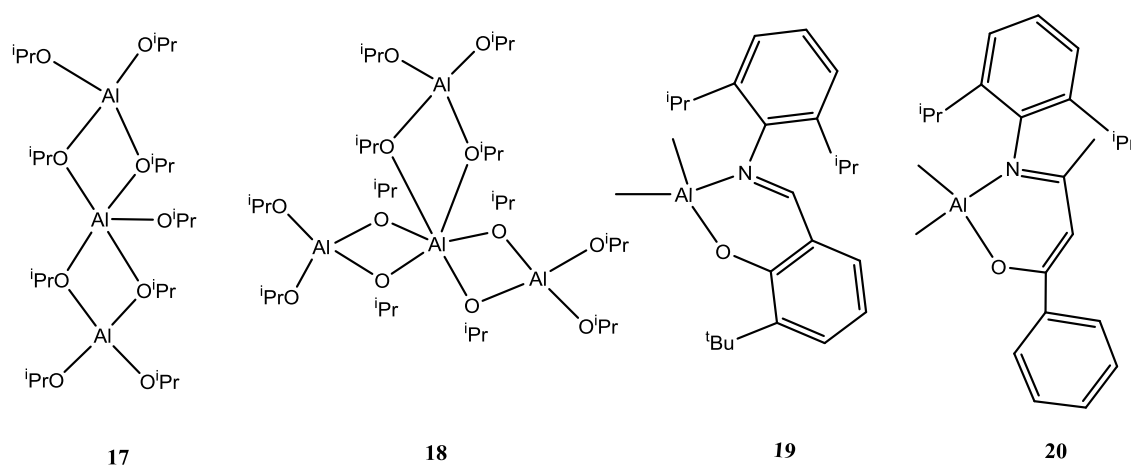
Figure 8. Literature examples of aluminum catalysts.

5. 4 Lithium complexes.

Recently, lithium compounds have been investigated as catalysts for the ring opening polymerization of cyclic esters. For example, Wang *et al*. published a paper in which they described using LiCl as a catalyst for ROP of lactide in the presence of ethylene glygol and methyl α-D-glucopyranoside.[60] Another study by Kasperczyk reported lithium *tert*-butoxide as an initiator for ROP of *rac*-lactide and *L*-LA. Although these catalysts showed activity toward polymerization the basicity of these species led to side reactions resulting in very broad or multimodal molecular weight.[61] Further work has been carried out by using a series of lithium complexes with different ligand sets. For instance, Carptentier and co-workers reported the synthesis of lithium complexes based on other-phenolate ligands, these systems were active in the presence of BnOH. [62] Kerton *et al.* reported coordinated tetradentate ligands with (*O,N,N,O*)-type bonding with lithium and sodium metals. These catalysts showed activity toward ROP of *rac*-lactide (**Figure 9**, **21**).[63]
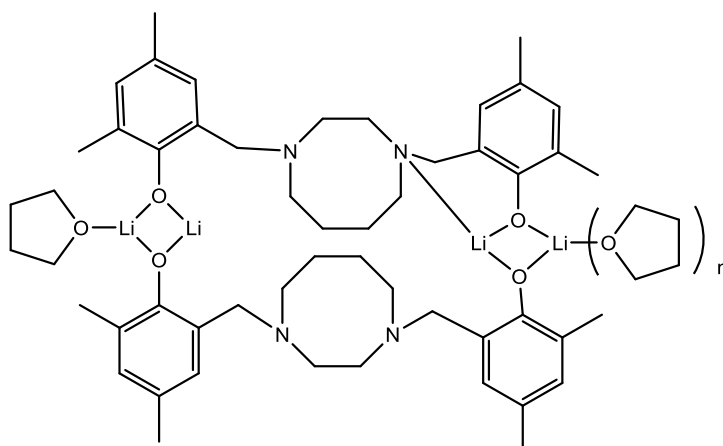
21

Figure 9. Literature examples of lithium catalysts**.**

5. 5 Zinc complexes.

Lately, ligands supported by a zinc ion for polymerization of lactones and lactides have been encouraged due to the valuable features of the zinc ion, such as, no colour, price (cheap) and lack of toxicity. These are key points for a number of purposes, e.g in medical applications of the resulting polymer. Recently, many zinc complexes have been investigated as catalysts in the ring opening polymerization of lactide and lactones for example, Coates *et al.* have used a β-diiminate bidentate ligand supported by zinc and magnesium ions and employed them in the ROP of *rac*-lactide (**Figure 10**, **22** and **23**).[64] Chisholm also presented the same ligand with an altered backbone and coordinated with Zn and Mg. The results revealed that the rate of ring opening polymerization based one Mg metal was greater than for Zn (**Figure 10**, **24**).[65]
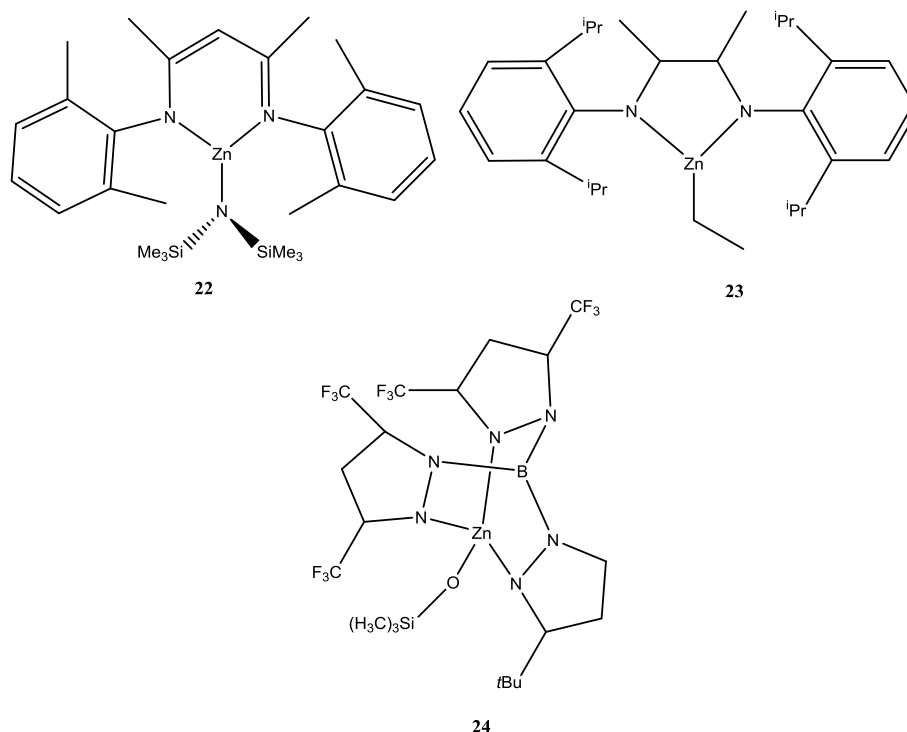
Figure 10. Literature examples of zinc catalysts**.**

6. Polymer Characterization.

6.1 NMR Spectroscopy

It is possible for significant information regarding a polymerization reaction and the successive polymer produced to be yielded from NMR spectroscopy. The presence of protons in most of the polymer chains and fast relaxation times makes it possible for fast analysis of produced polymeric material. This is the reason for the common use of ^{1}H NMR spectroscopy. Exhibition of somewhat different chemical shifts, within the monomeric environment, is often made by proton environments, compared to when they are incorporated into the polymer chain. With regards to polylactide, for example, polymer and monomer are soluble in a deuterated solvent, while it is possible to utilise ^{1}H NMR spectroscopy in calculating for the monomer conversion.[66]

6.2. Homonuclear-decoupled NMR

Quantification of polylactide stereochemical microstructure can be carried out through evaluation by employing homonuclear decoupled ^{1}H NMR spectroscopy. Observation of several methine proton resonances can be made as a result of several stereochemical environments. It is possible to assign these resonances to different stereo sequence combinations which are given the name '*r*' and '*m*' notation.[64],[67]

6.3. Gel Permeation Chromatography.

A size-exclusion technique capable of being utilised for the characterization of polymeric material is known as gel permeation chromatography (GPC). It is possible to pass the polymeric sample solution through porous beaded columns to separate the polymer. The polymer chains on the basis of size. Materials of

smaller molecular weight go into the beads and the time it takes to elute is longer, compared to the larger chains passing around the material.[68]

6.4. Differential Scanning Calorimetry

A material's thermal transitions can be measured with the aid of differential scanning calorimetry. A phase change due to thermal transitions is accompanied by a change in heat capacity. The material sample is placed in a pan and heat is applied at a similar rate to that of a blank reference. A graph of the heat flux difference can be made against temperature. A number of thermal properties can be made available by DSC. A material glass transition temperature is symbolised by T_g. An increase in the material heat capacity is brought about by a shift of the baseline in the endothermic direction on the DSC trace. Below its T_g, an amorphous polymer will become glassy and brittle, while above its T_g, it will become softer. The crystallisation temperature is symbolised by T_c. This happens to be a transition that is exothermic and signified by the highest point in the exothermic direction on the DSC trace. When enough energy is given to the material so that its regular crystalline state can be attained, crystallisation takes place, thereby decreasing its heat capacity. The material's melting temperature is symbolised by T_m. Adequate energy is made available in order to make the endothermic transition from solid to liquid possible.[69]

7. Thesis overview

This study focuses on ring opening polymerization of cyclic esters. A number of mono- or multi-nuclear pre-catalyst systems have been synthesized and characterized, and then tested for their ability to act as catalysts for the ring opening polymerization of ε-caprolactone, *rac*-lactide, *l*-lactide and δ-valerolactone.

In **Chapter 2**, the synthesis of niobium(v) and tantalum(v) complexes supported by α, α,α$^/$,α$^/$-tetra(3,5-di-*tert*-butyl-2-hydroxyphenyl–*p*-) xylene-*para*/*meta*-tetra phenol complexes have been screened for their ability for ring opening polymerization of ε-caprolactone.

In the second results and discussion chapter (**Chapter 3**), the focus is on molybdenum(VI) complexes supported by di-, tri- or tetra-phenol ligands. These systems were also be screened for their ability to produce poly(ε-caprolactone).

In the third section of the study (**Chapter 4**), the focus is on vanadium(V) complexes supported by also di-, tri-, and tetra-phenol ligands. These complexes have been screened for their ability to ring open polymerize ε-caprolactone, *L*-lactide or *rac*-lactide with and without solvent present.

The fourth part of the study (**Chapter 5)** involve the synthesis of organoaluminium complexes derived from anilines or Schiff bases for the ring opening polymerization of ε-caprolactone, δ-valerolactone *rac*-lactide and ε-caprolactone/*rac*-lactide copolymer.

(Chapter 6) include the synthesis of multimetallic lithium complexes derived from the acids $Ph_2C(X)CO_2H$ (X = OH, NH_2). All complexes were screened for their potential to

act as pre-catalysts for the ring opening polymerization (ROP) of ε-caprolactone (ε-CL), *rac*-lactide (*rac*-LA) and δ-valerolactone (δ-VL).

In **Chapter 7**, the synthesis of multimetallic alkyl zinc complexes derived from the acids $Ph_2C(X)CO_2H$ (X= OH, NH_2) is reported. These complexes have been screened for their potential to act as catalysts for the ring opening polymerization (ROP) of ε-caprolactone (ε-CL), δ-valerolactone (δ-VL) and *rac*-lactide (*rac*-LA); the co-polymerization of ε-CL with *rac*-LA was also studied.

(**Chapter 8**) presente all synthetic procedures, characterization data and polymerization methods are presented.

7.1 Ligands used in this study

L^{1}H$_4$

L^{2}H$_4$

R = Me (L^{3}H$_2$), Ph (L^{4}H$_2$)

L^{5}H$_3$

L^{6}H$_3$

L^{7}H

L^{8}H

L^{9}H

L^{10}H

Ph$_2$P

NH$_2$

Ph$_2$NH

Ph$_2$CHNH$_2$

NH$_2$

OH

O

OH

O

OH

L^{11}

L^{12}

L^{13}

dpgH

benzH
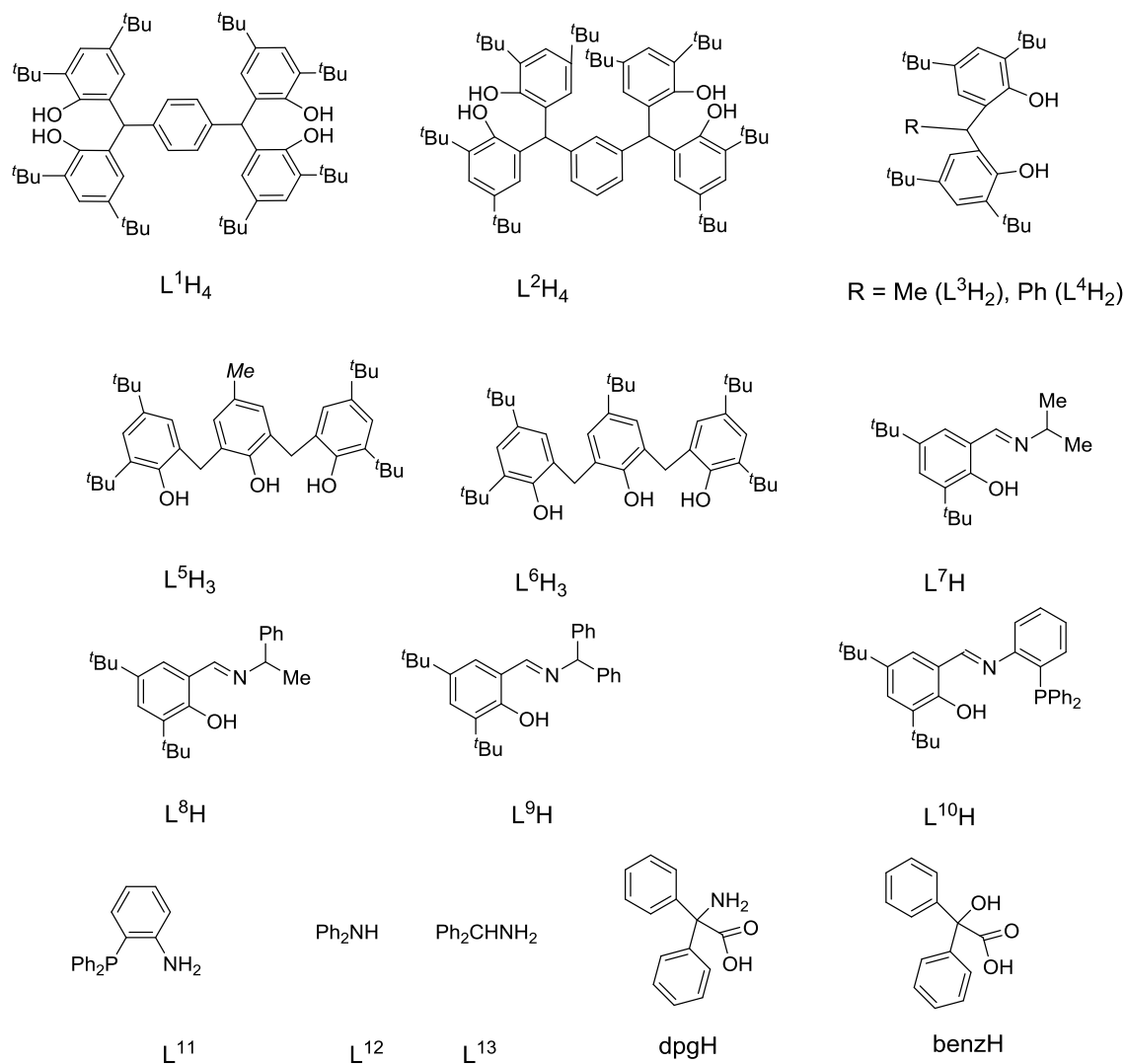
Figure 11. Ligands used in this study.

7.2 Complexes used in this study.
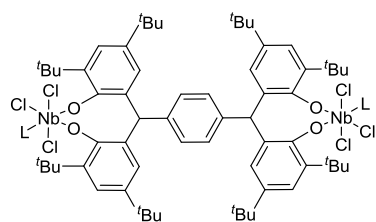
(1)
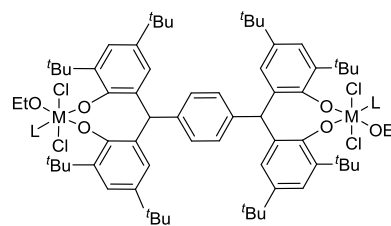
M = Nb (2), Ta (3)
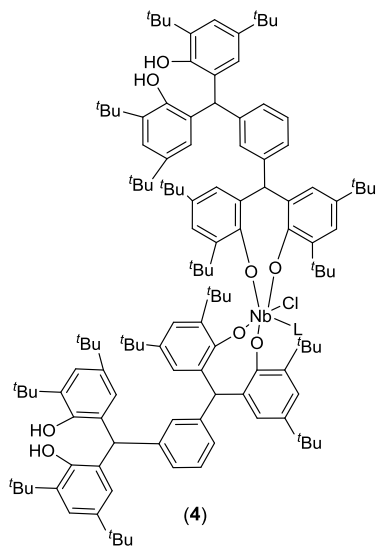
(4)
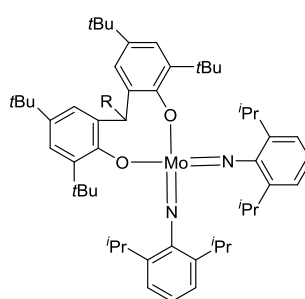
R = Me (5), Ph (6)

(7)

(8)

(9)

(10)

(11) (12) (13)

(14) R =
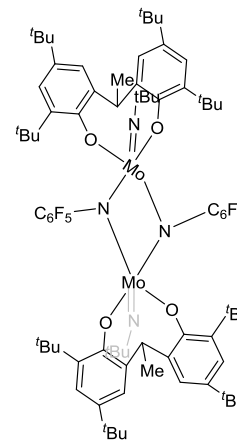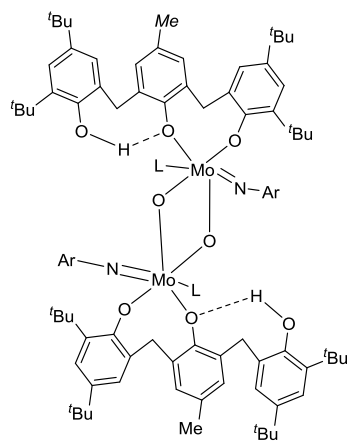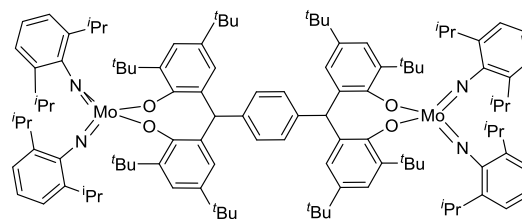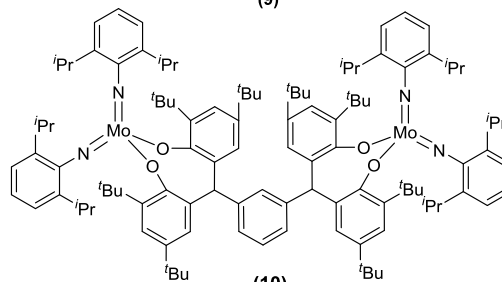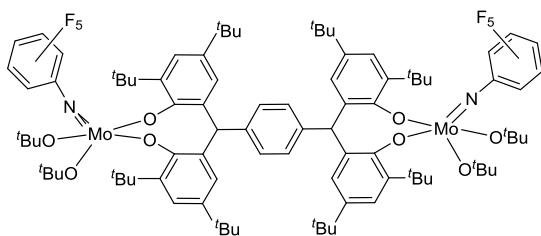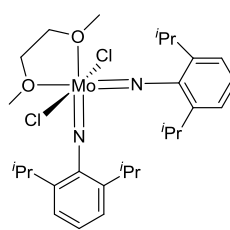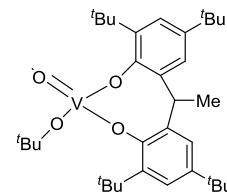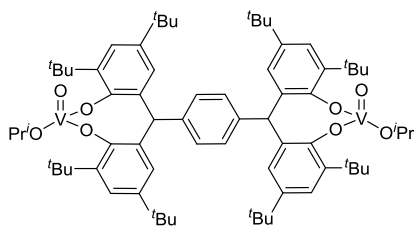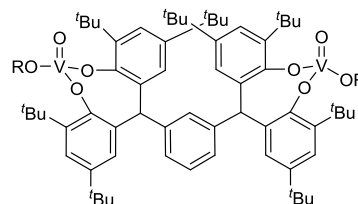
R = *i*Pr (15), *t*Bu (16)
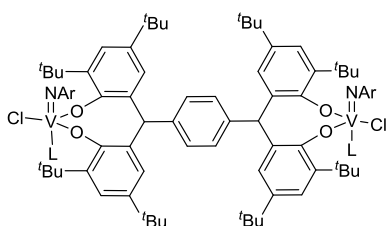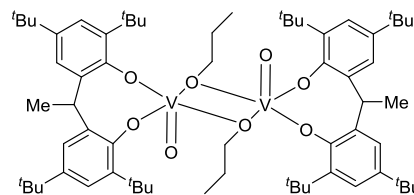
(17) (18)
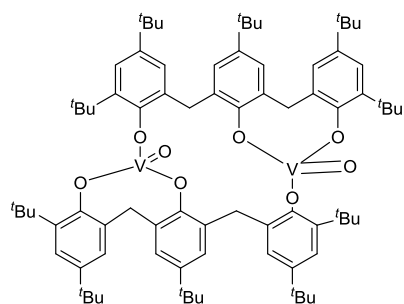
(19) R = Me (20), Et (21) R = Me (22), Et (23)

27
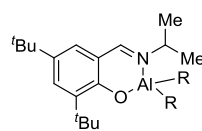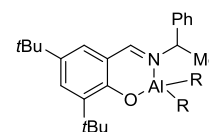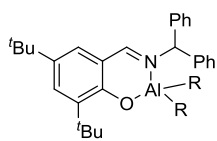
R = Me (**24**), Et (**25**)
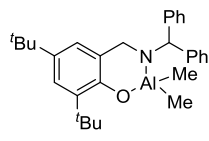
(**26**)
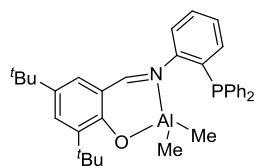
(**27**)
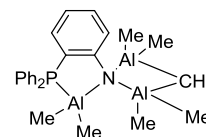
(**28**)
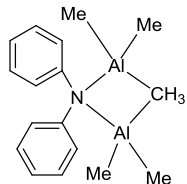
(**29**)
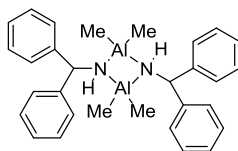
(**30**)
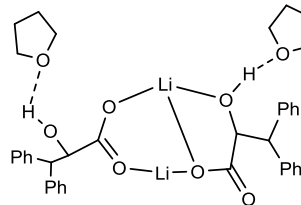
(**31**)
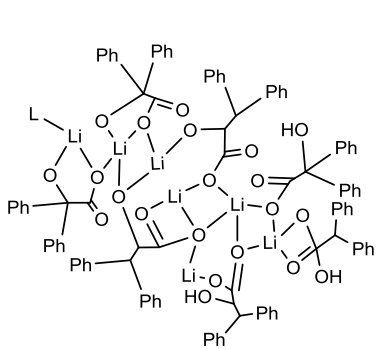
L= MeCN

(**32**)
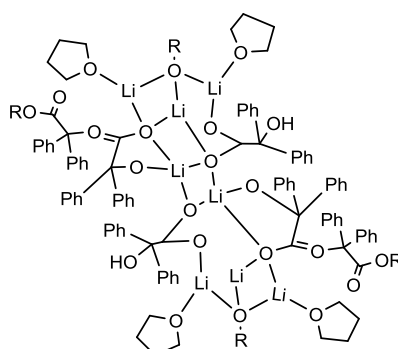
R= *t*-Bu

(**33**)
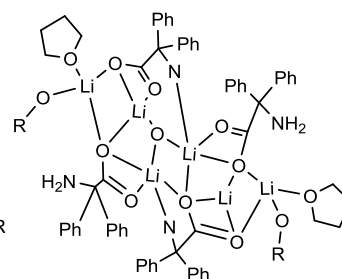
R= *t*-Bu

(**34**)
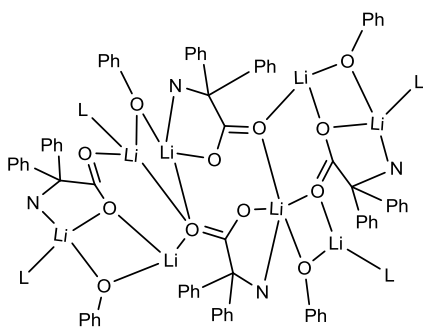
(**35**)   L= MeCN

R=Me (**36**), R=Et (**37**)

28
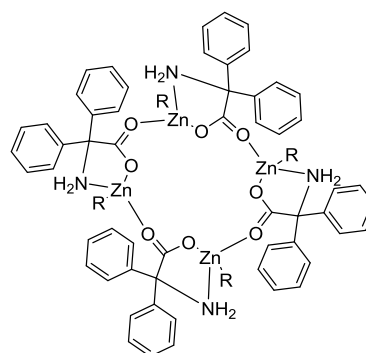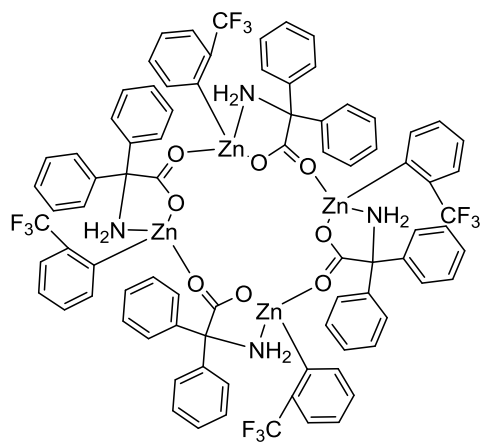
(38)
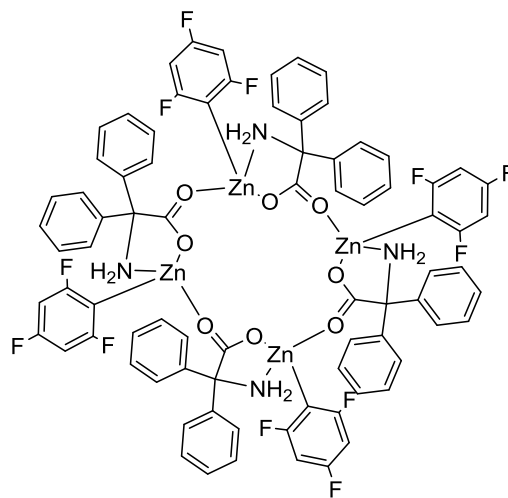
(39)
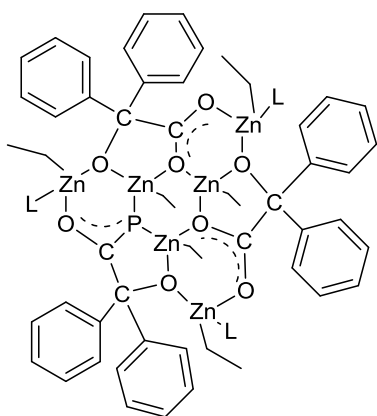
(40)

Ph=phenyl, L=MeCN

Figure 12. Complexes used in this study.

7. References

[1] R. O. Ebewele, *Polymer science and technology*, CRC Press, United States, **2000**,544.

[2] PlasticsEurope in *the Facts Vol.* PlasticsEurope, **2015**.

[3] C. E. Carraher and R. B. Seymour in *Introduction to Polymer Science and Technology*, *Vol. 285 A. Chem. Soc*, **1985**, 13.

[4] M. H. C. Ahmad Shamiri , S. Jahan , M. A. Hussain , W. Kaminsky , P. V. Aravind and W. A. Yehye, *Materials,* **2014**, 7.

[5] G. Natta, *J. Polym. Sci.,* **1959**, 34, 21.

[6] J. P. Claverie and F. Schaper, *MRS Bulletin* **2013**, 38, 213.

[7] S. D. Ittel, L. K. Johnson and M. Brookhart, *Chem. Rev.*, **2000**, 100, 1169.

[8] A. Clark, J. P. Hogan, R. L. Banks and W. C. Lanning, *Ind. Eng. Chem.*, **1956**, 48, 1152.

[9] F. Edmund and F. Morris in *Conversion of ethylene and/or propylene to solid polymers in the presence of group 6a metal oxides and alkali metals*, *Vol.* Google Patents, **1954**.

[10] V. K. Ziegler and H. Martin, *Die Makromolekulare Chemie* **1956**, 18, 186.

[11] D. S. Breslow and N. R. Newburg, *J. Am. Chem. Soc.*, **1957**, 79, 5072.

[12] H. Sinn, W. Kaminsky, H.-J. Vollmer and R. Woldt, *Angew. Chem. Int. Ed. Engl.* **1980**, 19, 390.

[13] W. Kaminsky, *J. Chem. Soc., Dalton Trans.,* **1998**, 1413.

[14] W. Kaminsky and A. Laban, *Appl. CataL., A: General,* **2001**, 222, 47.

[15] P. Europe in *The Compelling Facts About Plastics*, **2008**.

[16] A. Arbaoui and C. Redshaw, *Polym. Chem.*, **2010** , 1, 801.

[17] K. Sudesh and T. Iwata, *Clean (Weinh),* **2008**, 36, 433.

[18] V. R. Sinha, K. Bansal, R. Kaushik, R. Kumria and A. Trehan, *Int. J. Pharm.,* **2004**, 278, 1.

[19] Y. Kimura, *Polym. J,* **2009**, 41, 797.

[20] O. Dechy-Cabaret ,B. Martin-Vaca and D. Bourissou, *Chem. Rev.,* **2004**, 104, 6147.

[21] N. Hadjichristidis, S. Pispas and G. Floudas in *Block Copolymers by Anionic Polymerization*, *Vol. JWS.*, **2003**, 1.

[22] G. Odian in *Introduction*, JWS., **2004**, 1.

[23] A. Bhattacharya and P. Ray in *Introduction*, *Vol. J WS.*, **2008**, 1.

[24] C. X. Song, H. F. Sun and X. D. Feng, *Polym J.,* **1987**, 19, 485.

[25] K. M. Stridsberg, M. Ryner and A.-C. Albertsson in *Controlled Ring-Opening Polymerization: Polymers with designed Macromolecular Architecture*, *Vol.* Springer Berlin Heidelberg, Berlin, Heidelberg, **2002**, 41.

[26] C. Braud, R. Devarieux, A. Atlan, C. Ducos and V. Michel, *J. Chromatogr. B Biomed. Sci. Appl*. **1998**, 706, 73.

[27] F. J. v. Natta, J. W. Hill and W. H. Carothers, *J. Am. Chem. Soc.,* **1934**, 56, 455.

[28] C. K. Williams, *Chem. Soc. Rev.,* **2007**, *36*, 1573.

[29] B. A. Rozenberg, *Makromolekulare Chemie.macromol. symp*., **1992**, 60, 177.

[30] V. H. Cherdron, H. Ohse and F. Korte, *makromol. chem.,* **1962**, 56, 179.

[31] S. Penczek, *J. Polym. Sci. A Polym. Chem.,* **2000**, 38, 1919.

[32] V. J. Kleine and H.-H. Kleine, *makromol. chem.,* **1959**, 30, 23-38.

[33] H. R. Kricheldorf, T. Mang and J. M. Jonte, *Macromolecules* **1984**, 17, 2173-2181.

[34] F. Sanda, D. Jirakanjana, M. Hitomi and T. Endo, *J. Polym. Sci. A Polym. Chem.* **2000**, 38, 4057.

[35] O. Nuyken and S. Pask, *Polymers* **2013**, 5, 361.

[36] Z. Jedlinski, P. Kurcok and M. Kowalczuk, *Macromolecules* **1985**, 18, 2679.

[37] A. Hofman, S. Słomkowski and S. Penczek, *Makromol chem.,* **1984**, 185, 101.

[38] F. Sanda, D. Jirakanjana, M. Hitomi and T. Endo, *Macromolecules* **1999**, 32, 8010.

[39] Z. Jedliński, W. Wałach, P. Kurcok and G. y. Adamus, *Makromol Chem Rapid Comm.*, 1991, 192, 2051.

[40] I. dos Santos Vieira and S. Herres-Pawlis, *Eur. J. Inorg. Chem.,* **2012**, 765.

[41]G. Natta, I. Pasquon and A. Zambelli, *J. Am. Chem. Soc.,***1962**, 84, 1488.

[42]Y. Nakayama, H. Bando, Y. Sonobe and T. Fujita, *J. Mol. Catal. A: Chem.* **2004**, 213, 141.

[43] C. Redshaw, L. Warford, S. H. Dale and M. R. J. Elsegood, *Chem. Commun* **2004**, 1954.

[44] C. Redshaw, M. A. Rowan, D. M. Homden, S. H. Dale, M. R. J. Elsegood, S. Matsui and S. Matsuura, *Chem. Commun.,* **2006***,* 3331.

[45] Y. Mahha, A. Atlamsani, J.-C. Blais, M. Tessier, J.-M. Brégeault and L. Salles, *J. Mol. Catal. A: Chem.,* **2005**, 234, 63.

[46] A. Arbaoui, C. Redshaw, D. M. Homden, J. A. Wright and M. R. J. Elsegood, *Dalton Trans.***, 2009**, 8911.

[47] C.-T. Chen, L. H. Doerrer, V. C. Williams and M. L. H. Green, *J. Chem. Soc., Dalton Trans.,* **2000**, 967.

[48] J. M. Decams, S. Daniele, L. G. Hubert-Pfalzgraf, J. Vaissermann and S. Lecocq, *Polyhedron.,* **2001,** 20, 2414.

[49] C. Redshaw, D. M. Homden, M. A. Rowan and M. R. J. Elsegood, *Inorg. Chim. Acta* **2005**, 358, 4067.

[50] Y. Miyamoto, M. Fujiki and K. Nomura, *J. Polym. Sci., Part A: Polym. Chem.,* **2004**, 42, 4248.

[51] D. E. Bellone, J. Bours, E. H. Menke and F. R. Fischer, *J. Am. Chem. Soc.,* **2015**, 137, 850.

[52] (a) P. W. Dyer, V. C. Gibson, J. A. K. Howard, B. Whittle and C. Wilson, *J. Chem. Soc., Chem. Commun.* **199**2,1666. (b) R. R. Schrock, *J. Mol. Catal. A: Chem.,* **2004**, 213, 21.

[53] J. E. Báez and A. Martínez-Richa, *Polymer* **2005**, 46, 12118.

[54] W. Yang, K.-Q. Zhao, C. Redshaw and M. R. J. Elsegood, *Dalton Trans.,* **2015**, 44,.13140.

[55] Y. Wang and H. Ma, *Chem. Commun.*, **2012**, 48, 6729.

[56] H. von Schenck, M. Ryner, A.-C. Albertsson and M. Svensson, *Macromolecules* **2002**, 35, 1556.

[57] A. Duda, T. Biela, J. Libiszowski, S. Penczek, P. Dubois, D. Mecerreyes and R. Jérôme, *Polym. Degrad. Stab.,* **1998**, 59, 215.

[58] A. Kowalski, A. Duda and S. Penczek, *Macromolecules* **1998**, 31, 2114.

[59] Y. Liu, W.-S. Dong, J.-Y. Liu and Y.-S. Li, *Dalton Trans.,* **2014**, 43, 2244.

[60] W. Xie, D .Chen, X. Fan, J. Li, P. G. Wang, H. N. Cheng and R. G. Nickol, *J. Polym. Sci., Part A: Polym. Chem.,* **1999**, 37, 3486.

[61] J. E. Kasperczyk, *Macromolecules* **1995**, 28, 3937.

[62] S.-C. Rosca, D.-A. Rosca, V. Dorcet, C. M. Kozak, F. M .Kerton, J.-F. Carpentier and Y. Sarazin, *Dalton Trans.,* **2013**, 42, 9361.

[63] D. Alhashmialameer, N. Ikpo, J. Collins, L. N. Dawe, K. Hattenhauer and F. M. Kerton, *Dalton Trans.,* **2015**, 44, 20216.

[64] B. M. Chamberlain, M. Cheng, D .R. Moore, T. M. Ovitt, E. B. Lobkovsky and G. W. Coates, *J. Am. Chem. Soc.,* **2001**, 123, 3229.

[65] M. H. Chisholm, N. W. Eilerts, J. C. Huffman, S. S. Iyer, M. Pacold and K. Phomphrai, *J. Am. Chem. Soc.,* **2000,** 122, 11854**.**

[66] B. Miksa, M. Sochacki, J. Libiszowski, A. Duda, W. Ciesielski and M. J. Potrzebowski, *Anal. Methods.,* **2012**, 4, 377.

[67] H. R. Kricheldorf, C. Boettcher and K.-U. Tönnes, *Polymer* **1992**, 33, 2817.

[68] L. E. Maley, *J. Polym. Sci. Pol. Sym.,* **1965**, 8, 253.

[69] T. Hatakeyama, Hyoe Hatakeyama *Thermal properties of green polymers and biocomposites*, *Vol. 4* Boston : Kluwer Academic Publishers **2004**.

Chapter 2

Niobium(V) and tantalum(V) pre-catalysts supported by tetra-phenolate

1. Introduction

In recent years, the development of new ligand-metal systems for the production of biodegradable polymers via ROP of cyclic esters has met with great success. [1] Whilst some metals (and non-metals) have been employed in a variety of catalysts for such ROP processes, the use of other metals such as niobium and tantalum has received scant attention. Indeed, only two reports, namely on systems using a tripodal trialkoxyamine ligand with Ta-(OEt)$_5$[2] and more recently the use of bi-dentate phenoxyimines in combination with NbCl$_5$ or TaCl$_5$[3] have been reported for the ROP of either lactides or lactones. These metals are also now attracting interest for α-olefin polymerization catalysis. [4] Given the lack of use of these group V metals, we have initiated a program to explore their potential for ROP using a variety of ancillary ligands at the metal. We noted with interest the new family of tetraphenols recently reported by Wasserman *et al.*, [5] and also that they have since been exploited by the group of Wu to prepare multi-alkali metal complexes capable of the ROP of *L*-lactide. [6] In this chapter, we explore the coordination chemistry of these tetra-phenols towards niobium and tantalum, and investigate the capability of the resulting complexes (**Scheme 9**) towards the ROP of ε-caprolactone under a variety of conditions. The nature of the products has allowed us to also screen for possible cooperative effects. Our group has previously noted for organoaluminium-based ROP systems, that the presence of nearby metal centres can either be beneficial or detrimental depending on the separation distance and type of bonding present, [7] whilst others have noted large effects in olefin polymerization. [8]
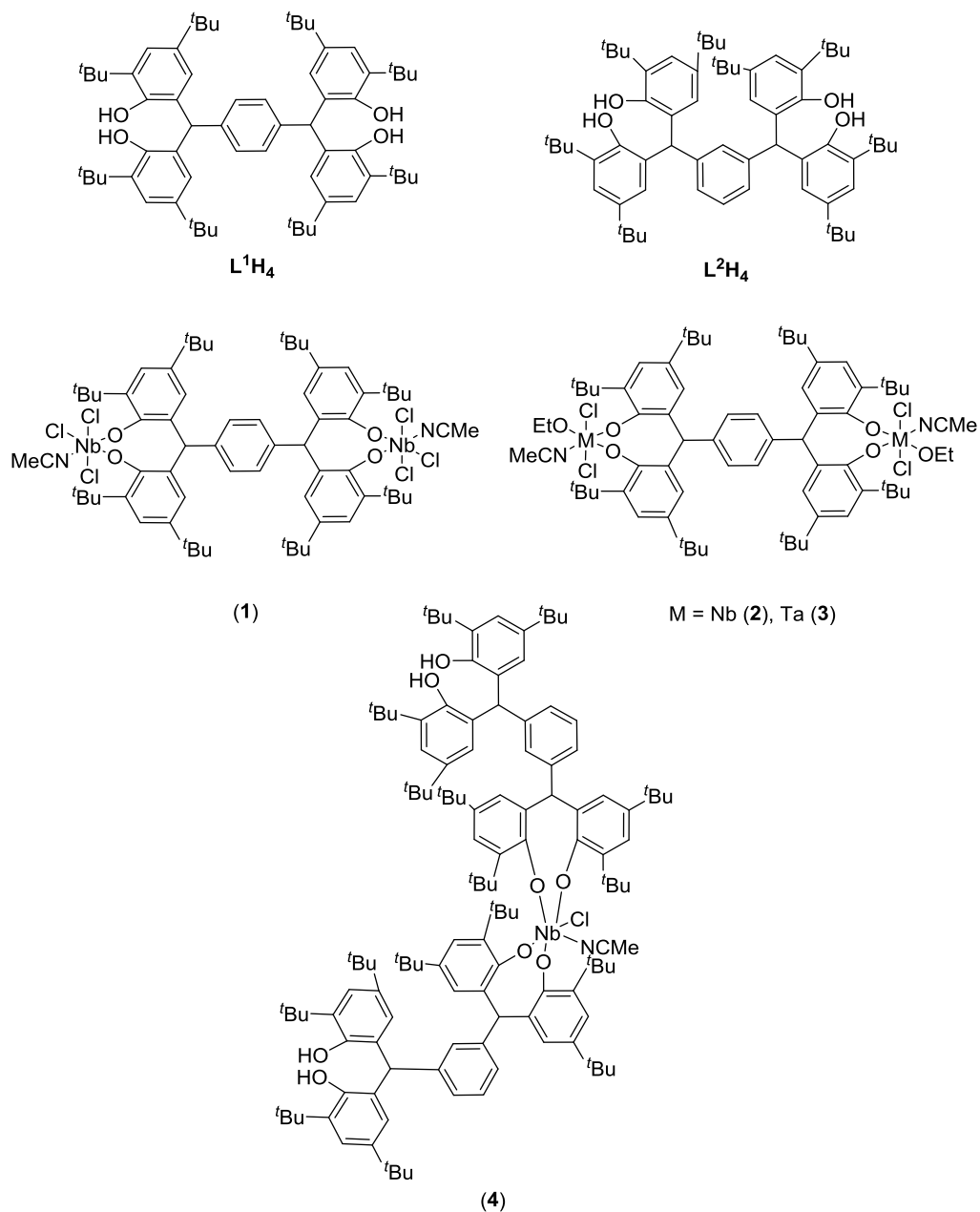
Scheme 9. Chemical structure of *para* and *meta* tetra-phenol complexes.

2. Results and Discussion

2.1 Synthesis and structure of p-L^{1}H$_4$ derived niobium and tantalum complexes

The ligand L^{1}H$_4$ was synthesized following the reported literature method. [5] It proved possible to grow small single crystals, which were suitable for X-ray diffraction using synchrotron radiation. The molecular structure is shown in (**Figure 13**), with crystallographic data presented in (**Appendix table 28**). There

are two half molecules on centres of symmetry in the asymmetric unit; there is no solvent of crystallization. Within both unique molecules, there are strong C–H···π interactions between one of the unique hydroxyl groups and the central C_6 ring: H(1)···C(16) = 2.18 Å, angle at H(1) = 144°; H(3A)···C(48) = 2.26 Å, angle at H(1) = 142°. There are also weaker O–H···O interactions between the other hydroxyl group 2.43Å between H(2) and O(4') and H(4) and O(2') compare with typical hydrogen bond variable in length 1.5-2.5 Å with angle of *ca.* 109, angle at H(1) = 139°; H(4)···C(38) = 2.38 Å, angle at H(1) = 142°. In the packing of the molecules, there are weak O–H···O intermolecular interactions at *ca.* 2.43 Å between H(2) and O(4') and H(4) and O(2') with angles of *ca.* 109°, but the lengths are very long and the angle sub-optimal for these interactions to be significant.

Figure 13. Molecular structure of L^1H_4, indicating the atom numbering scheme. Non-OH hydrogen atoms have been removed for clarity. The second unique molecule is not shown but has similar geometry.

The compound {[NbCl$_3$(NCMe)]$_2$(μ-p-L^1)} MeCN (**1**·6MeCN) was synthesized in good yield (*ca*. 83%) via the treatment of L^{1}H$_4$ with a slight excess (2.1 equiv.) of [NbCl$_5$] in refluxing toluene. The reaction proceeds with loss of two equivalents of HCl per metal centre. In the IR spectrum of **1**, infrared s[ectrum showed v(CN) at 2308/2286 cm^{-1} for the coordinated acetonitrile. Inaddition, the ^{1}H NMR is observed signals peak at 2.05 ppm with integrals (6H) are consistent with the formulation for **1**. Crystals suitable for a single crystal X-ray diffraction study were grown from a saturated acetonitrile solution at 0 °C; the crystal structure is presented in (**Figure 14**). Each niobium centre is present in a distorted octahedral geometry, and bears a *mer* arrangement of chlorides with the sixth position *trans* to one of the phenoxide groups occupied by an acetonitrile molecule. The two sets of diphenolates across the central phenyl ring are arranged in a *trans* fashion related by an inversion centre. The bond lengths and angles are given in the caption to (**Figure 14**); the Nb – O distances [1.860(5) and 1.879(5) Å] are typical of those observed in previous niobium(V) aryloxides, [9] with the shortest value found *trans* to the acetonitrile ligand. The Nb – Cl distances [*ca*. 2.38 Å] are slightly longer than those observed in [Nb$_2$Cl$_{10}$] [2.250(6) and 2.302(5) Å] and [NbCl(mtp)$_2$] [2.3357(9) Å] (mtpH$_2$ = 2,2$^/$-methylene-bis(2,4-di-*tert*-butylphenol), but shorter than observed in [Nb(NCMe)Cl(ebp)$_2$] [2.4339(10) Å] (ebpH$_2$ = 2,2$^/$-ethylidene-bis(2,4-di-*tert*-butylphenol).[10] The Nb – N distance of 2.270(6) is comparable with that of [NbCl$_5$(NCMe)] [2.236(4) Å],[11] and the binding is linear [Nb(1) – N(1) – C(33) 170.3(6)°]. An 8-membered metallocycle is formed at each end of the

tetraphenolate, with each adopting the boat conformation; the bite angle of the chelate is 96.6(2)°.
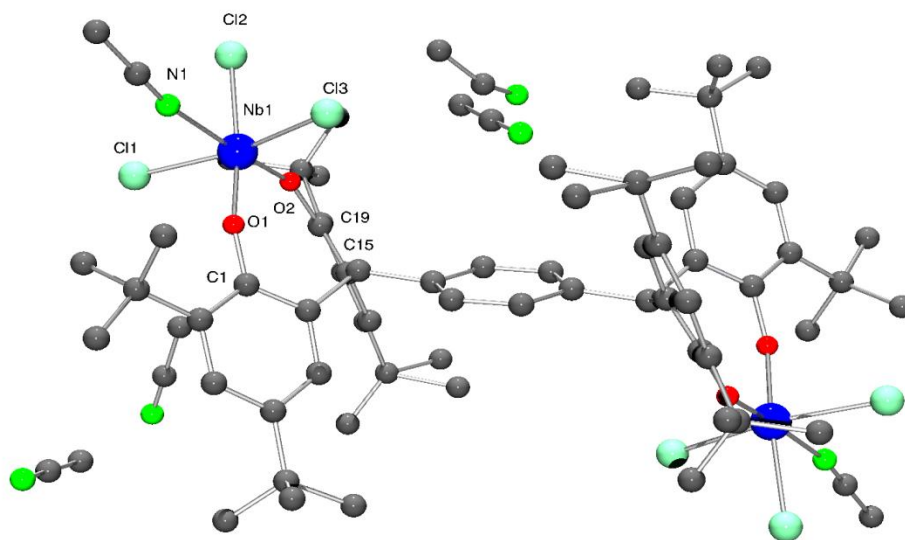
Figure 14. Representation of the molecular structure of complex **1**·6MeCN in the solid state, indicating the atom numbering scheme. Hydrogen atoms have been removed for clarity. Selected bond lengths (Å) and angles (°): Nb(1) – O(1) 1.879(5), Nb(1) – O(2) 1.860(5), Nb(1) – Cl(1) 2.380(2), Nb(1) – Cl(2) 2.3860(19), Nb(1) – Cl(3) 2.3828(19), Nb(1) – N(1) 2.270(6); O(1) – Nb(1) – O(2) 96.6(2), Nb(1) – O(1) – C(1) 159.5(4), Nb(1) – O(2) – C(19) 153.8(4), O(1) – Nb(1) – Cl(1) 170.45(14).

If the above reaction was conducted in the presence of excess ethanol, then a complex of formula $\{[NbCl_2(OEt)(NCMe)]_2(\mu\text{-}p\text{-}L^1)\}$·3½MeCN·0.614toluene (**2**·3½MeCN·0.614toluene) was isolated in good yield. In the IR spectrum of **2**, v(CN) for the coordinated acetonitrile is observed at 2312/2290 cm^{-1}. The ^{1}H NMR signals/integrals are consistent with the formulation for **2**. Crystals suitable for a single crystal X-ray diffraction study were grown from a saturated acetonitrile solution at 0 °C; the crystal structure is presented in (**Figure 15**).

Interestingly, the molecule has two distinct ends and two distinct faces. At one end, Nb(1) has ethoxide and acetonitrile trans, with both chlorides trans to phenolates. At the other end, Nb(2) has ethoxide trans to one chloride, whilst the two phenolates are trans to a chloride and acetonitrile. Furthermore, one face of the tetraphenolate supports both metal centres, whilst the other face has none. Thus, an acetonitrile lies below the central C_6H_4 ring at the Nb(1) end, while a chloride lies below the ring at the Nb(2) end; this contrasts with the centro-symmetric arrangement found in **1**. Molecules of **2** pack in layers giving zones with hetero atoms (Cl, N, O) and zones with hydrocarbon moieties (tBu groups and toluene molecules). There are a few weak, intermolecular C–H⋯Cl/O/N interactions.
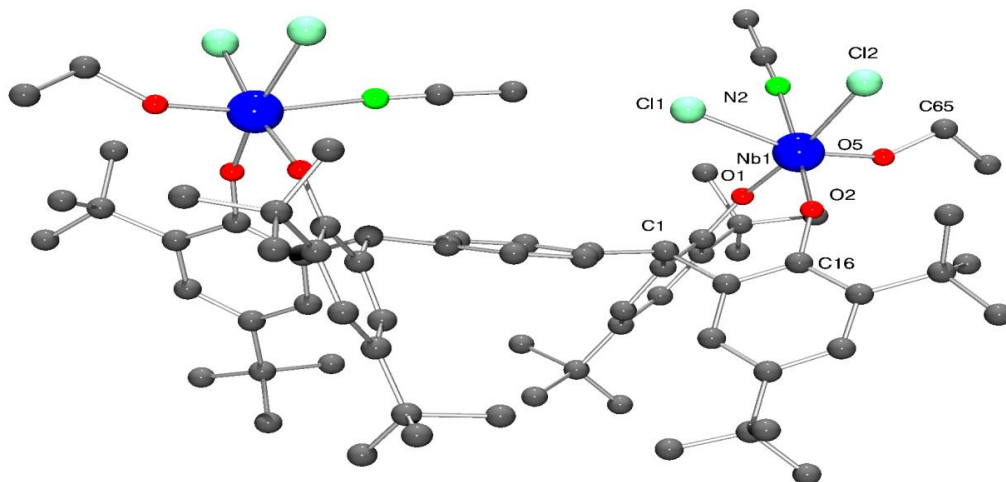
Figure 15. Representation of the molecular structure of complex **2**·3½MeCN·0.614toluene in the solid state, indicating the atom numbering scheme. Hydrogen atoms and unbound solvent molecules have been removed for clarity. Selected bond lengths (Å) and angles (°): Nb(1) – O(1) 1.897(2), Nb(1) – O(2) 1.915(2), Nb(1) – O(5) 1.826(2), Nb(1) – Cl(1) 2.4116(10), Nb(1) – Cl(2) 2.3964(10), Nb(1) – N(1) 2.300(3); O(1) – Nb(1) – O(2) 89.72(9), Nb(1) – O(1) – C(1) 154.1(2), Nb(1) – O(2) – C(16) 159.75(19), Nb(1) – O(5) – C(65) 148.9(3).

Similar use of [TaCl$_5$] led to the isolation of the complex {[TaCl$_2$(OEt)(NCMe)]$_2$(μ-p-L^1)}·5MeCN (**3**·5MeCN) in good yield. In the IR spectrum of **3**, ν(CN) for the coordinated acetonitrile is observed at 2334/2286 cm^{-1}. Crystals suitable for a single crystal X-ray diffraction study were grown from a saturated acetonitrile solution at 0 ^{o}C; the crystal structure is presented in (**Figure 16**), with crystallographic data presented in (**Appendix table 28**). The unit cells of **2**·3½MeCN and **3**·5MeCN are very similar as are the molecular structures. The tetraphenoxide ligand acts as a bidentate ligand to two pairs of Ta(V) cations; O(1) and O(2) are deprotonated and bind in a *cis* chelating fashion to Ta(1). The coordination is completed by a pair of *cis* chloride ligands, one ethoxide, and one molecule of acetonitrile. Ta(2) is bound by O(3) and O(4) and has very similar coordination. The ligands on the two Ta(V) ions are arranged such that the acetonitrile bound to Ta(2) is oriented towards Cl(2) along the long axis of the complex, a situation reminiscent of **2**. Adjacent complexes are packed such that there are weak C−H···Cl interactions between bound acetonitrile of one molecule and chloride ions in the next. These assemble the complexes into stacks running parallel to the crystallographic *a* axis. Unbound, but crystallographically well-determined, acetonitrile also forms weak C−H···Cl interactions. A portion of diffuse electron density was modelled using the SQUEEZE routine, in particular that centred on 0, ½, ½ in the unit cell. This suggested the presence of approximately two further molecules of acetonitrile per unit cell and a composition of [{TaCl$_2$(MeCN)(C$_2$H$_5$O)}$_2$(*tetra*-phen)].4MeCN.
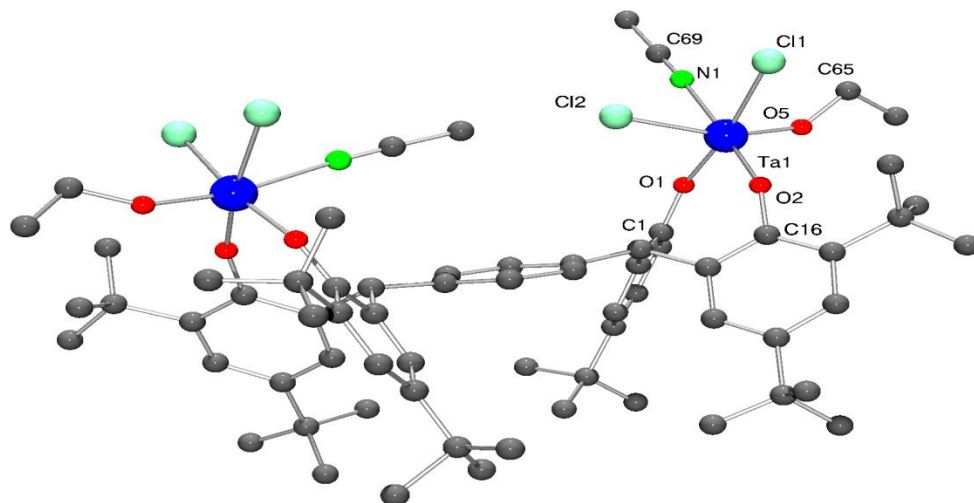
Figure 16. Representation of the molecular structure of complex **3**·5MeCN in the solid state, indicating the atom numbering scheme. Hydrogen atoms, and unbound solvent molecules have been removed for clarity. Selected bond lengths (Å) and angles (°):Ta(1) – O(1) 1.883(9), Ta(1) – O(2) 1.866(8), Ta(1) – O(5) 1.842(8), Ta(1) – Cl(1) 2.431(3), Ta(1) – Cl(2) 2.437(3), Ta(1) – N(1) 2.275(11); O(1) – Ta(1) – O(2) 92.5(3), Ta(1) – O(1) – C(1) 155.2(7), Ta(1) – O(2) – C(16) 155.9(8), Ta(1) – O(5) – C(65) 144.9(10).

2.2 Synthesis and structure of m-L²H₄ derived niobium

The ligand L^2H_4 was synthesized following the reported literature method.[5] It proved possible to grow small single crystals from a saturated acetonitrile solution. Although the diffraction data was weak, the connectivity is clear. The molecular structure is shown in (**Figure 17**), and there are two acetonitrile molecules of crystallization, both of which are H-bonded to an OH group. There is also an intramolecular O–H···π interaction: O(2)–H(2)···C(30) = 2.31 Å, akin to those seen in L^1H_4. Molecules form centrosymmetric pairs encapsulating pairs of symmetry-related acetonitrile molecules (**Appendix figure 139**). Otherwise there are only van der Waal's forces between molecules.
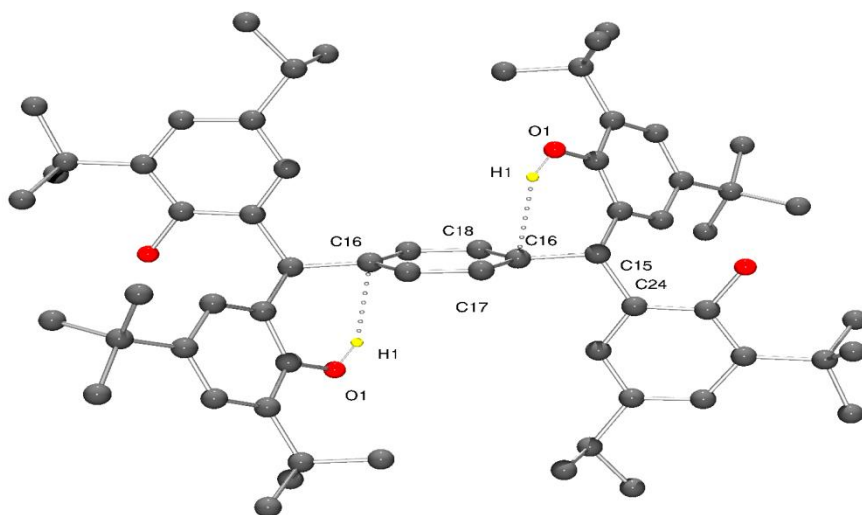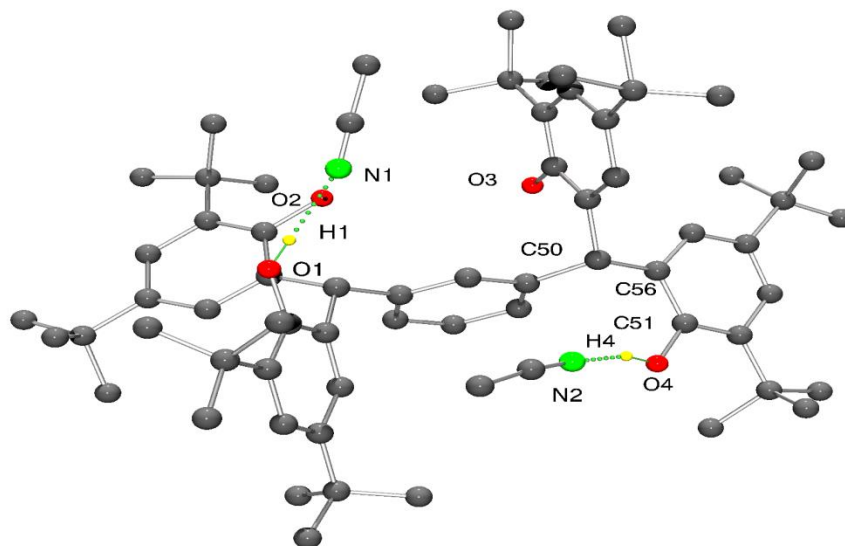
Figure 17. Molecular structure of $L^2H_4 \cdot 2MeCN$, indicating the atom numbering scheme. Non-OH hydrogen atoms have been removed for clarity.

Similar treatment (as for L^1H_4) of the *meta* ligand L^2H_4 with a slight excess of [NbCl$_5$] (or TaCl$_5$) failed to afford any crystalline material. Instead, it was found that only use of the oxychloride complex [NbOCl$_3$(NCMe)$_2$] allowed access to clean products. Reaction of [NbOCl$_3$(NCMe)$_2$)] (two equivalents) with L^2H_4 afforded, following work-up, an orange solid **4**. In the IR spectrum of **4**, v(CN) for the coordinated acetonitrile is observed at 2295/2261 cm^{-1}, whilst bands at 3545/3523/3428 cm^{-1} were assigned to v(OH). However, the structure of **4** was not obvious from the ^{1}H NMR signals/integrals. Single crystals were obtained from a saturated acetonitrile on prolonged standing at ambient temperature. The structure was found to comprise two L^2H_2 ligands per Nb centre, namely {[Nb(NCMe)Cl(*m*-L^2H_2)$_2$]}·3½MeCN (**4**·3½MeCN). Given the unexpected nature of this product, the reaction was repeated to verify reproducibility, and again single crystals were obtained from saturated acetonitrile solutions following work-up of the interaction of [NbOCl$_3$(NCMe)$_2$] (two equivalents) and L^2H_4. The

43

product on this again proved same complex only difference in the degree of solvation, *viz* {[Nb(NCMe)Cl(*m*-L^{2}H$_2$)$_2$]}·5MeCN (**4·5MeCN**). The molecular structure of **4·3½MeCN** is shown in (**Figure 18**), with selected bond lengths and angles given in (**Table 1**) and are compared with those of **4·5MeCN**; a diagram of **4·5MeCN** is given in (**Appendix figure 140**).

Table 1. Selected structural data for **4·3½MeCN** and **4·5MeCN**.

Bond lengths (Å)/Angles (°)	**4·3½MeCN**	**4·5MeCN**
Nb1−O1	1.886(3)	1.873(7)
Nb1−O2	1.933(3)	1.925(8)
Nb1−O5	1.921(3)	1.928(8)
Nb1−O6	1.946(3)	1.916(8)
O1−Nb1−O2	92.95(12)	93.8(3)
O2−Nb1−O5	174.37(13)	173.0(3)
Nb1−O1−C1	157.4(3)	156.6(8)
Nb1−O2−C16	154.1(3)	155.1(7)
Nb1−O5−C65	160.7(3)	158.2(9)
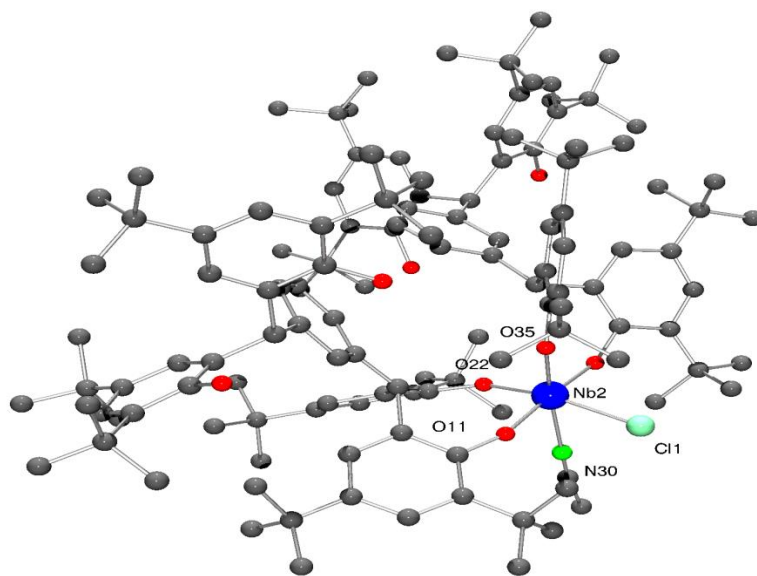
Figure 18. Molecular structure of **4·3½MeCN**. Hydrogen atoms except OH, and *t*-Bu groups have been removed for clarity.

In the asymmetric unit, the formula is 2[NbCl(NCMe)(*meta*-L^{2}H$_2$)$_2$]·5MeCN. The Nb(V) is octahedral, bonding to one chloride ligand, one acetonitrile, and two chelating *meta*-L^{2}H$_2$ ligands. The Cl$^-$ and NCMe are *cis*. Two diphenol-diphenolates bind through proximal phenolates and form a pair of 8-membered chelate rings. The phenols at the opposite end of each *meta*-L^{2}H$_2$ ligand are not deprotonated. One of the O (8) atoms forms a hydrogen bond to a molecule of MeCN. Further acetonitrile of solvation is included in the structure. For each Nb, 4.5 molecules of MeCN are modelled as point atoms. A further portion of diffuse electron density corresponding to 0.5MeCN was modelled using the SQUEEZE procedure. There are weak inter- and intra-molecular C–H···Cl interactions within the solid that knit together pairs of complexes into dimers held by Nb−Cl···H−C interaction. Otherwise, the packing is unremarkable.

The crystal of **4**·5MeCN examined was very weakly scattering. Diffraction data did not extend beyond $2\theta = 40$ ° (Mo radiation, $\lambda = 0.71073$ Å). Despite the poor scattering, a good solution was obtained. This gives very useful chemical information: the metal coordination is essentially the same as in **4**·3½MeCN. The major difference is the degree of solvation which gives rise to a different packing arrangement.

3. Polymerization Screening

Compounds **1**-**4** were screened for the ring opening polymerization of ε-caprolactone (ε-CL). Each catalyst has been screened for polymerization with and without addition of BnOH (benzyl alcohol) and at different temperatures, times and [ε-CL]:[Nb] ratios. From the screening (**Table 2**), it is evident that activity was only observed at temperatures in excess of 100 ^{o}C; recently reported niobium

phenoxyimines were also found to operate at high temperatures.[3] Comparing complexes **1** and **2** suggests that, in toluene, the presence of the ethoxides in **2** is beneficial in terms of conversion and control (runs 1 – 4 *versus* 6 – 10), whilst both systems appear to perform better in the absence of solvent (runs 5 and 11), though there was a slight increase in control. With or without toluene present, the niobium ethoxide **2** afforded a bimodal distribution of products (**Appendix figure 141)**, whereas the isostructural tantalum complex **3** afforded only a lower molecular weight fraction. Based on entries 11 to 15, plots (**Figures 19** and **20)**, of M_n (low or high molecular weight fraction) *versus* [CL]/[**2**] had a near linear relationship, suggestive of a living system. Increasing the molar ratio of [ε-Cl]:[Nb] (for **2**) from 200:1 to 800:1 led to an increase in the observed molecular weights (of both fractions) with the conversion rates and molecular weight distributions remaining relatively constant for the lower fraction (1.14 – 1.26), whilst as the ratio increased the spread of molecular weights for the higher fraction decreased; increasing the ratio beyond 800:1 had no further effect.

The results using complex **4** in toluene suggested that the presence of just one niobium centre can be beneficial in terms of conversion, for example runs 4 *vs* 27, however when an ethoxide is present at niobium, then the system performs better in terms of conversion, control and increased molecular weight (runs 12 *vs* 27). Interestingly, in the absence of benzyl alcohol, complex **4** was the only system involving niobium to afford PCL (run 26). When the ROP was conducted the absence of solvent, **4** exhibited inferior conversion (50 %) *versus* **1** and **2** (98 %), but better control (runs 6 and 16 *versus* 28).

In the MALDI-TOF spectrum (**Figure 21**), only one major population of peaks, possessing the spacing of 114 mass unit (the molecular weight of the monomer), was detected. The peaks are assigned to the sodium adducts of the polymer chains with benzyloxy end groups. A smaller series of peaks is associated with the use of protonated/sodiated (from the matrix) species from the matrix. [12]

The ^{1}H NMR spectrum of the polymer obtained using **1**(**Figure 22**), to verify the molecular weight of the polymer and identify the end chain group of the PCL (polycaprolactone). Typically, peaks at 7.38, 5.07 and 3.65 ppm (5:2:2) indicated that the polymer chains were capped by one benzyl ester and a hydroxyl group, consistent with insertion of a benzyloxy group during polymerization.

Table 2. Ring opening polymerization of ε-CL by precatalyst **1-4**[a]

Run	Cat.	Toluene	CL:X[b]:BnOH	T/ °C	t/h	m/g	Conversion (%)[c]	$M_n \times 10^{-4}$[d]	PDI[e]
1	**1**	5	400:1:2	25	1	---	---	---	---
2	**1**	5	400:1:2	80	1	---	---	---	---
3	**1**	5	400:1:0	100	20	---	---	---	---
4	**1**	5	400:1:2	110	1	0.03	50	0.12	1.07
5	**1**	5	400:1:2	110	20	0.10	86	0.66	1.25
6	**1**	---	200:1:0.5	100	1	4.65	98	0.18	1.77
7	**2**	5	400:1:2	25	1	---	---	---	---
8	**2**	5	400:1:2	80	1	---	---	---	---
9	**2**	5	400:1:2	110	1	---	---	---	---
10	**2**	5	400:1:0	110	20	---	---	---	---
11	**2**	5	200:1:2	110	20	0.03	96	0.70 (6.66)	1.18 (1.9)
12	**2**	5	400:1:2	110	20	0.39	99	0.94 (7.31)	1.14 (1.67)
13	**2**	5	600:1:2	110	20	0.17	98	1.09 (8.97)	1.12 (1.58)
14	**2**	5	800:1:2	110	20	0.49	97	1.18 (11.44)	1.26 (1.44)
15	**2**	5	1000:1:2	110	20	0.42	97	1.19 (12.13)	1.26 (1.4)
16	**2**	---	200:1:0.5	100	1	2.1	98	0.24 (7.34)	1.31 (1.80)
17	**3**	5	400:1:2	25	1	---	---	---	---
18	**3**	5	400:1:2	80	1	---	---	---	---
19	**3**	5	400:1:2	110	1	---	---	---	---
20	**3**	5	400:1:0	110	20	0.31	98	0.21	1.73
21	**3**	5	400:1:2	110	20	0.20	98	0.26	1.20
22	**3**	---	200:1:0.5	100	1	1.69	98	0.31	1.20
23	**4**	5	400:1:2	25	1	---	---	---	---
24	**4**	5	400:1:2	80	1	---	---	---	---
25	**4**	5	400:1:2	110	1	---	---	**---**	---
26	**4**	5	400:1:0	110	20	0.02	96	0.11	1.11
27	**4**	5	400:1:2	110	20	0.24	98	0.24	1.31
28	**4**	---	200:1:0.5	100	1	2.81	50	0.36	1.17

[a] Conditions: 12.3 μmol of cat.; 1.0 M ε-CL toluene solution. [b] X = Nb,Ta complexes. [c] Detrmined by ^{1}HNMR. [d, e] From GPC data in THF vs. polystyrene standards.
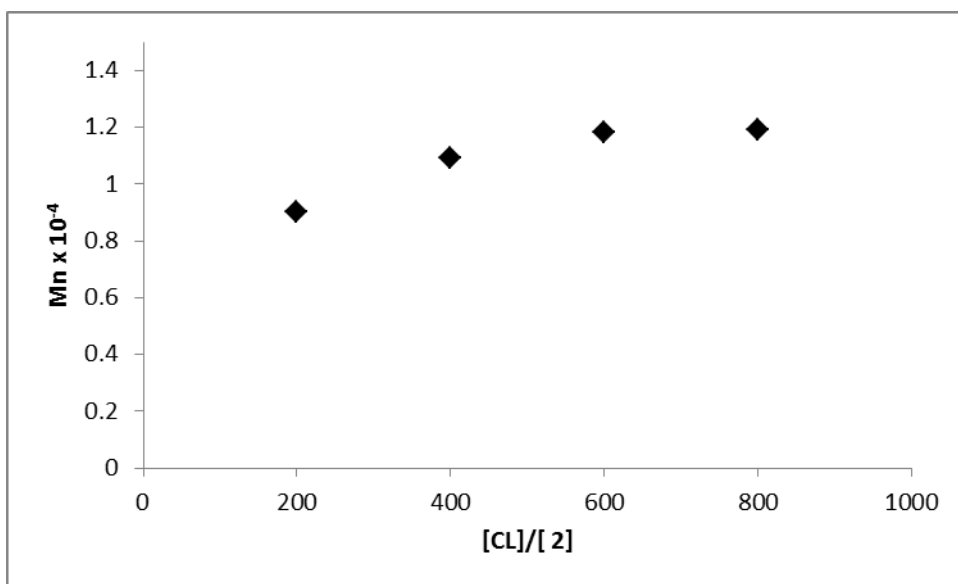
Figure 19. M_n (low molecular weight fraction) *versus* [CL]/[**2**]
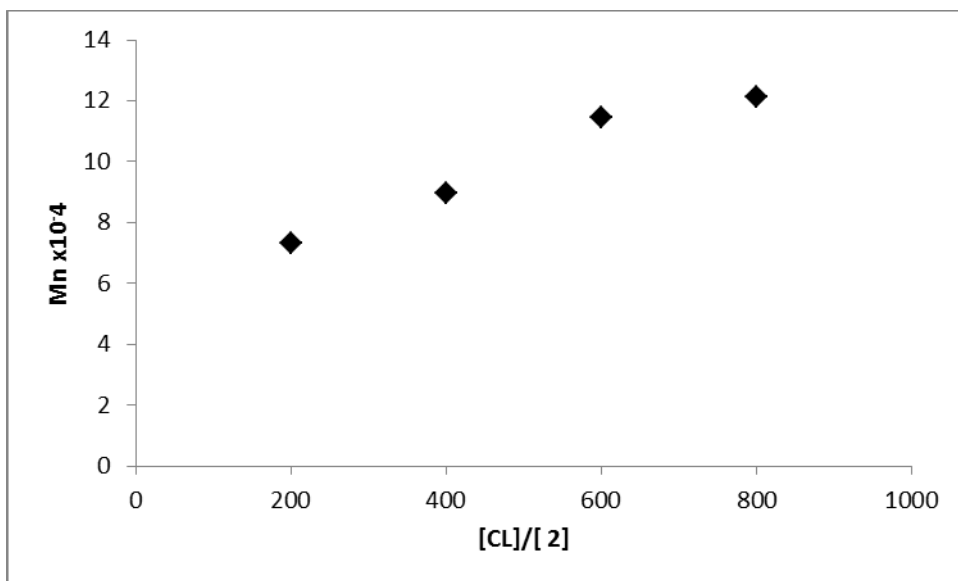
Figure 20. M_n (high molecular weight fraction) *versus* [CL]/[**2**]
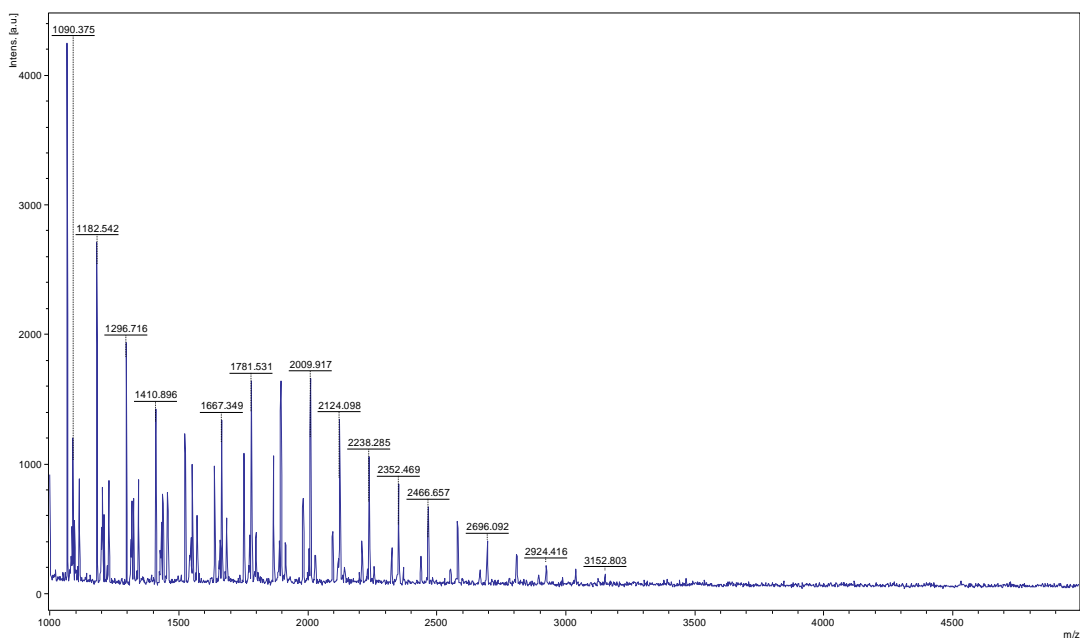
Figure 21. MALDI-TOF spectrum of PCL from (run 22 table 2) using **3**.
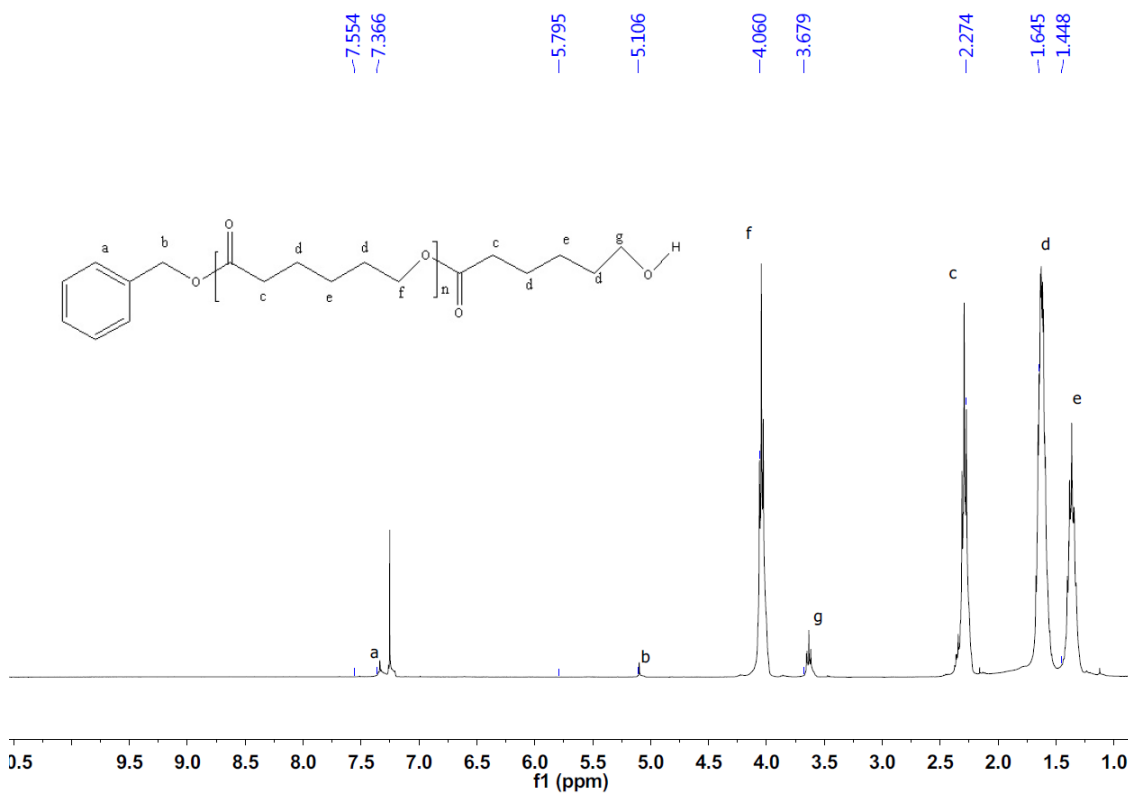
Figure 22 ^{1}H NMR spectrum of the PCL from (run 6 table 2) using **1**.

4. Conclusion

In summary, a number of new tetra-phenolate niobium (and tantalum) complexes have been prepared from the metal precursors [MCl$_5$] (M = Nb, Ta) or [NbOCl$_3$(NCMe)$_2$]. Crystal structure determinations reveal a preference for binding two metal centres when using then '*para*' ligand set L^{1}H$_4$, whereas use of the '*meta*' ligand L^{2}H$_4$ resulted in the isolation of a bis(chelate) mononuclear complex. In terms of the ROP of ε-caprolactone, only negligible polymer was isolated at temperatures below 100 ^{o}C. At 100 ^{o}C, in the absence of any solvent, these systems were capable of good conversions (≥98 %) in the case of the dinuclear systems; 50 % conversion was observed for the mononuclear system. In toluene, the presence of an ethoxide at the metal was generally advantageous in terms of conversion and control.

5. References

[1] A. Arbaoui and C. Redshaw, *Polym. Chem.,* **2010**, 1, 801.

[2] Y. Kim, P. N. Kapoor and J. G. Verkade, *Inorg. Chem.,* **2002**, 41, 4834.

[3] T. K. Saha, M. Mandal, M. Thunga, D. Chakraborty and V. Ramkuma, *Dalton Trans.*, **2013**, 42, 10304.

[4] (a) R. Galletti and G. Pampaloni, *Coord. Chem. Rev.*, **2010**, 254, 525; (b) Y. R. Patil, in Olefins Polymerisation Reactivity of Niobium-Based Metal Complexes, *Lambert Academic Publishing*, *US*, **2011**; (c) C. Redshaw, M. Walton, L. Clowes,D. L. Hughes, A.-M. Fuller, Y. Chao, A. Walton, V. Sumerin, P. Elo, I. Soshnikov, W. Zkao and W.-H. Sun, *Chem. – Eur. J.*, **2013**, 19, 8884.

[5] L. H. Tang, E. P. Wasserman, D. R. Neithamer, R. D. Krystosek, Y. Cheng, P. C. Price, Y. He and T. J. Emge, *Macromolecules,* **2008**, 41, 7306.

[6] 4. J. Zhang, C. Jian, Y. Gao, L. Wang, N. Tang and J. Wu,*Inorg. Chem.*, **2012**, 51, 1338**.**

[7] A. Arbaoui, C. Redshaw and D. L. Hughes, *Chem. Commun.*, **2008**, 4717.

[8] (a) S. Singh and H. W. Roesky, *Dalton Trans*., **2007**, 1360; (b) M. Delferro and T. J. Marks, *Chem. Rev*., **2011**, 111, 2450; (c) M. P. Weberski Jr., C. Chen, M. Delferro and T. J. Marks, *Chem. – Eur. J.*, **2012**, 18, 10715; (d) S. Liu, A. Motta, A. R. Mouat, M. Delferro and T. J. Marks, *J. Am. Chem. Soc*., **2014**, 136, 10460.

[9] T. W. Coffindaffer, B. D. Steffy, I. P. Rothwell, K. Folting, J. C. Huffman and W. E. Streib, *J. Am. Chem. Soc.,* **1989**, 111, 4749.

[10] (a) H. Kawaguchi and T. Matsuo, *Inorg. Chem.*, **2002**, 41, 6090. (b) C. Redshaw, D. M. Homden, M. A. Rowan and M. R. J. Elsegood, *Inorg. Chim. Acta*, **2005**, 358, 4067.

[11] G. R. Willey, T. J. Woodman and M. G. B. Drew, *Polyhedron*, **1997**, 16, 351.

[12] N. Ikpo, C. Hoffmann, L. N. Dawe and F. M. Kerton, *Dalton Trans.,* **2012**, 41, 6651.

Chapter 3

Molybdenum(VI) imido complexes derived from chelating phenols: synthesis, characterization and ε-caprolactone ROP capability

1. Introduction

As mentioned in Chapter 1, high valent bis(imido) molybdenum complexes have proven suitable for a range of catalytic reactions. [1] Moreover the ease of preparation of bisimido starting material of the type $Mo(NAr)_2Cl_2(dme)$ is advantageous. [2] In this chapter, were attracted to the potential use of molybdenum for the ROP of cyclic esters given its excellent track record over the last couple of decades in ring opening metathesis polymerization (ROMP) as well as being attracted by its low cost and toxicity. Such ROMP studies have revealed the ability of the molybdenum complexes to promote living polymerizations, and to tolerate a wide range of functionalities, which bodes well for the proposed studies herein.[3] Redshaw *et al*. reported the use of molybdenum chelate complexes derived from the oxydianiline $[(2\text{-}NH_2C_6H_4)_2O]$ and found that for the ROP of ε-caprolactone, conversion rates were good (>90 %) at high temperatures $(100 \ ^{o}C)$.[4] As part of that study, a siloxide complex was also isolated and was found to be active without the need for the addition of external alcohol; for the chloride species the addition of benzyl alcohol was necessary to generate an alkoxide. Previous use of molybdenum species in the ROP of cyclic esters is somewhat limited.[5]-[10] Given this, the high valent molybdenum imido phenolate chemistry has been probed herein where again the expectation is that the addition of an external alcohol would not be necessary for ROP activity. It was found that the use of bulky di-phenols in combination with bulky organoimido groups allows for the isolation of mono-nuclear four coordinate complexes, whilst variation of the imido group can lead to bridged di-nuclear species. The use of tri- and *tetra*-phenolates has also been explored, and in the case of the latter, in the

form of the *para* and *meta* pre-ligands, the possibility of possible cooperative effects has been explored. The complexes prepared/screened herein are shown in (**Scheme 10**)

R = Me (**5**), Ph (**6**)   (**7**)   (**8**) (L = MeCN)

(**9**)   (**10**)

(**11**)   (**12**)
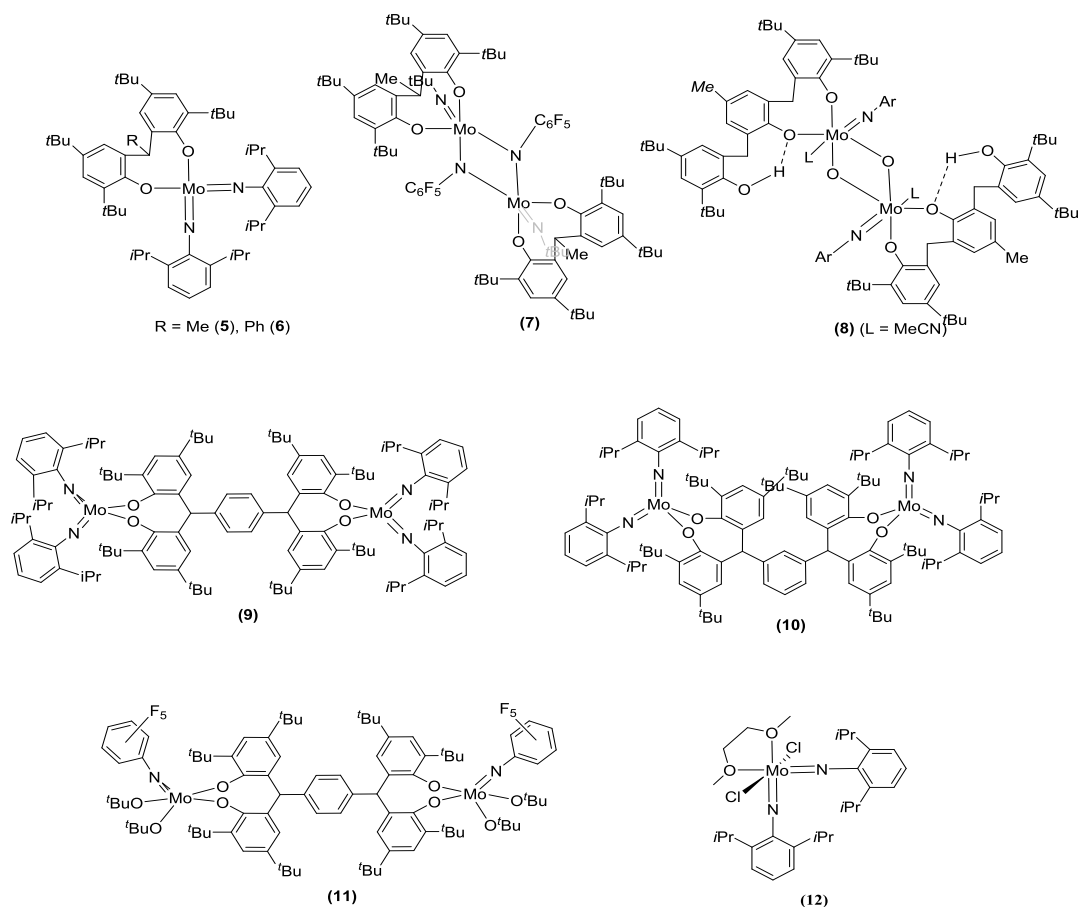
Scheme 10. Complexes **5–12** prepared and screened for ring opening polymerization (ROP) in this chapter.

2. Results and Discussion

2.1 Di-phenolate compounds

The interaction of [Mo(NC$_6$H$_3$$i$-Pr$_2$-2,6)$_2$(O$t$-Bu)$_2$] (formed *in-situ* from [Mo(NC$_6$H$_3$$i$-Pr$_2$-2,6)$_2Cl_2$(dme)] and a slight excess of LiOt-Bu) and the di-phenol 2,2'-CH$_3$CH[4,6-(t-Bu)$_2$C$_6$H$_2$OH]$_2$ (L^{3}H$_2$) in diethyl ether readily gives multigram quantities of [Mo(NC$_6$H$_3$$i$-Pr$_2$-2,6)$_2$L^3] (**5**) in yield (*ca.* 60 %). Stoichiometrically **5** is formed via the loss of two molecules of *tert*-butanol,

which can be removed during the reaction by removing volatiles *in-vacuo* and then adding more solvent (diethyl ether) and repeating the process several times. Small golden-yellow prisms of **5** suitable for an X-ray structure determination using synchrotron radiation were grown from a saturated heptane solution at ambient temperature. The molecular structure is shown in (**Figure 23**), with bond lengths and angles given in the caption; crystallographic data is presented in (**Appendix table 28**). There is one molecule in the asymmetric unit. The space group is chiral and essentially a single enantiomer has crystallized out.

The geometry about the Mo atom is essentially tetrahedral with distortions from ideal varying from 104.93(12) to 119.03(10) $^{\circ}$. The two Mo-N distances are similar [1.746(3) and 1.760(3) Ǎ], however the corresponding Mo-N-C angles are somewhat different [171.5(2) *versus* 158.7(3) $^{\circ}$]; the latter is thought to be at the lower limit anticipated for a linear imido group. A related complex [Mo(NPh)$_2$(edtc)$_2$] (edtc = S$_2$CNEt$_2$) has been shown to contain one bent [139.4(4) $^{\circ}$] and one linear [169.4(4) $^{\circ}$] imido ligand. [11] The eight membered ring chelate of **5** adopts a flattened chair-like conformation in-stark contrast to the boat-like conformations found previously in complexes containing the related biphenol ligand 2,2'-CH$_2$(4-Me,6-*t*-BuC$_6$H$_2$OH)$_2$,[12] the 'bite angle' of the chelate is 119.03(10) $^{\circ}$. In the IR spectrum of **5** the OH band of the free ligand (*ca* 3486 cm^{-1}) has disappeared, but there are new bands in the region 750 - 850 cm^{-1} assignable to *v*Mo-O. In the ^{1}H NMR spectrum, there is a significant shift in the position of the C*H* bridge proton; such sensitivity to coordination environment has been noted previously. [12a]

Figure 23. Molecular structure of $[Mo(NC_6H_3i\text{-}Pr_2\text{-}2,6)_2L^3]$ (**5**), showing the atom numbering scheme. Selected bond lengths (Å) and angles (°): Mo(1)-N(1) 1.746(3), Mo(1)-N(2) 1.760(3), Mo(1)-O(1) 1.929(2), Mo(1)-O(2) 1.921(2); N(1)-Mo(1)-N(2) 113.30(14), N(1)-Mo(1)-O(2) 106.91(12), N(2)-Mo(1)-O(2) 104.93(12), N(1)-Mo(1)-O(1) 106.91(12), N(2)-Mo(1)-O(1) 106.00(12).

Similar use of the di-phenol $2,2'\text{-}C_6H_5CH[4,6\text{-}(t\text{-}Bu)_2C_6H_2OH]_2$ (L^4H_2) led to the related complex $[Mo(NC_6H_3i\text{-}Pr_2\text{-}2,6)_2L^4]$ (**6**). In the ^1H NMR spectrum, the C*H* bridge proton is found at δ 4.89 (*cf* 5.16 ppm in **5**). Crystals of **6** suitable for X-ray analysis were grown from a saturated dichloromethane solution at 0 °C. The molecular structure is shown in (**Figure 24)** with bond lengths and angles given in caption and crystallographic data presented in (**Appendix table 28).**

Figure 24. Molecular structure of [Mo(NC$_6$H$_3$*i*-Pr$_2$-2,6)$_2$L^4] (**6**), showing the atom numbering scheme. Selected bond lengths (Å) and angles (°): Mo(1)-N(1) 1.7610(17), Mo(1)-N(2) 1.7476(17), Mo(1)-O(1) 1.9280(14), Mo(1)-O(2) 1.921(2); N(1)-Mo(1)-N(2) 112.38(8), N(1)-Mo(1)-O(2) 104.24(7), N(2)-Mo(1)-O(2) 108.10(7) (7), N(1)-Mo(1)-O(1) 104.79(7), N(2)-Mo(1)-O(1) 107.78(7), O(1)-Mo(1)-O(2) 119.59(6).

As for **5**, the metal centre has a distorted tetrahedral geometry, as seen in the bond angles for N(1)–Mo(1)–O(2) 104.24(7) and O(1)–Mo(1)–O(2) 119.59(6)°. Again, as in **5**, the two imido groups are somewhat different, with Mo–N–C angles of 172.30(15) and 157.26(15) °. The eight membered ring chelate again adopts a flattened chair-like conformation; the "bite angle" of the chelate is 119.59(6)°. One solvent molecule of crystallization (dichloromethane) forms a C–H··π interaction at 2.584(4) Å to the ring centroid C(13)–C(18). In contrast to the previous use of L^{3}H$_2$,[12-18] L^{4}H$_2$ has been relatively unexplored. Indeed, a search of the CSD revealed only one example (in titanium chemistry).[13]

Use of the mixed-imido precursor [Mo(N*t*-Bu)(NC$_6$F$_5$)(O*t*-Bu)$_2$] with L^{3}H$_2$ led, following work-up, to the orange complex [Mo(N*t*-Bu)(NC$_6$F$_5$)L^3]$_2$ (**7**), which

was readily crystallized from a saturated acetonitrile solution on prolonged standing (2 days) at ambient temperature. The molecular structure (**Figure 25)**, revealed that half of the complex comprises the asymmetric unit. The molecule lies on a centre of symmetry *i*, and possesses asymmetric imido (C_6F_5) bridges, the latter arising given the differing *trans* environments. The terminal *tert*-butylimido groups are near linear [Mo–N(1)–C(1) 178.0(2)°]. There is literature precedent for bending of C_6F_5N groups in preference to *tert*-butylimido groups when present in the same complex, which is attributed to the more electron-releasing nature of the latter. [11b] Furthermore, bridging arylimido groups have been structurally characterized in a complex also containing linear, terminal *tert*-butylimido ligation. [14] The eight membered ring chelates each adopt a flattened chair-like conformation; the "bite angle" of the chelates are 117.20(9)°.

Figure 25. Molecular structure of [Mo(N*t*-Bu)(NC$_6$F$_5$)L^3]$_2$ (**7**), showing the atom numbering scheme. Selected bond lengths (Å) and angles (°): Mo(1)-N(1) 1.721(2), Mo(1)-N(2) 1.856(2), Mo(1)-O(1) 1.9324(19), Mo(1)-O(2) 1.9260(19); N(1)-Mo(1)-N(2) 101.29(11), N(1)-Mo(1)-O(2) 98.61(10), N(2)-Mo(1)-O(2) 116.77(9), N(1)-Mo(1)-O(1) 98.73(10), N(2)-Mo(1)-O(1) 117.94(10), O(1)-Mo(1)-O(2) 117.20(9), Mo(1) – O(1) – C(11) 122.77(18), Mo(1) – O(2) – C(27) 123.83(16).

2.2 Tri-phenolate compound

When the tri-phenol 2,6-bis(3,5-di-*tert*-butyl-2-hydroxybenzyl)-4-methylphenol (L^{5}H$_3$),[15] was reacted with [Mo(NC$_6$H$_3$*i*-Pr$_2$-2,6)$_2$(O*t*-Bu)$_2$], the oxo-bridged complex [Mo(NC$_6$H$_3$*i*-Pr$_2$-2,6)(NCMe) (μ-O)L^{5}H]$_2$·6MeCN (**8**·6MeCN) was isolated from a saturated acetonitrile solution on prolonged standing at ambient temperature. The presence of the oxo bridges was thought to be the result of fortuitous hydrolysis (also resulting in the elimination of 2,6-diisopropylaniline). The molecular structure of **8** is shown in (**Figure 26)**, with selected bond lengths and angles given in the caption. Half of the complex and three acetonitrile molecules comprise the asymmetric unit. The molecule resides on a centre of symmetry *i*, and possesses asymmetric oxo bridges. Each molybdenum centre

exhibits a distorted octahedral environment, for example Mo(1) is 0.3349(6) Å out of the O_4 plane. Of the three acetonitrile molecules of crystallization, two lie in clefts of the phenol/di-phenolate ligand, namely those solvent molecules containing N(4) and N(5); the other containing N(3) lies between molecules of **8**. The bonding mode of the tri-phenol derived ligand in **8** is reminiscent of that observed for the tungsten(VI) complex [W(eg)$_2$L^{a}H] (eg = 1,2-ethanediolato, L^{a}H = doubly deprotonated form of 2,6-bis(3,5-dimethyl-2-hydroxybenzyl)-4-*t*-butylphenol) and the niobium complexes [NbCl$_3$(NCMe)L^{b}H] and [NbCl(NCMe)L$^{a/b}$H]$_2$ (L^{b}H = doubly deprotonated form of 2,6-bis(4-methyl-6-*t*-butylsalicyl)-4-*t*-butylphenol.[16] The eight membered ring chelates adopts a boat-like conformation; the "bite angle" of the chelate is 93.43(7)°, which is much smaller than observed in **5-7** (*ca.* 119°) due to the higher coordination number of **6** as opposed to **4** or **5**. In solution however, the ^{1}H NMR spectrum (in CDCl$_3$, C$_6$D$_6$ or CD$_3$CN) of **8** contained only two resonances for the *tert*-butyl groups, which is not consistent with the unsymmetrical nature of the tri-phenol derived ligand observed in the solid state.

Figure 26. Molecular structure of [Mo(NC$_6$H$_3$$i$-Pr$_2$-2,6)(NCMe)($\mu$-O)L^{5}H]$_2$(**8**), showing the atom numbering scheme. Selected bond lengths (Å) and angles (°): Mo(1) – O(1) 1.9072(16), Mo(1) – O(2) 2.0257(16), Mo(1) – O(4) 1.8688(16), Mo(1) - N(1) 1.728(2), Mo(1) – N(2) 2.400(2); O(1) – Mo(1) – O(2) 93.43(7), Mo(1) – O(1) – C(13) 145.46(15), Mo(1) – O(2) – C(28) 127.49(14), Mo(1) – N(1) – C(1) 174.59(17), Mo(1) – O(4) – Mo(1$^\prime$) 100.56(7).
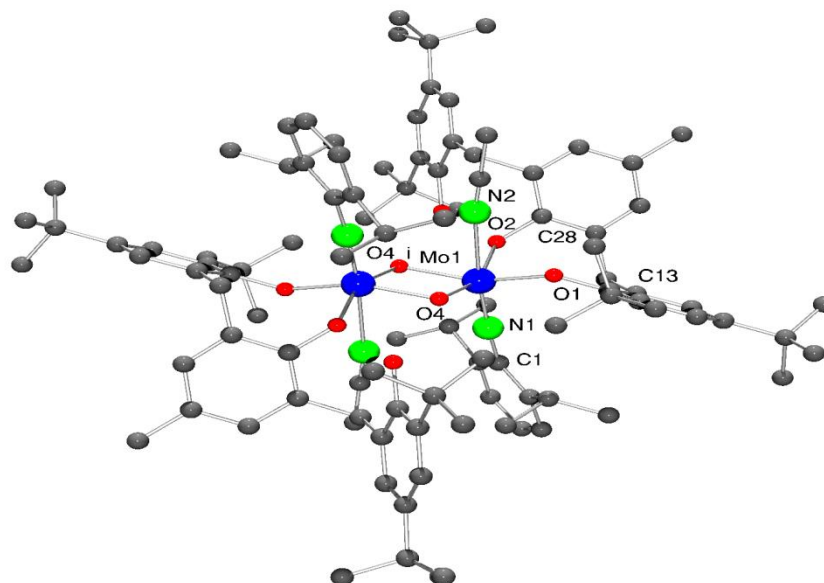
2.3 Tetra-phenolate compounds

The synthetic methodology was then extended to the relatively unexplored tetra-phenols α,α,α′,α′-tetrakis(3,5-di-*tert*-butyl-2-hydroxyphenyl)-*p*-xylene L^{1}H$_4$ and α,α,α′,α′-tetrakis(3,5-di-*tert*-butyl-2-hydroxyphenyl)-*m*-xylene L^{2}H$_4$.[17] Treatment of either L^{1}H$_4$ or L^{2}H$_4$ with [Mo(NC$_6$H$_3$$i$-Pr$_2$-2,6)$_2$(O$t$-Bu)$_2$] afforded tetra-imido complexes, namely {[Mo(NC$_6$H$_3$$i$-Pr$_2$-2,6)$_2$]$_2$($\mu$-L^1)} (**9**) and {[Mo(NC$_6$H$_3$$i$-Pr$_2$-2,6)$_2$]$_2$($\mu$–L^2)} (**10**), respectively in moderate to good yield. Red plate-like crystals of **10** suitable for an X-ray structure determination were obtained on recrystallization from a saturated hexane solution at 0 °C. The molecular structure of **10** is shown in (**Figure 27**), with selected bond lengths and angles given in caption, with crystallographic data presented in (**Appendix table**
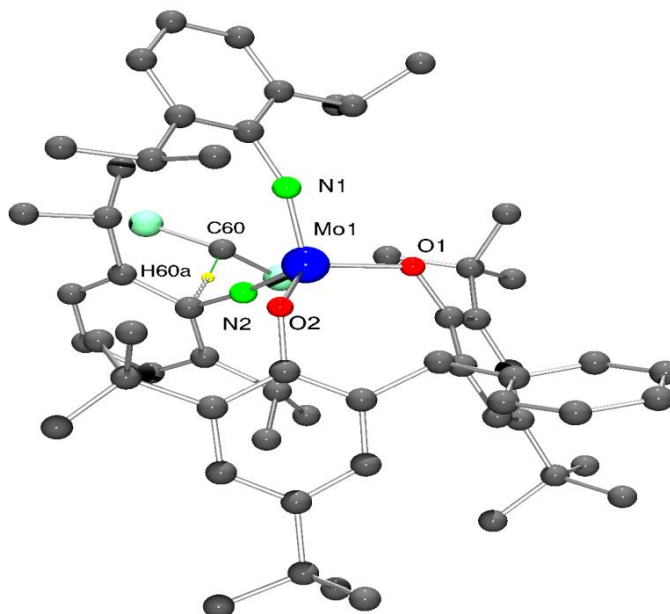
62

28) The molecule lies on a 2-fold axis that passes through the vector C(32)–C(33).

Figure 27. Molecular structure of {[Mo(NC$_6$H$_3$*i*-Pr$_2$-2,6)$_2$]$_2$(μ-L^2)} (**10**), showing the atom numbering scheme. Selected bond lengths (Å) and angles (°): Mo(1)-N(1) 1.7617(18), Mo(1)-N(2) 1.7506(19), Mo(1)-O(1) 1.9322(14), Mo(1)-O(2) 1.9293(14); N(1)-Mo(1)-N(2) 111.39(9), N(1)-Mo(1)-O(2) 106.85(7), N(2)-Mo(1)-O(2) 108.35(7), N(1)-Mo(1)-O(1) 105.33(8), N(2)-Mo(1)-O(1) 109.86(7), O(1)-Mo(1)-O(2) 115.04(6).

Each molybdenum center is four coordinate and exhibits a distorted tetrahedral geometry with distortions in the range 105.33(8) to 115.04(6)°, the largest angle being associated with the chelate. Each eight membered ring chelate adopts a flattened chair-like conformation. The imido groups are linear, with that at N(1) lying to the lower end of the range associated with linearity [Mo-N(1)-C(34) 156.29(16)°]. The difference between the imido angles here in **10** is *ca.* 13.6°, which compares favorably with that in **5** (*ca.* 13.0°) and is slightly smaller than that observed in **6** (*ca.* 15.0°). There is tendency in these complexes for the shorter Mo - N bond length to be associated with the larger Mo–N–C angle; a similar

situation has been observed in molybdenum and tungsten imido alkylidene chemistry.[18]The distance between Mo centers in this system is 10.588 Å.

Surprisingly, when the imido precursor employed was $[Mo(NC_6F_5)_2(Ot\text{-}Bu)_2]$ with $L^{1p}H_4$, the reaction proceeded via loss of aniline rather than alcohol, which must be due to the differing electronics associated with the C_6F_5 group. Crystals of $\{[Mo(NC_6F_5)(Ot\text{-}Bu)_2]_2(\mu\text{-}L^1)\}\cdot6MeCN$ (**11**·6MeCN) were grown from a saturated acetonitrile solution. The molecular structure is shown in (**Figure 28**), with selected bond lengths and angles given in the caption. Each molybdenum centre in **11** is five coordinate, bound by the chelate, one imido group and two *tert*-butoxide ligands. There are two similar metal complexes and twelve acetonitrile molecules in the asymmetric unit. The geometries at the metal can best be described as distorted trigonal bipyramidal with the imido group and one of the chelate phenoxide oxygen atoms occupying axial positions. The imido group is slightly bent [Mo(1)–N(1)–C(65) 161.3(5)°] though is still considered linear. However, the two *tert*-butoxides are clearly bent [Mo(1)–O(5)–C(71) 142.8(5), Mo(1)–O(6)–C(75) 138.6(5)°] with slightly different bond lengths [Mo–O(5) 1.821(5), Mo(1)–O(6) 1.884(5)]; neither alkoxide is required to act as a three electron donor to attain an overall eighteen electron count. Chisholm and coworkers have noted a correlation between M–OR bond distances and M–O–C angles. [19]

64

Figure 28. Molecular structure of {[Mo(NC$_6$F$_5$)(Ot-Bu)$_2$]$_2$(μ-L^1)}·6MeCN (**11**·6MeCN), showing the atom numbering scheme. Selected bond lengths (Å) and angles (°): Mo(1) – O(1) 1.921(5), Mo(1) – O(2) 1.945(5), Mo(1) – N(1) 1.766(6), Mo(1) – O(5) 1.821(5), Mo(1) – O(6) 1.884(5); Mo(1) – N(1) – C(65) 161.3(5), Mo(1) – O(1) – C(1) 141.1(5), Mo(1) – O(2) – C(15) 146.6(4), O(1) – Mo(1) – O(2) 85.3(2), Mo(1) – O(5) – C(71) 142.8(5), Mo(1) – O(6) – C(75) 138.6(5), O(5) – Mo(1) – O(6) 112.6(2), N(1) – Mo(1) – O(2) 168.6(2).

The molecular structure of the complex [Mo(NC$_6$H$_3i$-Pr$_2$-2,6)$_2$Cl$_2$(dme)] (**12**) has also been determined and is given in (**Figure 29**). A number of such mononuclear bis(imido) dichloro molybdenum(VI) complexes have been structurally characterized; a search of the CSD revealed 14 hits.[13a]

Figure 29. Molecular structure of [Mo(NC$_6$H$_3$$i$-Pr$_2$-2,6)$_2Cl_2$(dme)] (**12**) showing the atom numbering scheme. Selected bond lengths (Å) and angles (°): Mo(1) – O(1) 2.326(4), Mo(1) – O(2) 2.408(4), Mo(1) – N(1) 1.735(5); N(2) – Mo(1) – C(2) 160.8(2), N(1) – Mo(1) – O(2) 93.86(19).
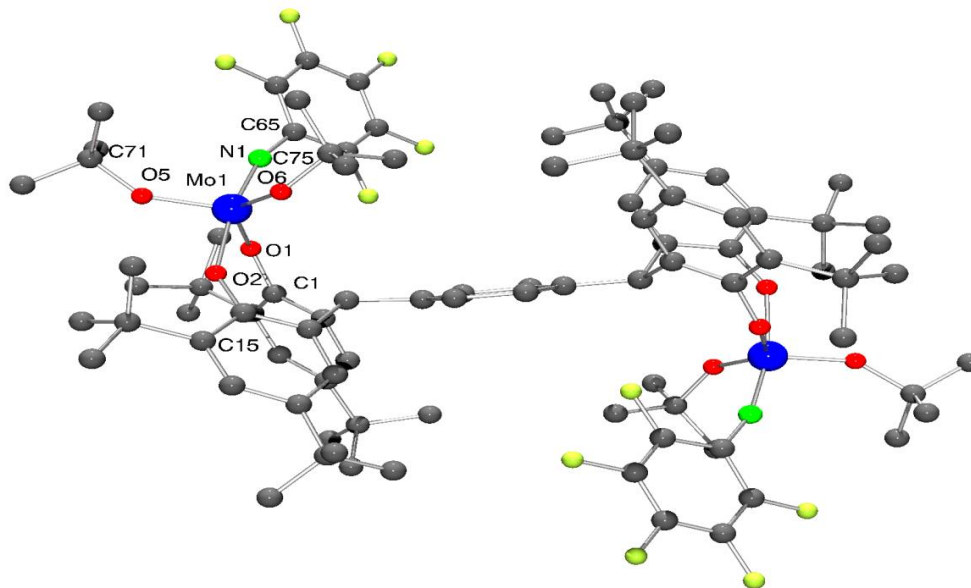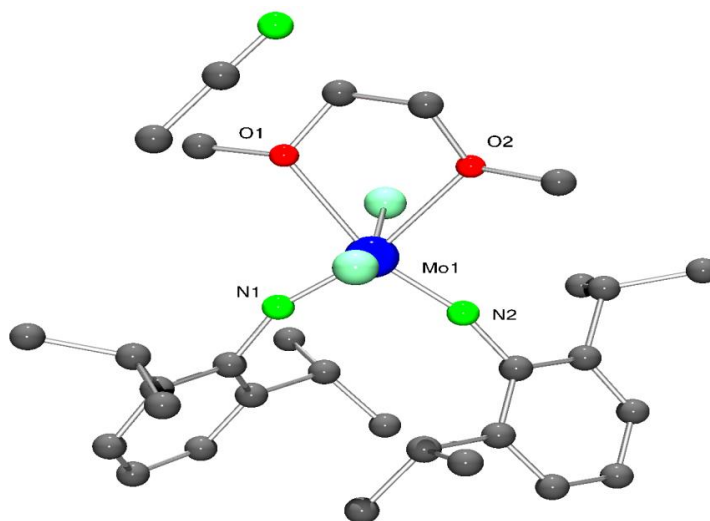
3. Polymerization Screening

Complexes **5**–**12** have been screened for their ability to act as catalysts for the ring opening polymerization (ROP) of ε-caprolactone and the results are presented in (**Table 3**). At temperatures below 80 °C, the systems were inactive. At 80 °C, the systems utilizing **5**, **6**, **10** and **11** exhibited moderate activities with conversions of about 45%–50%, whilst the combination of 12/BnOH exhibited good conversion (*ca.* 85%). At 100 °C, there was little or no activity for reaction times of less than one hour. In most cases, excellent conversions were achieved over 6 h, and little was gained by prolonging the reaction time beyond this point. Although the complexes **5**–**11** are phenolates (and **11** also a *tert*-butoxide), we have screened them both in the presence and absence of benzyl alcohol (BnOH) to monitor if this is beneficial or not. The presence or absence of BnOH had little effect on % conversion or control (eg runs 30 *v* 31 and 39 *v* 40), though

depending on the temperature there was either an increase or decrease in the observed molecular weight (M_n). All systems produced polyesters with narrow dispersities with unimodal characteristics (M_w/M_n 1.08 to 1.72); those at the higher end of the range were associated with increases in the [CL]:[cat]:[BnOH] ratio (runs 17, 19 and 20) and are perhaps indicative of some transesterification reactions occurring under such conditions. Such ratio changes (for **7**) however led to little change in the % conversion.

In terms of structure-activity relationships, in the case of **5** *versus* **6**, the presence of the bulkier phenyl group in the bridge of the di-phenol appears to have only a slight effect with **5** exhibiting a better conversion at 100 °C over 6 h (99 % *cf.* 95%). The bridging imido complex **7** exhibits activity on a par with **5** containing the same di-phenolate ligand. Analysis of the results for the tetra-phenolate systems **9** to **11** indicates that at 100 °C over various reaction times, the *meta* system out-performs the *para* system (*i.e.*, **9** *v* **10**; runs 24 *v* 29, 26 *v* 32, 27 *v* 33), which is tentatively assigned to the closer proximity of the metal centers in **6** and thus an enhanced cooperative effect. A comparison of the use of different imido group in the *meta* system (**10** *v* **11**) is not possible given the different structures adopted, however it is evident that *meta* system **11** is comparable with **10** over 6 or 12 h and is superior over shorter reaction periods (runs 35 and 36). There appears to be no advantage in having two metals present over one (**9**, **10** *cf.* **5**, **6**). Interestingly, the bis(imido) dichloride complex **12**, in the presence of BnOH, also exhibits excellent conversions at 100 °C when employed for 3 h or more.

In general, the observed polymer molecular weights were lower than expected, which indicates that in most cases, there were significant *trans*-esterification reactions occurring. Such a trend has been noted previously when using molybdenum-based species. [4-9] The MALDI-ToF spectra of the resultant PCL revealed is given in (**Figures 30** and **31**), a major series of peaks with separation 114 g·mol^{-1} (*i.e.*, the monomer) with evidence of a secondary minor set of peaks resulting from hydrolysis under ionization conditions. Examination of the ^{1}H NMR spectrum (**Figures 32** and **33**) of the same samples revealed peaks at δ 5.10 and 3.65 assigned to benzyl ester and hydroxymethylene end groups. Interestingly for **7**, a plot of number average molecular weight (*M*n) was approximately linear (**Figure 34**), which was suggestive of a well-controlled polymerization. Comparison of these systems with other molybdenum-based catalysts reveals that it is typical for high temperatures (≥80 °C) to be employed to achieve activity. Neutral chelate complexes derived from the oxydianiline [(2-NH$_2$C$_6$H$_4$)$_2$O] can achieve good conversion rates (>90%) at high temperatures (100 °C) over 12 h; the tetra-nuclear siloxide complex [Mo$_4$Cl$_3$(N*t*Bu)$_3$(OSiMe$_3$)(μ$_4$-O)(L)$_2$(L′)$_2$] (where L = (2-NC$_6$H$_4$)O, L′ = (2-NH$_2$C$_6$H$_4$)(2-NC$_6$H$_4$)O) performed best achieving a conversions >90% over 1 h.[4] Of the other Mo-based systems known, bis(salicylaldehyde) dioxomolydenum operates effectively at 110 °C in mesitylene, whilst ammonium decamolybdate functions as a melt at 150 °C.[7],[10] As observed herein, such molybdenum systems are susceptible to *trans*-esterification processes.

Table 3. Ring opening polymerization of ε-CL using complexes **5 – 12**

Entry	Cat.	CL:Mo:BnOH	Temp./°C	Time/h	Conversion (%)	M_ng/mol$_{,GPC}$	M_ng/mol$_{,Cal}$	PDI[d]
1	**5**	250:1:1	80	0.5	-	-	-	-
2	**5**	250:1:1	100	0.5	-	-	-	-
3	**5**	250:1:1	100	1	70	4.62	20.08	1.41
4	**5**	250:1:0	80	3	45	3.77	12.84	1.17
5	**5**	250:1:1	100	3	86	5.53	24.64	1.22
6	**5**	250:1:1	100	6	99	6.40	28.35	1.40
7	**5**	250:1:1	100	12	99.5	10.67	28.50	1.40
8	**6**	250:1:1	100	0.5	-	-	-	-
9	**6**	250:1:1	100	1	96	5.23	27.50	1.29
10	**6**	250:1:0	80	3	51	2.19	14.55	1.19
11	**6**	250:1:1	100	3	89	7.14	25.50	1.25
12	**6**	250:1:1	100	6	95	7.24	27.21	1.22
13	**6**	250:1:1	100	12	99	10.33	28.35	1.57
14	**7**	250:1:0	80	3	-	-	-	-
15	**7**	250:1:1	100	3	55	2.14	15.80	1.11
16	**7**	250:1:1	100	6	99	6.74	28.35	1.17
17	**7**	125:1:1	100	12	99	8.51	14.23	1.60
18	**7**	250:1:1	100	12	99	9.73	28.35	1.46
19	**7**	500:1:1	100	12	99.5	13.00	56.89	1.72
20	**7**	1000:1:1	100	12	98	16.14	111.96	1.72
21	**4**	250:1:1	100	12	99	7.80	28.35	1.25
22	**8**	250:1:0	80	3	-	0.68	-	1.22
23	**9**	250:1:1	30	24	-	-	-	-
24	**9**	250:1:1	100	1	45	0.822	12.94	1.23
25	**9**	250:1:1	100	3	98	2.84	28.07	1.23
26	**9**	250:1:1	100	6	93	3.13	26.64	1.17
27	**9**	250:1:1	100	12	98	4.39	28.07	1.17
28	**10**	200:1:1	100	0.5	-	-	-	-
29	**10**	200:1:1	100	1	68	5.43	19.51	1.13
30	**10**	250:1:0	80	3	50	1.93	14.26	1.24
31	**10**	250:1:1	80	3	48	3.75	13.80	1.22
32	**10**	250:1:1	100	6	100	7.15	28.64	1.34
33	**10**	250:1:1	100	12	100	7.27	28.64	1.26
34	**11**	250:1:0	80	3	-	-	-	-
35	**11**	250:1:0	100	1	95	2.14	27.10	1.11
36	**11**	250:1:0	100	3	98	2.25	27.96	1.08
37	**11**	250:1:0	100	6	99.5	8.79	28.39	1.33
38	**11**	250:1:0	100	12	99	9.11	28.24	1.37
39	**11**	250:1:1	100	12	99	6.10	28.35	1.46
40	**12**	250:1:1	80	3	85	2.64	24.36	1.21
41	**12**	250:1:1	100	3	99	5.97	28.35	1.19
42	**12**	250:1:1	100	6	98	8.21	28.07	1.36
43	**12**	250:1:1	100	12	100	14.32	28.64	1.46

[a] By ^{1}H NMR analysis. [b] Obtained from GPC analysis times 0.56 x 10^{-3}. [c] (F.W(Monomer).[M] /[BnOH])(conversion)10^{-3}, [d] from GPC.
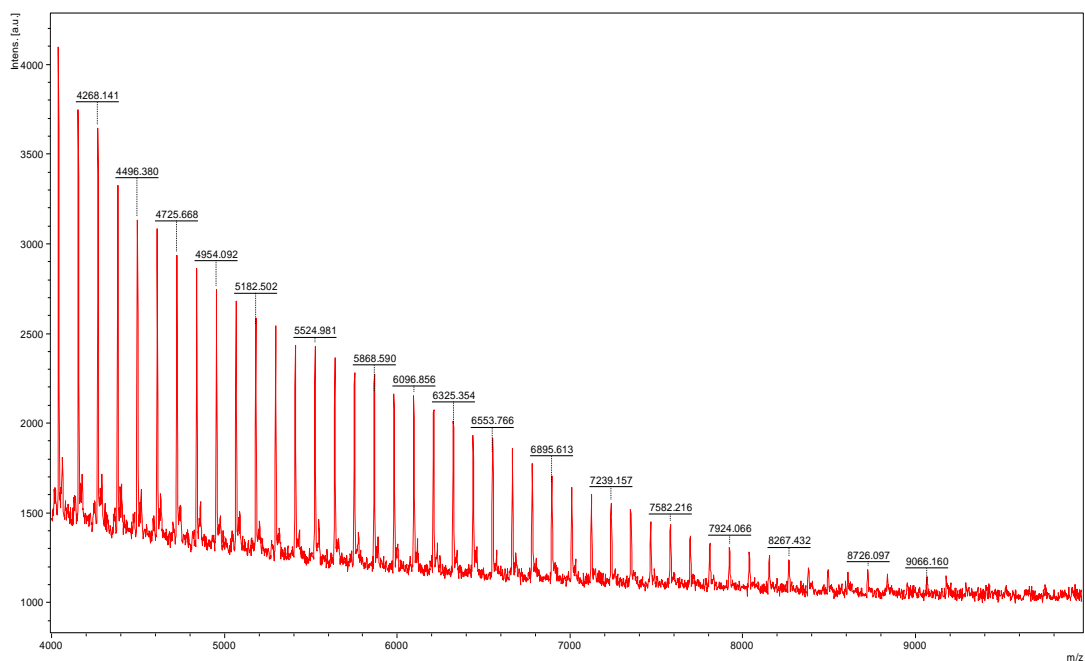
Figure 30. MALDI-TOF spectrum of PCL from (run 9 table 3).
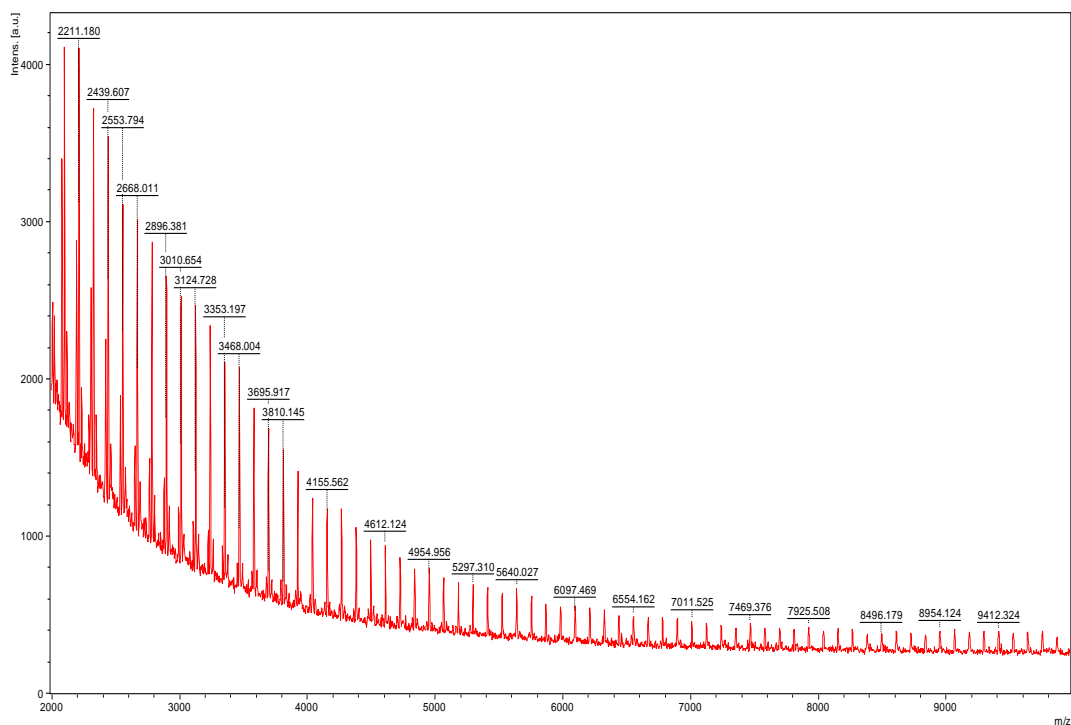
Figure 31. MALDI-TOF spectrum of PCL from (run 22 table 3).
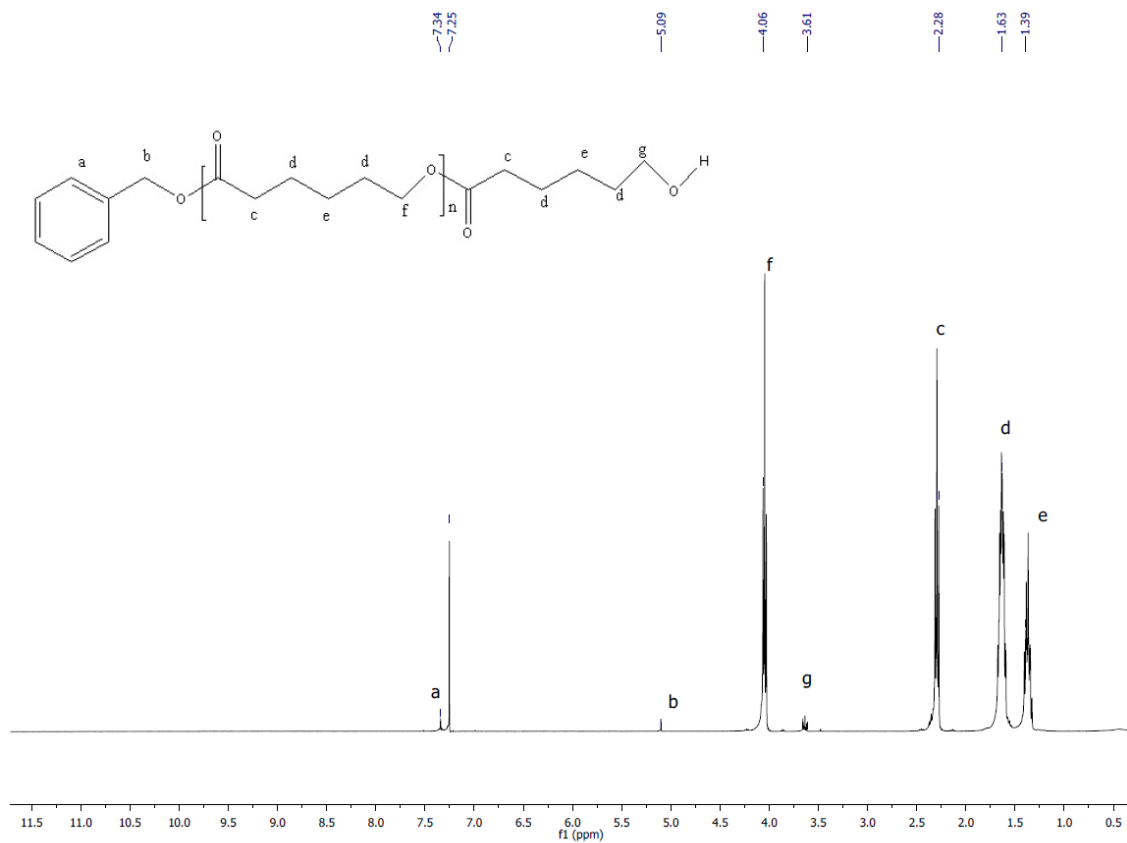
Figure 32. ^{1}H NMR spectrum of the PCL from run (6 table 3).
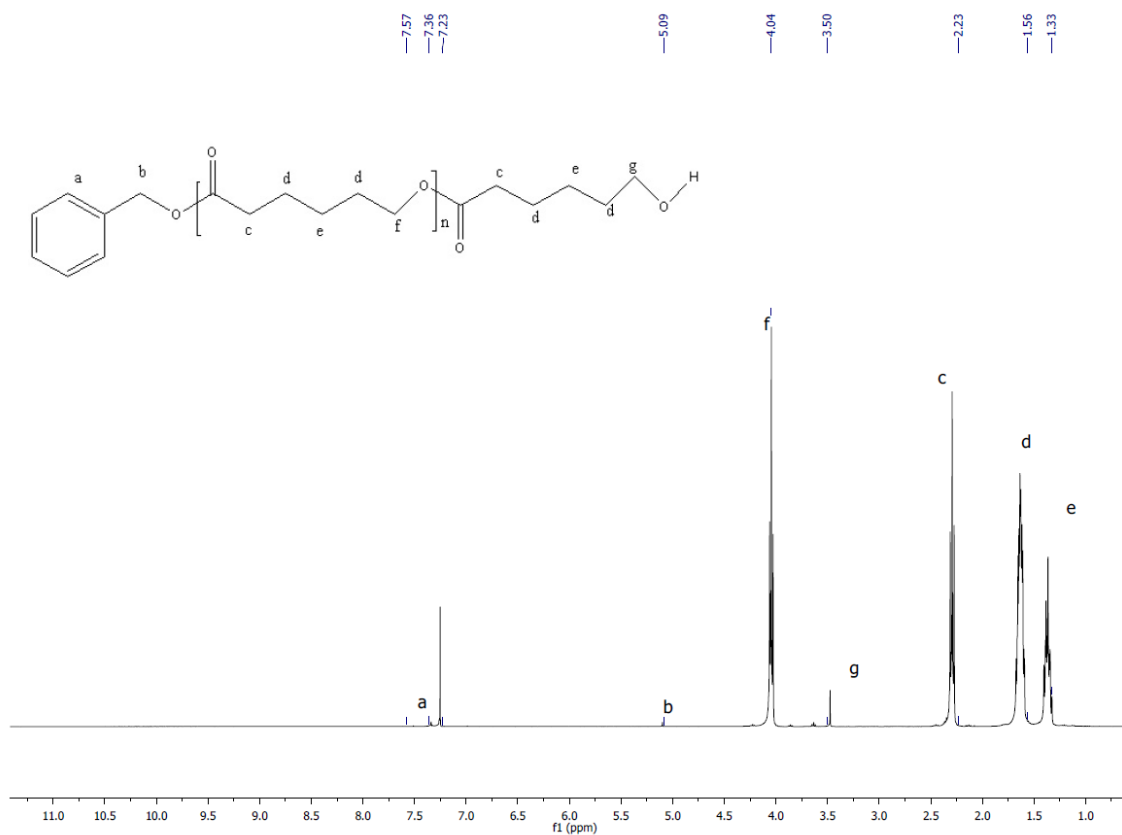
Figure 33. ^{1}H NMR spectrum of the PCL from run (27 table 3).
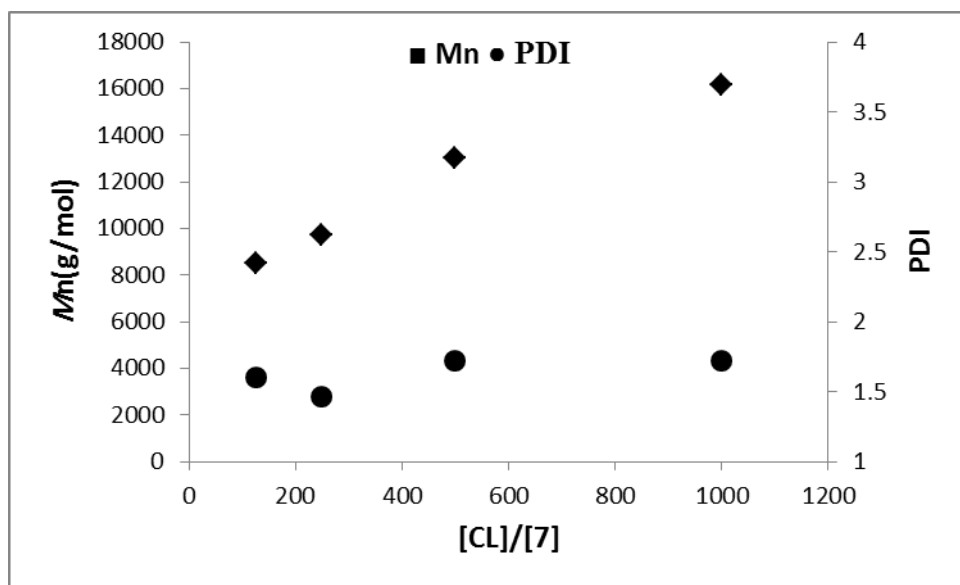
Figure 34. M$_n$ (■) and M$_w$/M$_n$ (●) *versus* [ε-CL]/[**7**].

4. Conclusion

In summary, a new family of molybdenum(VI) phenolate complexes have been structurally characterized and exploited as catalysts for the ring opening polymerization of ε-caprolactone. The ROP proceeded in a controlled fashion in terms of polydispersity, but polymer molecular weights (M_n) were lower than calculated values; MALDI-ToF spectra indicated a degree of *trans*-esterification was taking place. The ROP process using these Mo-based catalysts required high temperature ($\geq 100\ ^{o}C$) and longer reaction times (≥ 1 h). The ROP results were suggestive of some structure activity relationships, for example it was beneficial to employ a ligand set derived from a *meta* tetra-phenol rather than a *para* tetra-phenol, presumably as this brought the metals into closer proximity. However, there seemed to be no advantage gained by employing a complex containing more than one molybdenum centre.

4 Refrences.

[1] R. Sanz and M. R. Pedrosa, *Curr. Org Synth.*, **2009**, 6, 239.

[2] A. Bell, W. Clegg, P. W. Dyer, M. R. J. Elsegood, V. C. Gibson and E. L. Marshall, *J. Chem. Soc., Chem. Commun*, **1994**, 4, 2547.

[3] R. R. Schrock, *J. Mol. Catal. A.,* **2004**, 213, 21.

[4] W.Yang, K. -O. Zhao, C. Redshaw and M. R. J. Elsegood, *Dalton Trans.*, **2015**, 44, 13133.

[5] M. M. Kubo, M. Nakanishi and M. Kimura, *US Patent DE2947978*, 15 September, **1981**.

[6] E. J. Báez, M. Martĭnez-Rosales and A. Martĭnez-Richa, *Polymer.,* **2003**, 44, 6767.

[7] E. J. Báez and A. Martĭnez-Richa, *Polymer.,* **2005**, 46, 12118.

[8] E. J. Báez, A. Marcos-Fernández and A. Martĭnez-Richa, *Macromolecules.,* **2005**, 38, 1599.

[9] Y. Mahha, A. Atlamsani, C. J. Blais, M. Tessier, M. J. Brégeault and L. Salles, *J. Mol. Catal. A.,* **2005**, 2, 234, 63.

[10] Y. Maruta and A. Abiko, *Polym. Bull.*, **2014**, 71, 1413.

[11] (a) L. B. Haymore, A. E. Maatta and D. A. R. Wentworth, *J. Am.Chem. Soc.*, **1979**, 101, 2063. (b) V. C. Gibson, C. Redshaw, W. Clegg and M. R. J. Elsegood, *Polyhedron,* **2007**, 26, 3161.

[12] (a) C. Floriani, F. Corazza, W. Lesueur, A. Chiesi-Villa, and C. Guastini, *Angew. Chem. Int.* **1989**, 28,66. (b) P. J. Toscano, E. J. Schermerhorn, C. Dettelbacher and D. Macherone, *Chem. Commun*, **1991**, 933. (c) F. Corazza, C. Floriani, A. Chiesi-Villa and G. Guastini, *Inorg. Chem.* **1991**, 30, 145. (d) J. Okuda, S. Fokken, C. H. Kaug and W. Massa, *Chem. Ber.* **1995**, 128, 221. (e) M. H. Chisholm, J. H. Huang, J. C. Huffmann, E. W. Streib and D. Tiedtke, *Polyhedron.,* **1997**, 16,2941. (f) M. H. Chisholm, J. H. Huang, J. C. Huffmann and I. P. Parkin, *Inorg. Chem.*, **1997**, 36, 1642. (g) D. R. Mulford, P. R. Fanwick and I. P. Rothwell, *Polyhedron.,* **2000**, 19**,** 35.

[13] (a) F. H. Allen, *Acta. Crystallogr. Sect. B,* **2002**, 58, 380. (b) A. G. Maestri and S. N. Brown, *Inorg. Chem.*, **2004**, 43, 6995.

[14] C. Redshaw, V. C. Gibson, M. R. J. Elsegood and W. Clegg, *Chem. Commun.*, **2007**, 1951.

[15] B. W. F. Gordon and M. J. Scott, *Inorg. Chim. Acta,* **2000**, 297, 206.

[16] (a) T. Matsuo and H. Kawaguchi, *Inorg. Chem.*, **2002**, 41, 6090. (b) C. Redshaw, S. M. Humphrey, *Polyhedron,* **2006**, 25, 1946.

[17] L. Tang, E. P. Wasserman, D. R. Neithamer, R. D. Krystosek, Y. Cheng, P. C. Price, Y. He, and T. J. Emge, *Macromolecules,* **2008**, 41, 7306.

[18] (a) T. R. Cundari and M. S. Gordon, *J. Am. Chem. Soc.*, **1991**, 113, 5231. (b) H. H. Fox, M. H. Schofield and R. R. Schrock, *Organometallics,* **1994**, 13, 2804. (c) A. Poater, X. Solans-Monfort, E. Clot and C. Copéret, *Dalton Trans.*, **2006**, 25, 3077. (d) J. H. Oskam, H. H. Fox, B. K. Yap, H. D. McConville and R. Dell, *J. Organomet.Chem.*, **1993**, 459, 185.

[19] M. H. Chisholm, F. A. Cotton, K. Folting, J. C. Huffman, A. L. Raterman and E. S. Shamshoum, *Inorg. Chem.*, **1984**, 23, 4423.

Chapter 4

Vanadyl phenolate complexes for ring opening homo-polymerization of ε-caprolactone, *L*-lactide and *rac*-lactide

1. Introduction

As mentioned in chapter 1, one metal attracting attention in polymerization catalysis of both lactides and lactones is vanadium given the toxicity associated with this metal is relatively low.[1] It is noted that reports on the use of group 5 complexes for the ROP of cyclic esters are scant.[2] Herein, the potential of vanadyl complexes with ligands derived from di- (L^3H_2), tri- (L^6H_3) or tetra-phenols ($L^{1p/2m}H_4$) (**Scheme 11**) for the ROP of ε-caprolactone, *L*-lactide, *rac*-lactide and the co-polymerization thereof is investigated. Also reported are the effects of the structures of the complexes on the properties of the final polymeric products. Such chelating phenoxide ligation has proved useful in olefin polymerization, [3] but their use in the ROP of lactides and lactones, particularly that of the tri- and tetra-phenolic ligand sets, is rather limited. [2d],[4],[5] Use of a tetra-phenolate ligand set, both *meta* and *para* forms, also allowed for probing for possible cooperative effects, *viz* **13** *versus* **14**-**16**. With this in mind, the crystal structures of the monomeric vanadyl complex [VO(OtBu)L^3] (**13**) and the dinuclear vanadyl complexes {[VO(Oi-Pr)]$_2$(μ-p-L^1)} (**14**), {[VO(OR)]$_2$(μ-p-L^2)} (R = iPr **15**, tBu **16**) are also presented; the molecular structures of **18** and **19** have been reported elsewhere. [6]

(13)

(14)

R = *i*Pr (**15**), *t*Bu (**16**)

(17)

(**18**)

(**19**)
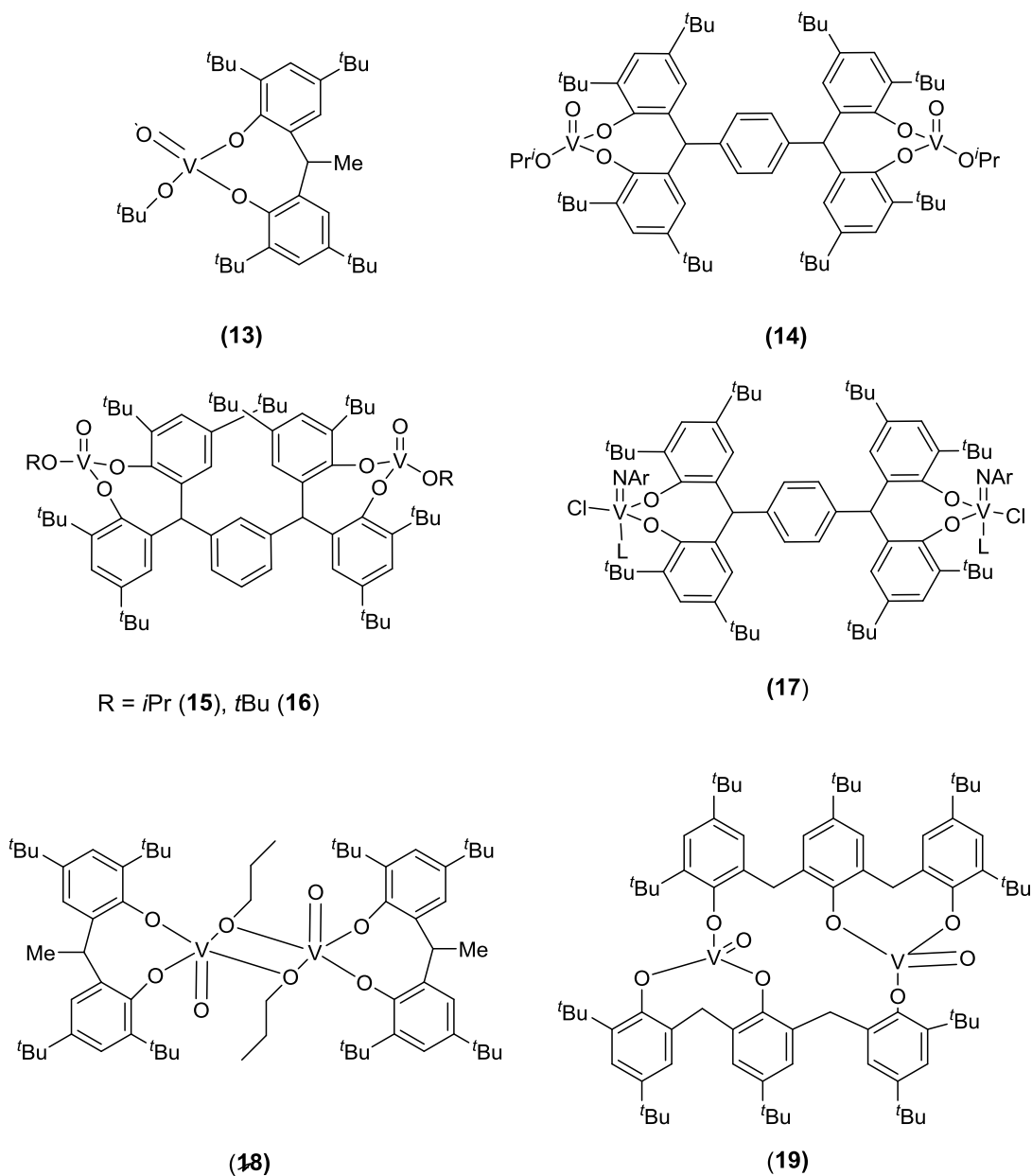
Scheme 11. Vanadyl complexes screened herein (Ar = p-tolyl, L = MeCN).

2. Results and discussion

2.1 Vanadyl phenolate complexes

Interaction of [VO(O*t*-Bu)$_3$] with the 2,2$'$-CH$_3$CH[4,6-(*t*-Bu)$_2$C$_6$H$_2$OH]$_2$ (L^{3}H$_2$) in reluxing toluene afforded, after workup, the monomeric complex [VO(O*t*Bu)L^3] (**13**) in good isolated yield (*ca*. 76%). Complex **13** is presumed to form via displacement of two molecules of *tert*-butanol in a similar fashion reported for

78

related *n*-propoxide complexes. [6] In the IR spectrum of **13**, there is a strong stretch at 1003 cm^{-1} assigned to the v(V=O) group. Crystals of **13** suitable for X-ray diffraction were readily grown from a saturated acetonitrile solution at 0 $^{\circ}$C. The structure of **13** is shown in (**Figure 35**), with selected bond lengths and angles given in the caption, with crystallographic data presented in (**Appendix table 28**).

The vanadium centre adopts a distorted tetrahedral environment with angles varying from ideal in the range 107.7(2) to 112.1(2) $^{\circ}$. The chelating ligand forms an eight membered metallocycle adopting a flattened chair conformation, with a bite angle of 110.1(2) $^{\circ}$, which is somewhat larger than that found in the monomeric vanadyl complex {VOCl[2,2$^{\prime}$-CH$_2$(4-Me,6-*t*-BuC$_6$H$_2$O)$_2$]} [106.9(2) $^{\circ}$] and the dimeric complex [VO(O*n*-Pr)L]$_2$ [94.49(10) $^{\circ}$].[6a],[7] The V–O bond lengths to the bisphenolate ligand [1.789(5) and 1.783(5) Å] are typical of those previously observed for vanadium aryloxides,[6],[7] whilst the V–O alkoxide distance [1.739(5) Å] is shorter than those typically observed in alkoxy vanadium complexes, but similar to that reported in the monomeric imido vanadium complex [V(NAr)(O*t*Bu)L] [1.738(2) Å] (Ar = *p*-ClC$_6$H$_4$). The alkoxide ligand is best described as bent with a V(1) – O(4) – C(40) angle of 145.9(5) $^{\circ}$, which is slightly smaller than the analogous angle in the imido complexes [V(NAr)(O*t*Bu)L] [146.77(12) – 151.9(2) $^{\circ}$] (Ar = *p*-ClC$_6$H$_4$, *p*-tolyl).[8]
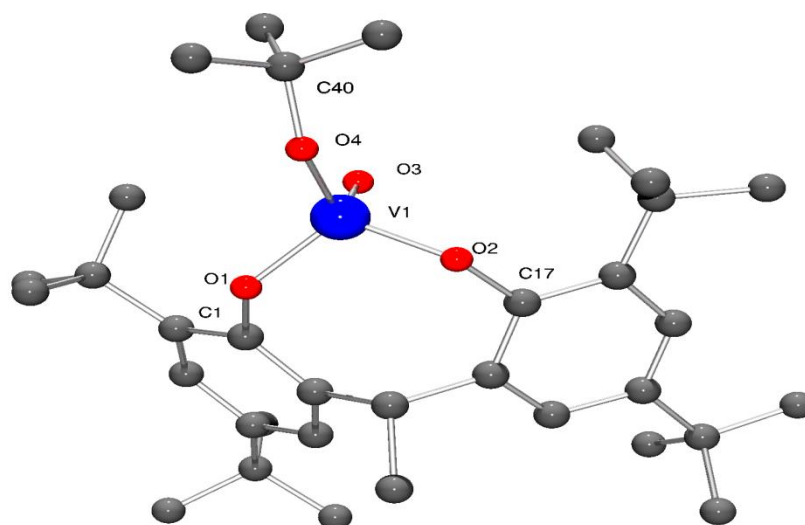
Figure 35. Molecular structure of **13**. Selected bond lengths (Å) and angles (°): V(1) – O(1) 1.789(5), V(1) – O(2) 1.783(5), V(1) – O(3) 1.581(5) ,V(1) – O(4) 1.739(5) ; O(1) – V(1) – O(2) 110.1(2), V(1) – O(1) – C(1) 124.4(4), V(1) – O(2) – C(17) 130.9(4), V(1) – O(4) – C(41) 145.9(5).

Extension of this synthetic methodology to the tetra-phenol $\alpha,\alpha,\alpha',\alpha'$-tetra(3,5-di-*tert*-butyl-2-hydroxyphenyl–*p*-)xylene-*para*-tetra-phenol (L^1H_4) afforded the dinuclear complex $\{[VO(Oi\text{-}Pr)]_2(\mu\text{-}p\text{-}L^{1p})\}$ (**14**) in good yield. Crystals of **14** suitable for X-ray diffraction were readily grown from a saturated dichloromethane solution at 0 °C. The structure of **14** is shown in (**Figure 36**), with selected bond lengths and angles given in the caption. The tetra-phenolate ligand is centrosymmetric with one vanadyl cation bound above the plane of the central aromatic ring and one beneath. The separation of these two identical metal centres is 11.756 Å. Each vanadium centre can be described as adopting a pseudo tetrahedral geometry. The bite angle formed by the tetra-phenolate at each vanadium is 109.4(2) °, which is slightly smaller than that observed for **13** (110.1(2) °) and for the recently reported alkoxide complexes $\{[VO(OR)]_2(\mu\text{-}p\text{-}L^1)\}$ [R = *n*-Pr, 111.73(7)°; *t*Bu, 112.0(2) °]; and the metallocycle adopts a

flattened boat conformation. The isopropoxide ligand can be described as bent with a V2 – O8 – C68 angle of 130.1(5)^o.
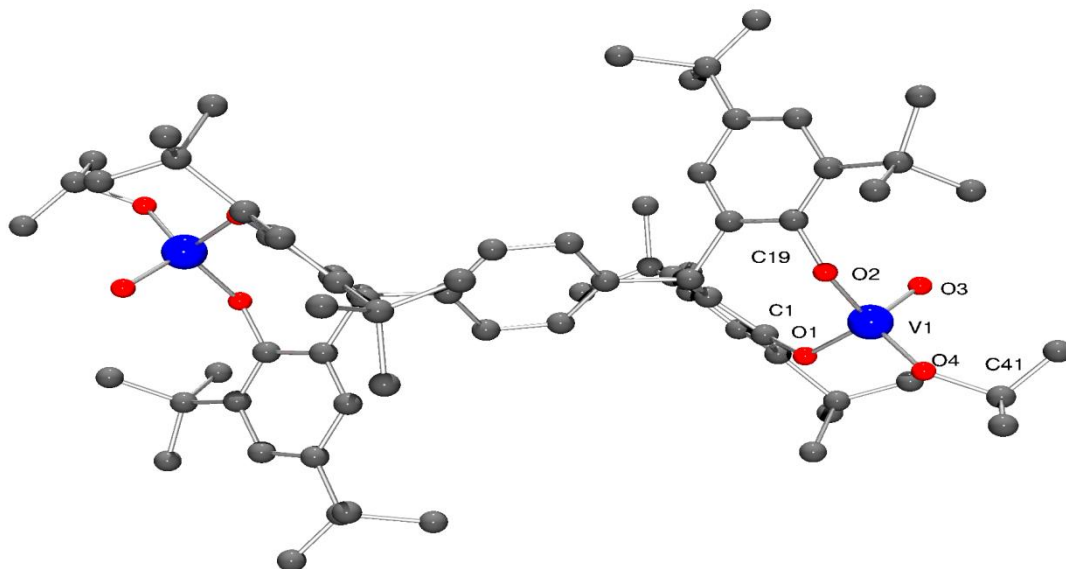
Figure 36. Molecular structure of **14**. Selected bond lengths (Å) and angles (^{o}): V(1) – O(1) 1.750(5), V(1) – O(2) 1.777(4), V(1) – O(3) 1.575(4),V(1) – O(4) 1.759(5) ; O(2) – V(1) – O(1) 109.4(2), V(1) – O(1) – C(1) 139.7(5), V(1) – O(2) – C(19) 151.7(4), V(1) – O(4) – C(41) 130.1(5).

Similar use of the *meta* tetra-phenol α,α,α$^/$,α-tetra(3,5-di-*tert*-butyl-2-hydroxyphenyl–*m*-)xylene-*meta*-tetra-phenol (L^{2}H$_4$) with [VO(OR)$_3$] (R = *n*-Pr or *t*Bu) afforded the dinuclear complexes {[VO(OR)]$_2$(μ-*m*-L^3)} (R = *i*-Pr **15**, *t*-Bu **16**) in good yield. Crystals of **15** and of **16** suitable for an X-ray diffraction studies were obtained on cooling (to –20 ^{o}C) their respective saturated dichloromethane solutions. The molecular structure of **15**·2CH$_2$Cl$_2$ is shown in (**Figure 37)**, and for **16**·2CH$_2$Cl$_2$ in (**Figure 38)** with selected bond lengths (Å) and angles (^{o}) given in (**Table 4)** where they are compared with those of **16**·2CH$_2$Cl$_2$ and **16**·3CH$_2$Cl$_2$.
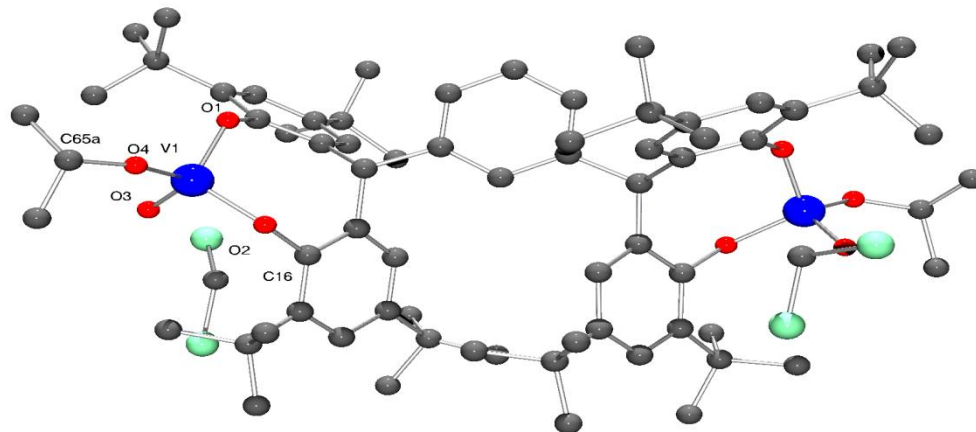
Figure 37. Molecular structure of complex **15**·2CH$_2$Cl$_2$, indicating the atom numbering scheme. Hydrogen atoms have been removed for clarity.
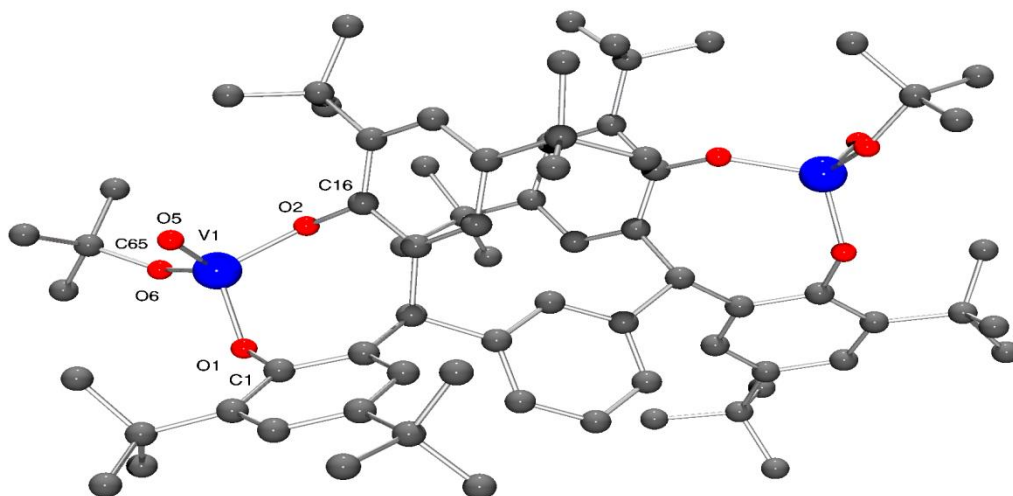
Figure 38. Molecular structure of complex **16**·2CH$_2$Cl$_2$, indicating the atom numbering scheme. Hydrogen atoms have been removed for clarity.
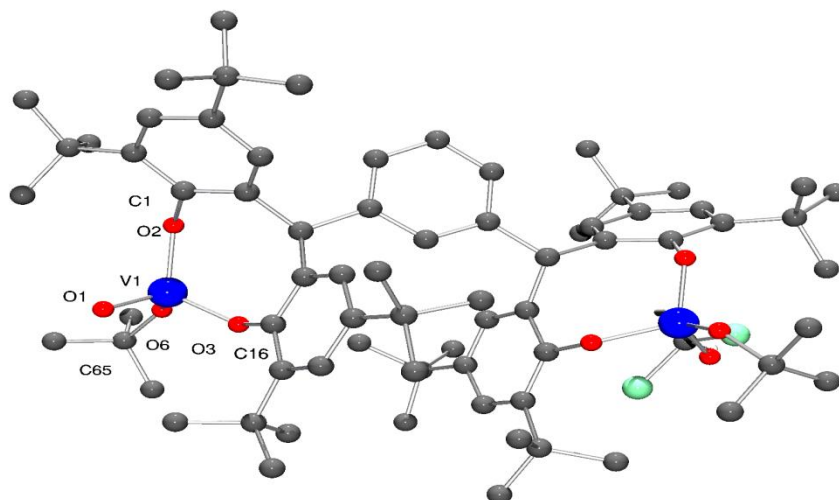
Figure 39. Molecular structure of complex **16**·3CH$_2$Cl$_2$, indicating the atom numbering scheme. Hydrogen atoms have been removed for clarity.

Table 4. Selected bond lengths for **15**, **16**·2CH$_2$Cl$_2$ and **16**·3CH$_2$Cl$_2$.

Bond lengths (Å)/Angles (°)	15	16·2CH$_2$Cl$_2$	16·3CH$_2$Cl$_2$
V1−O(phenolate)	1.790(2)	1.7908(15)	1.790(6)
	1.790(2)	1.7963(15)	1.806(5)
V1=O(vanadyl)	1.581(3)	1.5890(16)	1.577(6)
V1−O(alkoxide)	1.733(3)	1.7298(16)	1.736(6)
V2−O(phenolate)	1.791(2)	1.7891(16)	1.792(6)
	1.793(2)	1.7904(15)	1.796(5)
V2=O(vanadyl)	1.584(3)	1.5908(17)	1.572(7)
V2−O(alkoxide)	1.734(3)	1.7323(16)	1.735(6)
O1−V1−O2		111.31(7)	
O2−V1−O5		106.92(8)	
O5−V1−O6		112.95(8)	
V1−O1−C1		126.91(13)	
V1−O16−C1		126.91(13)	
V1−O6−C65		143.63(15)	

In **15**, the vanadium centres can be described as adopting a pseudo tetrahedral geometry. The bite angle formed by the tetra-phenolate at each vanadium is 110.55(11) °, which is slightly larger than that observed for **13**; again the metallocycle adopts a chair-boat conformation. The *iso*-propoxide ligand can be described as bent with a V2 – O8 – C68 angle of 140.5(3) °; the V – O *iso*-propoxide bond lengths are similar to those observed elsewhere.[9]

For **16**·2CH$_2$Cl$_2$, there is one molecule of the complex and two molecules of CH$_2$Cl$_2$ (modelled by the Platon SQUEEZE procedure) in the asymmetric unit.[10] Each vanadium center adopts a pseudo-tetrahedral geometry, with bond angles in the range 106.92(8) – 112.95(8) ^{o}; the bite angle of the chelate is 111.31(7) ^{o}. The *tert*-butoxide ligand is somewhat bent [V1 – O6 –C65 = 143.63(15) ^{o}], with a slightly larger angle than that observed in the *iso*-propoxide **15** and presumably reflects the greater steric bulk of the *tert*-butoxide. The molecules pack in layers, however there is no significant interaction between the layers.

From a repeated synthesis of **16**, a different solvate was obtained, namely **16**·3CH$_2$Cl$_2$. In the molecular structure of **16**·3CH$_2$Cl$_2$, determined using synchrotron radiation,[11] there is one well-defined dichloromethane which is involved in intramolecular interactions (**Figure 39**). In particular, there is a C-H···O H-bond to the oxo group O7 and a C-H ···π interaction with the aromatic ring C51>C56 {H (73B) ··· ring centroid = 2.56(2) Å}. Crystallographic data presented in (**Appendix table 28**).

2.2 Vanadium imido phenolate complex

Given the oxo group is isoelectronic with the imido group, studies were extended the studies to the reaction of [V(N*p*-MeC$_6$H$_4$)Cl$_3$],[12] with *p*-L^{1}H$_4$ in the presence of Et$_3$N. Following work-up (extraction into MeCN), the red/brown imido complex {[V(N*p*-MeC$_6$H$_4$)(NCMe)Cl]$_2$(μ-*p*-L^1)}·2MeCN (**17**·2MeCN) was isolated in good yield. Single crystals of **17**, obtained on prolonged standing at ambient temperature, were subjected to an X-ray diffraction study. The structure of **17** is shown in (**Figure 40**), with selected bond lengths and angles given in the

caption. The geometry at each vanadium is best described as trigonal bipyramidal with the imido and MeCN groups occupying axial positions [N(1) − V(1) − N(2) 178.74(14) °]. Distortions are in the range 111.59(11) − 122.47(9) °, with the largest equatorial deviation associated with the angle subtended at the metal by the phenolic oxygen centres.

The imido ligand has the geometrical parameters associated with a linear imido function [V(1) − N(1) 1.670(3) Å; V(1) − N(1) − C(40) 170.5(3) °]. The structure of **17** closely resembles that of the recently reported complexes {[V(NAr)(THF)Cl]$_2$(μ-*p*-L^{1p})} (Ar = *p*-MeC$_6$H$_4$, *p*-CF$_3$C$_6$H$_4$), in which THF occupies one of the axial position at the metal as opposed to MeCN in **17**.[3d]
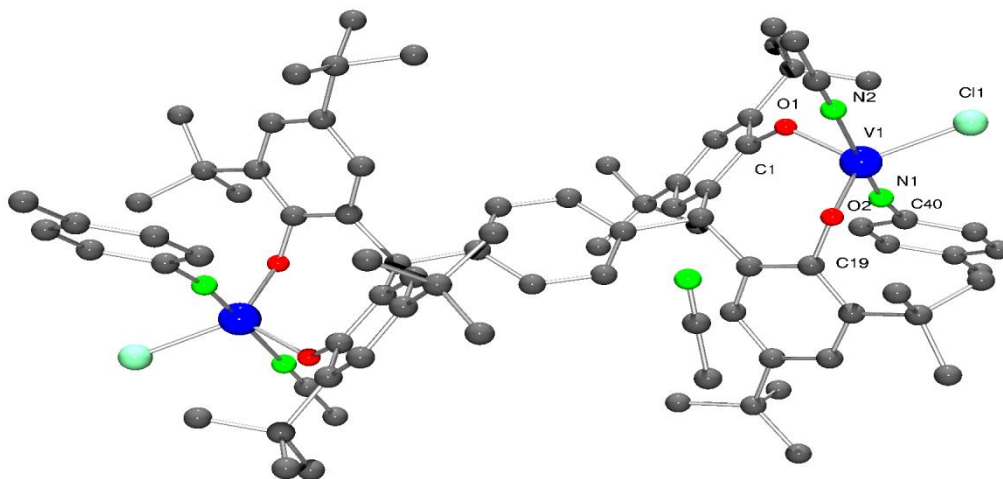
Figure 40. Molecular structure of complex **17**·2MeCN, indicating the atom numbering scheme. Hydrogen atoms have been removed for clarity. Selected bond lengths (Å) and angles (°): V(1) − N(1) 1.670(3), V1–O1 1.818(3), V1–O2 1.831(2), V1–Cl1 2.2609(11); O1–V1–N1 98.33(13), O1–V1–O2 111.59(11), Cl1–V1–N1 94.74(11), V1–O1–C1 124.4(2), V1–O2–C19 121.4(2), V1–N1–C50 170.5(3). Symmetry operation used to generate equivalent atoms: i = −*x*, −*y*, −*z*.

[51]V NMR data for **13 – 19** are presented in (**Table 5)**, and all vanadyl complexes appear in the range δ -410 to -498 ppm, with the 5-coordinate VO_4 centre in **19** slightly upfield of the other 4-coordinate VO_3 containing species. The imido complex **17** appears somewhat downfield, a position which also reflects the presence of the chloride ligand; line widths are also increased in the presence of imido groups. [12]

Table 5. [51]V NMR data for compounds **13 – 19** (recorded in $CDCl_3$ at 298 K *versus* $VOCl_3$ as standard).

Compound	δ (ppm)	$\omega_{1/2}$ (Hz)
13	−482.4	63
14	-410.3[1]	–
15	−498	340[4]
16	−449.6	184
17	−449.6	190
18	-468.9	652
19	−218.9	1074

3. Ring opening polymerization (ROP) studies

3.1 ε-Caprolactone (ε-CL)

Given its ease of preparation on a multi-gramme scale, complex **16** was used to determine the optimum conditions (temperature, time and concentration) needed for the ROP of ε-caprolactone. It was observed that the ratio 200:1 for [CL]:[cat] was best both in the presence or absence of BnOH, over a period of 24 h at 80 ^{o}C. For all catalysts systems, runs conducted at temperatures of ≤45 ^{o}C or for ≤12 h led to either no polymer or low yields (**Table 6**). All systems were well behaved with only one runs (run 3 and 29) affording a PDI of over 2.01 and 1.80, whilst the majority of runs were below 1.40. The presence of BnOH was also examined

86

for **16** (runs 19 – 21), and under the optimized conditions, the conversion was about 10% lower whilst the observed M_n was about 30 % lower. For **17**, bearing a terminal chloride ligand, the use of BnOH was beneficial in terms of % conversion, and the observed molecular weights (M_n) were also higher. In terms of pro-catalyst structure, there appeared to be no advantage in having two metals present given the % conversion for **13** $\approx$ **18** and **19** under optimized conditions (runs 3, 30 and 33).

In the case of the tetra-phenolate systems, it appears that use of systems (**15** and **16**) derived from the *meta* pro-ligand set m-L^2H_4 are more effective than those (**14**) derived from the *para* pro-ligand p-L^1H_4 (runs 7 – 9 and 10 – 21 *versus* 4 – 6) (**Table 6**). This suggests in **15** and **16** that there is a favourable V$^{...}$V separation, which may favour the coordination of a single monomer to both catalytic centres of the same complex. One centre can then be used as a Lewis acid and the other using its V-OR functionality to attack the carbonyl group. The chloride complex **17**, in the presence of BnOH, afforded the highest yield (85 %). In the ^{1}H NMR spectra of the resulting PCL (**Figure 41**), for runs involving pro-catalysts with a V-OR moiety present, signals were assignable to a hydroxyl end group (CH_2OH) and an alkyl ester (eg, isopropyl ester for **15**). This indicated that the polymerization procedure involved rupture of the monomer acyl-oxygen bond and insertion in the alkoxide-vanadium bond. For runs conducting in the presence of BnOH, ^{1}H NMR spectra were more complicated in terms of end group, with both OBn and OR (eg.*t*-Bu for **16**) (**Figure 42**).

Table 6. Ring-opening polymerization of ε-caprolactone catalyzed by the vanadyl phenolate complexes **13 – 19**.

Run	Cat	Temp/°C	Time/h	[CL]:[Cat]:[BnOH]	$M_{n,GPC}$[b]	M_n cal[c]	PDI[d]	Yield%
1	**13**	45	24	200:1:0	2440	19400	1.11	45
2	**13**	60	24	200:1:0	4450	22600	1.43	67
3	**13**	80	24	200:1:0	5430	22600	2.01	68
4	**14**	45	24	200:1:0	1620	12560	1.17	39
5	**14**	60	24	200:1:0	2850	21830	1.20	42
6	**14**	80	24	200:1:0	4110	22600	1.14	50
7	**15**	45	24	200:1:0	---	---	---	---
8	**15**	60	24	200:1:0	1610	11410	1.15	57
9	**15**	80	24	200:1:0	2880	22600	1.35	77
10	**16**	80	1	200:1:0	---	---	---	---
11	**16**	80	6	200:1:0	1120	11414	1.12	30
12	**16**	80	12	200:1:0	2501	20316	1.23	40
13	**16**	45	24	200:1:0	---	---	---	---
14	**16**	60	24	200:1:0	1620	11560	1.12	55
15	**16**	80	24	100:1:0	2143	10272	1.16	60
16	**16**	80	24	200:1:0	3520	22740	1.33	75
17	**16**	80	24	400:1:0	4922	45199	1.42	68
18	**16**	80	24	600:1:0	5720	67799	1.47	77
19	**16**	45	24	200:2:1	800	2280	1.13	23
20	**16**	60	24	200:2:1	1200	22250	1.29	58
21	**16**	80	24	200:2:1	2510	22710	1.30	65
22	**17**	45	24	200:1:0	---	---	---	---
23	**17**	60	24	200:1:0	2170	22370	1.16	70
24	**17**	80	24	200:1:0	3150	22600	1.21	67
25	**17**	45	24	200:2:1	440	---	1.16	40
26	**17**	60	24	200:2:1	3260	22710	1.14	85
27	**17**	80	24	200:2:1	5780	22710	1.43	84
28	**18**	45	24	200:1:0	4600	22370	1.15	47
29	**18**	60	24	200:1:0	5760	22600	1.80	66
30	**18**	80	24	200:1:0	5110	25600	1.66	68
31	**19**	45	24	200:1:0	2860	22370	1.20	36
32	**19**	45	24	200:1:0	2860	22370	1.20	36
33	**19**	80	24	200:1:0	5950	22600	1.32	70

[a]All reactions were carried out in toluene under nitrogen. [b]M_n values were determined by GPC in THF vs PS standards and were corrected with a Mark-Houwink factor of 0.56. [c]Calculated by (F.W.monomer x [Monnomer]/[cat]) x conversion + Fw BnOH. [d](M_w/M_n) were determined by GPC.
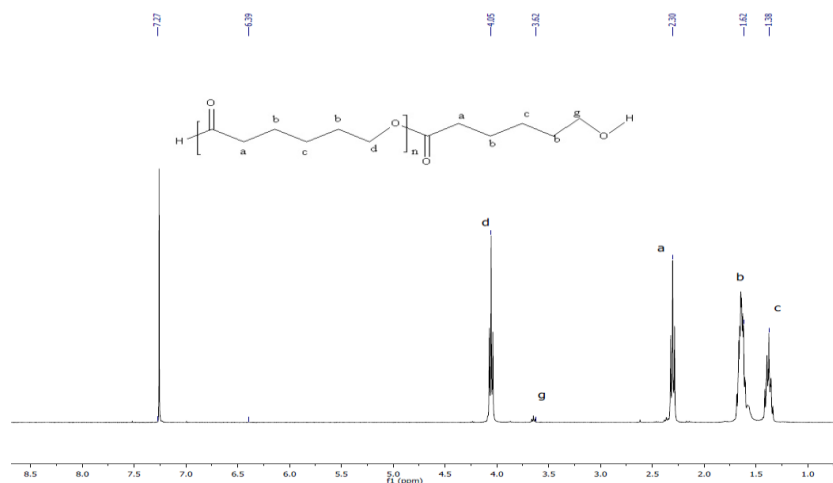
Figure 41. ¹H NMR spectrum of the resulting PCL (run 3, table 6).
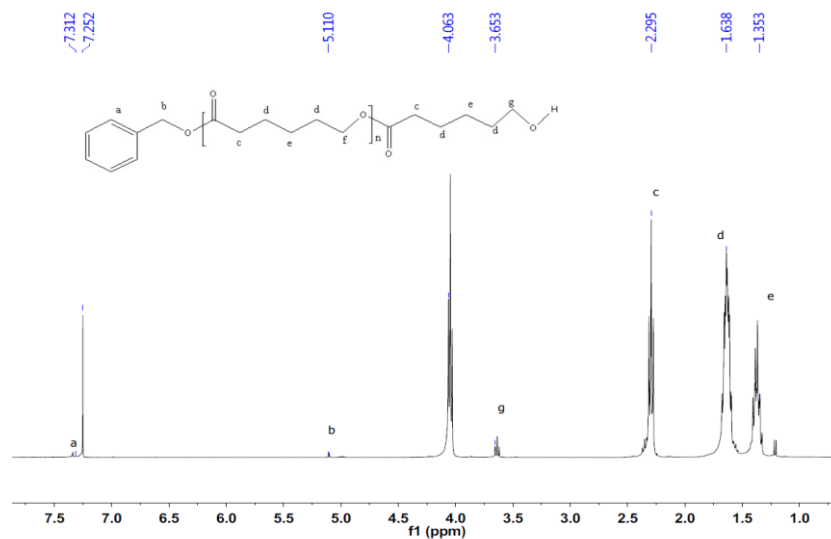
Figure 42. ¹H NMR spectrum of the resulting PCL (run 21, table 6).

Interestingly, in the absence of solvent, these systems performed far better at 80 °C, with conversions ≥ 95%, polydispersities ≤ 1.62 (**Table 7**), and in general afforded higher observed molecular weight (M_n) polymers. The monomeric *tert*-butoxide complex **13** was found to afford the best yield (90 %) and highest molecular weight (M_n) PCL (~16,300). By contrast, **19** afforded lowest conversion and highest PDI, which we assume is due to the lack of a readily

accessible alkoxide bond (a phenoxide linkage of the tri-phenolate would need to be broken). Interestingly, the isopropoxides **14** and **15** gave very similar results, whilst the *tert*-butoxide **16** afforded a polymer of much lower molecular weight (M_n). For complex **17**, it was necessary to add an equivalent of BnOH to achieve ROP activity run 5 *vs* 6 (**Table 7)**, and the resulting polymer was of higher molecular weight (M_n) ~14,000 g mol^{-1}.

Table 7. Ring-opening polymerization of ε-caprolactone catalyzed by vanadyl phenolate complexes **13 – 19** in the absence of solvent.

Run	Cat	Time/min	$[CL]_0:[Cat]_0:[BnOH]_0$	$M_{n,GPC}$[a]	$M_n$cal[b]	PDI[c]	Conv.%[d]	Yield/%
1	**13**	20	200:1:0	16,269	22,599	1.45	99	90
2	**14**	30	200:1:0	7,196	22,143	1.34	97	75
3	**15**	30	200:1:0	7,134	21,914	1.50	96	63
4	**16**	40	200:1:0	2,658	22,371	1.20	98	79
5	**17**	30	200:1:1	14,052	22,251	1.49	97	84
6	**17**	60	200:1:0	---	---	---	---	---
7	**18**	20	200:1:0	4,926	22,599	1.26	99	78
8	**19**	30	200:1:0	11,743	21,686	1.62	95	84

[a] M_n values were determined by GPC in THF *vs* PS standards and were corrected with a Mark-Houwink factor of 0.56. [b] F.W.monomer x [Monomer]/[cat]) x conversion + Fw BnOH. [c] M_w/M_n were determined by GPC. [d] From ^{1}HNMR spectrum.

In general, for the CL runs, despite the narrow polydispersity, the polymer molecular weights (M_n) were much lower than expected, indicating in all cases that significant *trans*-esterification reactions were occurring. Further evidence was provided by the MALDI-ToF mass spectra, where as well as the major population of peaks, there was evidence of a second, albeit minor, population (**Figure 43)** and (**Appindex Figures 142-145**). For **16**, a plot of number average molecular weight (*Mn*) *versus* conversion (**Figure 44)** runs 15 – 18 (**Table 6**), exhibited a linear relationship. Given the plot also shows that the PDI remained narrow, it suggests that under these conditions the ROP by **16** is proceeding in a living manner.
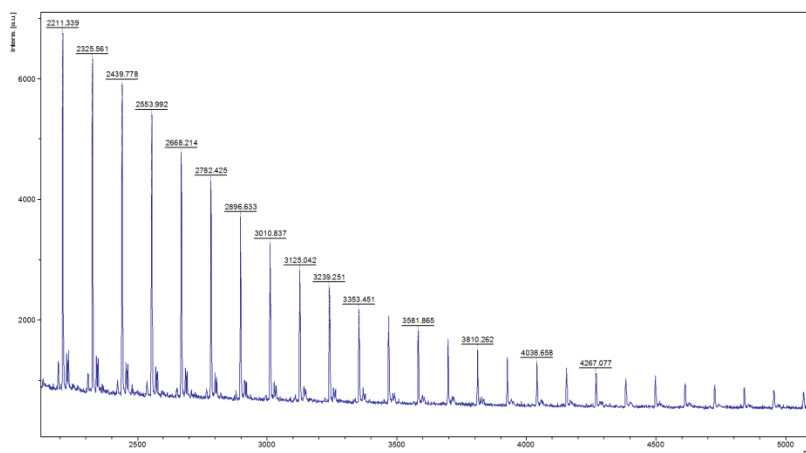
Figure 43. MALDI-ToF spectrum of PCL (run 16, table 6) obtained using **16**.
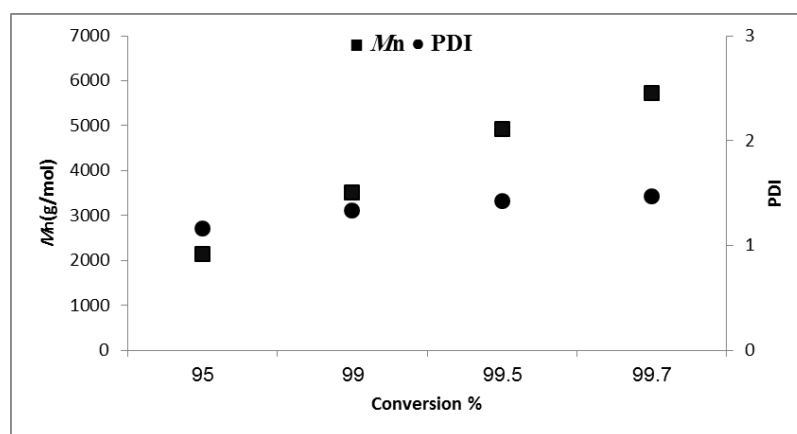
Figure 44. M_n (■) and M_w/M_n (●) vs. monomer conversion in the ROP of ε-CL.

The production of only low molecular weight polymers using alkoxy vanadium

systems has been noted previously.[6] Herein, there was little correlation of [51]V

NMR signal (**Table 5**) *versus* catalytic activity (**Figure 45.**).
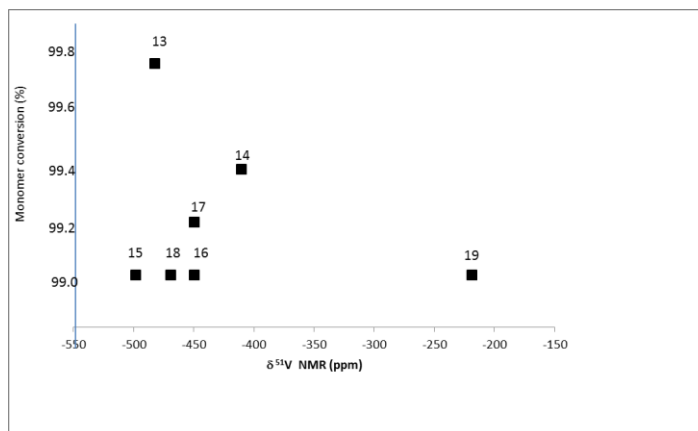
Figure 45. Plot of [51]V NMR signal (from Table 5) *versus* catalytic activity.

3.2 L-Lactide (L-LA)

Complexes **13** to **19** have been screened for their potential to act as catalysts for the ROP of *L*-Lactide. In this case, complex **15** was chosen to establish the optimized conditions for the ROP of *L*-lactide (*L*-LA). Using a ratio of 200:1 for *L*-LA to catalyst, it was found that at temperatures below 80 °C, there was no catalytic activity even after 35 h. At 80 °C, there was no activity after 6 h, and polymer was only isolated at 24 h affording a yield of 20%. Prolonging the reaction time increased the yield to 50%. Further increasing the temperature to 110 °C afforded only a slight improvement in yield, with a slight increase in PDI. Varying the ratio of *L*-LA to catalyst led to a slight improvement in the yield (55 %), together with an increase in the molecular weight (M_n) and a slight broadening of the PDI. Given these results, the other complexes were screened using a ratio of 200:1 for *L*-LA to catalyst and in the case of **17**, screening was conducted both in the absence and presence of BnOH (**Table 8**).

In the case of **16**, differing from **15** only in the nature of the alkoxide (*tert*-butoxide *versus* isopropoxide) there was some activity at 60 °C over 30 h, though the yield was low (10 %). Reactions conducted at 80 °C afforded yields slightly lower than observed for **15**; molecular weights (M_n) were similar. In the case of complex **14**, which differs from **15** in the nature of the tetra-phenolate employed (*para versus meta*), activity was observed at 80 °C on prolonging the reaction time. Yields using **14** after 24 h were typically higher than for **15**, but then after 36 h, the yields were approximately the same (slightly higher using **15**); molecular weights (M_n) followed the same trend. PDIs for runs employed **14** were higher than those for **15**. However, these results, unlike those for ε-

caprolactone, did not suggest that use of the *meta* ligand had any beneficial effect in terms of the distance between the two vanadium centres and the result ROP activity. In the case of the imido complex **17** (a chloride complex), it proved necessary here to add BnOH to afford an active system. We note however that chlorides have previously been shown to be capable of the ROP of lactide. [13] At 80 ^{o}C, activity was observed after 24 h, with yields similar to the vanadyl complex**14**, but with higher molecular weight (M_n) polymers formed.

Comparing results for **13** *versus* **18** suggests that there is no benefit in having two vanadyl centers present rather than one**.** Indeed, results for **13** suggest the opposite given than **13** can operate at 60 ^{o}C and also affords superior yields at 80 ^{o}C. Results for **19** are similar to those of **18**.

In all cases, observed molecular weights (M_n) are far lower than calculated values. In contrast to the ε-caprolactone screening, conducting the *L*-LA ROP runs in the absence of any solvent did not afford improved results and actually afforded little or no polymer.

As for PCL, the observed molecular weights (M_n) for the PLA are lower than the calculated values, and in the MALDI-ToF spectra (**Figure 46**) and (**Appendix figure 146),** there was evidence of a second population consistent with some transesterification processes occurring.

For **15**, a plot (**Figure 47**), (**Table 8,** runs 14 – 17), of the number average molecular weight (M_n) of the poly(*L*-LA) as a function of the monomer conversion was linear, and with consistently low PDI values suggestive of a living process.

Table 8 Ring-opening polymerization of *L*-lactide catalyzed by vanadyl phenolate complexes **13 – 19**.

Run[a]	Cat	Temp/°C	Time/h	$[LA]_0:[Cat]_0:[BnOH]_0$	$M_{n,GPC}$[b]	$M_{n,Cal}$[c]	PDI[d]	Conv.%[f]
1	**13**	45	31	200:1:0	---	---	---	---
2	**13**	60	24	200:1:0	1480	2882	1.57	10
3	**13**	80	6	200:1:0	---	---	---	---
4	**13**	80	24	200:1:0	2311	15566	1.24	54
5	**13**	80	35	200:1:0	2098	14413	1.26	50
6	**14**	60	31	200:1:0	---	---	---	--
7	**14**	80	6	200:1:0	---	---	---	--
8	**14**	80	24	200:1:0	2122		1.34	50
9	**14**	80	36	200:1:0	2192		1.30	58
10	**15**	45	33	200:1:0	---	---	---	---
11	**15**	60	35	200:1:0	---	---	---	---
12	**15**	80	6	200:1:0	---	---	---	---
13	**15**	80	24	200:1:0	1338		1.11	15
14	**15**	80	36	100:1:0	2146		1.11	52
15	**15**	80	36	200:1:0	2511		1.09	52
16	**15**	80	36	400:1:0	3320		1.26	60
17	**15**	80	36	600:1:0	3762		1.29	62
18	**15**	110	31	200:1:0	2006		1.26	51
19	**16**	60	30	200:1:0	865		1.23	9
20	**16**	80	6	200:1:0	---	---	---	---
21	**16**	80	24	200:1:0	1930		1.01	20
22	**16**	80	31	200:1:0	2462		1.10	45
23	**17**	80	31	200:1:0	---	---	---	---
24	**17**	80	6	200:1:1	---	---	---	---
25	**17**	80	24	200:1:1	3400		1.29	53
26	**17**	110	31	200:1:1	3640		1.35	55
27	**18**	45	34	200:1:0	---	---	---	---
28	**18**	60	34	200:1:0	---	---	---	---
29	**18**	80	6	200:1:0	---	---	---	---
30	**18**	80	24	200:1:0	2931	15854	1.73	54
31	**18**	80	31	200:1:0	2639	15854	1.16	54
32	**19**	60	34	200:1:0	---	---	---	---
33	**19**	80	6	200:1:0	---	---	---	---
34	**19**	80	24	200:1:0	3008	16719	1.46	58
35	**19**	80	34	200:1:0	3436	17295	1.31	60

[a] All reactions were carried out in toluene under nitrogen. [b] M_n values were determined by GPC in THF *vs* PS standards and were corrected with a Mark-Houwink factor of 0.58. [c] F.W.monomer x [Monomer]/[cat]) x conversion + Fw BnOH. [d] (M_w/M_n) were determined by GPC. [f] Detrmined by ^{1}H NMR.
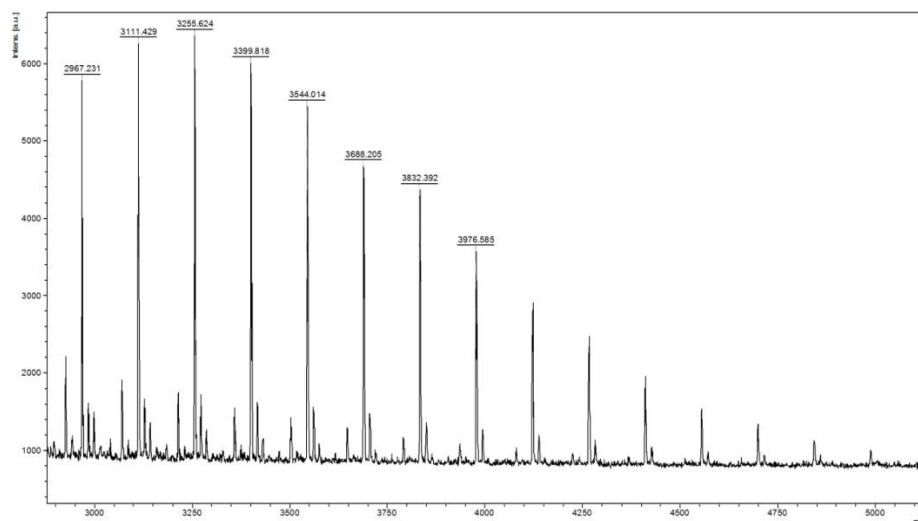
Figure 46. MALDI-ToF spectrum of PLA (run 1, table 8).
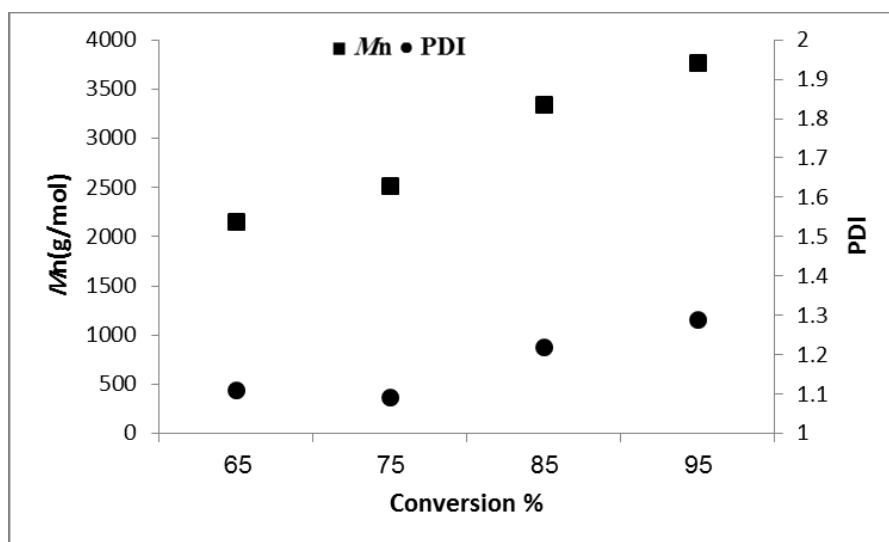
Figure 47. M_n (■) and M_w/M_n (●) *vs*. monomer conversion in the ROP of *L*-LA.

3.3 rac-Lactide (rac-LA)

Complexes **13 – 19** were also screened for their ability to ROP *rac*-lactide and the results are given in (**Table 9**). Temperatures of at least 80 ^{o}C were found necessary to achieve activity and yield were found to be at best moderate ≤50 % as found for *L*-lactide. The ROP appeared to be well controlled in terms of PDI with values in the range 1.09 – 1.30 observed (**Figure 48**). There was no obvious advantage in the use of *meta vs para* ligation in **14** and **15** at either 80 or 110 ^{o}C. Looking at **15** *vs* **16** (O*i*-Pr *vs* O*t*-Bu), at 80 ^{o}C, the isopropoxide **15** afforded

higher molecular polymer (M_n) in higher yield, whereas at 110 ^{o}C the trend was reversed.

Observed molecular weights (M_n) were again lower than calculated values, and MALDI-Tof spectra (**Figure 49)** and (**Appendix figure 147)** also revealed a number of minor populations. As for *L*-lactide, use of no solvent afforded little or no observed catalytic activity.
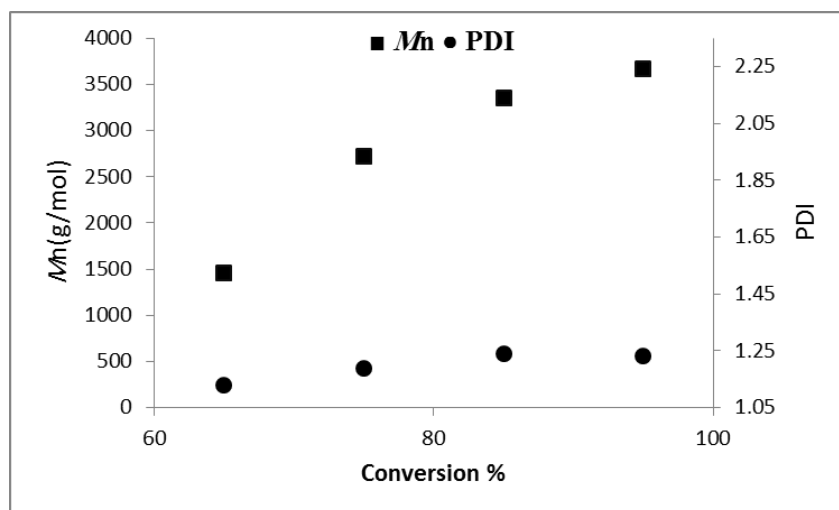
Figure 48. M_n (■) and M_w/M_n (●) *vs*. monomer conversion in the ROP of *rac*-LA**.**
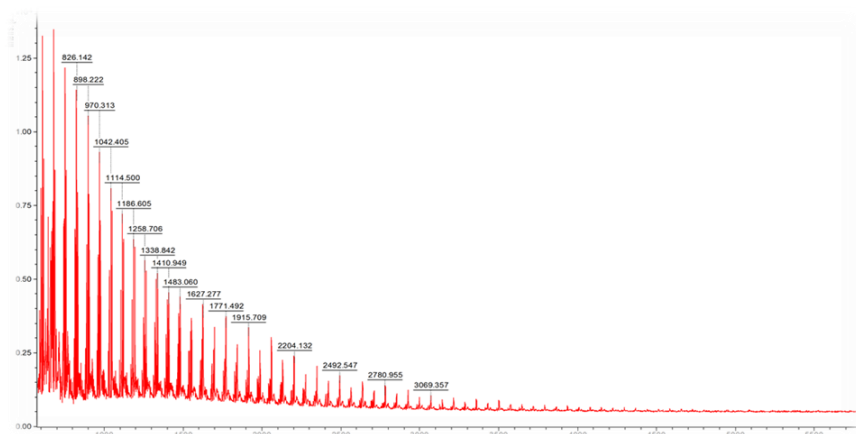
Figure 49. MALDI-ToF spectrum of *r*ac-PLA (run 19, table 9).

Table 9. Ring-opening polymerization of *rac-Lactide* catalyzed by vanadyl phenolate complexes **13 – 19**.

Run	Cat	Temp/^{o}C	Time/h	[LA]:[Cat]:[BnOH]	$M_{n,GPC}$[a]	$M_{n,Cal}$[b]	PDI[c]	Conv.%[d]	Pr[e]
1	**13**	80	24	200:1:0	6055	23060	1.30	---	0.61
2	**14**	60	24	200:1:0	---	---	---	---	---
3	**14**	80	24	100:1:0	1460	9368	1.13	---	---
4	**14**	80	24	200:1:0	2720	23060	1.19	---	0.58
5	**14**	80	24	400:1:0	3447	43239	1.24	54	0.58
6	**14**	80	24	600:1:0	3567	64858	1.23	54	0.58
7	**14**	110	24	200:1:0	2437	21619	1.21	---	0.58
8	**15**	60	24	200:1:0	---	---	---	---	---
9	**15**	80	12	200:1:0	786	12971	1.17	58	---
10	**15**	80	24	200:1:0	2855	25943	1.18	60	0.58
11	**15**	110	24	200:1:0	2475	21619	1.27	--	0.61
12	**16**	80	24	200:1:0	2117	23060	1.25	--	0.61
13	**16**	110	24	200:1:0	4116	21619	1.23	50	0.61
14	**17**	80	24	200:1:1	---	---	---	58	---
15	**17**	110	24	200:1:1	2206	22592	1.10	---	0.58
16	**17**	130	24	200:1:0	---	---	---	---	---
17	**18**	60	24	200:1:0	---	---	---	10	---
18	**18**	80	24	200:1:0	3649	20178	1.15	---	0.60
19	**19**	60	24	200:1:0	---	---	---	54	---
20	**19**	80	24	200:1:0	3856	22484	1.09	50	0.63

[a]M_n values were determined by GPC in THF *vs* PS standards and were corrected with a Mark-Houwink factor of 0.58. [b]Calculated from F.W.monomer x [Monomer]/[cat]) x conversion + Fw BnOH. [c]M_w/M_n were determined by GPC. [d] From ^{1}HNMR spectrum. [e] Determined by analysis of the tetrad signal in the ^{1}H NMR spectrum**.**

To assign the stereochemistry of the PLA polymers we employed 2D J-resolved ^{1}H NMR spectroscopy and assigned the peaks by reference to the literature.[14] Representative spectra for runs 1, 6 and 20 are given in the (**Figures 50)** and (**Appendex figures 148** and **149**)**,** with the assignments given on the respective figures. These systems gave moderately isotactic PLA with a *P*r value in the range 0.58 – 0.63.

Runs conducted in different solvents, namely THF and CH_2Cl_2 resulted in little or no polymer. The presence of cyclic PLA was ruled out by comparison with literature MALDI-ToF and ^{1}H NMR spectra. [15]
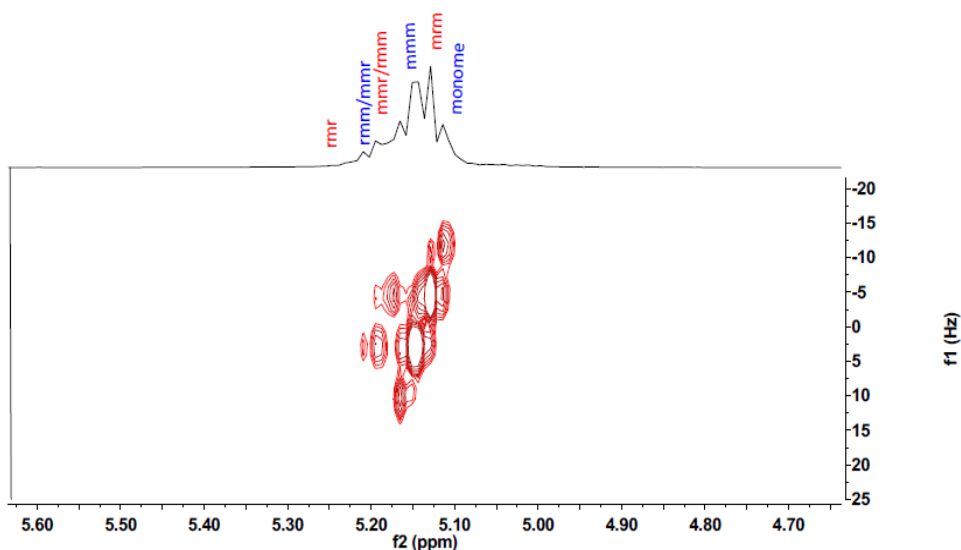
Figure 50. 2D J-resolved ^{1}H NMR spectrum of PLA (run 1, table 9).

3.4 Co-polymerization of ε-caprolactone and L-Lactide.

Complexes **13** to **19** have been screened for their potential to act as catalysts for the co-polymerization of CL with L-Lactide under the optimized conditions found for the homo-polymerization in toluene, ie 80 ^{o}C, 200:200:1 for CL:LA:cat over 24h (x2). In all cases (**Table 10**), good yields (65 − 83 %) of co-polymer were formed, but with low lactide content (2.5 − 9.0 %) as observed from ^{1}H NMR spectra (**Figure 51**), the highest % incorporation of LA (9 %) was found for **17** in the presence of BnOH. According to ^{1}H NMR spectrum the end groups for alkoxide and hydroxyl were also evident. Observed molecular weights were in general higher than those observed for the homo-polymerizations conducted in toluene. Thermal analysis of the co-polymer by DSC revealed two melting points

at 55.1 °C (PCL) and 170.5 °C (PLA) (**Figure 52**). If the addition of the monomers was reversed, *ie L*-LA added first, no co-polymer was isolated after work-up. This suggested that a PLA chain end was not capable of PCL chain growth.

Table 10. Synthesis of diblock copolymers from cyclic ester monomers (LA = *L*-lactide)

Run[a]	Complex	CL:LA[b]	Yield%	M_n[c]	M_w/M_n[d]
1	**13**	390:10	83	15463	2.58
2	**14**	385:15	73	8766	1.54
3	**15**	383:17	71	8143	1.66
4	**16**	380:20	66	5910	1.43
5	**17**	364:46	65	6111	1.26
6	**18**	383:17	77	6875	1.24
7	**19**	379:21	68	6398	1.16

.[a]All reactions were carried out in toluene under nitrogen under optimum condition 24h CL/24h *L*-LA (80 °C). [b] Ratio of CL to LA observed in the co-polymer by ^{1}H NMR. [c]M_n values were determined by GPC in THF *vs* PS standards and were corrected with a Mark-Houwink factor(Mn,GPC $\times$ 0.56 $\times$ %PCL + Mn,GPC$\times$ 0.58 $\times$ %PLLA. [d] PDI were determined by GP.

Figure 51. ^{1}H NMR spectrum of co-polymer from CL and *L*-LA (run 4, table 10).
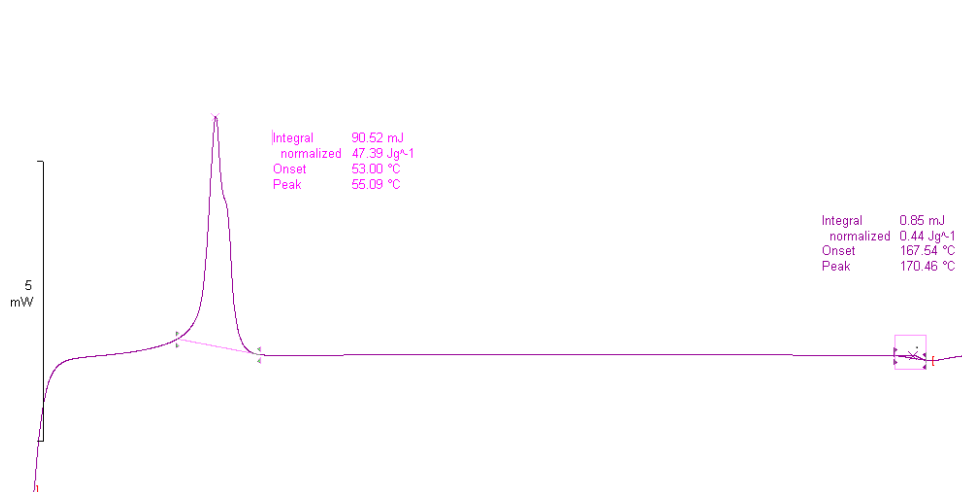
Figure 52. DSC plot of co-polymer from CL and *L*-LA (run 4, table 10).

3.5 Co-polymerization of ε-caprolactone and rac-Lactide

Co-polymerizations involving CL and *rac*-LA gave similar results to the co-polymerization with *L*-LA (**Table 11**). Yields were in the range $60 - 88\%$ and the incorporation of *rac*-lactide was $4.5 - 14.3\%$, and again the highest incorporation was noted for **17**. ^{1}H NMR spectrum showed the end groups for alkoxide and hydroxyl were also evident for form copolymer, (**Figure 53**), DSC (**Figure 54**).

Table 11. Synthesis of diblock copolymers from cyclic ester monomers (LA = *rac*-lactide).

Run[a]	Complex	CL:LA[b]	Yield%	M_n[c]	M_w/M_n[d]
1	**13**	382:18	88	10445	1.42
2	**14**	360:40	75	6428	1.71
3	**15**	375:25	68	6754	1.60
4	**16**	367:33	60	5835	1.46
5	**17**	343:57	70	3364	1.18
6	**18**	375:25	73	5929	1.92
7	**19**	363:73	70	7003	1.21

[a]All reactions were carried out in toluene under nitrogen under optimum condition 24h CL/24h *rac*-LA (80 °C). [b]Ratio of LA to CL observed in the co-polymer by ^{1}H NMR. [c]M_n values were determined by GPC in THF *vs* PS standards and were corrected with a Mark-Houwink factor (Mn,GPC $\times$ 0.56 $\times$ %PCL + Mn,GPC$\times$ 0.58 $\times$ %PLLA, [d] PDI were determined by GPC.
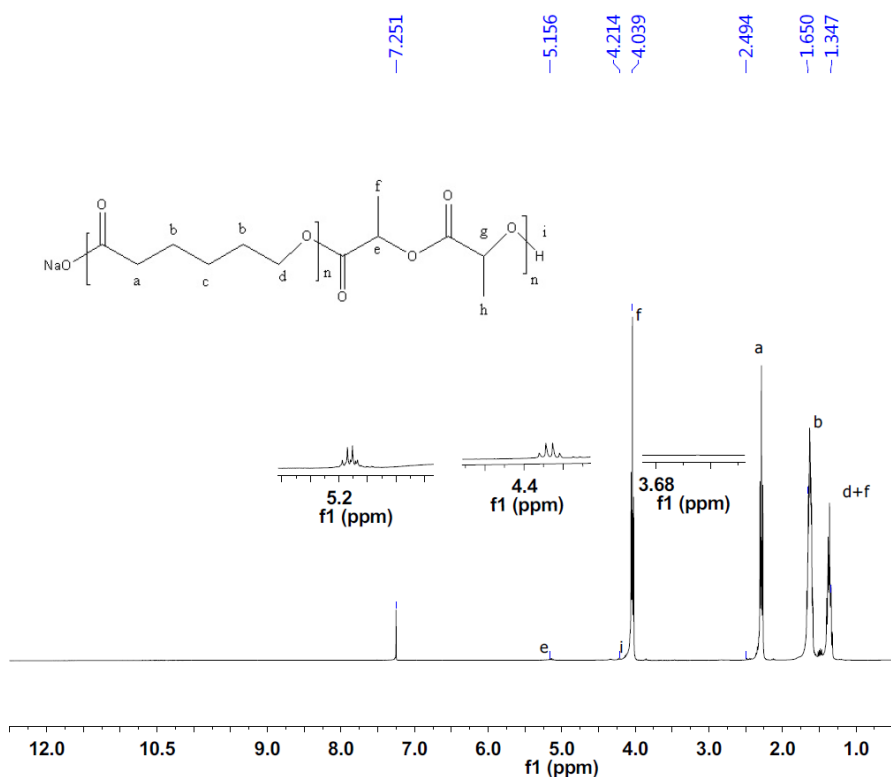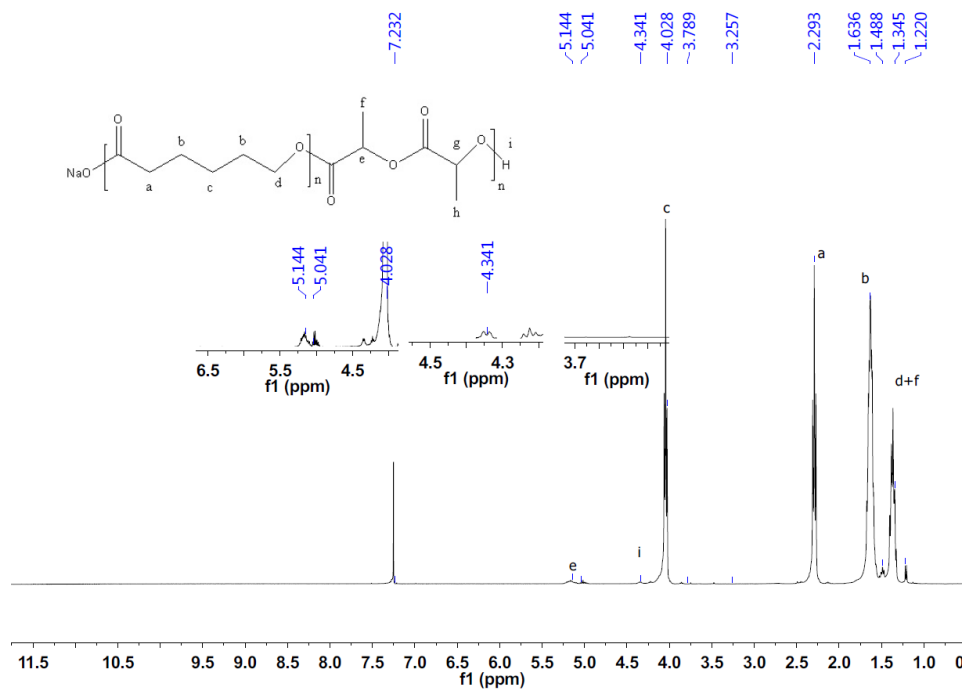
Figure 53. ^{1}H NMR spectrum of co-polymer from CL and *rac*-LA (run 6, table 11).
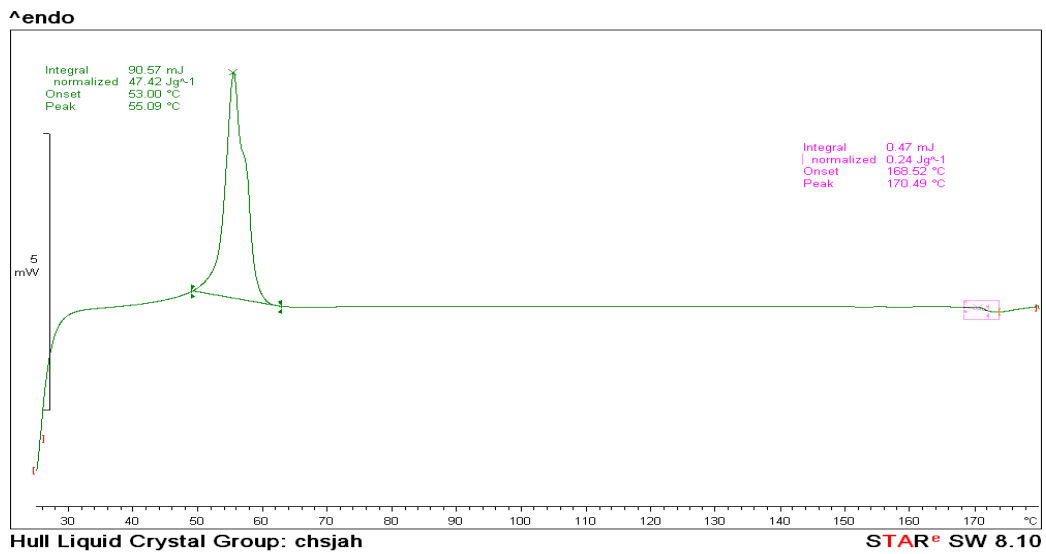
Figure 54. DSC plot of co-polymer from CL and *rac*-LA (run 4, table 11).

4. Conclusions

In conclusion, the ROP behaviour of a series of vanadyl complexes bearing chelating di-, tri- and tetra-phenolate ligands towards ε-caprolactone, *L*-lactide or *rac*-lactide with and without solvent present, and the co-polymerization of ε-CL with lactide has been examined and a good yields (54 - 88%) of co-polymer were formed, and with appreciable lactide content (35 to 62.6%) as observed. For the homo-polymerization of ε-CL, under the optimized conditions in toluene, yields were typically of the order of 70 %. It was observed that there was no advantage in having two metals present (*cf* to one), whilst for the tetra-phenolates use of the *meta* ligand set appeared beneficial (*cf* the *para* ligand set), which perhaps reflects the closer proximity of the metal centres. Conducting the runs in the absence of solvent led to higher conversions, typically > 95 %.

5. References

[1] C. Redshaw, M. R. J. Elsegood, J. A. Wright, H. Baillie-Johnson, T. Yamato, S. de Giovanni and A. Mueller, *Chem.Commun*., **2012**, 48, 1129.

[2] (a) Y. Kim, P. N. Kapoor and J. G. Verkade, *Inorg. Chem*., **2002**, 41, 4834; (b) C. Alonso-Moreno, A. Antinolo, J. C. Garcia-Martinez, S. Garcia-Yuste, I. Lopez-Solera, A. Otero, J. Perez-Flores and M. Tercero-Morales, *Eur. J. Inorg.Chem*., **2012**, 1139 (c) T. K. Saha, M. Mandel, M. Thunga, D. Chakraborty and V. Ramkumar, *Dalton Trans*., **2012**, 42,10304; (d) Y. Al-Khafaji, X. Sun, T. J. Prior, M. R. J. Elsegood and C. Redshaw, *Dalton Trans*., **2015**, 44,12349.

[3] (a) C. Redshaw, *Dalton Trans*., **2010**, 39, 5595; (b) K. Nomura and W. Zhang, *Chem. Rev*., **2011**, 111, 2342; (c) J.-Q. Wu and Y.-S. Li, Coord. *Chem. Rev*., **2011**, 255, 2303; (d) C. Redshaw, M. J. Walton, M. R. J. Elsegood, T. J. Prior and K. Michiue, *RSC Adv*., **2015**, 5, 89783.

[4] Use of di-phenols: (a) B.-T. Ko and C.-C. Lin, *Macromolecules,* **1999**, 32, 8296; (b) I. Taden, H.-C. Kang, W. Massa, T. P. Spaniol and J. Okuda, *Eur. J. Inorg. Chem*., **2000**, 441; (c) H.-L. Chen, B.-T. Ko, B.-H. Huang and C.-C. Lin, *Organometallics*, **2001**, 20, 5076; (d) B. T. Ko and C.-C. Lin, *J. Am. Chem. Soc*., **2001**, 123, 7973; (e) Y.-C. Liu, B.-T. Ko and C.-C. Lin, *Macromolecules*, **2001**, 34, 6196; (f) M.-L. Hsueh, B.-H. Huang and C.-C. Lin, *Macromolecules*, **2002**, 35, 5763; (g) M. H. Chisholm, C.-C. Lin, J. C. Gallucci and B.-T. Ko, *Dalton Trans*., **2003**, 406; (h) T.-C. Liao, Y.-L. Huang, B.-H. Huang and C.-C. Lin, *Macromol. Chem. Phys*., **2003**, 204, 885; (i) Y. Takashima, Y. Nakayama, T. Hirao, H. Yasuda and A. Harada, *J. Organomet. Chem*., **2004**, 689, 612; (j) M.-L. Shueh, Y.-S. Wang, B.-H. Huang, C.-Y. Kuoand C.-C. Lin, *Macromolecules*, **2004**, 37, 5155; (k) R.-M. Ho, Y.-W. Chiang, C.-C. Tsai, C.-C. Lin,

B.-T. Ko and B.-H. Huang, *J. Am. Chem. Soc*., **2004**, 126, 2704; (l) T.-L. Yu, C.-C. Wu, C.-C. Chen, B.-H. Huang, J. Wu and C.-C. Lin, *Polymer*, **2005**, 46, 5909; (m) Y. Yao, X. Xu, B. Liu, Y. Zhang, Q. Shen and W.-T. Wong, *Inorg. Chem*., **2005**, 44, 5133; (n) X. Xu, Z. Zhang, Y. Yao, Y. Zhang and Q. Shen, *Inorg. Chem*., **2007**, 46, 9379; (o) M.-L. Hsueh, J. Wu and C.-C. Lin, *Macromolecules*, **2005**, 38, 9482; (p) J. Wu, Y.-Z. Chen, W.-C. Hung and C.-C. Lin, *Organometallics*, **2008**, 27, 4970; (q) Z. Liang, X. Ni, X. Li and Z. Shen, *Inorg. Chem. Commun*., **2011**, 14, 1948; (r) C.-Y. Li, P.-S. Chen, S.-J. Hsu, C.-H. Lin, H.-Y. Huang and B.-T. Ko, *J. Organomet. Chem*., **2012**, 716, 175; (s) X. Xu, X. Pan, S. Tang, X. Lv, L. Li, J. Wu and X. Zhao, Inorg. *Chem. Commun*., **2013**, 29, 89; (t) Z. Liang, M. Zhang, X. Ni, X. Li and Z. Shen, Inorg. *Chem. Commun*., **2013**, 29, 145.

 [5] Use of tetra-phenols: J. Zhang, C. Jian, Y. Gao, L. Wang, N. Tang and J. Wu, *Inorg. Chem*., **2012**, 51, 13380.

[6] (a) C. Redshaw, L. Warford, S. H. Dale and M. R. J. Elsegood, *Chem. Commun*., **2004**, 1954; (b) D. Homden, C. Redshaw, L. Warford, D. L. Hughes, J. A. Wright, S. H. Dale and M. R. J. Elsegood, *Dalton Trans*., **2009**, 8900.

[7] P. J. Toscano, E. J. Schermerhorn, C. Dettelbacher, D. Macherone and J. Zubieta, *J. Chem. Soc., Chem. Commun.*, **1991**, 933.

[8] A. Arbaoui, D. Homden, C. Redshaw, J. A. Wright, S. H. Dale and M. R. J. Elsegood, *Dalton Trans*., **2009**, 8911.

[9] T. Moriuchi, M. Nishina and T. Hirao, *Angew. Chem. Int. Ed*., **2010**, 49, 83.

[10] (a) A. L. Spek, *Acta Crystallogr*., **1990**, A46, C34. (b) P. v. d. Sluis and A. L. Spek, *Acta Crystallogr*., **1990**, A46, 194.

[11] (a) W. Clegg, M. R. J. Elsegood, S. J. Teat, C. Redshaw and V. C. Gibson, *J. Chem. Soc., Dalton Trans.* **1998**, 3037. (b) W. Clegg, *J. Chem. Soc., Dalton Trans.*, **2000,** 3223.

[12] (a) E. A. Maatta, *Inorg. Chem.* **1984**, 23, 2561. (b) D. D. Devore, J. D. Lichtenhan, F. Takusagawa and E. A. Maatta, *J. Am. Chem. Soc.* **1987**, 109, 7408.

[13] (a) Y. Takashima, Y. Nakayama, K. Watanabe, T. Itono, N. Ueyama, A. Nakamura, H. Yasuda, A. Harada and J. Okuda, *Macromolecules.,***2002**, 35, 7358. (b) Y. Kim, G. K. Jnaneshwara and J. G. Verkade, *Inorg. Chem.*, **2003**, 42, 1437.

[14] A. Grala, J. Ejer, L. B. Jerzykiewicz and P. Sobota, *Dalton Trans.*, **2011**, 40, 4042.

[15] E. Piedra-Arroni, C. Ladavi`ere, A. Amgoune and D. Bourissou, *J. Am. Chem. Soc.*, **2013**, 135, 13305.

Chapter 5

Organoaluminium complexes derived from Anilines or Schiff bases for ring opening polymerization of ε-caprolactone, δ-valerolactone and *rac*-lactide

1. Introduction

As mentioned in Chapter 1, aluminium complexes are capable of forming efficient catalytic systems for the ring opening of lactones and lactide. Easily prepared pro-ligands are also a prerequisite if such systems are to be employed on a bulk scale. With this in mind, the use of phenoxyimine type ligation has attracted interest, and a number of structure/activity relationships have been identified.[1] Indeed, a search of the CSD revealed 343 hits for dialkylaluminium where N and O complete the coordination environment, and of these hits, 76 contained chelating phenoxyimine ligand sets.[2] For an overview of the phenoxyimine aluminium systems that have previously been employed in the ROP of cyclic esters, (**Appendix Table 27**).[3-4] Having employed this type of ligand set recently in vanadium-based α-olefin polymerization,[5] in this chapter results on the series of complexes $[R^1R^2CHN=CH(3,5\text{-}t\text{-}Bu_2C_6H_2\text{-}O\text{-}2)AlMe_2]$ ($R^1 = R^2 = R^3 = Me$ **20**; $R^1 = R^2 = Me$, $R^3 = Et$ **21**; $R^1 = R^3 = Me$, $R^2 = Ph$ **22**; $R^1 = Me$, $R^2 = Ph$, $R^3 = Et$ **23**; $R^1 = R^2 = Ph$, $R^3 = Me$ **24**; $R^1 = R^2 = Ph$, $R^3 = Et$ **25**) are reported and are compared their behaviour against organoaluminium complexes derived from the amine component only (i.e. minus the phenoxy-containing 3,5-di-*tert*-butylsalicyl motif, (**Schemes 12** and **13**). Nomura has previously investigated the effect of the imino substituent on the ROP of ε-CL, and observed greatly enhanced activity for aryl substituents (C_6F_5, $2,6\text{-}i\text{-}Pr_2C_6H_3$) versus aliphatic substituents (adamantyl, *tert*-butyl). [4] Herein, we initially targeted diphenylglycine and derivatives thereof given the tendency of related

motifs to form highly crystalline products, [5] by lossing of CO_2 during the formation **L³**H (dpg).

2. Results and Discussion

2.1 Pre-ligands $L^{7-13}H$

The Schiff-base ligands used herein were prepared by standard condensation procedures. [6]

L⁷H   L⁸H   L⁹H

L¹⁰H   L¹¹   L¹²   L¹³
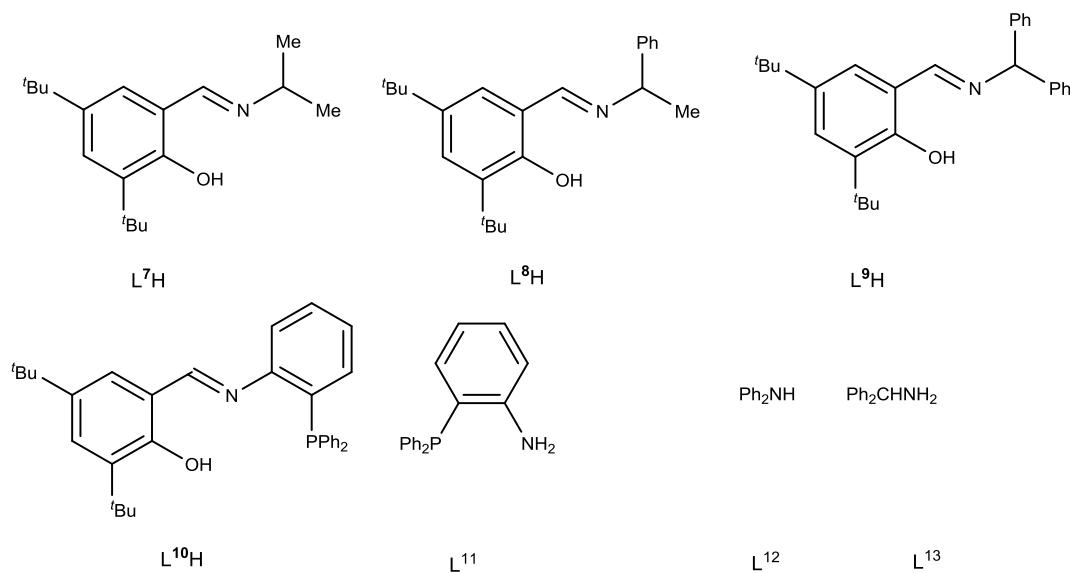
Scheme 12. Compounds (pre-ligands) employed in this chapter.

R = Me (**20**), Et (**21**)   R = Me (**22**), Et (**23**)   R = Me (**24**), Et (**25**)   (**26**)

(**27**)   28)   (**29**)   (**30**)
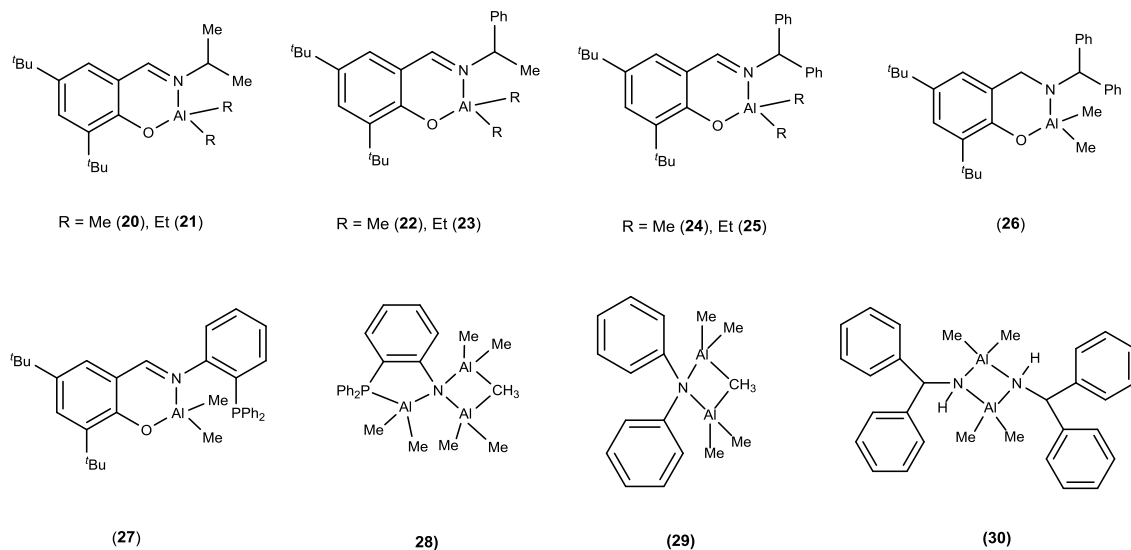
Scheme 13. Complexes used in this chapter.

The IR spectra of ligands contained a relatively strong v(C=N) band at *ca.* 1628 cm^{-1}, whilst in the ^{1}H NMR spectrum, δ OH typically appeared around 13.68 ppm. The pro-ligands **L^{6}H** and **L^{9}H** have been previously reported. [6],[7] Crystals suitable for single crystal X-ray diffraction of the pro-ligand **L^{9}H** (dpa), obtained via the use of benzhydrylamine (dpa) were grown from a saturated acetonitrile solution at ambient temperature. The molecular structure is shown in (**Figure 55**), with selected bond lengths and angles given in the caption. There are two unique molecules in the asymmetric unit with slightly different arrangement of the phenyl groups and methyl groups. In each of the two molecules the core is essentially planar; there is an intramolecular hydrogen bond between the phenol and the imine groups.
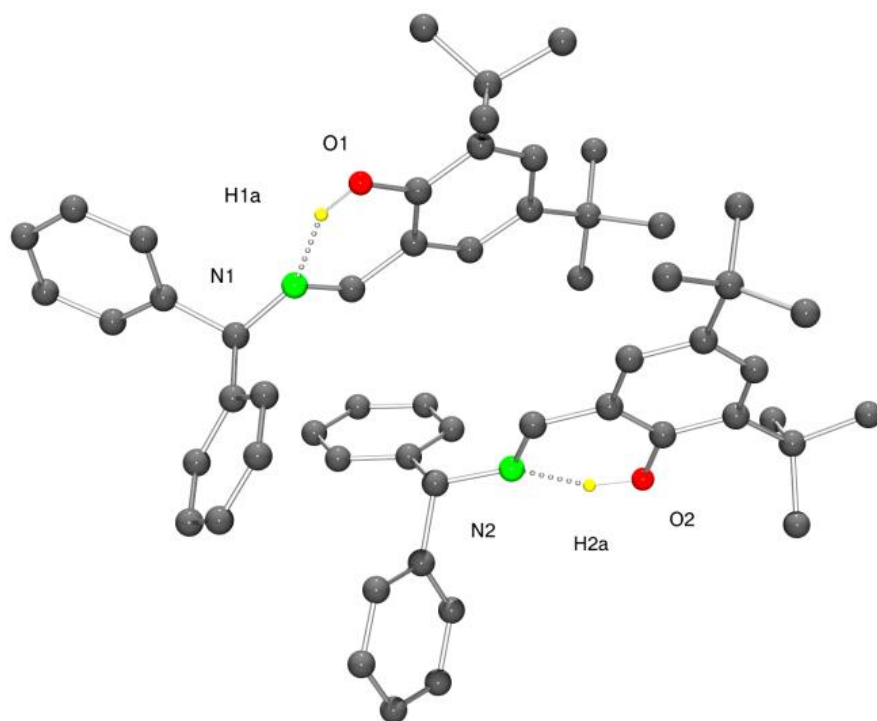
Figure 55. Representation of the asymmetric unit of pro-ligand L^{9}H (dpa). Hydrogen atoms attached to carbon have been omitted for clarity. Dashed lines indicate intramolecular hydrogen bonds. Selected bond lengths (Å) and angles (°): O1–H1A 0.96(4), O1···N1 2.602(3), O2–H2A 1.02(4), O2···N2 2.597(3) Å; O1–H1A···N1 149(4), O2–H2A···N2 154(3).

The packing of the molecules is largely unremarkable. There is some evidence of short C–H⋯π distances (e.g. H15 lies approximately 2.80 Å above the plane of ring C31–C36; H35 lies approximately 2.95 Å from the plane of ring $C3^i$–$C8^I$ [i = 1=x, y, z]).

Similar use of diphenylglycine (dpg), $2,2'$-$Ph_2C(CO_2H)(NH_2)$, resulted in loss of CO_2 during the conditions employed herein and formation of a pale yellow product. A crystal structure determination revealed that the structure of L^9H (dpg) was identical to that obtained using dpa (**Figure 56**) for overlap of the structures and (**Figure 57**) for the molecular structure and bond lengths and angles for L^9H (dpg). A phase change accounts for the differing unit cells in (**Appendix table 28**) which were collected at 150 and 293 K.

Figure 56. Overlay of molecular structures of L^9H (dpa) and L^9H (dpg).
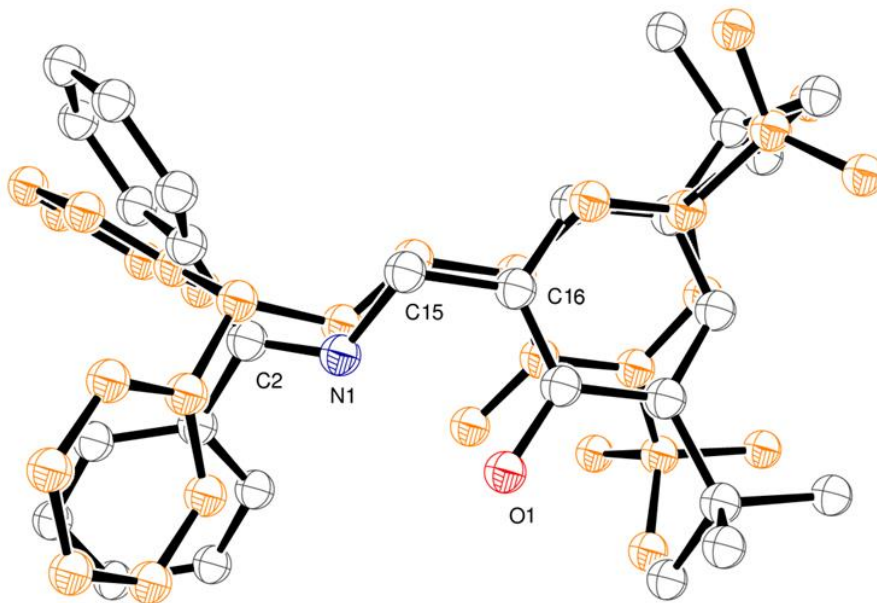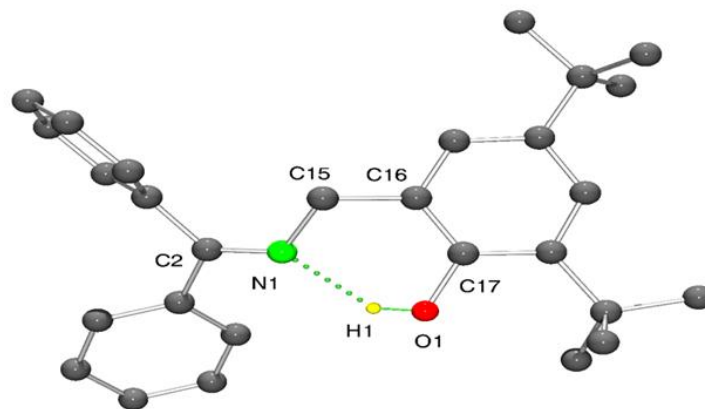
Figure 57. Molecular structure of the asymmetric unit of pre-ligand L^9H_2 (dpg). Hydrogen atoms attached to carbon have been omitted for clarity

2.2 Organoaluminium complexes

Reaction with 1.1 equivalents of Me_3Al with the parent Schiff bases in refluxing toluene afforded,after work-up, good yields of the complexes $[R^1R^2CHN=CH(3,5\text{-}t\text{-}Bu_2C_6H_2\text{-}O\text{-}2)AlMe_2]$ ($R^1 = R^2 = R^3 = Me$ **20**; $R^1 = R^2 = Me$, $R^3 = Et$ **21**; $R^1 = R^3 = Me$, $R^2 = Ph$ **22**; $R^1 = Me$, $R^2 = Ph$, $R^3 = Et$ **23**; $R^1 = R^2 = Ph$, $R^3 = Me$ **24**; $R^1 = R^2 = Ph$, $R^3 = Et$ **25**). Complex **20** was previously reported by Milione *et al*, and used for halide anion binding via H-bonding,[7] whilst the debutylated version of complex **24** has recently been employed by Chiang, Chen and Chen and coworkers for the ROP of ε-Cl and *L*-lactide; the structure of debutylated **24** was not reported.[3z] Herein, crystals of **24** suitable for an X-ray diffraction study were grown from acetonitrile on prolonged standing at ambient temperature. The molecular structure is shown in (**Figure 58**) with selected bond lengths and angles given in the caption; crystallographic data are presented in (**Appendix table 28**). The asymmetric unit of **24** contains one

molecule of the complex; there is no solvent of crystallization. The C–N bond at 1.32(3) Å is consistent with an imine linkage, whilst the Al–N bond length (1.98(2) Å) is typical of reported Al–N imine bonds.[8] In the packing of the complex, the structure adopted is layered, with C–H···π interactions between layers.
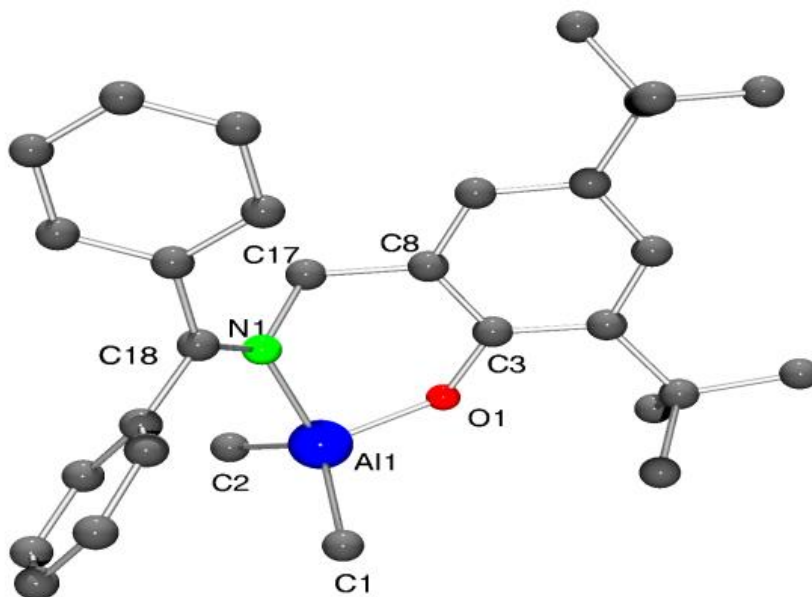
Figure 58. Molecular structure of [Ph$_2$CHN=CH(3,5-t-Bu$_2$C$_6$H$_2$-O-2)AlMe$_2$] (**24**), showing the atom numbering scheme. Hydrogen atoms have been omitted for clarity. Selected bond lengths (Å) and angles ($^{\circ}$): Al(1)–O(1) 1.769(11), Al(1)–N(1) 1.991(14), Al(1)–C(1) 1.965(16), Al(1)–C(2) 2.04(2), N(1)–C(17) 1.317(19), N(1)–C(18) 1.522(19), C(8)–C(17) 1.50(2); O(1)–Al(1)–N(1) 92.5(6), C(1)–Al(1)–C(2) 118.0(10), Al(1)–O(1)–C(3) 125.7(11), Al(1)–N(1)–C(18) 126.0(9).

On one occasion, the amine complex [Ph$_2$NCH$_2$(3,5-t-Bu$_2$C$_6$H$_2$-O-2)AlMe$_2$] (**26**), was also isolated, the molecular structure of which is shown in (**Figure 59**). The longer Al–N and N–C bond lengths are consistent with an amine linkage.[9] The nitrogen N(1) is not protonated here as the sum of the angles is 360° and planar (i.e. not pyramidal), whilst N(1) – C(18) is 1.29 Å (double bond) and N(1) – C(17) is 1.49 Å (single bond). The situation is reminiscent of that reported for the amine nitrogen in the complex {MoCl(Nt-Bu)[1-μ(N),2-(Ph$_2$P)C$_6$H$_4$]}$_2$.[9a] The formation of **26** is thought to be due to the presence of excess Me$_3$Al acting as a reducing agent. Interestingly, Stephan *et al* have recently reported imine hydrogenation by alkylaluminium catalysts (eg i-Bu$_3$Al) albeit under more forcing conditions; a hydroalumination/hydrogenolysis mechanism was invoked.[10]
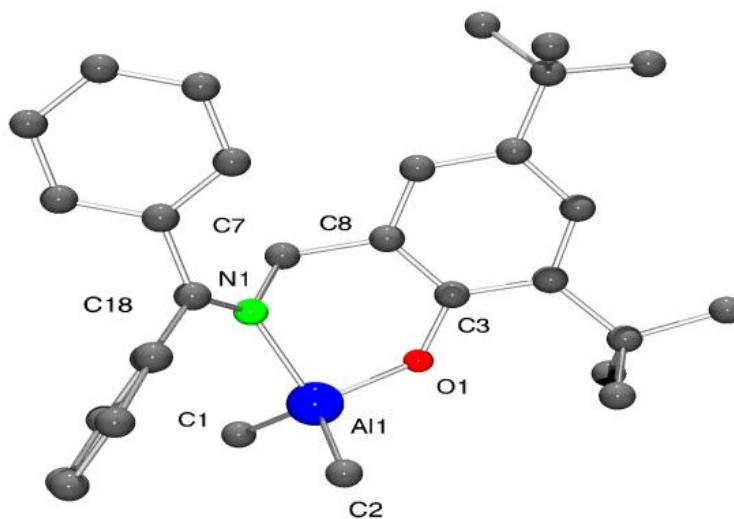
Figure 59. Molecular structure of [Ph$_2$CNCH$_2$(3,5-t-Bu$_2$C$_6$H$_2$-O-2)AlMe$_2$] (**26**), showing the atom numbering scheme. Hydrogen atoms and non-coordinated solvent molecules have been omitted for clarity. Selected bond lengths (Å) and angles (°): Al(1)–O(1) 1.7675(11), Al(1)–N(1) 2.0088(13), Al(1)–C(1) 1.9636(17), Al(1)–C(2) 1.9537(16), N(1)–C(17) 1.4900(17), N(1)–C(18) 1.2894(19), C(8)–C(17) 1.512(2); O(1)–Al(1)–N(1) 94.06(5), C(1)–Al(1)–C(2) 119.65(8), Al(1)–O(1)–C(3) 129.65(9), Al(1)–N(1)–C(18) 129.57(10).

For comparative ROP studies, we also prepared the known Schiff base complex [2-Ph$_2$PC$_6$H$_4$CH$_2$(3,5-t-Bu$_2$C$_6$H$_2$-O-2)AlMe$_2$] **27**,[6] and studied the interaction of 2-diphenylphosphinoaniline, 1-NH$_2$,2-PPh$_2$C$_6$H$_4$, with an excess of Me$_3$Al. In the case of diphenylphosphinoaniline, following work-up, small colourless crystals suitable for X-ray diffraction using synchrotron radiation were isolated.[11] (**Figure 60**), As shown in (**Figure 60**), the complex (**28**) contains three tetrahedral dimethylaluminium centres, two of which are bound to what was the amino nitrogen N(1), and also to each other via a methyl bridge. A search of the CSD revealed 30 hits for methyl bridging of aluminium centres (**Appendix chart 1**).[12], [13] In **28**, two out of three H atoms on the CH$_3$ group at C(7) are disordered. In the difference electron density map, one clear peak is seen with a peak height of *ca*. 0.9 eÅ^{-3} which is refined fully occupied as H(7A). There are also *ca*. four smaller peaks of between 0.4-0.5 eÅ^{-3} which are refined in pairs as the other bridging methyl H atoms. The third aluminium centre Al(1) bridges N(1) and P(1). The structure is reminiscent of [(Me$_2$Al)$_2$(μ-Me)(μ-NPh$_2$)] (**I**, **Appendix chart 1**), obtained via the reaction between diphenylamine and Me$_3$Al.[12b] In **I**, the three H atoms were modelled as all pointing away from the Al–C bonds, i.e. no equivalent of the H(7A) atom in **28**. The Al–C bond lengths {2.145(5) and 2.139(5) in **I** and 2.176(3) and 2.146(3) Å in **28**} and Al–C–Al angle {78.92(17) in **I** and 77.40(11) ° in **28**} are, however, remarkably similar. Mild geometrical restraints were applied to make all the C(7)–H distances similar, and also to keep the H⋯H distances similar for the pairs of disordered H atoms. While a model could be refined with restraints for all three H atoms

pointing away, there remained the large peak nearer the Al atoms, and the *R* factor was worse. The two approximately trigonal planar disorder components are approximately 90° apart, with the minor disorder {48(4)% occupancy) component being less planar than the major. There is no solvent of crystallization in (28).
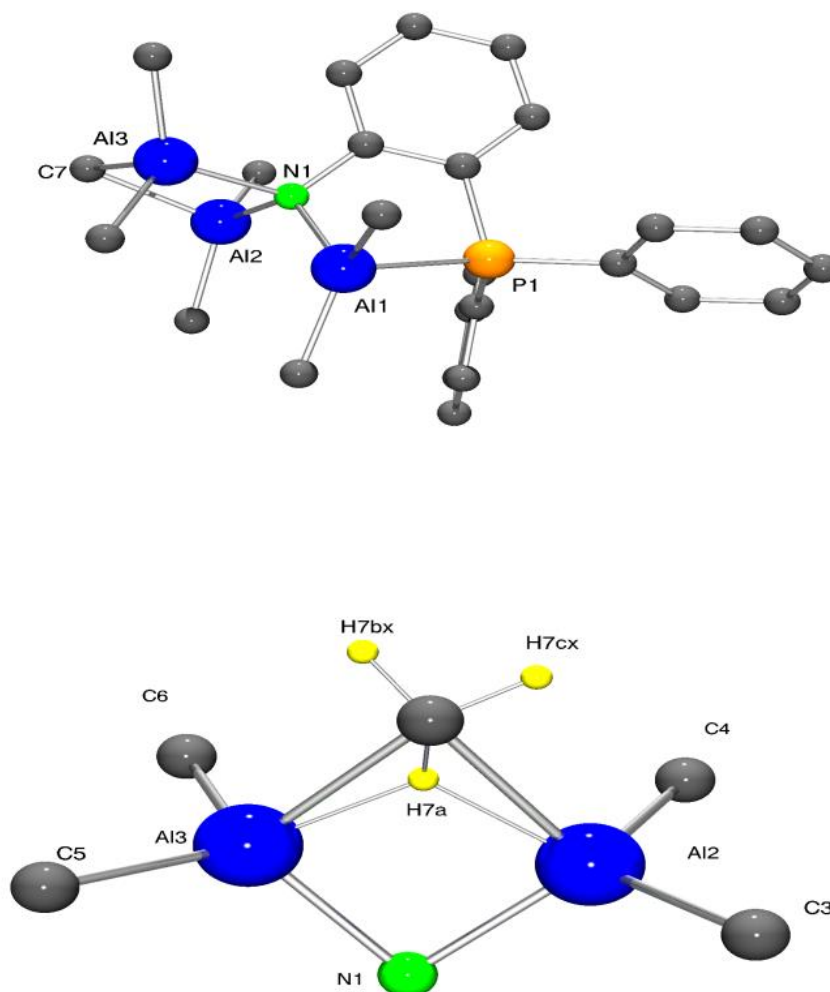
Figure 60. Top: Molecular structure of {Ph$_2$PC$_6$H$_4$N[(Me$_2$Al)$_2$μ-CH$_3$](μ-Me$_2$Al)} (**28**), showing the atom numbering scheme. Bottom: Structure around Al(2) and Al(3) core. Selected bond lengths (Å) and angles (°): Al(1)–N(1) 1.9432(19), Al(1)–P(1) 2.4481(9), Al(2)–N(1) 1.9465(18), Al(2)–C(7) 2.176(3), Al(3)–N(1) 1.9551(18), Al(3)–C(7) 2.146(3), Al(1)–Al(2) 3.4374(10), Al(2)–Al(3) 2.7022(10); N(1)–Al(1)–P(1) 83.76(6), Al(2) –C(7)–Al(3) 77.40(11), Al(2)–N(1)–Al(3) 87.67(7).

Given the nature of the bridging methyl cation in **28** *versus* that reported for (**I, Appendix chart 1**),[10b] we decided to re-examine the structure of the diphenylamine derived aluminium structure. Single crystals of **29** suitable for X-ray diffraction were grown from hexane, which proved to be a two component twin with domains related by a 180 ° rotation about real and reciprocal axes 010. There is one molecule of **29** in the asymmetric unit (no solvent of crystallization), which is shown in **Figure 61** with selected bond lengths and angles given in the caption.

The group at C(5) tallies with the conclusion for (**I, Appendix chart 1**). The Al$_2$NC butterfly in **29** has a shallow hinge angle of 28.24(10)°, which is somewhat shallower than that observed in **28** at 15.19(18)°. Again, VSEPR theory suggests this cation should be trigonal planar. We note that in **I**, the three H atoms are modelled as all pointing away from the Al–C bonds, i.e. no equivalent of the H(7A) atom in **28** or the H(5A) atom in **29**. The Al–C bond lengths {2.145(5) and 2.139(5) in (**I, Appendix chart 1**), 2.176(3) and 2.146(3) in **28**, and 2.145(2) and 2.146(2) Å in **25**} and Al–C–Al angle {78.92(17) in (**I, Appendix chart 1**), 77.40(11) in **28**, and 78.77(8)° in **29**} are, however, remarkably similar. Mild geometrical restraints were applied to make all the C(5)–H distances similar, and also to keep the H⋯H distances similar for the pairs of disordered H atoms. While a model could be refined with restraints for all three H atoms pointing away, there remained the large peak nearer the Al atoms, and again the *R* factor was worse. The two approximately trigonal planar disorder components are approximately 90° apart, with the minor disorder

{47(4)% occupancy) component being less planar than the major one. One electron density peak remained approximately 180° away from H(5A).
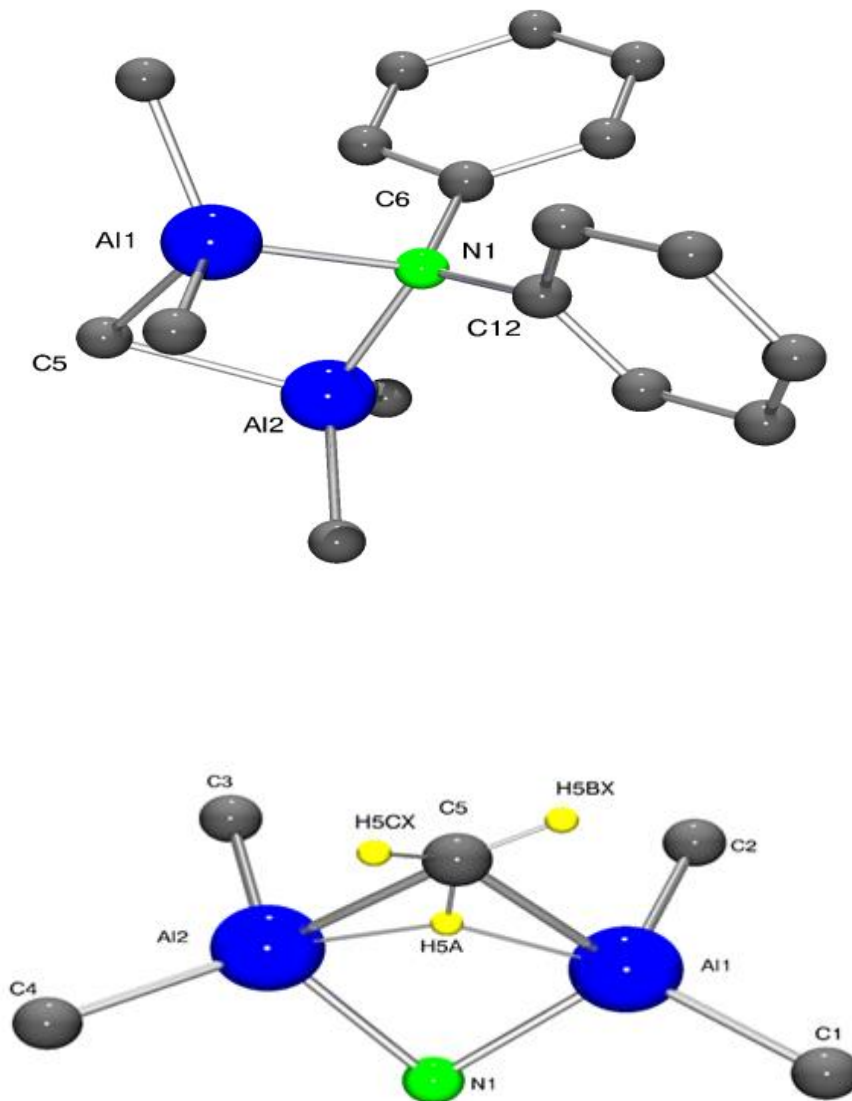

Figure 61. Top**:** Molecular structure of {Ph$_2$N[(Me$_2$Al)$_2$μ-Me]} (**29**), showing the atom numbering scheme. Bottom: Structure around Al(1) and Al(2) core. Selected bond lengths (Å) and angles (°): Al(1)–N(1) 2.0014(18), Al(2)–N(1) 1.9944(18), Al(1)–C(5) 1.957(2), Al(2)–C(5) 2.145(2); Al(1)–N(1)–Al(2) 85.90(7), Al(1)–C(5)–Al(2) 78.77(8), C(6)–N(1)–C(12) 113.15(15).

Introduction of an extra carbon in the form of benzhydrylamine and subsequent treatment with two equivalents of Me_3Al led to the formation of $[Ph_2CHNH(\mu-Me_2Al)]_2 \cdot MeCN$ (**30·MeCN**) in good yield. Single crystals were grown from a saturated acetonitrile solution on prolonged standing (12 h) at 0 °C. The molecular structure is shown in (**Figure 62**); selected bond lengths and angles given in the caption. One Al dimer and one MeCN of crystallization comprise the asymmetric unit. The Al_2N_2 core adopts a shallow butterfly shape with a dihedral angle of 9.66(6)°. Interestingly, the geometrical parameters associated with the Al_2N_2 square are somewhat of a hybrid of those observed for the anisidine derived complexes $\{[1,2-(OMe),N-C_6H_4(\mu-Me_2Al)](\mu-Me_2Al)\}_2$, $[1,3-(Me_3AlOMe),NH-C_6H_4(\mu-Me_2Al)]_2$ and $[1,4-(Me_3AlOMe),NH-C_6H_4(\mu-Me_2Al)]_2$ and the pyrrolyl-methylamide complexes $\{[C_4H_3N(2-CH_2HtBu)]AlH\}_2$ and $\{[C_6H_3N(2-CH_2HtBu)]Al(OCHMe_2)\}_2$ in that the Al–N bond lengths are *ca*. 1.96 Å (found in the 1,4-anisidine derived complex and the pyrrolyl-methylamide), whilst the angles are *ca*. 88 °(found in the 1,2/1,3-anisidine derived complexes).[14] In **30·MeCN**, both N–H groups point 'up', and there is one, well-behaved MeCN solvent molecule of crystallization which is H-bonded to one of the two N–H moieties; the dimensions associated with the H-bonding are given in the (**Appendix table 28**).

118
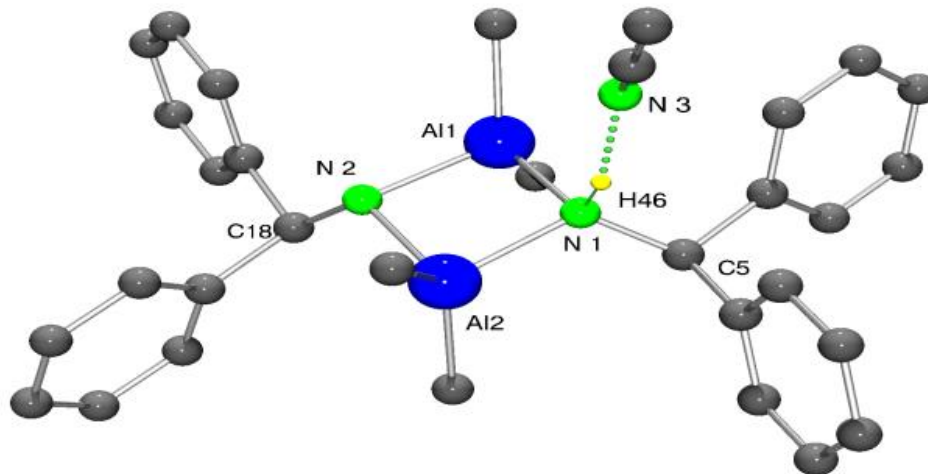
Figure 62. Molecular structure of [Ph$_2$CHNH(μ-Me$_2$Al)]$_2$·MeCN (**30**·MeCN), showing the atom numbering scheme. Most hydrogen atoms have been omitted for clarity. Selected bond lengths (Å) and angles (°): Al(1)–N(1) 1.9597(10), Al(1)–N(2) 1.9484(10), Al(2)–N(1) 1.9620(10), Al(2)–N(2) 1.9528(10), N(1)–C(5) 1.4771(14), N(2)–C(18) 1.4836(13); Al(1)–N(1)–Al(2) 91.72(4); Al(1)–N(2)–Al(2) 92.35(4), N(1)–Al(1)–N(2) 86.67(4), N(1)–Al(2)–N(2) 87.48(4).

3. Ring Opening Polymerization.

3.1 Ring Opening Polymerization of ε-Caprolactone (ε-CL)

Given that aluminium compounds are known to be efficient catalysts for ring opening polymerization (ROP) of cyclic esters, [15] the catalytic behaviour **20 – 30** was explored toward the ROP of ε-CL in the presence of benzyl alcohol (BnOH). One equivalent (per aluminium) of BnOH was employed in the runs herein. Despite the apparent mismatch of stoichiometry, the use of one equivalent of BnOH (per aluminium) for R_2Al containing pre-catalysts is well established; the use of two equivalents (per aluminium) has been found to afford inferior results. [3a,c,e]. Pre-catalyst **21** was employed to ascertain the optimum conditions (**Table 12**), and was found to be effective in the ROP of ε-CL at temperatures of 80 to 110 ^{o}C affording conversions > 67%. According to the entries (1-5), there is an exponential relationship between monomer conversions and M_n values, possibly due to severe catalyst decomposition, with molecular weight distributions [1.08 – 2.14] that suggest there is some degree of control. A linear relationship between [CL]/[Al] ratio and average molecular weight (M_n), suggests the systems still retain the classical features of a living polymerization process (**Figurs 63** and **64**). Elevation of the temperature generally resulted in higher molecular weight polymer and high conversion (**Figure 65)** with an increase in the monomer/Al ratio from 62.5:1 to 1000:1 at 110 °C, the molecular weight increased from 3.1 × 10^3 to 38.5 × 10^3, with little change of PDI (1.23 - 2.08), but producing polymers with lower molecular weight than the calculated M_n values. Prolonging the

reaction time to 12 h (runs 8 and 9) led to decreased conversions rates, presumably due to catalyst decomposition.

Table 12. ROP of ε-caprolactone using Al complex **21**

Run	T (°C)	[CL] : [M]:[BnOH]	Time (h)	Conv^a (%)	$M_n{}^b{}_{GPC}$	$M_{n,Cal}{}^c$	PDI^d
1	110	62.5:1:1	3	55	3100	4030	1.23
2	110	125 : 1:1	3	75	8240	13520	1.64
3	110	1000:1:1	3	99	38530	113110	2.08
4	110	125 : 1:1	5	96	11720	13540	1.66
5	110	250 : 1:1	5	95	17190	27080	2.03
6	110	500: 1:1	12	87	18450	49030	1.08
7	110	750 : 1:1	12	62	--	--	--
8	80	125 : 1:1	3	91	10340	12970	1.77
9	80	250 : 1:1	3	95	17340	26790	1.54
10	60	125 : 1:1	3	97	12310	13820	2.14
11	60	250 : 1:1	3	95	18170	27080	1.76
12	40	125 : 1:1	3	94	7400	13150	1.43
13	40	250 : 1:1	3	45	--	--	--
14	20	125 : 1:1	3	89	3210	12680	1.12
15	20	250 : 1:1	3	35	--	--	--
16	80	125 : 1:1	5	95	11100	13540	1.65
17	80	250 :1:1	5	96	18640	27360	1.60
18	60	125:1:1	5	72	--	--	--
19	60	250:1:1	5	79	3440	22520	1.28

Runs conducted in toluene using 0.05 mmol of catalyst; CL = ε-caprolactone. ^{a} Determined by ^{1}H NMR spectroscopy; ^{b} M_n GPC values corrected considering Mark-Houwink factors (0.56 poly(ε-caprolactone)) from polystyrene standards in THF. ^{c} Calculated from ([Monomer]$_0$/[OH]$_0$) × conv.(%) × Monomer molecular weight + Molecular weight of BnOH. ^{d} From GPC.
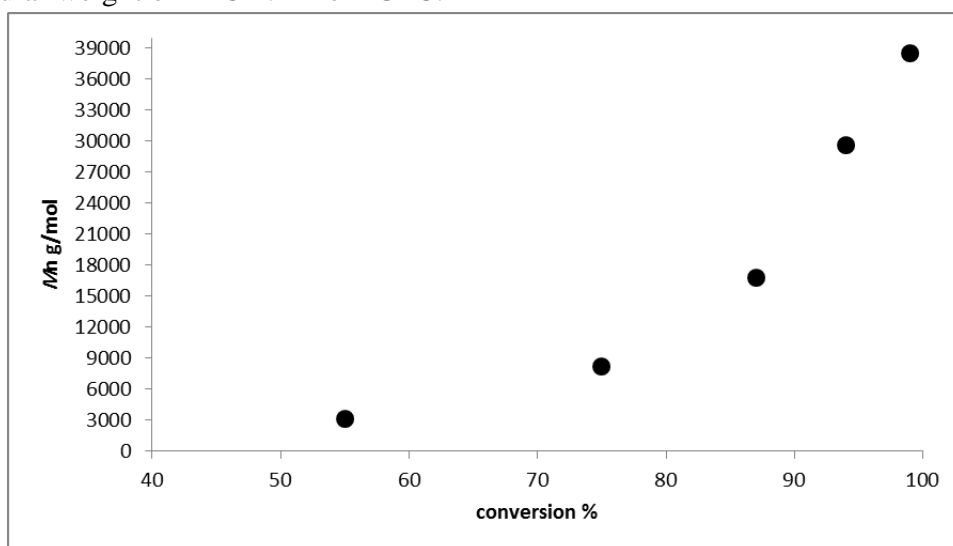

Figure 63. Plot of monomer conversion *versus* number average molecular weight for **21**.
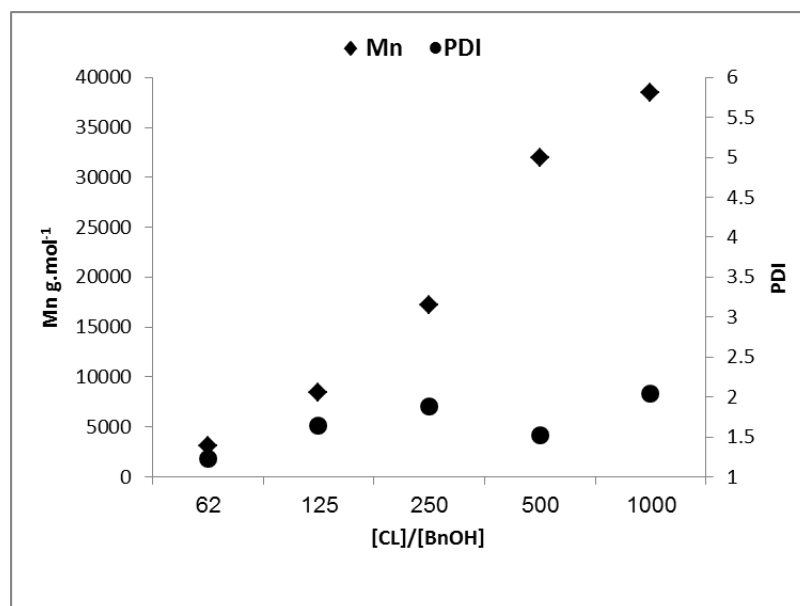
Figure 64. Relationship between M_n and PDI of the polymer and the mole ratio [CL]/[BnOH] using **21**.
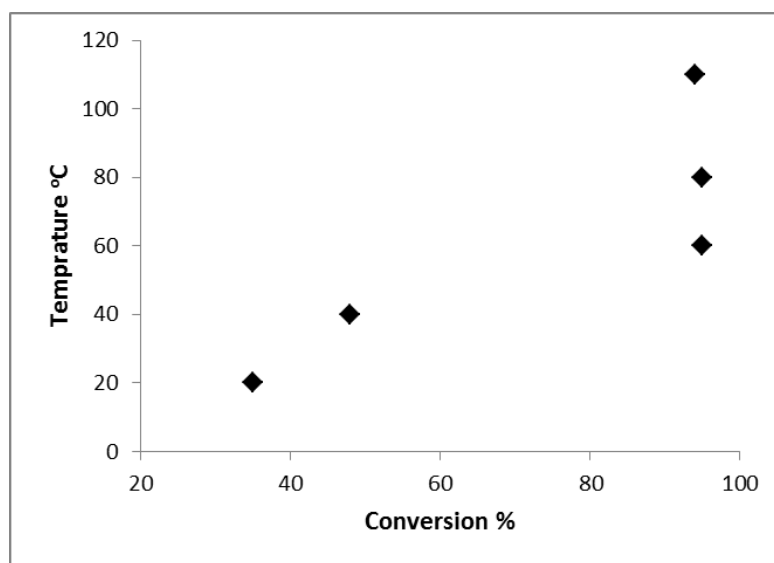

Figure 65. Temperature *versus* monomer conversion in the ROP of CL catalysed by **21**/BnOH.

In addition, we investigated the behaviour of the other complexes herein towards the ROP of ε-CL, using the ratio 250:1:1 (**Table 13**). Generally, these aluminium complexes displayed good catalytic conversions, particularly at temperatures of 80 °C or higher (> 92%). Catalytic systems employing complexes **26**, **28**, **29** and **30** outperformed the others at 110 °C, affording quantitative conversions in over

122

13 mins or less. For complexes **20-25**, the trend is for the methyl derivatives to outperform the ethyl derivatives at both 80 and 100 °C, a trend that has been seen previously[16]. the opposite trend has also been reported.[3z] Within the series **20-25**, on changing the sterics of the precursor aniline, there is little change in the conversion rates for either the methylaluminium or ethylaluminium derivatives. Typically, on increasing the temperature, the conversion rates increase, e.g. (**Appendix figure 150)** for complex **24**. In the case of the systems derived from 1-NH$_2$,2-PPh$_2$C$_6$H$_4$ (**27** and **28**), use of complex **28** appears to be more efficient and more controlled (narrower PDI). Similar trends are observed for those systems derived from diphenylaniline with complex **29** outperforming the systems bearing the phenoxyimine motif.

Again, these systems produced polymers with lower molecular weight than the calculated M_n values, particularly at lower temperatures. When conducting the polymerizations in the absence of solvent (**Table 14)**, the observed molecular weights were in general much closer to the calculated M_n values, and at 80 °C for 13 mins or less, all complexes achieved excellent conversions (> 97%) with mostly good control (PDIs 1.33 - 3.55).

^{1}H and ^{13}C NMR spectra of selected polymers (table 13, entries 4 and 11) were obtained in order to verify the molecular weights and to identify the end groups present (**Figures 66.** and **67**). For entries using pre-catalyst **22** (and **24**), peaks at δ 7.33 ppm (C$_6$H$_5$CH$_2$-), 5.27 ppm (C$_6$H$_5$CH$_2$-), and 3.62 ppm (CH$_2$CH$_2$OH) with an integral ratio of 5:2:2 indicated that the polymers were capped by a benzyl alkoxy group and a hydroxyl end group. ^{13}C NMR data also revealed peaks at δ

127.52 ppm (C$_6$H$_5$CH$_2$-), 69.21 ppm (C$_6$H$_5$CH$_2$-) and 64.24 ppm (CH$_2$CH$_2$OH).

The MALDI TOF spectrum of the PCL (**Figure 68**) revealed the presence of a

benzyloxy initiating group and a series of peaks separated by 114.14 mass units
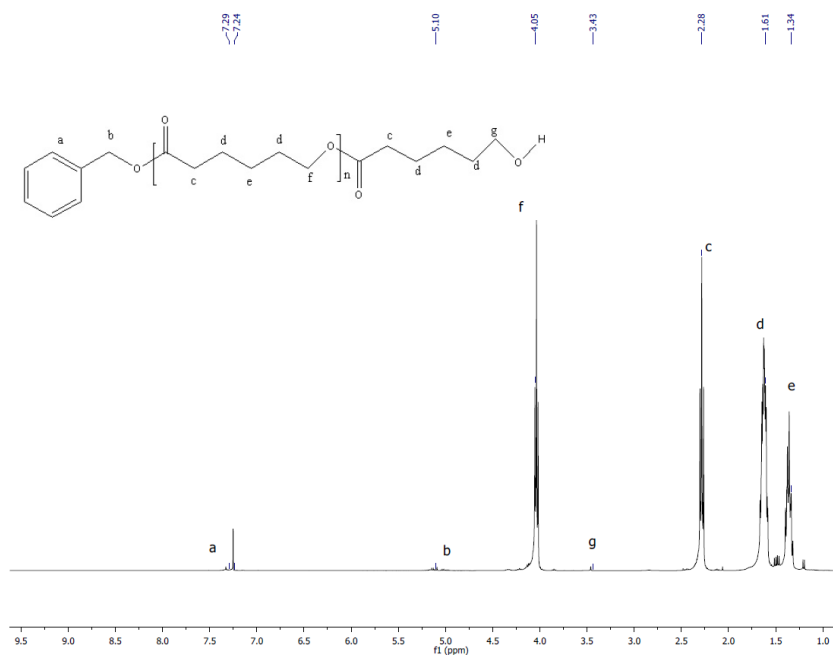
(the molecular weight of the monomer).

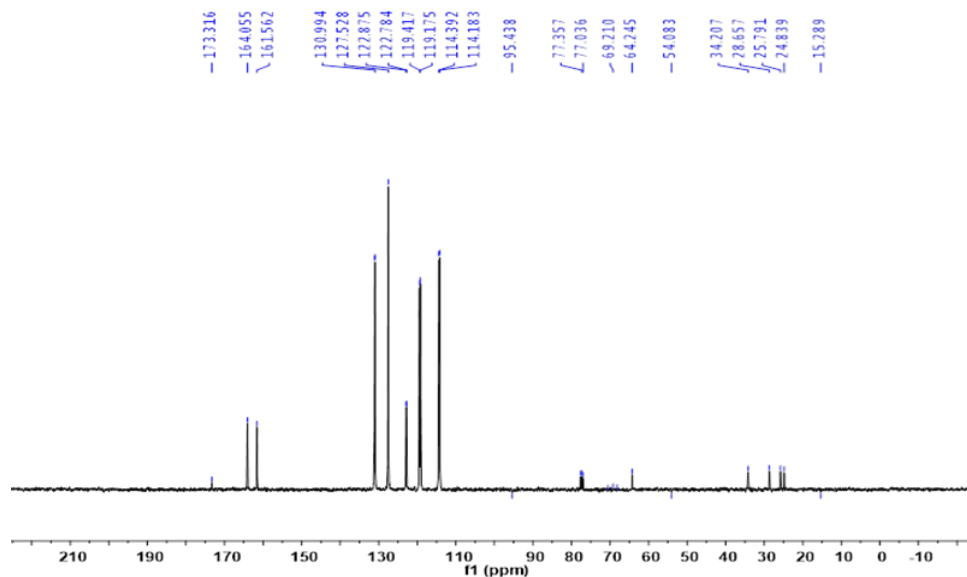**Figure 66.** ^{1}H NMR spectrum of PCL (run 4 table 13).

Figure 67. ^{13}C NMR spectrum of PCL (run 11 table 13).

124

Table 13. ROP of ε-caprolactone using complexes **20 – 30**.

Run	Cat	T (°C)	[CL]: [M]: [BnOH]	Time (h)	Conv^a (%)	M_n^b,GPC	$M_{n,Cal}^c$	PDI^d
1	**20**	80	250 : 1:1	3	97	24690	27790	1.23
2	**20**	110	250 : 1:1	3	96	13340	27500	1.73
3	**20**	110	250 : 1:2	3	89	4670	12750	1.65
4	**22**	80	250 : 1:1	3	95	17340	27220	1.54
5	**22**	110	250 : 1:1	3	93	13480	26650	1.73
6	**22**	110	250 : 1:2	3	94	4150	13470	1.52
7	**23**	80	250 : 1:1	3	65	3660	18660	1.23
8	**23**	110	250 : 1:1	3	92	6300	26360	1.46
9	**24**	25	250 : 1:1	3	67	3840	19230	1.12
10	**24**	45	250:1:1	3	75	4690	21510	1.17
11	**24**	60	250 : 1:1	3	90	5650	25790	1.19
12	**24**	80	250 : 1:1	3	95	15830	27220	1.76
13	**24**	110	250 : 1:1	3	96	16050	27500	1.36
14	**24**	110	250 : 1:2	3	85	5120	12180	1.47
15	**25**	80	250 : 1:1	3	84	2500	24080	1.63
16	**25**	110	250 : 1:1	3	95	2770	27220	1.21
17	**26**	25	250 : 1:1	1	35	1180	10000	1.01
18	**26**	80	250 : 1:1	1	99.5	7120	28360	1.69
19	**26**	110	250 : 1:1	13min	100	10770	28650	1.81
20	**27**	80	250 : 1:1	3	80	---	---	---
21	**27**	110	250 : 1:1	1	99	4670	28360	1.52
22	**27**	110	250 : 1:1	3	99.7	10190	28560	1.60
23	**28**	25	250 : 1:1	1	65	2070	18660	1.11
24	**28**	80	250 : 1:1	1	98	7770	28070	1.28
25	**28**	110	250 : 1:1	5min	98	7690	28070	1.32
26	**28**	110	250 : 1:1	1	100	17240	28640	1.28
27	**28**	110	250 : 1:2	1	96	9000	13750	1.28
28	**29**	25	250 : 1:1	1	45	4950	12950	1.08
29	**29**	110	250 : 1:1	10min	100	29040	28640	1.63
30	**29**	110	250 : 1:2	1	93	3730	13270	1.19
31	**30**	25	250 : 1:1	1	94	10520	26930	1.12
32	**30**	110	250 : 1:1	3 min	100	27380	28640	1.66
33	**30**	110	250 : 1:2	1	95	5470	13610	1.95

Runs conducted in toluene using 0.05 mmol of catalyst; CL = ε-caprolactone. ^{a} Determined by ^{1}H NMR spectroscopy; ^{b} M_n GPC values corrected considering Mark-Houwink factors (0.56 poly(ε-caprolactone)) from polystyrene standards in THF. ^{c} Calculated from ([Monomer]$_0$/[OH]$_0$) × conv.(%) × Monomer molecular weight + Molecular weight of BnOH. ^{d} From GPC.

Table 14. ROP of ε-caprolactone catalyzed by aluminium complexes **20**-**30** in the absence of solvent.

Run	Cat	Time/min	T /°C	[CL]:[Cat]:[BnOH]	$M_{n,GPC}$[a]	$M_n$cal[b]	PDI[c]	Conv.%[d]
1	**20**	7	80	250:1:1	13500	28590	2.76	99.8
2	**21**	5	80	250:1:1	9340	28560	1.74	99.7
3	**22**	5	80	250:1:1	13460	28560	2.03	99.7
4	**23**	5	80	250:1:1	2920	28360	2.91	100
5	**24**	5	80	250:1:1	31230	28640	3.55	99.7
6	**25**	5	80	250:1:1	28860	28500	2.04	100
7	**26**	5	80	250:1:1	39400	28650	2.09	100
8	**27**	60	80	250:1:1	7600	27680	1.32	97
9	**28**	3	80	250:1:1	15450	28650	1.75	100
10	**29**	13	80	250:1:1	28880	28640	1.33	100
11	**30**	15	25	250:1:1	5220	22930	1.28	80
12	**30**	3	80	250:1:1	27480	28640	1.64	99.6

[a] M_n values were determined by GPC in THF *vs*. PS standards and were corrected with Mark–Houwink factor of 0.56. [b] (F.W. monomer × [monomer]/[cat]) × conversion + F.W. BnOH. [c] M_w/M_n were determined by GPC. [d] Determined by ^{1}H NMR spectroscopy.
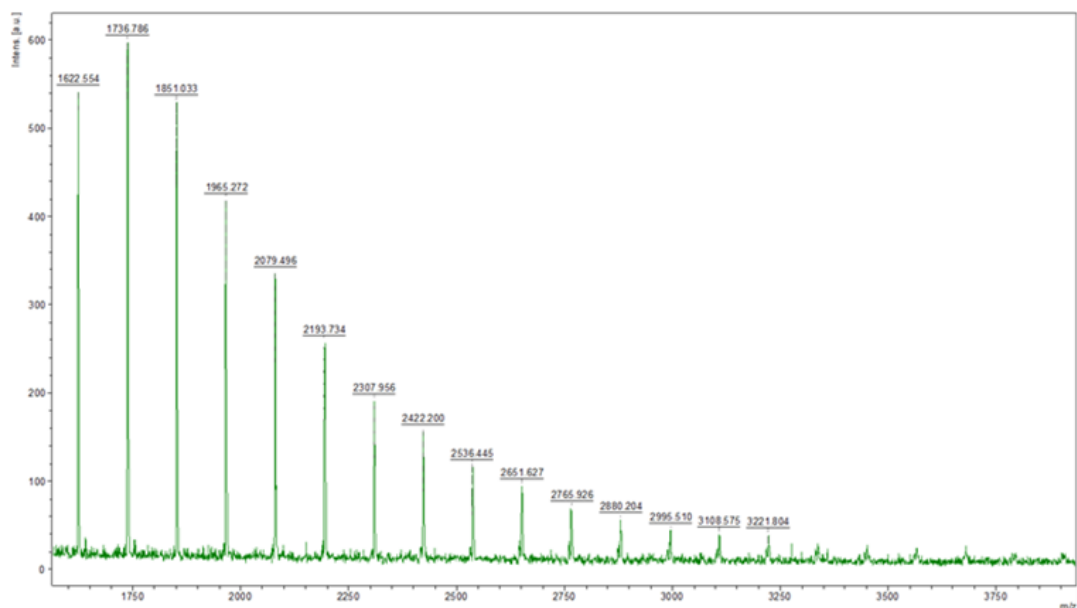

Figure 68. MALDI-ToF spectrum of PCL (run 21, table 13)

A kinetic study of the CL polymerization using **20, 24, 28** and **29 Figure 68** was undertaken by removing 0.3 ml from the reaction mixture and analyzing by ^{1}H NMR spectroscopy at the appropriate time under the conditions [CL]:[**Cat**]:[BnOH] = [250]:[1]:[1] at 80 °C in toluene. The polymerization rate of the ROP of CL exhibited a first order dependence on the CL concentration (Figure 68, left) and that the CL conversion reached >95 % over 80 min (**Figure 69,** right). From (**Figure 69**), the rate order **20** > **24** > **28** > **29** was observed suggesting that the presence of the phenoxy (salicylaldimine) motif may well be beneficial, although this is only a tentative suggestion given the differing structures of the complexes. Indeed, it could be argued that the presence of the multiple metal centres in **28** and **29** is detrimental to the rate. The data here (and that for the ROP of *rac*-LA) also suggested that these catalysts require an induction period, suggestive of slow activation.
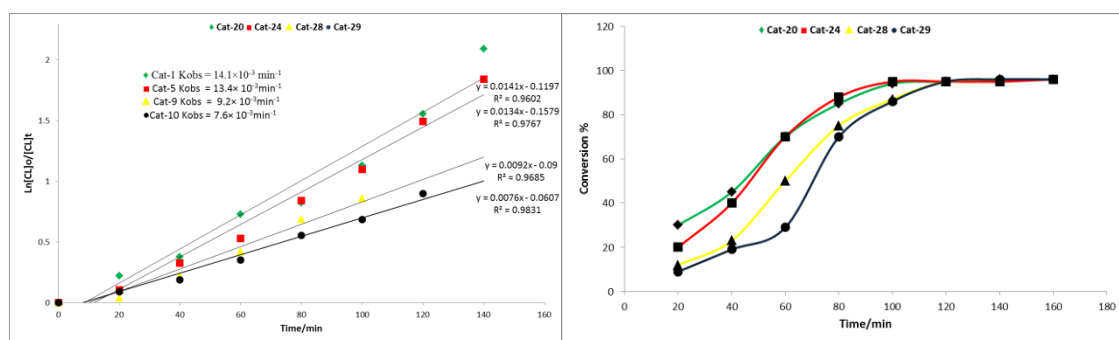

Figure 69. Left: Plot of ln[CL]$_o$/[CL]$_t$ *vs* time using complex **20**, **24**, **28** and **29**; Right : Relationship between conversion and time for the polymerization of CL using complex **20**, **24**, **28** and **29**

3.2 Ring Opening Polymerization (ROP) of rac-Lactide (LA)

The ROP of *rac*-Lactide (LA) was conducted using **20 – 30** in the presence of BnOH. All complexes were active, and the polymerizations were mostly well controlled (PDIs 1.04 – 2.36; only 3 runs gave PDIs > 1.5), although conversions were somewhat lower than those observed for ε-CL. Indeed, in most cases, it proved necessary to conduct the polymerizations over 12 h to achieve reasonable conversion. Increasing the molar ratio of [*rac*-LA] to [Al] did not drastically influence the conversion rates but appeared, in general, to increase the polymer molecular weight (M_n); increasing the polymerization time tended to have the same effect. The relationship between M_n and PDI of the polymer and the mole ratio [*rac*-LA]/[BnOH] for **22** (**Table 15**) entries 4-8 is displayed in (**Figure 70**), and reveals a saturation curve for the former. In the case of the PDI, the relationship with [LA]/[BnOH] suggests that transesterification might be an issue at high monomer loadings leading to molecular weight suppression. For **22** (**Table 15,** entries 4-8) the relationship between monomer conversions and M_n values (**Figure 71)** is exponential.

^{1}H and ^{13}C NMR spectra of selected polymers (**Table 15**), entries 3 and 14 were obtained in order to verify the molecular weights and to identify the end groups present (**Figures 72)** and **73**. For entries using pre-catalyst **24** and **25**) peaks at δ 7.12, 5.11, and 3.60 ppm (5:2:2) indicated that the polymers were capped by a benzyl alkoxy group and a hydroxyl end group consistent with insertion of a benzyloxy group during polymerization. ^{13}C NMR data also revealed peaks at δ 127.63 ($C_6H_5CH_2$-), 69.06 ($C_6H_5CH_2$-) and 63.99 ppm (CH_2CH_2OH). The

MALDI TOF spectrum of the *rac*-LA (**Figures 74**, **75**) revealed the presence of a

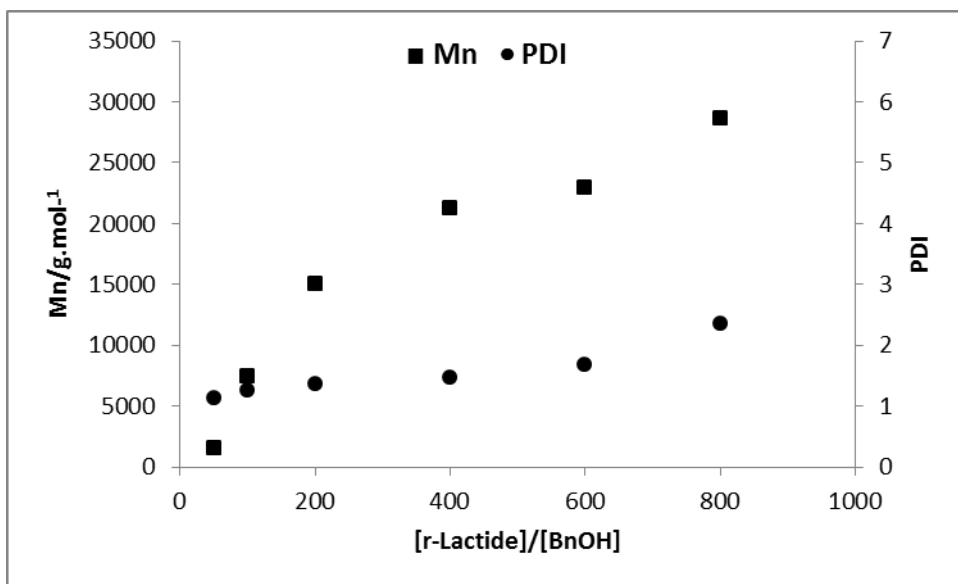benzyloxy initiating group and a series of peaks separated by 72 mass units.

Figure 70. Relationship between M_n and PDI of the polymer and the mole ratio [*rac*-LA]/[BnOH] for **22** (table 15).
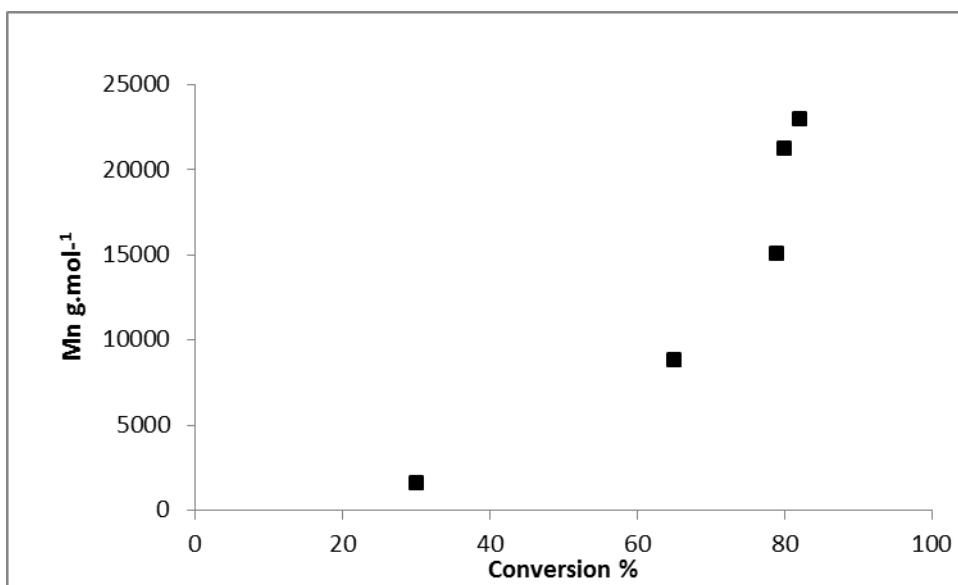

Figure 71. Plot of monomer conversion *versus* number average molecular weight using **22** (runs 4-8, table 15).

Table 15 ROP of *rac*-Lactide (LA) using complexes **20-30**.

Run	Cat	T (°C)	[*r*-lactide] :[cat]:[BnOH]	Time (h)	Conv[a] (%)	M_n^b,GPC	M_n,cal[c]	PDI
1	**20**	110	100 : 1:1	12	75	8770	10920	1.76
2	**20**	110	200 : 1:1	12	78	10180	22590	1.32
3	**21**	110	100:1:1	12	64	9800	9330	1.21
4	**22**	110	50:1:1	12	30	1560	2270	1.13
5	**22**	110	100 : 1:1	12	65	7480	9480	1.26
6	**22**	110	200 : 1:1	12	79	15050	22880	1.37
7	**22**	110	400 : 1:1	12	80	21240	46230	1.46
8	**22**	110	600 : 1:1	12	82	22950	70910	1.68
9	**22**	110	800 : 1:1	12	73	28660	84280	2.36
10	**22**	110	400 : 1:1	1	71	6600	41040	1.15
11	**22**	110	100 : 1:1	5	75	4260	10920	1.41
12	**22**	110	400 : 1:1	6	75	6010	43350	1.28
13	**22**	70	400 : 1:1	12	78	6750	45080	1.25
14	**23**	110	400 : 1:1	12	79	11060	45650	1.60
15	**24**	110	100 : 1:1	12	78	6750	11350	1.16
16	**24**	110	200 : 1:1	12	84	8280	24320	1.23
17	**24**	110	400 : 1:1	12	86	7640	49690	1.15
18	**25**	110	100:1:1	12	72	6530	10380	1.19
19	**26**	110	100:1:1	1	---	---	---	---
20	**26**	110	100:1:1	6	65	4370	9480	1.09
21	**26**	110	50:1:1	12	49	2260	3640	1.04
22	**26**	110	100:1:1	12	74	4370	10780	1.09
23	**26**	110	150:1:1	12	80	4520	17400	1.21
24	**26**	110	200:1:1	12	85	6870	24610	1.23
25	**27**	110	100:1:1	1	---	---	---	---
26	**27**	110	100:1:1	6	---	---	---	---
27	**27**	110	100:1:1	12	74	4270	10770	1.27
28	**28**	110	100:1:1	1	---	---	---	---
29	**28**	110	100:1:1	6	55	2810	8040	1.11
30	**28**	110	100:1:1	12	78	4680	11350	1.21
31	**29**	110	100:1:1	12	56	3870	8180	1.23
32	**30**	110	100:1:1	12	72	5330	10380	1.18
33	**30**	110	100:1:2	12	66	3270	4810	1.50

Runs conducted in toluene using 0.02 mmol of catalyst; [a] Determined by ^{1}H NMR spectroscopy; [b] M_n GPC values corrected considering Mark-Houwink factors (0.58 poly (*rac*-lactide)) from polystyrene standards in THF. [c] Calculated from ([Monomer]$_0$/[OH]$_0$) × conv.(%) × Monomer molecular weight;
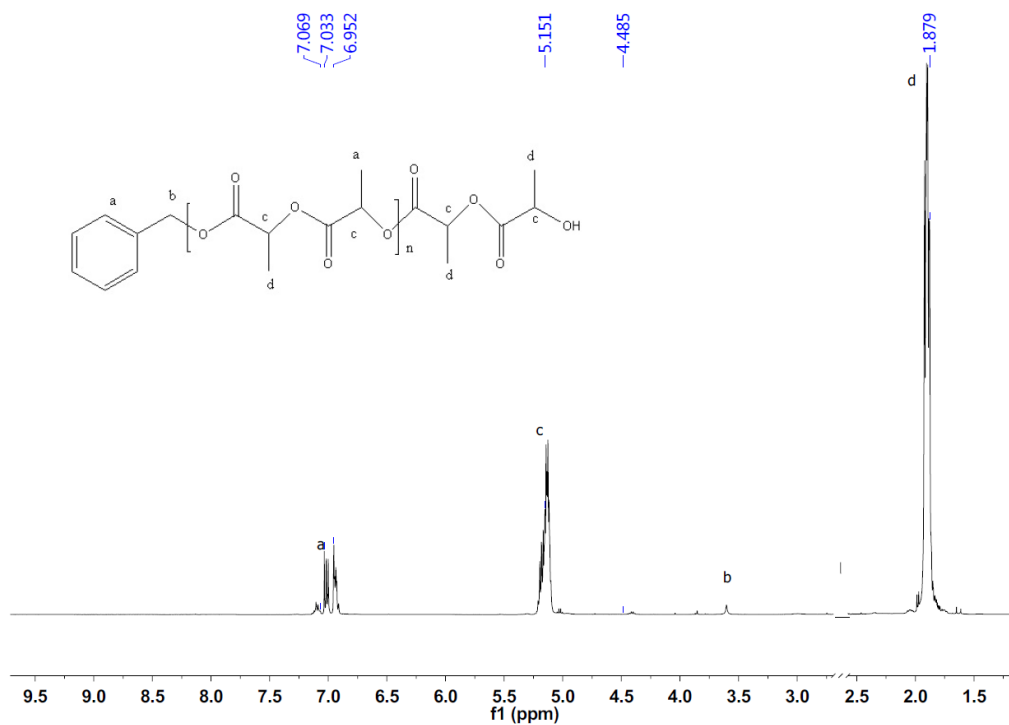
Figure 72. ^{1}H NMR spectrum of poly(*r*ac-LA) (run 14, table 15).
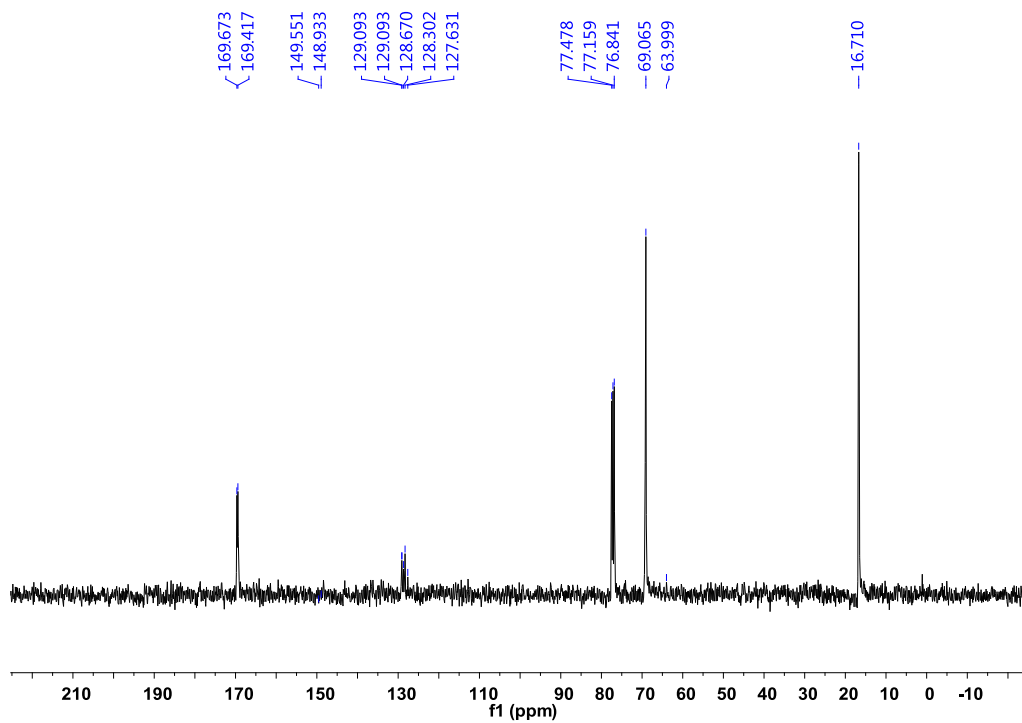

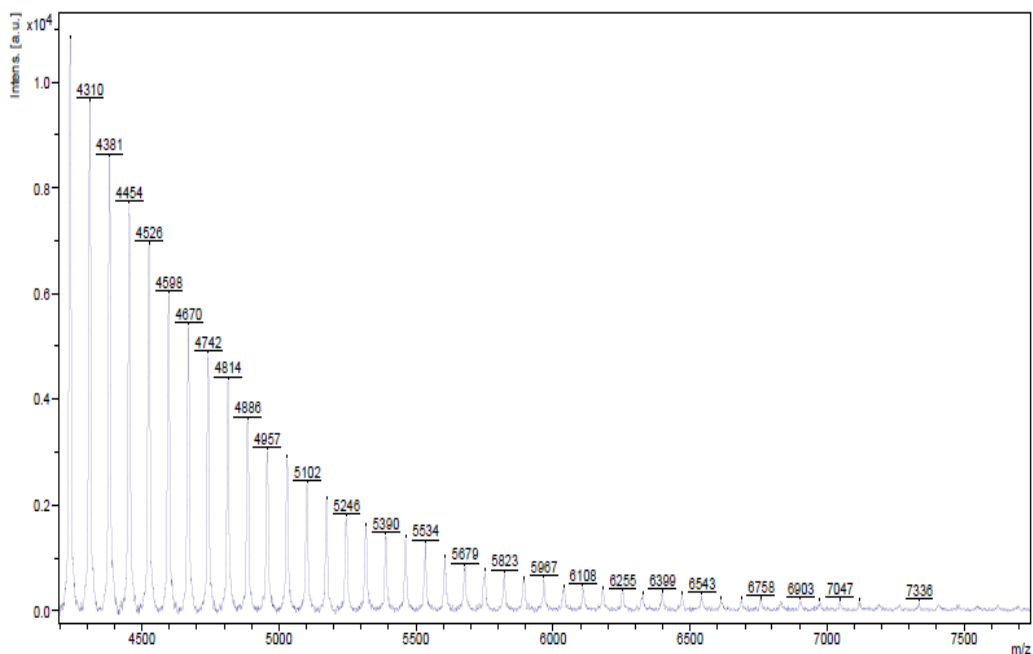**Figure 73**. ^{13}C NMR spectrum of poly(*r*ac-LA) (run 3, table 15).

Figure **74**. MALDI-ToF spectrum of poly(*rac*-LA) (run 16, table 15).
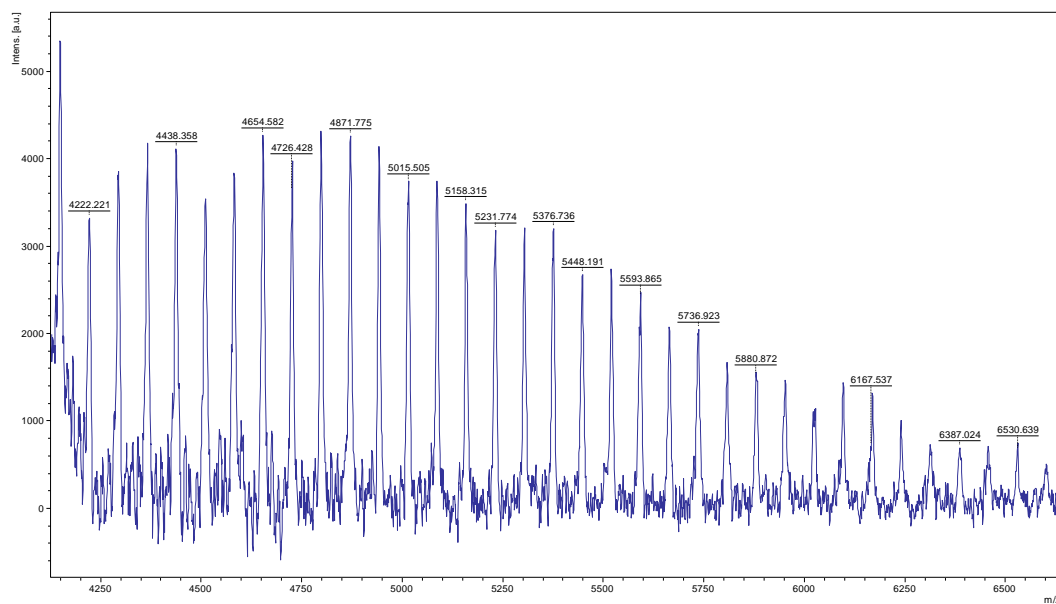

Figure 75. MALDI-ToF spectrum of poly(*rac*-LA) (run 23, table 15).

A kinetic study of the *rac*-LA polymerization using **20**, **24**, **28** and **29** was undertaken by removing 0.3 ml from the reaction mixture and analyzing by ^{1}H NMR spectroscopy at the appropriate time under the conditions [*rac*-LA]:[**Cat**]:[BnOH] = [100]:[1]:[1] at

110 °C in toluene. The polymerization rate of the ROP of *r*ac-LA exhibited a first order dependence on the *r*ac-LA concentration (**Figure 76**), left and that the *rac*-LA conversion reached >70% over 12 h. (**Figure 76**), right. The same order of reactivity was observed here as for the ε-CL case, although for **20** and **24** there was a clear rate enhancement after 6 and 8 h respectively.
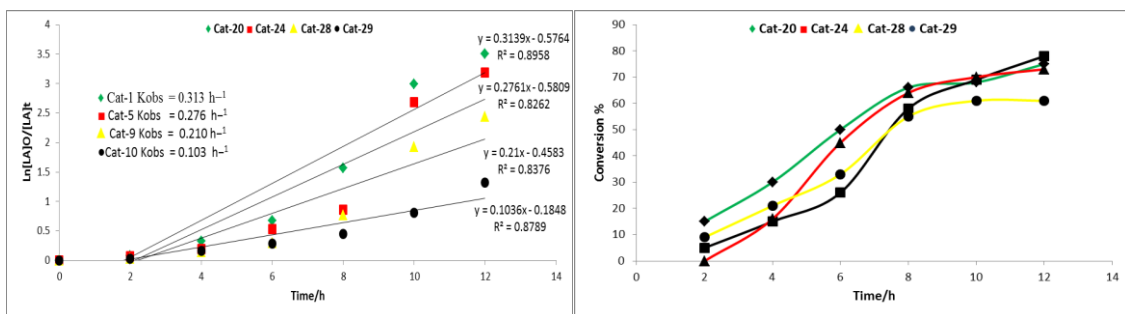

Figure 76. Left: Plot of ln[*r*ac-LA]$_o$/[*r*ac-LA]$_t$ *vs* time using **20**, **24**, **28** and **29**; Right: Relationship between conversion and time of polymerization *r*ac-LA using **20**, **24**, **28** and **29**.

To assign the stereochemistry of the PLA polymers, we employed 2D *J*-resolved and homonuclear decoupled ^{1}H NMR spectroscopy, and assigned peaks by reference to the literature.[15] Representative spectra for runs 21 and 26 are given in the (**Figures 77 – 80**), with the assignments given on the respective figures; these systems gave atactic PLA as reported elsewhere for this observed spectral pattern.[17]
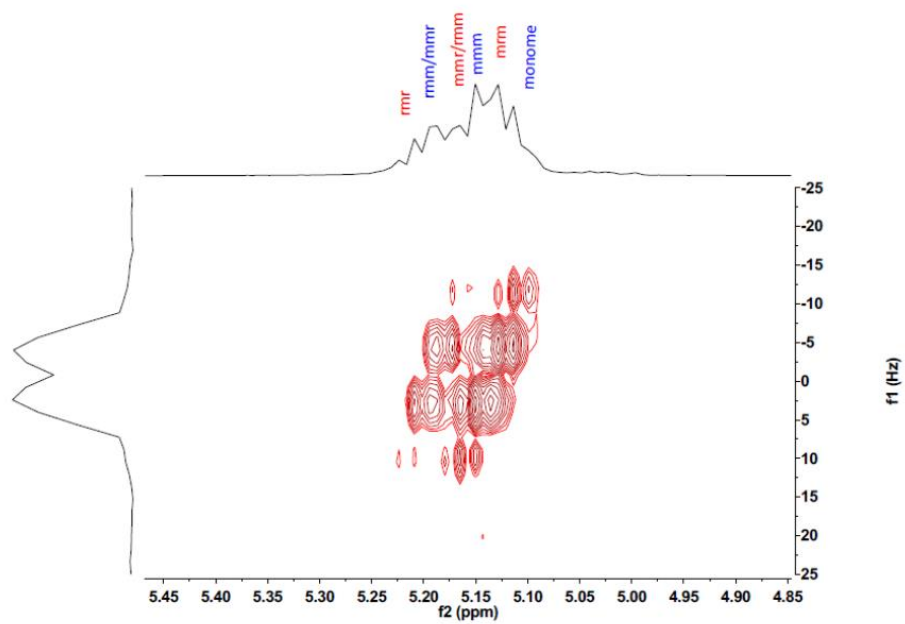
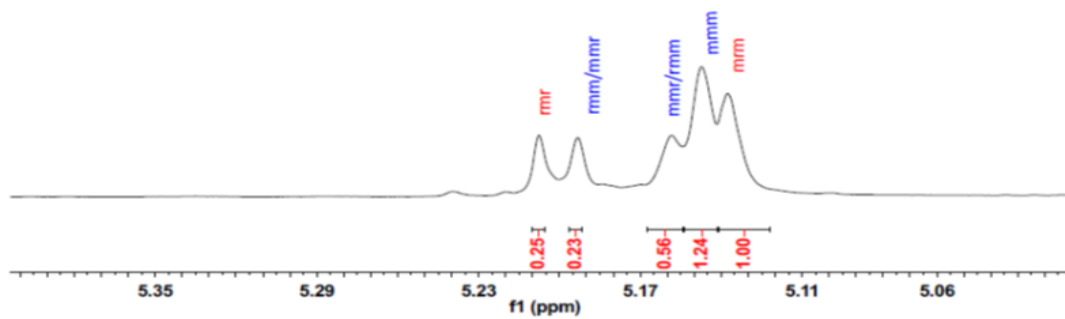**Figure 77.** 2D J-resolved ^{1}H NMR spectrum of poly(*r*ac-LA) (run 11, table 15).

Figure 78. Homonuclear decoupled ^{1}H NMR spectrum of of poly(*r*ac-LA), (run 11, table 15).
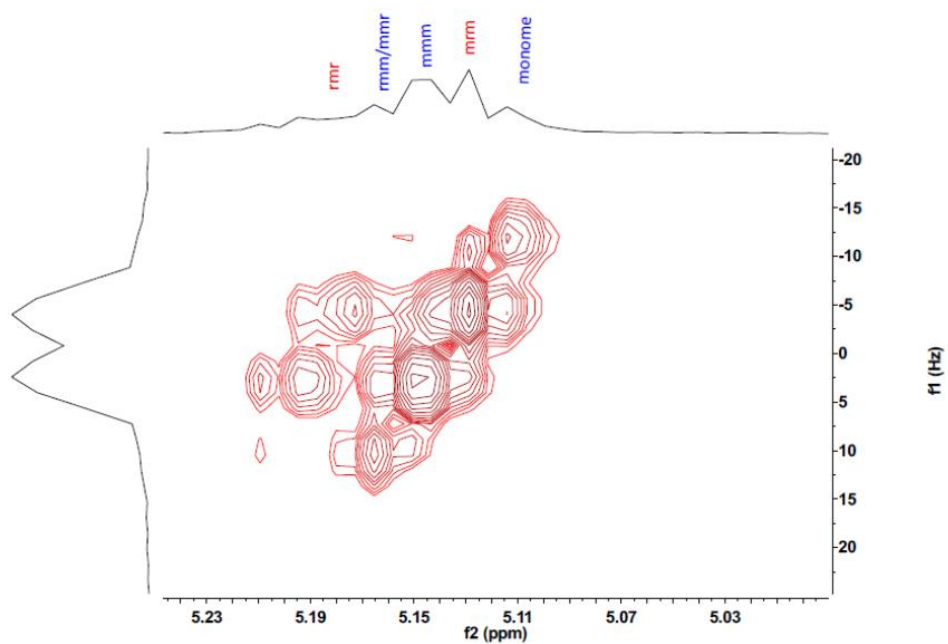
Figure 79. 2D J-resolved ^{1}H NMR spectrum of poly(*r*ac-LA) (run 16, table 15).
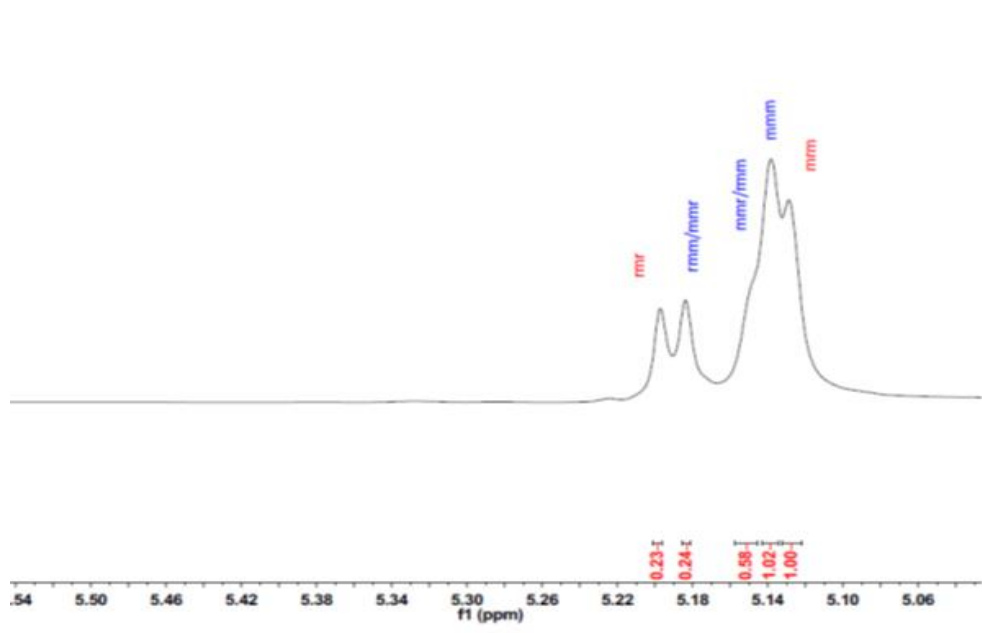

Figure 80. Homonuclear decoupled ^{1}H NMR spectrum of of poly(*r*ac-LA), (run 16, Table 15).

Of the complexes displayed in (**Appendix table 1)**, pre-catalysts **III**, **V**, **X** and **XXVII** closely resemble structures **20** - **27** herein. System **III** bearing an imine-bound pentafluorophenyl group and only one (*ortho*) *tert*-butyl substituent on the phenoxy moiety is more active at lower temperatures over shorter reaction times affording higher molecular weight products, particularly in the case of ε-CL and δ-VL. [3c] Pre-catalyst **V**, bearing a 2,4-difluorophenyl group at N, is a little slower than **III** for the ROP of ε-CL and is comparable with **20** − **27** herein, although the polymer molecular weight is somewhat reduced *cf* **III**, it is still higher than observed for the PCL herein.[3e] System **X**, possessing a *para* isopropyl substituent on the N bound aryl but bearing 3, 5-di-*tert*-butyl groups on the phenoxy as for **20** − **27** herein, has comparable activity for the ROP of *r*-LA requiring 48 h to achieve complete conversion but affords higher molecular weight PLA.[3i] Pre-catalysts **XXVII** possess an N bound CHPh$_2$, but with no *tert*-butyl substituents on the phenoxy (or thiophenoxy) motif,[3z] and these Me$_2$Al systems can most closely be compared with **24**. For ε-CL, results using **24** (run 9, **Table 13**) at ambient temperature are similar to those of the phenoxy version of **XXVII** (M_{nGPC} = 3100, PDI, 89 %) albeit under slightly different conditions (ROP of **XXVII** employed a ratio of 100:1:2 [ε-CL]:[Al]:[OH] over 6 h). For the ROP of *L*-LA, **XXVII** required a higher temperature than for ε-CL (as observed herein) and afforded PLA with M_{nGPC} in the 5000 − 6000 region.

3.3 Co-polymerization of ε-Caprolactone and rac-Lactide (LA)

Complexes **20** - **30** have also been screened for their potential to act as catalysts for the co-polymerization of ε-CL with *rac*-lactide under the optimum conditions found for the homo-polymerizations in toluene, i.e. 80 (ε-CL) or 110 (*rac*-LA) °C over 1 h and 12 h, respectively. In all cases (**Table 16**), good yields (54 - 88%) of co-polymer were formed, and with appreciable lactide content (35 to 62.6%) as observed by ^{1}H NMR spectroscopy (**Figure 81**); both ^{1}H and ^{13}C NMR spectra (**Figue 82**) were assigned as per the literature. [18] The highest % incorporation of LA was found for **1** (62.6%). Observed molecular weights (3680 - 6670) are best described as low to moderate, however we note there is interest in low molecular weight poly(lactide/caprolactone) polymers as bio-adhesives.[19] Thermal analysis of the co-polymers by DSC revealed two melting points at 55.7 °C (PCL) and 125.9 °C (PLA), (**Figure 83**)

Table 16. Synthesis of diblock co-polymers from cyclic ester monomers (ε-CL+ *rac*-LA).

Run[a]	Cat	CL:*r*-LA[b]	Yield	M_n[c]	PDI[d]
1	**20**	37.5:62.5	70	4850	1.31
2	**21**	38.5:61.5	77	5000	1.23
3	**22**	45:55	54	6670	1.43
4	**23**	44.5:55.5	80	6500	1.26
5	**24**	59:41	62	4620	1.29
6	**25**	57.5:42.5	56	4650	1.22
7	**26**	57:43	88	5840	1.34
8	**27**	65:35	55	3680	1.66
9	**28**	55.5:44.5	70	6000	1.23
10	**29**	43.5:56.5	60	5500	1.48
11	**30**	42.5:57.5	65	5770	1.41

[a] Optimum conditions: 1h CL 80 °C/12h *r*-LA 110 °C, (100 ε-CL: 100 *rac*-LA: 1 BnOH). [b] Ratio of ε-CL to *rac*-LA observed in the co-polymer by ^{1}H NMR. [c] M_n values were determined by GPC in THF *vs* PS standards and were corrected with a Mark−Houwink factor ($M_{n, GPC} \times 0.56 \times$ % PCL + $M_{n,GPC} \times 0.58 \times$ % P *r*-LA). [d] PDI were determined by GPC.
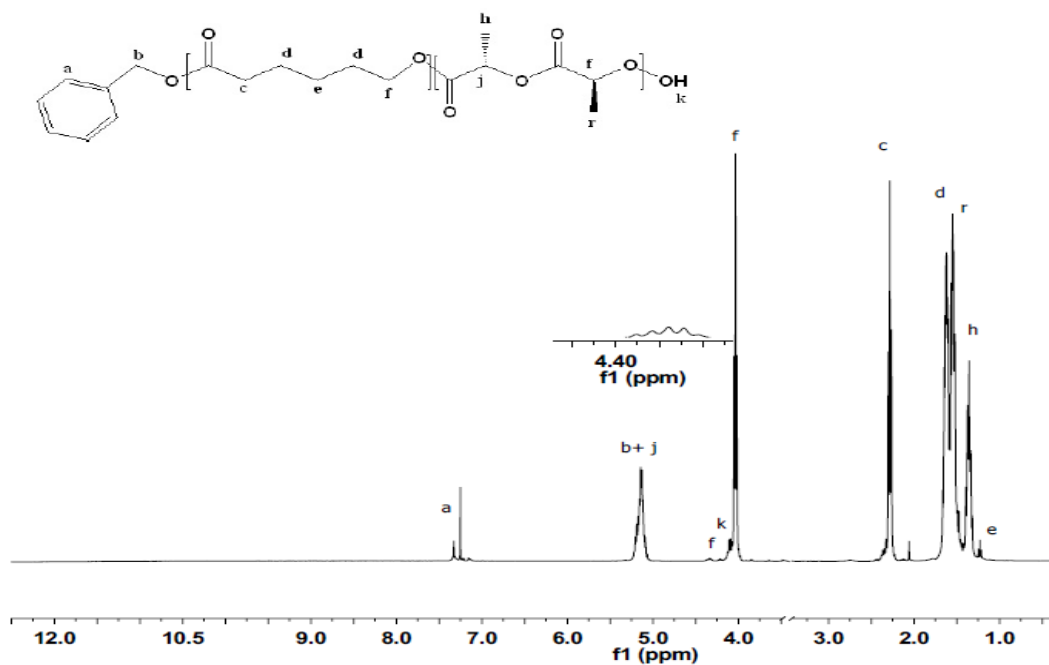
Figure 81. ^{1}H NMR spectrum of copolymer PCL+ poly(*r*-LA), (table 16 run 7).
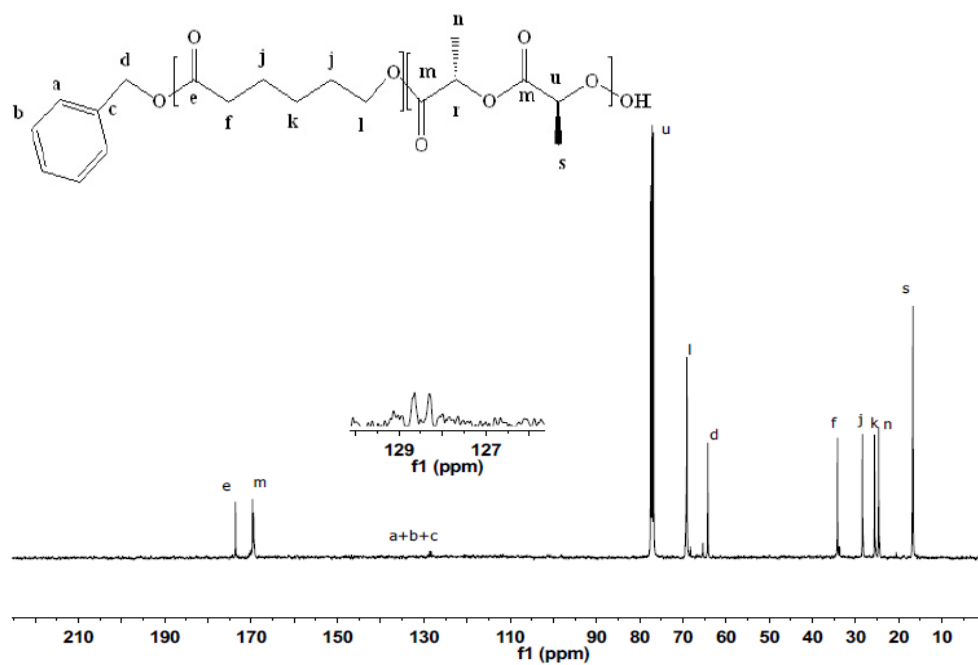

Figure 82. ^{13}C NMR spectrum of co-polymer PCL+ poly(*r*-LA), table 16, run 7.
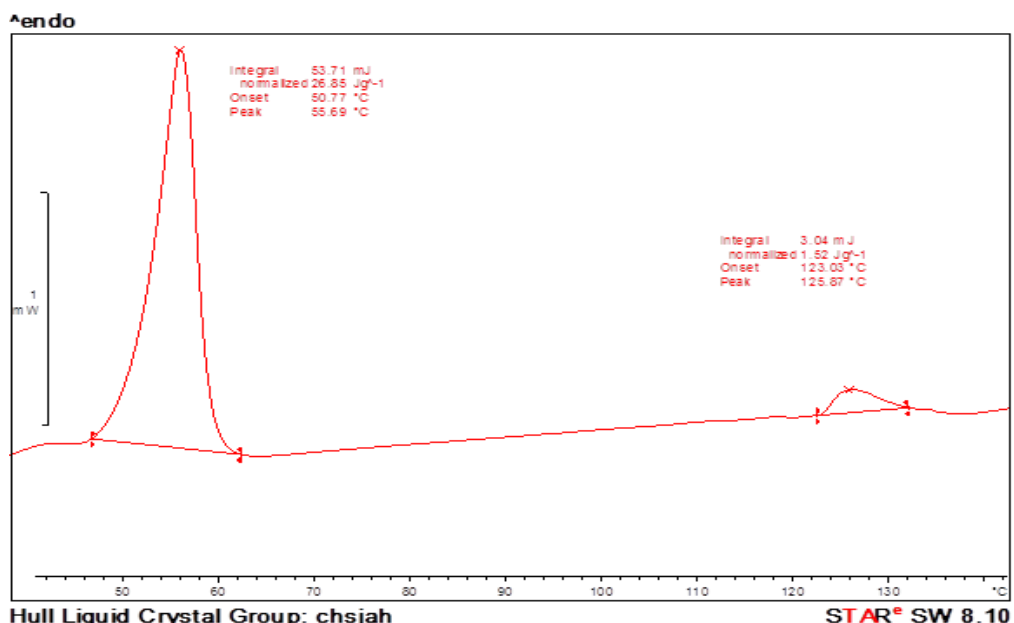
Figure 83. DSC plot of co-polymer from CL and *r*-LA (table 16, run 6).

3.4 Ring Opening Polymerization (ROP) of δ-valerolactone

For the δ-VL ROP reactions (**Table 17**), 110 °C over 12 h was generally required to achieve reasonable conversion, and the resulting ROP reactions were all well-behaved with PDIs in the range 1.10 - 1.73. The relationship between M_n and PDI of the PVL and the mole ratio [VL]/[BnOH] for **24** (**Table 17,** entries 7-10) are near linear (**Figure 84**). Thus, in general, the ROP of δ-VL was slower than that of ε-CL, which is consistent with the thermodynamic parameters for these lactones. [20] Within the series **20** - **25**, % conversions increased on increasing bulk of the aniline derived moiety. In the case of **26** and **27**, the presence of either the amine linkage or phosphine function respectively, appeared to be detrimental to the activity. The non-Schiff-base systems **28** - **30** required longer (24 h) to achieve reasonable % conversion. Molecular weights (M_n) for all systems were

somewhat lower than calculated values. ^{1}H NMR spectra of the resultant polymers (**Figure 85**) indicated the presence of benzyloxy and OH end groups.

Table 17. ROP of δ-valerolactone using Al complex **20-30**

Run[a]	Cat	[δVL] : [Cat] :[BnOH]	Time/h	Conv.%[b]	M_n[c]	$M_{n,Cal}$[d]	PDI[e]
1	**20**	100:1:1	12	34	1920	3510	1.35
2	**21**	100:1:1	12	20	1500	2110	1.23
3	**22**	100:1:1	12	89	3220	9010	1.29
4	**23**	100:1:1	12	60	1900	6110	1.35
5	**24**	100:1:1	6	---	---	---	---
6	**24**	100:1:1	12	97	2790	9820	1.75
7	**24**	50:1:1	24	77	2370	3960	1.43
8	**24**	100:1:1	24	98	3850	9920	1.36
9	**24**	150:1:1	24	97	5350	14680	1.73
10	**24**	200:1:1	24	98	8310	19710	1.38
11	**25**	100:1:1	12	---	500	---	1.03
12	**25**	100:1:1	24	90	3670	9120	1.38
13	**26**	100:1:1	12	72	2280	7310	1.44
14	**27**	100:1:1	12	50	1700	5110	1.13
15	**28**	100:1:1	12	---	510	---	1.01
16	**28**	100:1:1	24	80	4520	8120	1.32
17	**29**	100:1:1	12	---	---	---	---
18	**29**	100:1:1	24	99	7340	10020	1.1
19	**30**	100:1:1	12	---	---	---	---
20	**30**	100:1:1	24	88	3960	8920	1.52

[a]Runs conducted in toluene using 0.05 mmol of catalyst at 110 °C. [b] Determined by ^{1}H NMR spectroscopy; [c,e]GPC. [d]Calculated from ([Monomer]$_0$/[OH]$_0$) × conv.(%) × Monomer molecular weight + Molecular weight of BnOH.
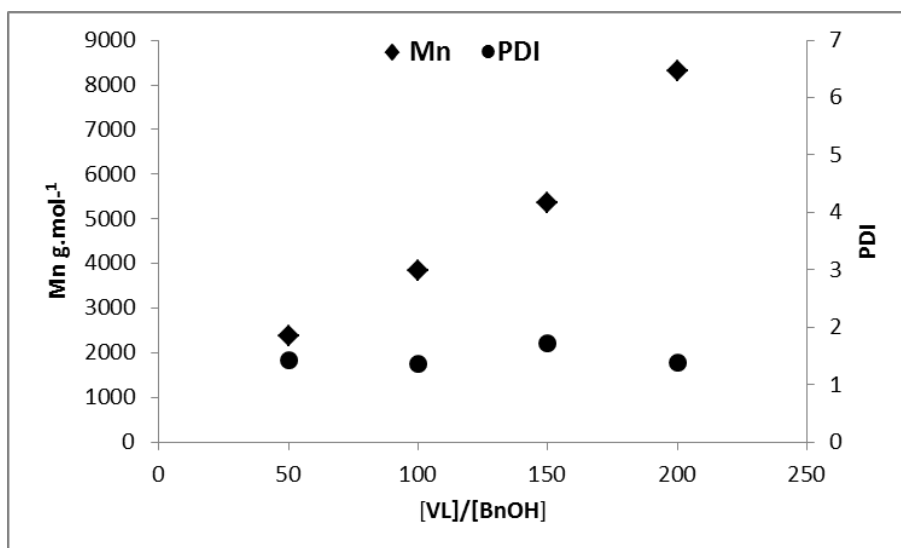

Figure 84. Relationship between M_n and PDI of the polymer and the mole ratio [VL]/[BnOH] using **24**.

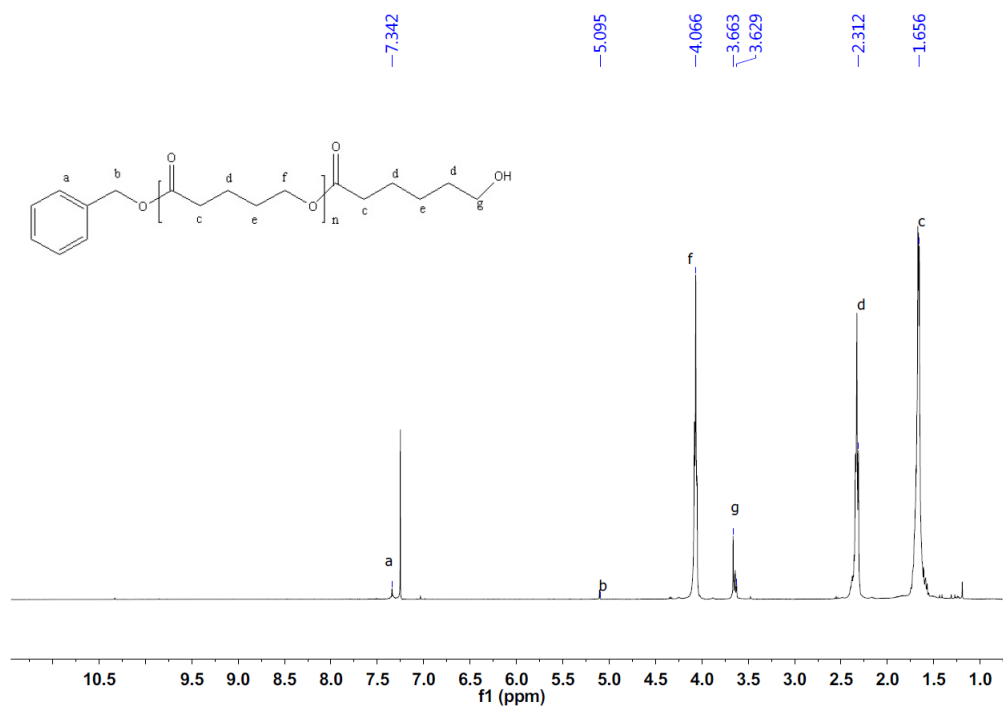**Figure 85.** ^{1}H NMR spectrum of PVL (run 8 table 17) using **24**.

4. Conclusion

In conclusion, a number of organoaluminium phenoximine complexes and have also investigated the structures of the complexes resulting from reaction of the precursor anilines with organoaluminium reagents. In the presence of benzyl alcohol, the complexes were active for the ROP of ε-caprolactone, δ-valerolactone and *rac*-lactide and were also capable of the co-polymerization of ε-caprolactone/*rac*-lactide with decent lactide incorporation. In the case of the ROP of ε-CL and *rac*-LA, there was indication of catalytic misbehaviour with non-linear plots and slightly broad (c.a. 2.0) PDIs. The systems bearing the salicylaldimine motif exhibited increased rates for these ROP studies. However, given that those complexes which did not possess this motif had more than one metal centre present, we can only tentatively propose that the presence of the salicylaldimine (phenoxy) motif is beneficial in the systems studied herein. In the case of δ-valerolactone, shorter polymerization times were possible for the Schiff-base systems.

5. References

[1] (a) N. Iwasa, M. Fujiki and K. Nomura, *J. Mol. Cat. A, Chem.,* **2008**, 292, 67;

(b) C. Zhang and Z. -X. Wang, *J. Organomet. Chem.*, **2008**, 613, 3151; (c) N. Iwasa, J. Liu and K. Nomura, *Catal. Commun.*, **2008**, 9, 1148; (d) J. Liu, N. Iwasa and K. Nomura, *Dalton Trans.*, **2008**, 3978; (e) N. Iwasa, S. Katao, J. Liu, M. Fujiki, Y. Furukawa and K. Nomura, *Organometallics,* **2009**, 28, 2179; (f) N. Nomura, T. Aoyama, R. Ishii and T. Kondo, *Macromolecules,* **2005**, 38, 5363; (g) D. Pappalardo, L. Annunziata and C. Pellecchia, *Macromolecules,* **2009**, 42, 6056. (h) X. -F. Yu and Z. -X. Wang, *Dalton Trans*, **2013**, 42, 3860. (i) T. -L. Huang and C. -T. Chen. *J. Organomet. Chem.*, **2013**, 725, 15. (j) A. Meduri, T. Fuoco, M. Lamberti, C. Pellecchia and D. Pappalardo, *Macromolecules*, **2014**, 47, 534. (k) B. Gao, D. Li, X. Li, R. Duan, X. Pang, Y. Cui, Q. Duan and X. Chen, *Cat. Sci & Tech*. **2015**, 5, 4644.

[2] Of 343 hits for dialkylaluminium where N and O complete the coordination environment, 76 contained chelating phenoxyimine as of March **2016**. F. H. Allen, *Acta Crystallogr., Sect. B: Struct. Sci*., **2002**, 58, 380.

[3] For ROP of cyclic esters utilising aluminium phenoxyimine catalysts see also (**Appendix table 27**.), (a) S. M. Kirk, H. C. Quilter, A. Buchard, L. H. Thomas, G. Kociok-Kohn and M. D. Jones, *Dalton Trans.,* **2016**, 45**,** 13846. (b) B. Gao, D. Li, X. Li, R. Duan, X. Pang, Y. Cui, Q. Duan and X. Chen, *Cat. Sci. & Tech.* **2015**, 5, 4644. (c) M. F. N. Iwasa, K. Nomura, *J. Mol. Cat. A,* **2008**, 292, 67. (d) H. -L. Chen, S. Dutta, P. -Y. Huang and C. -C. Lin, *Organometallics,* **2012**, 31, 2016. (e) N. Iwasa, S. Katao, J. Liu, M. Fujiki, Y. Furukawa and K. Nomura, *Organometallics* **2009**, 28, 2179. (f) J. Yang, Y. Yu, Q. Li, Y. Li and A. Cao, *J.*

Polym. Sci. A: Polym. Chem., **2005**, 43, 373. (g) E. L. Whitelaw, G. Loraine, M. F. Mahon and M. D. Jones, *Dalton Trans.,* **2011**, 40, 11469. (h) D. J. Darensbourg and O. Karroonnirun, *Organometallics,* **2010**, 29, 5627. (i) W. Zhang, Y. Wang, W. -H. Sun, L. Wang and C. Redshaw, *Dalton Trans,.* **2012**, 41, 11587. (j) C. Zhang and Z.-X. Wang, *J. Organomet. Chem.,* **2008**, 693, 3151. (k) C. Di Iulio, M. D. Jones and M. F. Mahon, *J. Organomet. Chem.,* **2012**, 718, 96. (l) C. Agatemor, A. E. Arnold, E. D. Cross, A. Decken and M. P. Shaver, *J. Organomet., Chem.* 2013, **745**, 335. (m) Z. Tang, X. Chen, X. Pang, Y. Yang, X. Zhang and X. Jing, *Biomacromolecules,* **2004**, 5**,** 965-970. (n) X. -F. Yu and Z.-X. Wang, *Dalton Trans.,* **2013**, 42, 3860. (o) H. -L. Han, Y. Liu, J. -Y. Liu, K. Nomura and Y. -S. Li, *Dalton Trans.,* **2013**, 42, 12346. (p) B. Gao, R. Duan, X. Pang, X. Li, Z. Qu, Z. Tang, X. Zhuang and X. Chen, *Organometallics,* **2013**, 32, 5435. (q) I. Taden, H. -C. Kang, W. Massa and J. Okuda, *J. Organomet. Chem.,* **1997**, 540, 189. (r) S. L. Hancock, M. F. Mahon and M. D. Jones, *New J. Chem.,* **2013**, 37, 1996. (s) N. Zhao, Q. Wang, G. Hou, H. Song and G. Zi, *Inorg. Chim. Acta,* **2014**, 413, 128. (t) A. Arbaoui, C. Redshaw and D. L. Hughes, *Chem. Commun.,* **2008**, 4717. (u) A. Alaaeddine, C. M. Thomas, T. Roisnel and J. -F. Carpentier, *Organometallics,* **2009**, 28, 1469. (v) M. Normand, T. Roisnel, J. -F. Carpentier and E. Kirillov, *Chem. Commun.,* **2013**, 49, 11692. (w) C. Kan, J. Ge and H. Ma, *Dalton Trans.,* **2016**, 45, 6682. (x) P. Hormnirun, E. L. Marshall, V. C. Gibson, R. I. Pugh and A. J. P. White, *Proc. Nat. Acad. Sci.,* **2006**, 103, 15343. (y) P. A. Cameron, D. Jhurry, V. C. Gibson, A. J. P. White, D. J. Williams and S. Williams, *Macromol. Rapid Commun.,* **1999**, 20, 616. (z) M. –C. Chang, W. –Y.

Lu, H. –Y. Chang, Y. –C. Lai, M. Y. Chiang, H. –Y. Chen and H. –Y. Chen. *Inorg. Chem.*, **2015**, 54, 11292.

[4] N. Iwasa, J. Liu and K. Nomura, *Cat. Commun.*, **2008**, 9, 1148.

[5] M. Braun, *Angew Chemie.* **1996**, 108, 565; *Angew Chemie. Int. Ed.*, **1996**, 35, 519.

[6] P. A. Cameron, V. C. Gibson, C. Redshaw, J. A. Segal, M. D. Bruce, A. J. P. White and D. J. Williams, *Dalton Trans.*, **1999**, 1883.

[7] S. Milione, F. Grisi, R. Centore and A. Tuzi, *Eur. J. Inorg. Chem.*, **2008**, 5532.

[8] V. C. Gibson, D. Nienhius, C. Redshaw, A. J. P. White and D. J. Williams, *Dalton Trans.*, **2004**, 1761.

[9] (a) C. Redshaw, V. C. Gibson, M. R. J. Elsegood and W. Clegg, *Chem. Commun.*, **2007**, 1951. (b) M. Lappert, A. Protchenko and P. Power in metal Amide Chemistry, *Wiley and Sons*, **2008**. (c) X. –F. Yu and Z. –X. Wang, *Dalton Trans.*, **2013**, 42, 3860.

[10] J. A. Hatnean, J. W. Thomson, P. A. Chase and D. W. Stephan, *Chem. Commun.*, **2014**, 50, 301.

[11] (a) W. Clegg, M. R. J. Elsegood, S. J. Teat, C. Redshaw and V. C. Gibson, *J. Chem. Soc., Dalton Trans.*, **1998**, 3037. (b) W. Clegg, *J. Chem. Soc., Dalton Trans.* **2000**, 3223.

[12] For structurally characterized examples of Al − Me − Al bridges, see (a) R.V. Vranka and E. L. Amma *J. Am. Chem. Soc*., **1967**, 89, 3121. (b) V. R. Magnuson, G. D. Stucky, *J. Am. Chem. Soc.,* **1969***,* 91**,** 2544. (c) S. K. Byram, J. K. Fawcett, S. C. Nyburg and R. J. O'Brien, *J. Chem. Soc. D.*, **1970**, 16. (d) J. C. Huffman and W. E. Streib, *J. Chem. Soc. D.*, **1971**, 911. (e) W. J. Evans, R. Anwander and J. W. Zille, *Organometallics,* **1995**, 14**,** 1107. (f) S. D. Waezsada, F. -Q. Liu, E. F. Murphy, H. W. Roesky, M. Teichert, I. Uson, H.-G. Schmidt, T. Albers, E. Parisini and M. Noltemeyer,

Organometallics, **1997**, 16, 1260. (g) S. D. Waezsada, C. Rennekamp, H. W. Roesky, C. Ropken and E. Parisini, *Z. Anorg. Allg. Chem.*, 1998, 624, 987. (h) W. T. Klooster, R. S. Lu, R. Anwander, W. J. Evans, T. F. Koetzle and R. Bau, *Angew. Chem., Int. Ed.*, **1998**, 37, 1268. (i) E. Ihara, V. G. Young Jr. and R. F. Jordan, *J. Am. Chem. Soc.*, **1998**, 120, 8277. (j) R. Wochele, W. Schwarz, K. W. Klinkhammer, K. Locke and J. Weidlein, *Z. Anorg. Allg. Chem.*, **2000**, 626, 1963. (k) J. E. Kickham, F. Guerin, J. C. Stewart and D. W. Stephan, *Angew Chem. Int. Ed.*, **2000**, 39, 3263. (l) Z. Yu, J. M. Wittbrodt, M. J. Heeg, H. B. Schlegel and C. H. Winter, *J. Am. Chem. Soc.*, **2000**, 122, 9338. (m) J. Klosin, G. R. Roof, E. Y. –X. Chen and K. A. Abbound, *Organometallics,* **2000**, 19, 4684. (n) E. Y. –X. Chen and K. A. Abbound, *Organometallics,* **2000**, 19, 5541. (o) A. Cottone III and M. J. Scott, *Organometallics,* **2000**, 19, 5254. (p) J. E. Kickham, F. Guerin, J. C. Stewart, E. Urbanska and D. W. Stephan, *Organometallics,* **2001**, 20, 1175. (q) A. Cottone III and M. J. Scott, *Organometallics,* **2002**, 21, 3610. (r) G. S. Hair, A. H. Cowley, J. D. Gorden, J. N. Jones, R. A. Jones and C. L. B. Macdonald, *Chem. Commun.*, **2003**, 424. (s) A. J. R. Son, M. G. Thorn, P. E. Fanwick and I. P. Rothwell, *Organometallics,* **2003**, 22, 2318. (t) B. C. Bailey, A. R. Fout, H. Fan, J. Tomaszewski, J. C. Huffman, J. B. Gary, M. J. A. Johnson and D. J. Mindiola, *J. Am. Chem. Soc.*, **2007**, 129, 2234. (u) G. B. Nikiforov, H. W. Roesky, B. C. Heisen, C. Grosse and R. B. Oswald, *Organometallics,* **2008**, 27, 2544. (v) H. M. Dietrich, J. W. Ziller, R. Anwander and W. J. Evans, *Organometallics,* **2009**, 28, 1173. (w) A. –L. Schmitt, G. Schnee, R. Welter and S. Dagorne, *Chem. Commun.*, **2010**, 46, 2480. (x) A. Heman-Gomez, A. Martin, M. Mena and C. Santamaria, *Inorg. Chem.*, **2010**, 49, 8401. (y) G. Occhipinti, C. Meermann, H. M. Dietrich, R. Litlabo, F. Auras, K. W. Tomroos, C. Maichle-Mossmer,

V. R. Jensen and R. Anwander, *J. Am. Chem. Soc.*, **2011**, 133, 6323. (z) N. Dettenrieder, H. M. Dietrich, C. Schadle, C. C. Maichle-Mossmer, K. W. Tomroos and R. Anwander, *Angew. Chem., Int. Ed.,* **2012**, 51, 4461.

[13] (a) S. Hamidi, H. M. Dietrich, D. Werner, L. N. Jende, C. Maichle-Mossmer, K. W. Tomroos, G. B. Deacon, P. C. Junk and R. Anwander, *Eur. J. Inorg. Chem*., **2013**, 2460. (b) G. Theurkauff, A. Bondon, V. Dorcet, J. –F. Carpentier and E. Kirillov, *Angew Chem. Int. Ed*., **2015**, 54, 6343. (c) H. G. Stammler, S. Blomeyer, R. J. F. Berger and N. W. Mitzel, *Angew Chem. Int. Ed*., **2015**, 54, 13816.

[14] (a) Y. Li, K. –Q. Zhao, M. R. J. Elsegood, T. J. Prior, X. Sun, S. Mo and C. Redshaw, *Cat. Sci. & Tech*., **2014**, 4, 3025. (b) Y. –C. Chen, C. –Y. lin, C. –Y. Li, J. –H. Huang, L. –C. Chang and T. –Y. Lee, *Chem. Eur. J.*, **2008**, 14, 9747.

[15] Y. Wei, S. Wang and S. Zhou, *Dalton Trans.*, **2016**, 45, 4471.

[16] (a) N. Iwasa, S. Katao, J. liu, M. Fujiki, Y. Furukawa and K. Nomura, *Organometallics*, **2009**, 28, 2179. (b) D. Li, Y. Peng, C. Geng, K. Liu and D. Kong, *Dalton Trans*., **2013**, 42, 11295. (c) W. –L. Kong, Z. –Y. Chai and Z. –X. Wang, *Dalton Trans*., **2014**, 43, 14470. (d) W. Zhang, Y. Wang, L. Wang, C. Redshaw and W. –H. Sun, *J. Organomet. Chem*., **2014**, 750, 65.

[17] (a) J. –C. Buffet and J. Okuda, *Chem. Commun*., **2011**, 47, 4796. (b) P. Piromjitpong, P. Ratanapanee, W. Thumrongpatanaraks, P. Kongsaeree and K. Phomphrai, *Dalton Trans*., **2012**, 41, 12704.

[18] Y. Liu, W. -S. Dong, J. -Y. Liu and Y. -S. Li, *Dalton Trans*., **2014**, 43, 2244.

[19] S. Sriputtirat, W. Boonkong, S. Pengprecha, A. Petsom and N. Thongchul, *Adv. Chem. Eng. Sci*., **2012**, 2, 15.

[20] P. Dubois, O. Coulembier and J. –M. Raquez, Ring-Opening Polymerization, *Wiley-VCH, Eds*., **2009**.

Chapter 6

Ring opening polymerization of lactides and lactones by multimetallic lithium complexes derived from the acids $Ph_2C(X)CO_2H$ (X = OH, NH_2)

1. Introduction

Coordination chemistry plays a central role in the ring opening polymerization (ROP) of cyclic esters field by allowing for the development of new, efficient, metal-based initiators by manipulation of the coordination environment about the metal centre. In other words, the choice of both the metal centre and the ligand set is crucial in terms of being able to control the features associated with the ROP process such as catalytic activity (% conversion) and the resultant polymer properties. The use of chelating and/or bulky ligands with a variety of metals has proved particularly successful.[1] Redshaw *et al.* have been investigating the use of ligands derived from acids bearing the motif $Ph_2(X)CO_2H$, where X = OH, NH_2, and have previously reported some intriguing molecular structures.[2] The ability of this motif to promote highly crystalline samples was first recognised by Braun.[3] A search of the CSD for compounds incorporating the $Ph_2C(X)$ motif revealed only a limited number of compounds (<40), the majority of which contained no metal.[4] We are also interested in the use of alkali metal species for ROP, given that their use in a number of systems has resulted in promising results with little in the way of side reactions.[5] With this in mind, and given the aforementioned limited coordination chemistry of acids containing the $Ph_2C(X)$ motif, in this chapter our investigations on the use of lithium complexes bearing ligands derived from $Ph_2(X)CO_2H$ are presented, which as well as resulting in some unusual structural motifs incorporating lithium-oxygen rings and ladders (**Scheme 14**), has afforded ROP systems exhibiting reasonable activities and low polydispersities (PDIs). We note that a number of lithium-containing cages, rings

and ladders, supported primarily by phenolate-type ligation, have previously been employed for the ROP of cyclic esters. [5, 6]
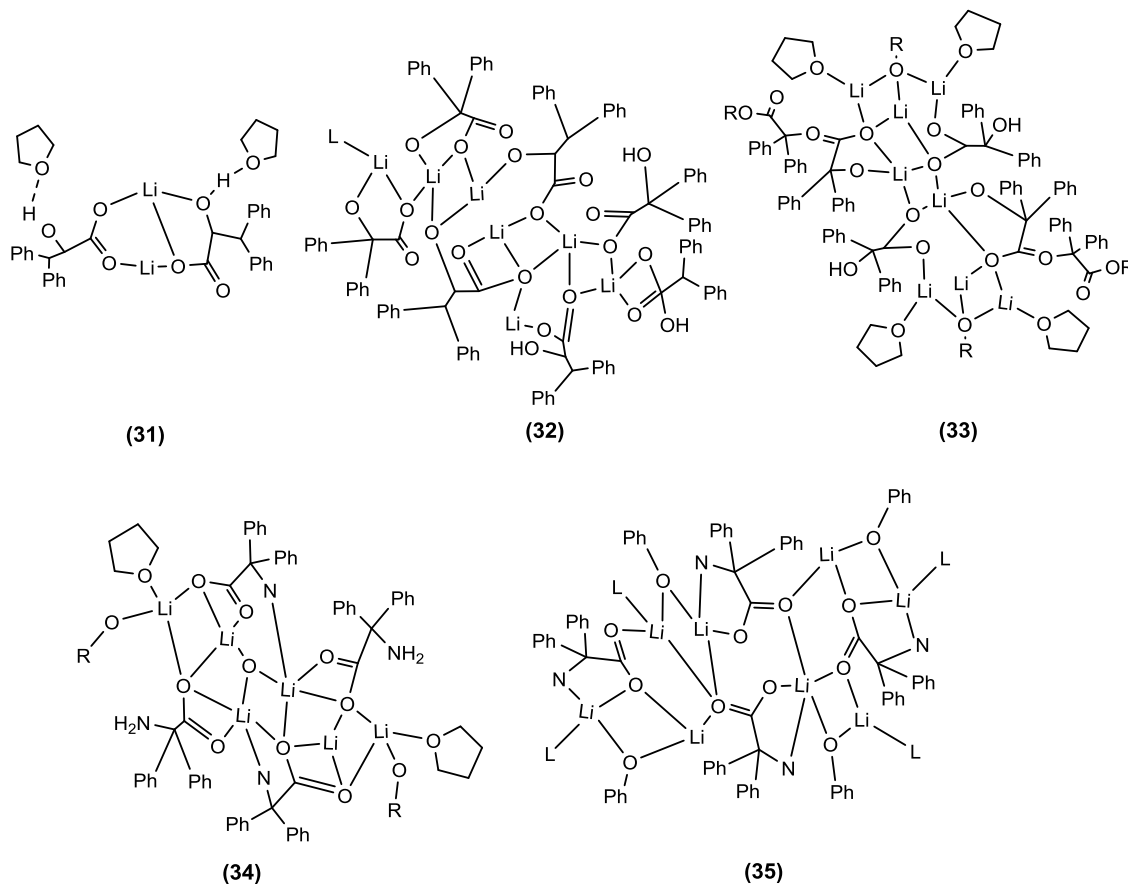
Ph= phenyl, R= ^{t}Bu, L=MeCN

Scheme 14. Complexes used in this chapter.

2. Results and Discussion

2.1 Use of benzilic acid

Our initial studies have focused on the use of benzilic acid, given it is available in bulk quantities at relatively low cost. [7] Using a 1:1 mole ratio of benzylic acid and lithium *tert*-butoxide in THF afforded, following work-up, colourless prisms [Li(benz)(THF)]$_2$·2THF (**31**·2THF) in moderate yield. Single crystals suitable for X-ray diffraction were obtained upon prolonged standing (2 − 3 days) at ambient

temperature. The molecular structure is shown in (**Figure 86**) with selected bond lengths and angles given in the caption. The structure is best described as mono-deprotonated benzilic acid which via Li^+ coordination forms 1D chains. The chains comprise a number of fused 5- and 6-membered rings along the chain/ladder, rather than the more commonly observed Li_2O_2 diamond-like motifs. Both Li1 and Li2 are four coordinate, with distorted tetrahedral geometry and are bound by an 'acid' oxygen from each of three benz ligands plus the hydroxyl from one of them. The Li – O bond lengths [1.89 (2) - 1.97 (2) Å] are comparable with other bimetallic lithium systems in the literature,[8] with those to the μ^3-O atoms O(2) and O(4) being the longest. The carboxylate at C(1) binds in *syn* fashion. The O–H hydrogens of both benz ligands are involved in H-bonding to THF which resides in clefts along the chain (**Appendix figure 151**).
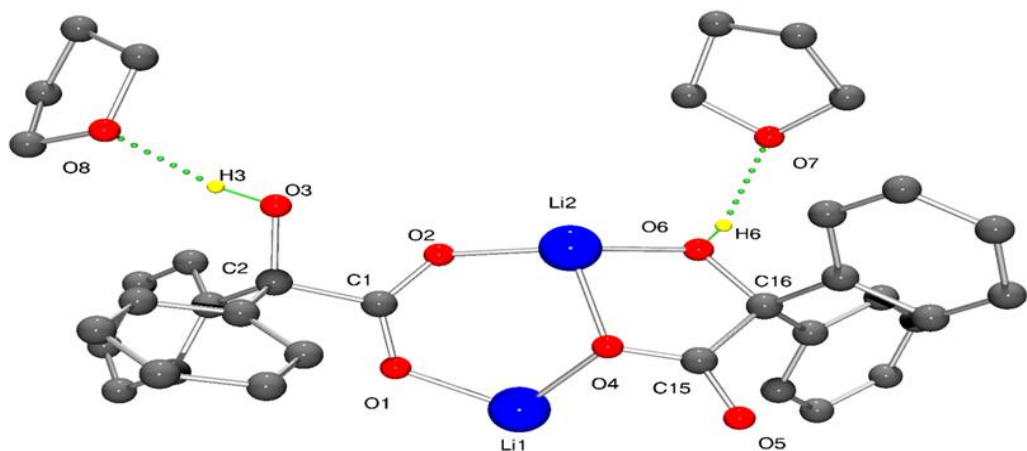
Figure 86. The asymmetric unit in the 1D chain structure of **31**·2THF. Selected bond lengths (Å) and angles (°): Li(1)–O(1) 1.89(2), Li(1)–O(2′) 1.912(19), Li(1)–O(4) 1.96(2), Li(2)–O(2) 1.92(2), Li(2)–O(4) 1.97(2), Li(2)–O(5′) 1.99(2), Li(2)–O(6) 1.94(2); Li(1)–O(2)–Li(2) 109.6(10), Li(1)–O(4)–Li(2) 110.2(9), O(6)–Li(2) – O(4) 80.6(8).

In the packing of the **31**, the 1D chains are aligned parallel to the crystallographic *a* direction. Neighbouring chains connect via van der Waals forces only (**Appendix figures 152**).

Conducting the same reaction, but utilising acetonitrile (MeCN) during work-up under mild conditions, (stirring at room temperature for 10 mins) afforded crystals with two distinct morphologies, namely small needles together with much larger blocks in approximately 70:30 ratio. Both morphologies were subjected to single crystal X-ray diffraction and gave different unit cells, one of which matched **31**. Both structures are 1D polymers, and in each phase, each lithium is surrounded by four oxygen atoms in a flattened tetrahedron. The key difference is in the location of the THF and associated composition and geometry of the Li-benz chain. For **31**, the THF is not bound to Li^+ but is localised by a hydrogen bond from the alcohol of benzilic acid. The chain is composed of five- and six-membered rings.

The structure of the second polymorph **31$^{\prime}$**, which crystallises in the chiral space group $P2_12_12_1$ with a single lithium ion, one benzilic acid and one molecule of THF in the asymmetric unit, could be described as a chain made up from discrete Li(benz)(THF) moieties in which the benzilic acid is bound to Li(1) through a single oxygen of the carboxylate and the alcohol in a 5-membered chelate ring, in other words the benzilic acid is bidentate to the lithium through the O(1) of the carboxylate and the alcohol O(3). The same oxygen atom of the carboxylate also coordinates to a second Li(1) ion generated by symmetry (the so-called

monatomic bridging coordination mode). Critically, in this polymorph, the THF is bound to the Li$^+$ (**Appendix figure 153)**.

The coordination of the lithium is completed by another O(1) atom generated by symmetry to give a tetrahedral arrangement of oxygen atoms. This generates a zigzag chain composed of Li(1) and O(1) atoms that runs parallel to the crystallographic *a* direction (**Appendix figure 154)** O(2) takes no part in binding to Li(1). There is a hydrogen bond between H(3) and O(2) of a neighbouring benzylic acid. This hydrogen bond is approximately along the *a* direction, strengthening the chain.

If, during work-up when employing LiO*t*Bu, the complex is recrystallized from acetonitrile after 10 mins of refluxing, then the complex [Li$_7$(benz)$_7$(MeCN)] (**32**·2MeCN·THF) is formed. In this case, the asymmetric unit contains three molecules of acetonitrile. The crystal structure of **32** (**Figure 87)** was determined using synchrotron radiation for alternative view (**Appendix figure 155)**; the crystal was weakly scattering and has a large asymmetric unit but displays a beautiful structure. The structure crystallises in the centrosymmetric space group $P2_1/n$ with 140 crystallographically-unique non-hydrogen atoms in the asymmetric unit.
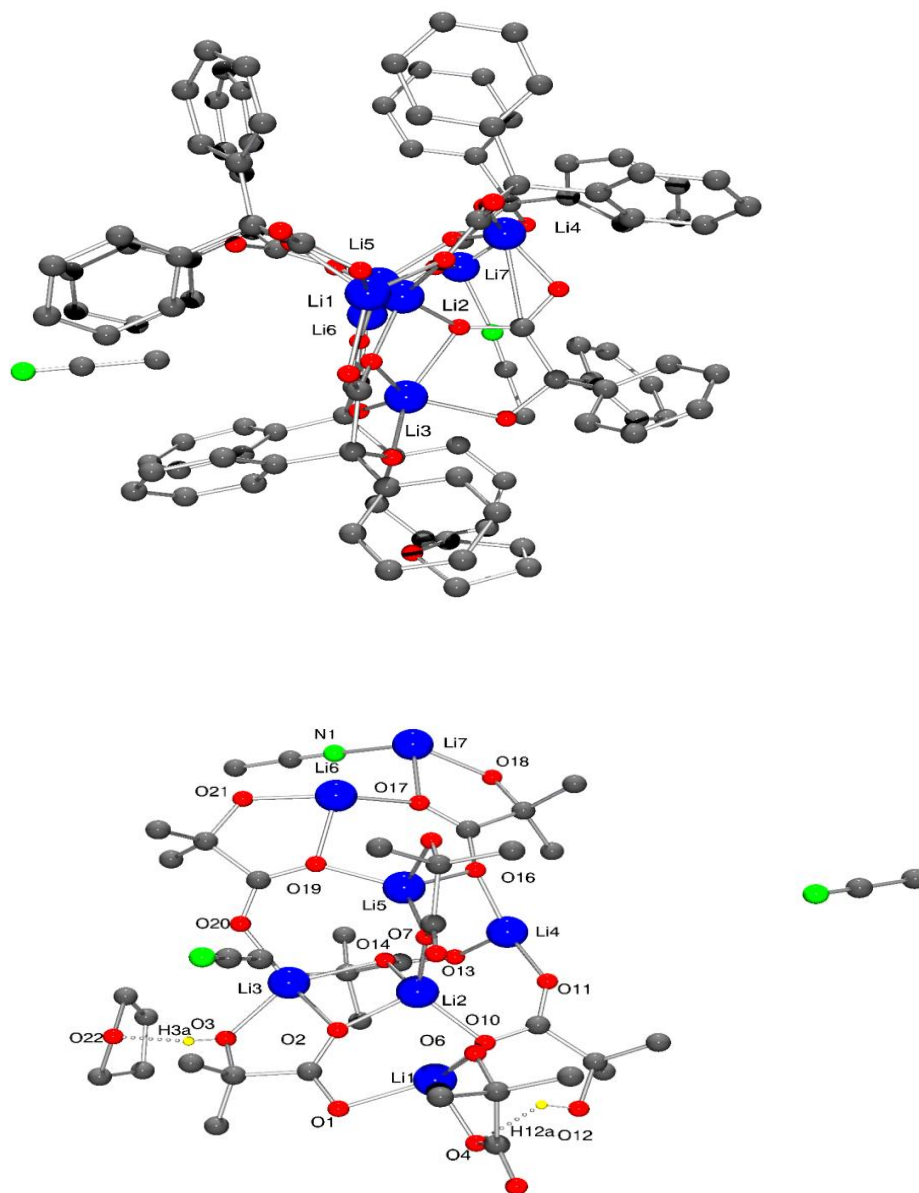
Figure 87. Two approximately orthogonal views of the asymmetric unit of chain polymer **32**. Selected bond lengths (Å) and angles (°): Li(1)–O(1) 2.052(3), Li(2)–O(2) 1.933(3), Li(3)–O(3) 1.994(4), Li(4)–O(13) 1.830(5), Li(5)–O(9) 2.032(4), Li(6)–O(7) 1.971(3), Li(7–O(18 1.982(3); Li(1)–O(10)–Li(2) 85.1(1), Li(2)–O(2)–Li(3) 88.4(2), Li(2)–O(14)–Li(3) 86.3(2), Li(2)–O(7)–Li(5) 95.9(1), Li(4)–O(16)–Li(5) 101.4(2), Li(5)–O(19)–Li(6) 99.2(1), Li(6)–O(17)–Li(7) 97.8(1).

The benzilates bind to lithium through the carboxylate and through the alcohol.

The carboxylate is observed as bridging bidentate [*e.g.* O(1)–C(1)–O(2)] and also

mono-dentate coordination where a single oxygen of the carboxylate binds to two lithium ions [*e.g.* O(7)]. In this case, the free C=O carbonyl is stabilised by a hydrogen bond from the alcohol [*e.g.* O(6)−H(6)···O(8)]. The three centres Li(1), Li(2), Li(3) adopt a distorted square-based pyramidal geometry surrounded by 5 oxygen atoms, whilst Li(5) and Li(6) adopt a distorted trigonal bipyramidal geometry. Li(7) adopts a distorted square planar geometry, with the apical position occupied by $NCCH_3$.

There are four oxygen atoms around Li(4) in a trigonal pyramidal arrangement, with apparently vacant space at the base of this pyramid. This ion is not really naked as it lies directly below one of the C–H bonds of a benzilic acid [Li(4)···C(84) = 2.715(5) Å; Li(4)···H(84) = 2.81 Å] at a distance of 2.689(5) Å from the mean plane of the phenyl ring.

The arrangement of lithium ions coordinated by benzilates leads to tapes that run in the [101] direction (**Figure 88**). Each tape is essentially a linear arrangement of five unique Li ions bridged by benzilic acid that is augmented by two further lithium ions and further benzilic acid. The tapes are packed in layers parallel to the *ac* plane; layers are packed ABAB parallel to *b*.
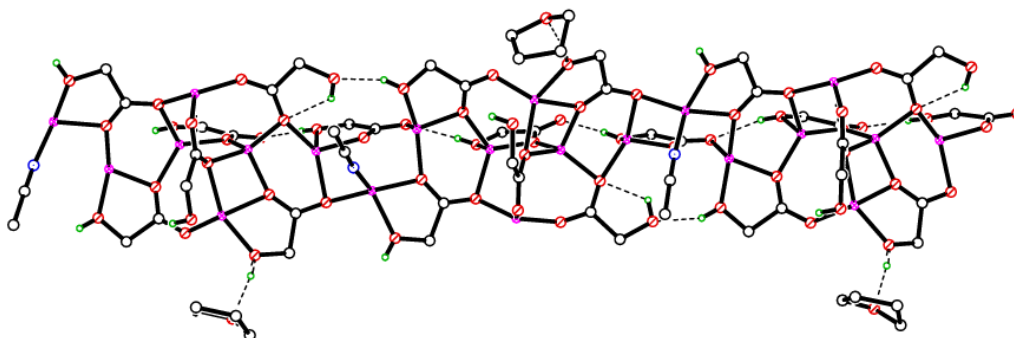
Figure 88. Portion of a single tape of **32** that runs parallel to the [101] direction.

Conducting the reaction under similar conditions, but using a 1:2 mole ratio of benzilic acid and lithium *tert*-butoxide afforded a somewhat different complex, namely [Li$_8$(benz)$_2$(Ot-Bu)$_2$(OC(Ph)$_2$CO$_2$C(Ph)$_2$CO$_2$$t$-Bu)$_2(THF)_4$] (**33**). The molecular structure is shown in (**Figure 89**) (for alternative view (**Appendix figure 156**), with selected bond lengths and angles given in the caption.
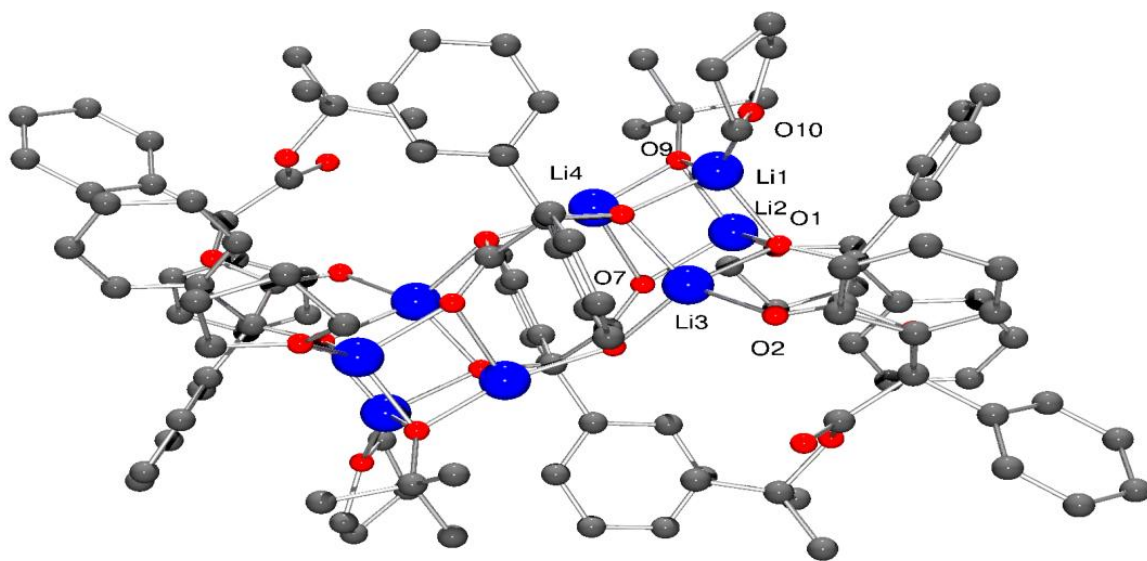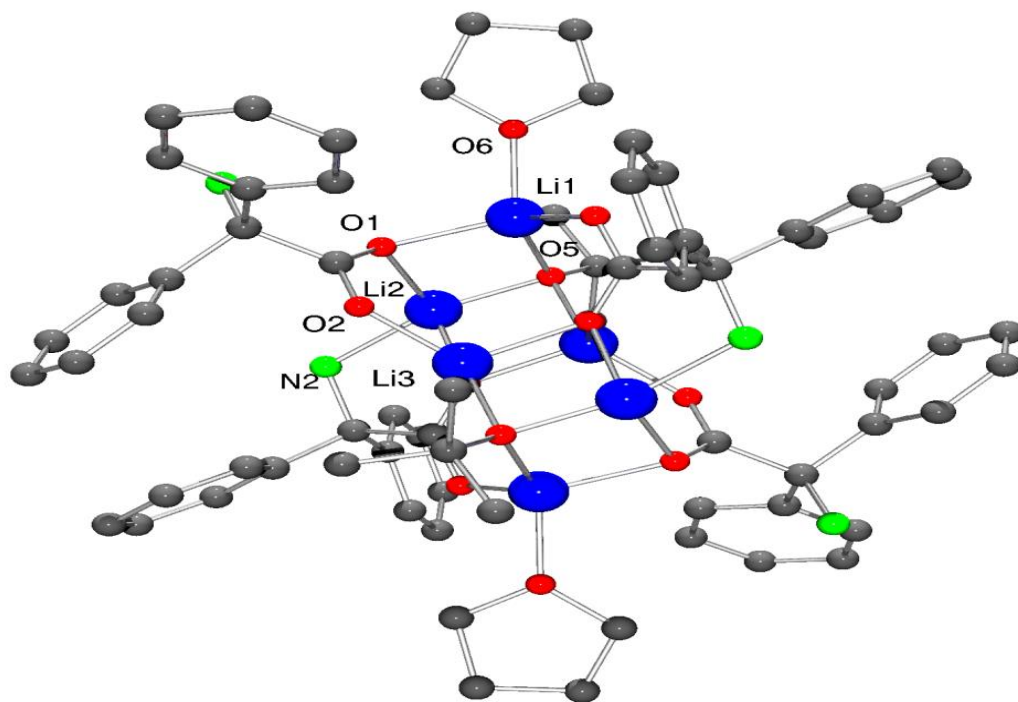

Figure 89. Molecular structure of **33**. Selected bond lengths (Å) and angles (°): Li(1)–O(1) 2.000(9), Li(1)–O(9) 1.948(9), Li(1)–O(10) 1.991(9), Li(2)–O(1) 1.917(9), Li(2)–O(7) 1.961(9), Li(3)–O(1) 1.959(9), Li(3)–O(2) 2.040(9), Li(3)–O(8) 2.052(9), Li(4)–O(9) 1.892(8); O(9)–Li(1)–O(10) 133.0(5), Li(1)–O(1)–Li(3) 82.0(3), Li(2)–O(1)–Li(3) 98.9(4), Li(1)–O(9)–Li(4 83.6(4), Li(2)–O(9)–Li(4) 86.9(3).

Half of the formula is the asymmetric unit because the molecule sits on a centre of symmetry. Two open cubes are linked by a pair of deprotonated benzilic acids. Each half of the molecule contains four different types of lithium centre. Li(1) and O(1) are bound by a bridging chelate ligand which formally results from the coupling of two benz and a *tert*-butoxide ligand. A search of the CSD revealed no examples of this type of coupled motif. [4] Within the central core, the Li – O

bonds are in the range 1.892(8) – 2.142(8) Å, with the longest associated with the μ_3 atoms O(7) and O(8). In **33**, there are no significant intermolecular interactions (or H-bonding).

2.2 Use of 2,2′-diphenylglycine

Having established suitable synthetic condition for the synthesis and isolation of lithium complexes derived from $Ph_2C(OH)CO_2H$, we extended our studies to the somewhat more expensive 2,2′-diphenylglycine, $Ph_2C(NH_2)CO_2H$.[7] Using 1:2 mole ratio from 2,2′-diphenylglycine and lithium _tert_-butoxide led to the isolation of the complex $[Li_6(Ot\text{-}Bu)_2(dpg)_4(THF)_2]$ (**34**). In the infrared spectrum, v_{NH} stretching modes are detected at approximately 3358, 3296 and 3159 cm^{-1}.

The molecular structure is shown in (**Figure 90)** and (**Appendix figure 157)**. Half of this formula comprises the asymmetric unit, and the molecule lies on a centre of symmetry. The core of the molecule comprises an Li_2O_2 ladder which has 6 steps supported by four dpg-derived ligands and two _tert_-butoxides. Such Li_2O_2 ladders are common in lithium chemistry and can varying in the number of steps present. Indeed, a search of the CSD revealed 26 hits for Li_2O_2 containing ladders; there were another 205 hits for Li–O containing cages (including cubes).[4] In **34**, there is intramolecular H-bonding: N(1)–H(1A)···O(1) (**Table 18)**.

Table 18. Hydrogen-bond geometry (Å, º) for complex **34**.

D—H···A	D—H	H···A	D···A	D—H···A
N1—H1A···O1	0.97 (6)	2.09 (6)	2.694 (6)	119 (4)
N2—H2A···N1^{ii}	0.88 (6)	2.35 (6)	3.190 (7)	160 (5)

Symmetry code: (ii) -x+1, -y+1, -z+1.

Figure 90. The molecular structure of **34**. Selected bond lengths (Å) and angles (^{o}): Li(1)–O(5) 1.910 (11), Li(1)–O(6) 1.960(11), Li(1)–O(4) 1.972(10), Li(2)–O(3) 1.952(10), Li(2)–O(5) 1.898(10), Li(2)–N(2) 2.122(11), Li(3)–O(2) 1.879(10), Li(3)–O(3) 2.006(10); O(5)–Li(1)–O(6) 124.4(5), O(5)–Li(2)–O(3) 98.2(4), O(2)–Li(3)–O(3) 103.8(4).

Furthermore, molecules of **34** are linked into 1D chains via head-to-tail pairs of intermolecular H-bonds N(2′)–H(2B′)···N(1). The chains run parallel to *a* (**Figure 91**). However, there are no significant interactions between chains.
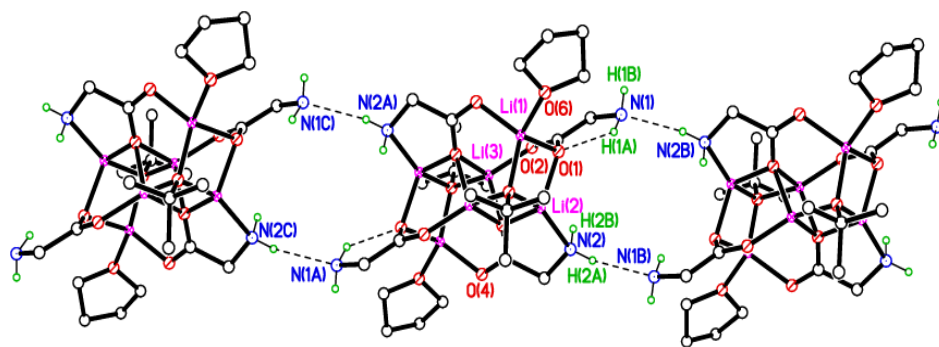
Figure 91. Chains of **34** parallel to *a*.

Using 1:2 mole ratio from 2,2$'$-diphenylglycine and lithium phenoxide results in a product for which the asymmetric unit contains two symmetry-unique portions each of composition Li$_2$:dpg:phenoxide:MeCN (**35**). The overall structure is best viewed (**Figure 92)** as an 8×Li cluster with formula [Li$_8$(dpg)$_4$(phenoxide)$_4$(MeCN)$_4$]. Clusters of **35** are essentially an Li$_8$O$_8$ core that is formed from four Li$_2$O$_2$ square planes arranged alternately by rotation of 90 °degrees to give a Li$_8$O$_8$ capsule. This capsule is then further stabilised by the nitrogen ligands (bidentate dpg) around the central portion of the capsule at 90 ° to each other (like sails on a windmill). The capsules are terminated by mono-dentate acetonitrile.

159
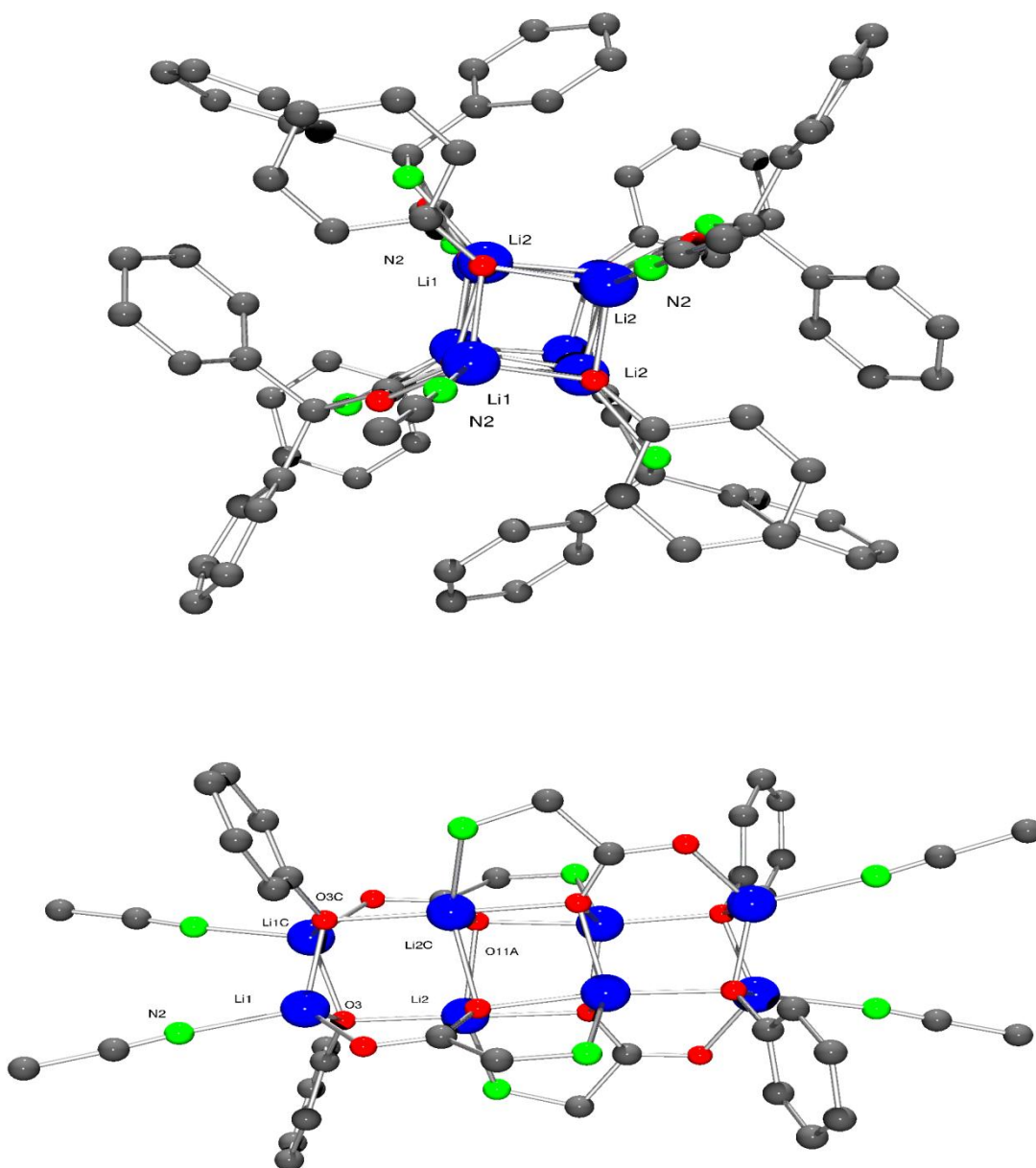
Figure 92. Two orthogonal views of the molecular structure of **35**·4MeCN. Selected bond lengths (Å) and angles (°): Li(1)–O(3) 1.920(15), Li(1)–N(2) 2.103(14), Li(2)–O(1) 2.003(15), Li(2)–O(3) 2.064(12), Li(2)–N(1) 2.151(15); Li(1)–O(3)–Li(2) 100.9(6), O(3)–Li(1)–N(2) 113.0(3), N(1)–Li(2)–O(1) 75.9(5).

In solution, complexes **31** – **35** exhibit only a single peak in their ^{7}Li NMR spectra, which is consistent with the disaggregation observed by O'Hara, Kozak and Kerton. [6d, h, i]

3. Ring opening polymerization (ROP)

3.1 ROP of ε-caprolactone

Complexes **31** – **35** have been screened for their ability to ring open polymerize ε-caprolactone (in the presence of benzyl alcohol (BnOH) in case of **31**). Complex **34** was selected to determine the optimum conditions (**Table 19**), and the results revealed that this catalyst was most effective for the ROP of **ε**-CL at temperatures of 80 to 110 ^{o}C. According to the entries (12-17, (**Table 19**), there is a near exponential relationship between monomer conversions and M_n values (**Figure 93**), possibly due to severe catalyst decomposition, with molecular weight distributions [1.13 – 1.66] that suggest there is some degree of control. There is an approximate linear relationship between conversion ratio and average molecular weight (M_n), which suggests the system still retains the classical features of a living polymerization process (**Figure 94**). In the ^{1}H and ^{13}C NMR spectra of the PCL (**Figures 95** and **96**), no peaks associated with end groups could be identified. This suggests the formation of cyclic PCL; this has been noted previously when using pre-catalysts containing Li/O rings. [6g] The MALDI TOF spectrum of the PCL (**Figure 97**) revealed peaks separated by 114 mass units (the molecular weight of the monomer ε-CL).

ROP of ε-CL in the absence of solvent was also investigated (**Table 20**), with higher conversions achieved over short times periods, but at the expense of (i.e.

lower) observed M_n values for the respective pre-catalysts; PDIs are in the range 1.21 to 2.01.

From a kinetic study of the ROP of ε-CL using **31** and **33** - **35** (**Figure 98**), it was observed that the polymerization rate exhibited a first order dependence on the ε-CL concentration (**Figure 98**, left), and the conversion of monomer achieved was >80 % over 100 min (**Figure 98**, right). Figure 96 indicates that the rate order is **33** > **34** > **35** > **31 Table 21** suggesting that for **33** and **34**, the presence of the O-*t*Bu and/or THF ligation at lithium may well be beneficial. For **35** (as for inactive **32**), the presence of acetonitrile may well be detrimental, though the additional presence of phenoxide ligation in **35** appears to be a more dominant factor. The relative poor activity observed for **31** is surprising in view of the open environments about the lithium centers, and is thought to be due to the inability of **31** to generate a lithium alkoxide. It should be noted however that this discussion of activity *versus* coordination environment/ligation is somewhat tentative given the differing nature of the Li/O ring systems present. The data here (and that for the ROP of *rac*-LA) also suggested that these catalysts require an induction period, suggestive of slow activation.

Table 19. Ring opening polymerization screening of ε-caprolactone using lithium complexes **31** – **35**.

Run	Cat	T (°C)	CL:Cat:BnOH	Time (h)	Conv^a (%)	M_n^b,GPC	$M_{n,Cal}^c$	PDI^d
1	**31**	110	150:1:0	3	---	---	---	---
2	**31**	110	150:1:1	3	86	4170	14830	1.12
3	**32**	110	150:1:1	3	---	---	---	---
4	**32**	110	150:1:2	24	---	---	---	---
5	**33**	110	150:1:1	3	79	5790	13630	1.46
6	**33**	110	150:1:0	3	88	4440	15070	1.56
7	**33**	110	150:1:0	1	69	4310	11810	1.43
8	**34**	60	150:1:0	6	---	---	---	---
9	**34**	80	150:1:0	3	45	1860	7700	1.24
10	**34**	110	150:1:0	1	52	3360	8900	1.22
11	**34**	110	150:1:1	3	74	5470	12780	1.21
12	**34**	110	100:1:0	3	59	2890	6730	1.13
13	**34**	110	150:1:0	3	70	4560	11980	1.17
14	**34**	110	200:1:0	3	70	10350	15980	1.19
15	**34**	110	250:1:0	3	71	13390	20260	1.23
16	**34**	110	300:1:0	3	82	15580	28080	1.66
17	**34**	110	350:1:0	3	88	32690	35160	1.58
18	**34**	110	150:1:0	24	91	7430	15580	1.48
19	**35**	110	150:1:0	1	76	2530	13010	1.12
20	**35**	110	150:1:0	3	82	9360	14040	1.31

^{a} Determined by ^{1}H NMR spectroscopy; ^{b} M_n GPC values corrected considering Mark-Houwink factors (0.56 poly(ε-caprolactone)) from polystyrene standards in THF. ^{c} Calculated from ([Monomer]$_0$/[Cat]$_0$) x conv.(%) x Monomer molecular weight. ^{d} From GPC.

Table 20. ROP of ε-caprolactone catalyzed by lithium complexes **31** - **35** in the absence of solvent.

Run	Cat	Time/min	T /°C	CL:Cat:BnOH	Conv.%^{a}	$M_{n,GPC}^b$	$M_n$cal^c	PDI^d
1	**31**	60	110	150:1:1	83	3500	14320	1.59
2	**32**	120	110	150:1:1	---	---	---	---
3	**33**	25	110	150:1:0	93	8250	15920	1.56
4	**33**	2h	25	150:1:0	82	4180	14040	1.64
5	**34**	30	110	150:1:0	91	6750	15580	2.01
6	**35**	35	110	150:1:0	87	4880	14900	1.21

^{a} Determined by ^{1}H NMR spectroscopy. ^{b}M$_n$ values were determined by GPC in THF vs. PS standards and were corrected with a Mark–Houwink factor of 0.56. ^{c} (F.W. monomer × [monomer]/[cat]) × conversion + F.W. BnOH. ^{d} Mw/Mn were determined by GPC.

Table 21. Observed rate constant for polymerization (K_{obs}) of ε-CL, *r*-LA and δ-VL.

Cat.	ε-CL / min⁻¹	*r*-LA	δ-VL
33	12.9×10^{-3}	0.143	0.102
34	10.3×10^{-3}	0.112	0.069
35	8.6×10^{-3}	0.103	0.058
31	7.1×10^{-3}	0.092	0.057
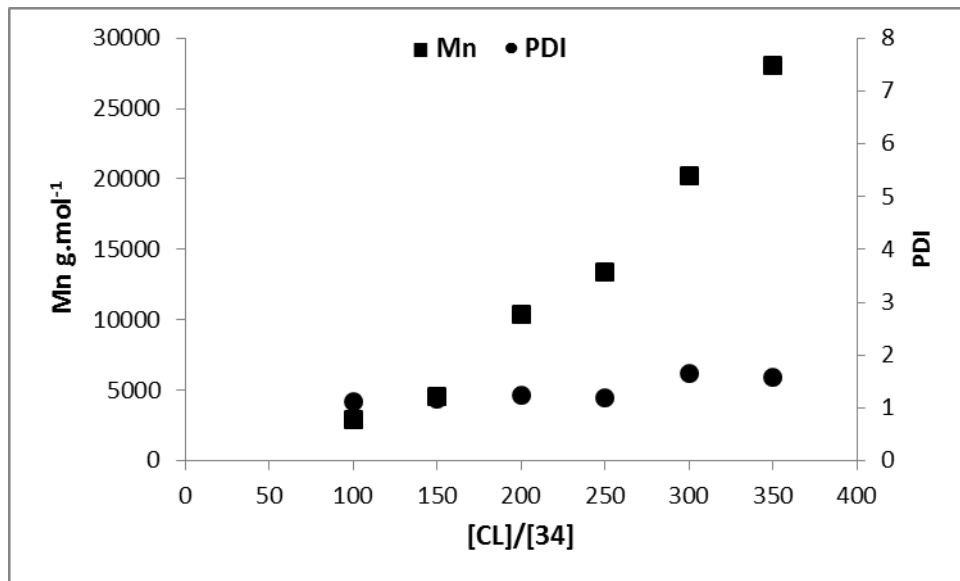
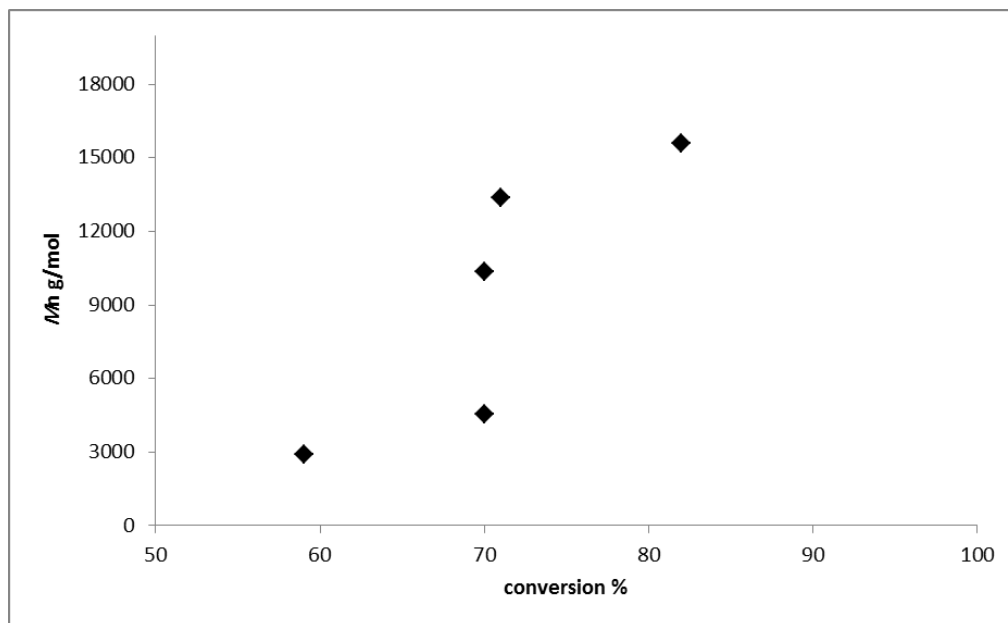**Figure 93.** M_n (■) and M_w/M_n ● *vs.* [CL]/[Cat] in the ROP of ε-CL using **34**.

Figure 94. Plot of monomer conversion *versus* number average molecular weight using **34** for PCL.
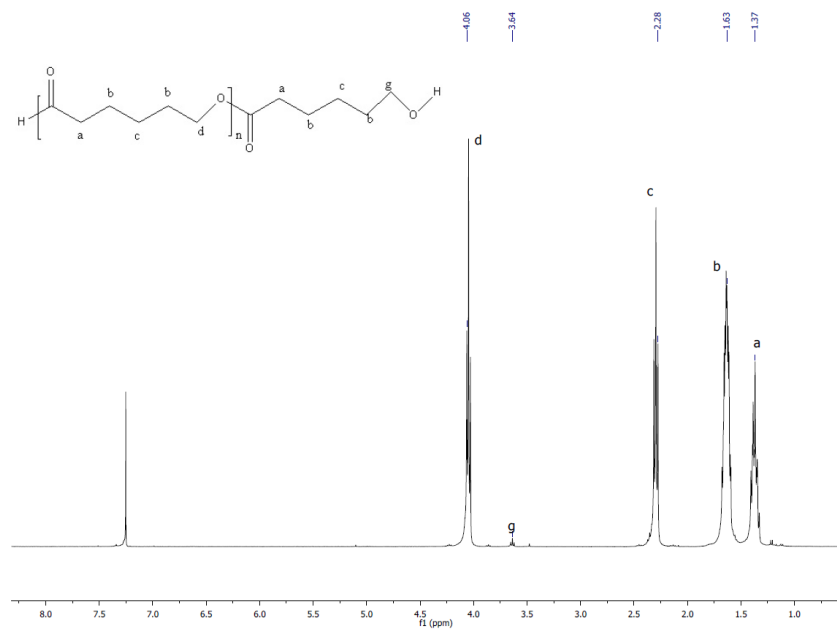
Figure 95. ^{1}H NMR spectrum of PCL (run 6 table 18).
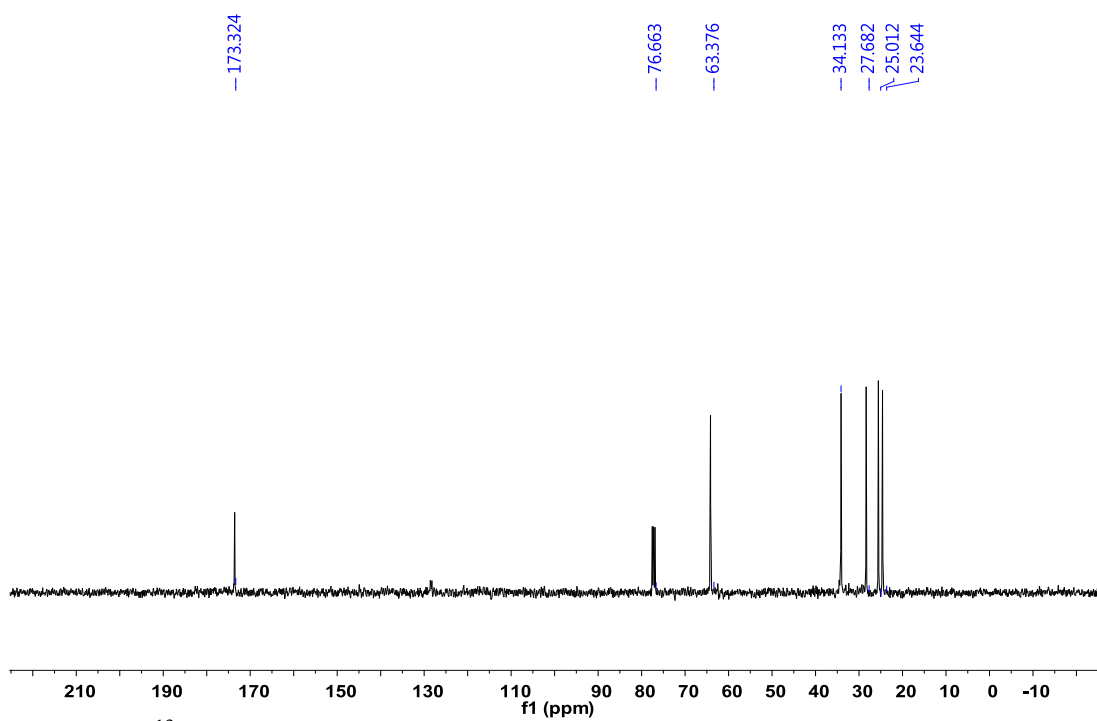
Figure 96. ^{13}C NMR spectrum of PCL (run 6 table 18).
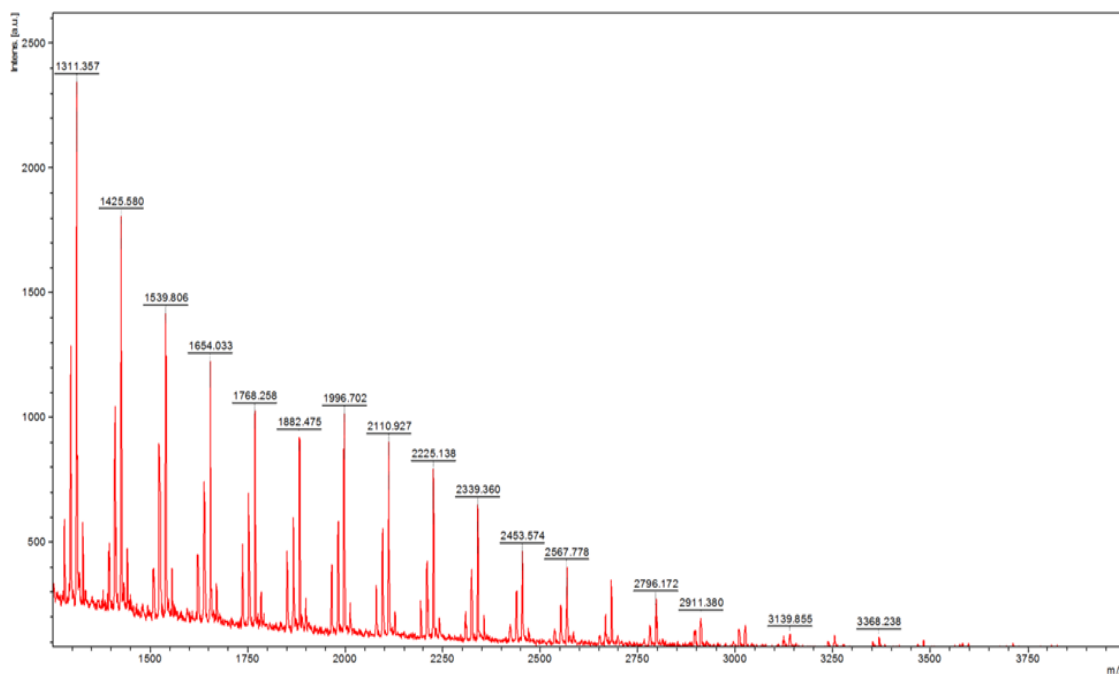
Figure 97. MALDI-ToF spectrum of PCL (run 6, table 18).
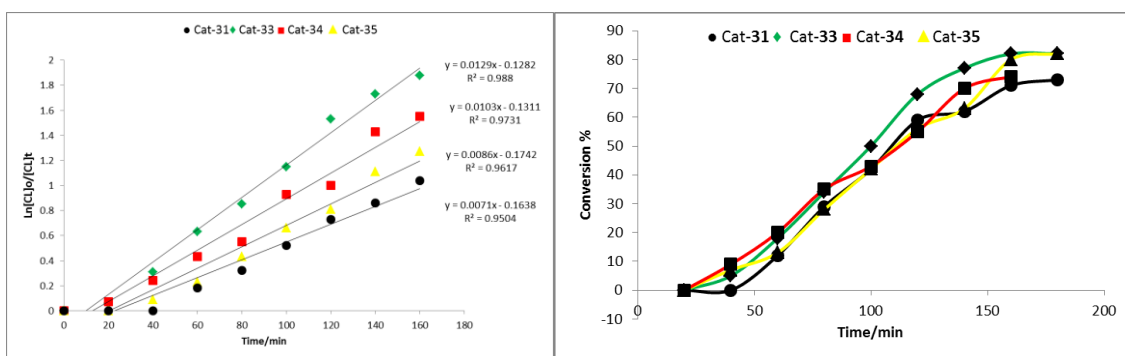
Figure 98. Left: Kinetic plots for ε-CL ROP using Li catalysts **31** and **33** - **35**; Right: Relationship between conversion and time for ε-CL ROP using **31** and **33** - **35**.

3.2 ROP of rac-lactide

Complexes **31** to **35** have also been screened for the ROP of *rac*-Lactide, with, in the case of **31**, addition of benzyl alcohol (BnOH). Here, complex **33** was selected to determine the optimized conditions (**Table 22)**. It was observed that at temperatures below 110 ^{o}C, these systems were generally inactive even after 24 h. However, at 110 ^{o}C, a linear relationship between average molecular weight and monomer mole ratio was observed for **33** (**Figure 99)**, whilst there is a near

166

exponential relationship between monomer conversions and M_n values (**Figure 100**), possibly due to severe catalyst decomposition; molecular weight distributions [1.14 – 1.43] that suggest there is some degree of control. The ^{1}H NMR and ^{13}C NMR spectra of the PLA (**Figures 101** and **102**), are consistent with the presence of O*t*Bu/OH end groups when the ROP is conducted in the absence of BnOH and BnO/OH end groups when conducted in the presence of BnOH). The MALDI-ToF spectrum for PLA using **31** (**Figure 103)** comprises a series of peaks separated by 72 Da with end groups OBn and ONa, for example with n = 82 = 6040 Da.

For runs conducted in the absence of BnOH, the MALDI-ToF spectrum for the PLA (**Figure 104)** is more bimodal in structure, and comprises a sizeable fraction of oligomers with peak separation 72 Da and end groups of ONa and OH; for the higher molecular weight fraction, the peak separation is 144 Da.

Table 22. ROP screening of *rac*-lactide using **31 – 35**.

Run	Cat	T (°C)	*r*-LA:Cat:BnOH	Time (h)	Conv[a] (%)	M_n^b,GPC	$M_{n,Cal}^c$	PDI[d]
1	**31**	110	100:1:1	12	63	4360	9190	1.09
2	**32**	110	100:1:1	12	---	---	---	---
3	**33**	60	100:1:1	24	---	---	---	---
4	**33**	80	100:1:0	12	23	1370	3310	1.15
5	**33**	110	100:1:0	3	---	---	---	---
6	**33**	110	100:1:0	6	33	1460	4760	1.34
7	**33**	110	50:1:0	12	19	690	1370	1.17
8	**33**	110	100:1:0	12	61	3970	8790	1.14
9	**33**	110	150:1:0	12	63	4620	13620	1.19
10	**33**	110	200:1:0	12	65	6160	18740	1.18
11	**33**	110	250:1:0	12	71	7820	25580	1.17
12	**33**	110	100:1:0	24	73	5780	10520	1.24
13	**33**	150	100:1:0	12	62	3470	8936	1.43
14	**34**	110	100:1:0	12	69	6990	9940	1.15
15	**35**	110	100:1:0	12	65	4700	9370	1.18

[a] Determined by ^{1}H NMR spectroscopy; [b,d] From GPC, M_n GPC values corrected considering Mark-Houwink factors (0.58 poly (rac-lactide)) from polystyrene standards in THF. [c] Calculated from ([Monomer]0/[Cat]0) × conv.(%) × Monomer molecular weight.
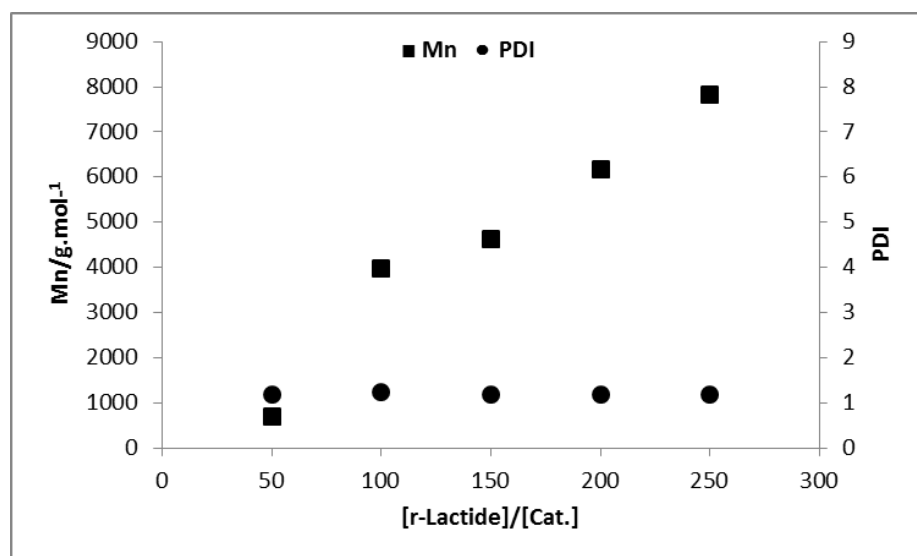
Figure 99. M_n (▲) and M_w/M_n ♦) *vs*. [*rac*-LA]/[Cat] in the ROP of *rac*-LA.
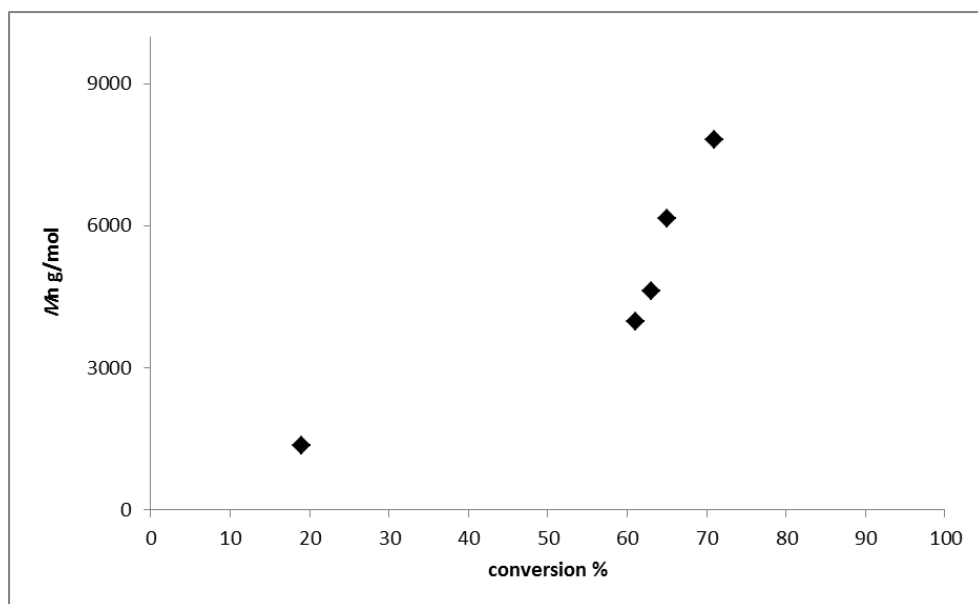
Figure 100. Plot of monomer conversion *versus* number average molecular weight for **33** for poly(*rac*-LA).
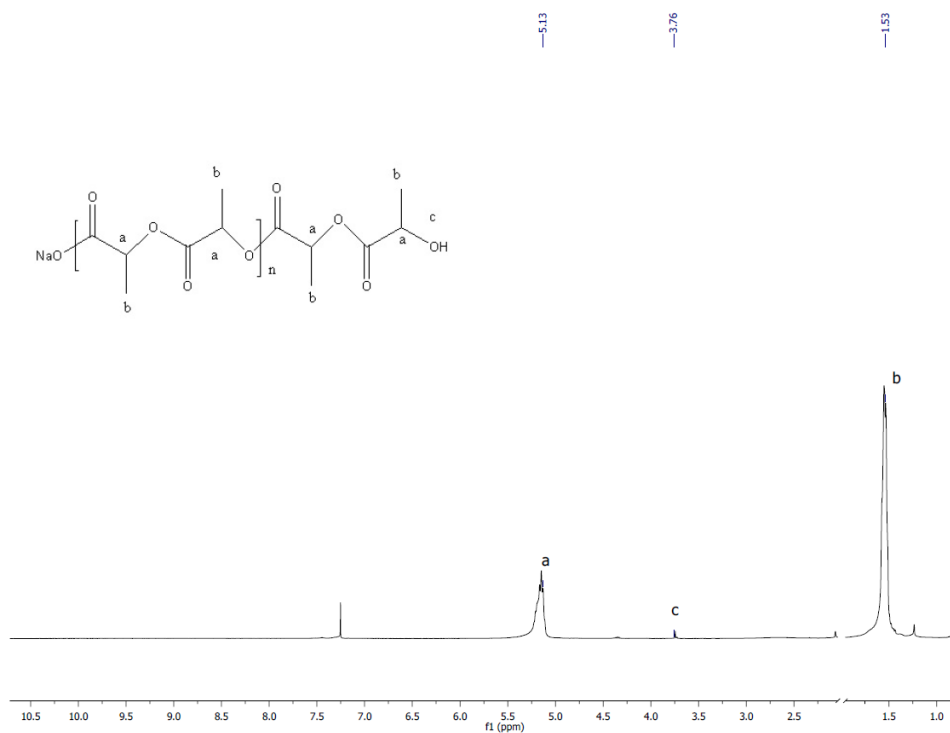
Figure 101. ¹H NMR spectrum of poly(*rac*-LA) (run 14, table 22).

Figure 102. ^{13}C NMR spectrum of poly(*rac*-LA) (run 14, table 22).
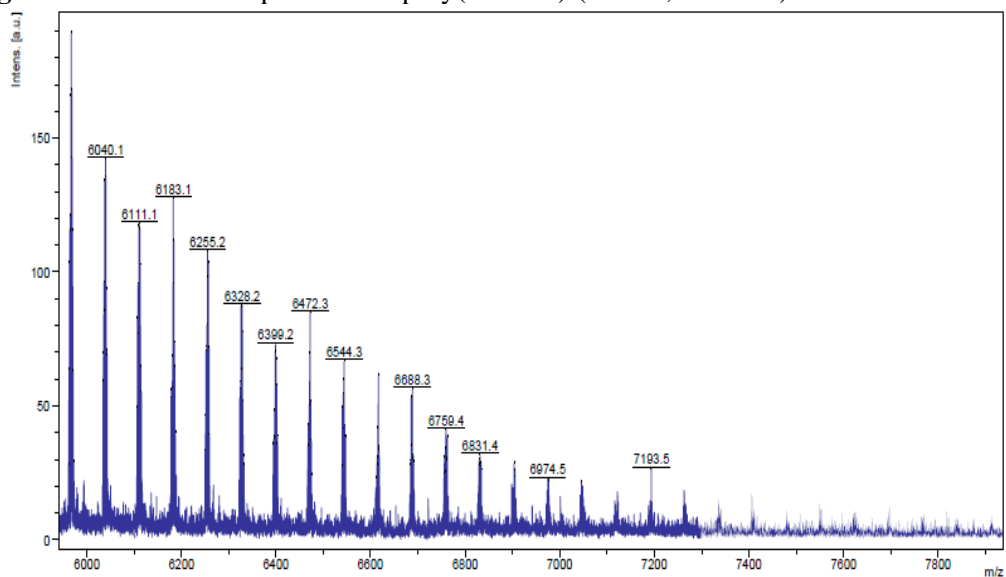
Figure 103. MALDI-ToF spectrum of poly(*rac*-LA) (run1, table 22).
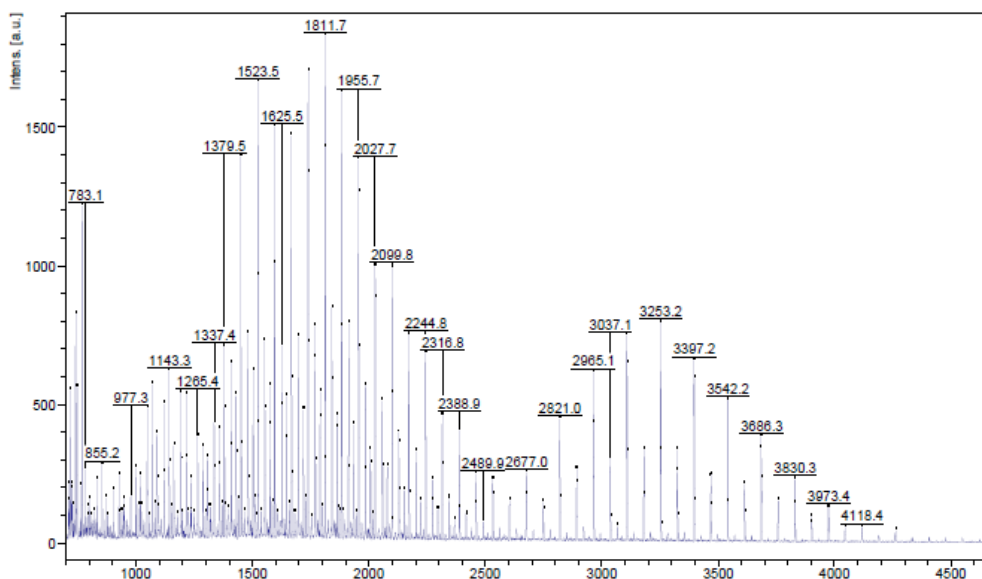
Figure 104. MALDI-ToF spectrum of poly(*rac*-LA) (run14, table 22).

To determine the stereo-chemical microstructure of the resulting PLA, homonuclear decoupled ^{1}H NMR spectra were recorded of the methine region, and the results revealed that the polymers were atactic (**Figures 105** - **108**);. 2D

NMR spectroscopy proved the polymers were atactic (**Figure 109)** is an example for 2D NMR.
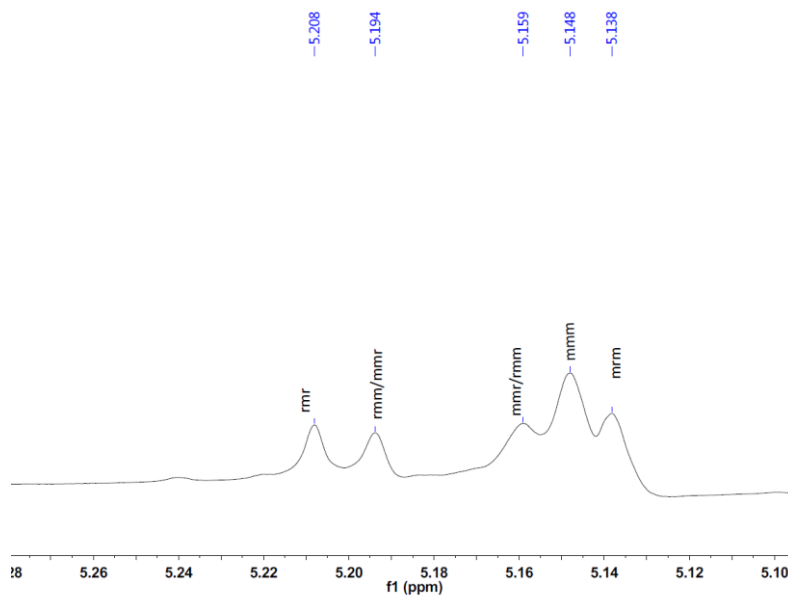
Figure 105. Homonuclear decoupled ^{1}H NMR spectrum of PLA (run 1, table 22).
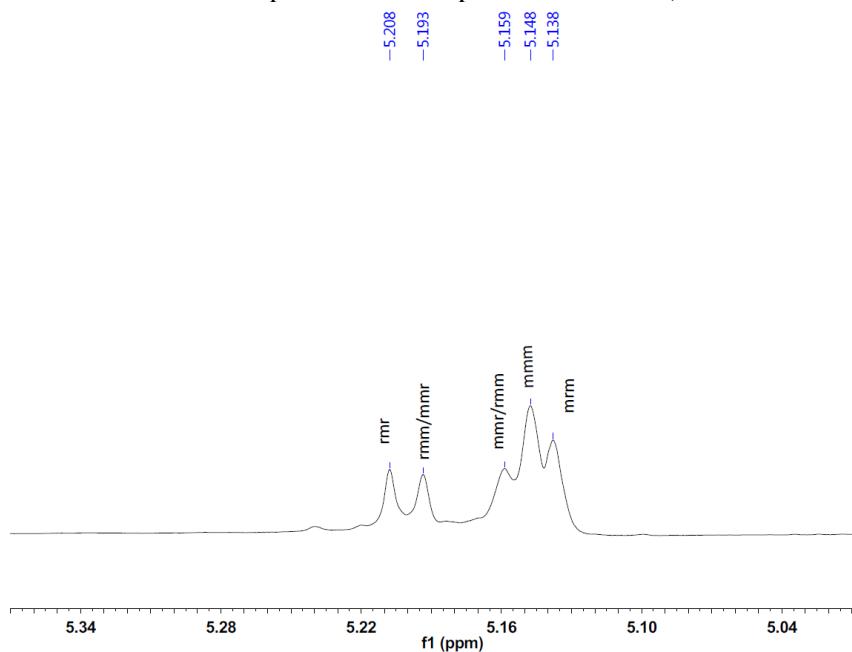
Figure 106. Homonuclear decoupled ^{1}H NMR spectrum of PLA (run 8, table 22).
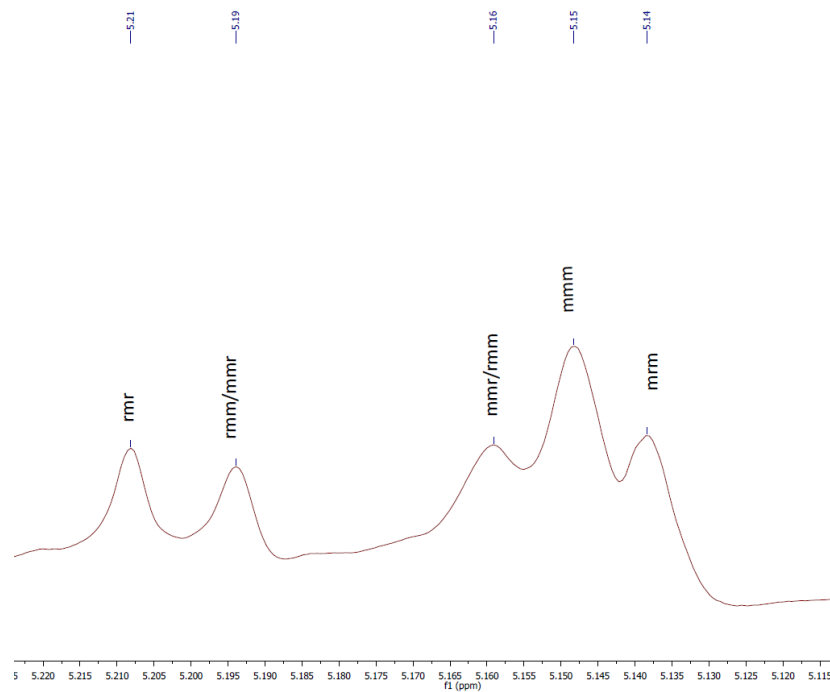
Figure 107. Homonuclear decoupled ^{1}H NMR spectrum of PLA (run 14, table 22).
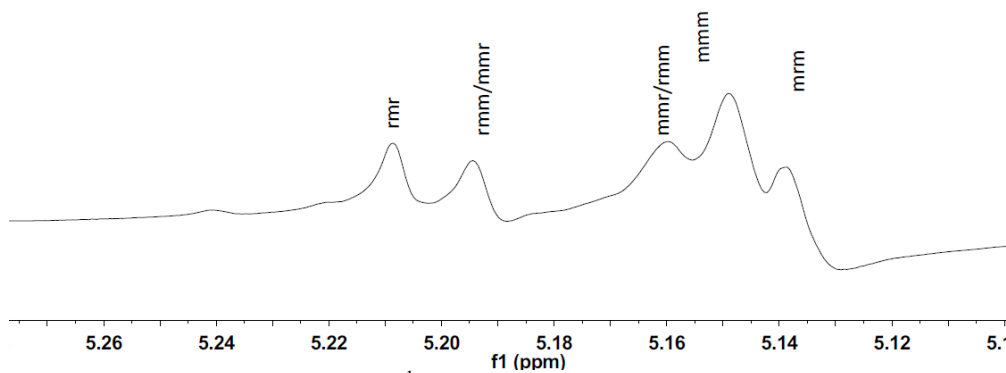
Figure 108. Homonuclear decoupled ^{1}H NMR spectrum of PLA (run 15, table 22).
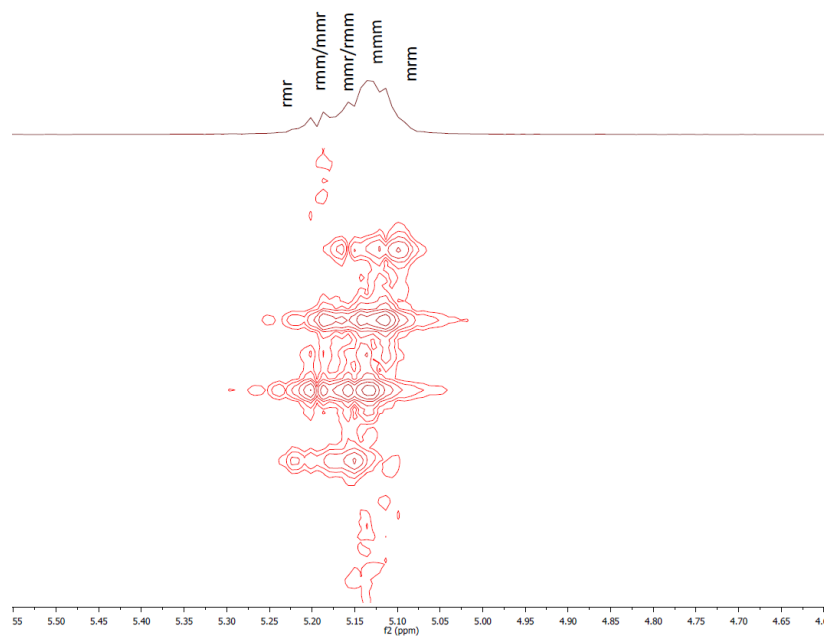
Figure 109. 2D J-resolved ^{1}H NMR spectrum of PLA (run 15, table 22).

From a kinetic study of the ROP of *r*ac-LA using **31, 33, 34** and **35** (**Figure 110**) at 110 ^{o}C, it was observed that the polymerization rate exhibited a first order dependence on the *rac*-LA concentration (**Figure 110**, left), and the monomer conversion reached >70 % over 8 h (**Figure 110**, right). The same activity trend as observed for the ROP of ε-CL was observed here (**Table 21**).
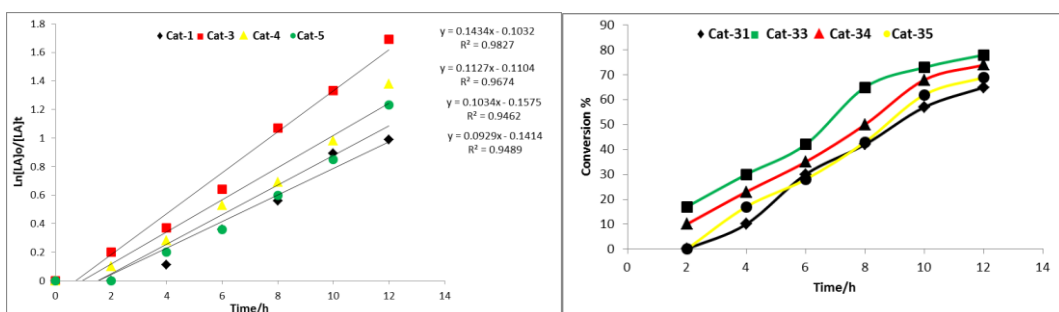
Figure 110. Left: Plot of ln[*r*-LA]$_o$/[*rac*-LA]$_t$ *vs* time using **31** and **33** - **35**; Right: Relationship between conversion and time of polymerization *r*-LA using **31** and **33** - **35.**

3.3 Ring Opening Polymerization (ROP) of δ-valerolactone

Complexes **31** – **35** were also evaluated as catalysts for the ROP of δ-valerolactone (**Table 23**). The relationship between M_n and PDI and monomer mole ratio (**Figure 111**) are near linear using catalyst system **33**. The ^{1}HNMR spectra of the resultant PVL (**Figure 112**) revealed the presence of benzyloxy and hydroxy end groups an example of ^{1}HNMR without addition of benzyl alcohol (**Figure 113**). The MALDI-ToF spectrum of the PVL (**Figure 114**) reveals a family of peaks separated by 100 Da (the molecular weight of the monomer), consistent with the presence of only oligomeric PVL. A kinetic study using **31** and **33 - 35** (**Figure 115**) at 110 ^{o}C revealed that the polymerization rate of the ROP of δ-valerolactone exhibited a first order dependence on the δ-valerolactone concentration (**Figure 115**, left). The monomer conversion was >70 % over 8 h (**Figure 115**, right) and the activity trend was as observed for the ROP of ε-CL and *r*ac-LA (**Table 21**).

Table 23. ROP of δ-valerolactone using lithium complex **31 - 35**

Run[a]	Cat	δ–VL:Cat:BnOH	Time/h	Conv.%[b]	M_n[c]	$M_{n,Cal}$[d]	PDI[e]
1	**31**	100:1:1	12	61	2760	6210	1.20
2	**32**	100:1:1	12	---	---	---	---
3	**33**	50:1:0	12	43	1170	2150	1.89
4	**33**	100:1:0	12	62	1580	6200	1.91
5	**33**	150:1:0	12	64	2240	9600	1.87
6	**33**	200:1:0	12	63	4870	12600	2.15
7	**33**	250:1:0	12	64	5690	16000	1.74
8	**33**	100:1:0	24	72	6790	7200	1.99
8	**34**	100:1:0	12	66	4530	6600	1.17
9	**35**	100:1:0	12	59	3780	5900	1.19

[a] Runs conducted in toluene at 110 °C. [b] Determined by ^{1}H NMR spectroscopy; [c, e] GPC. [d] Calculated from ([Monomer] /[Cat]) × conv.(%) × monomer molecular weight + molecular weight of BnOH.

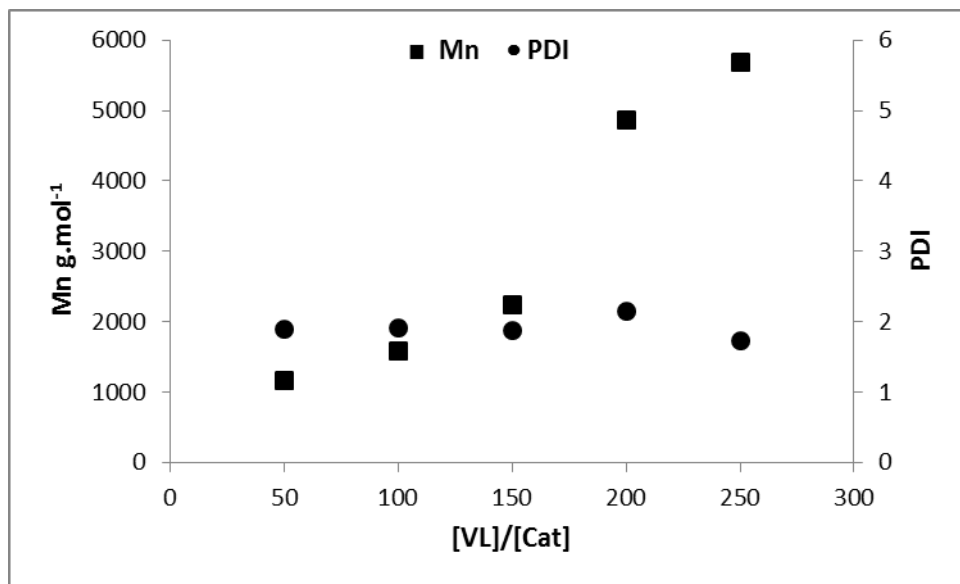**Figure 111.** Relationship between M_n and PDI of the polymer and the mole ratio [δ-VL]/[Cat] using **33**.
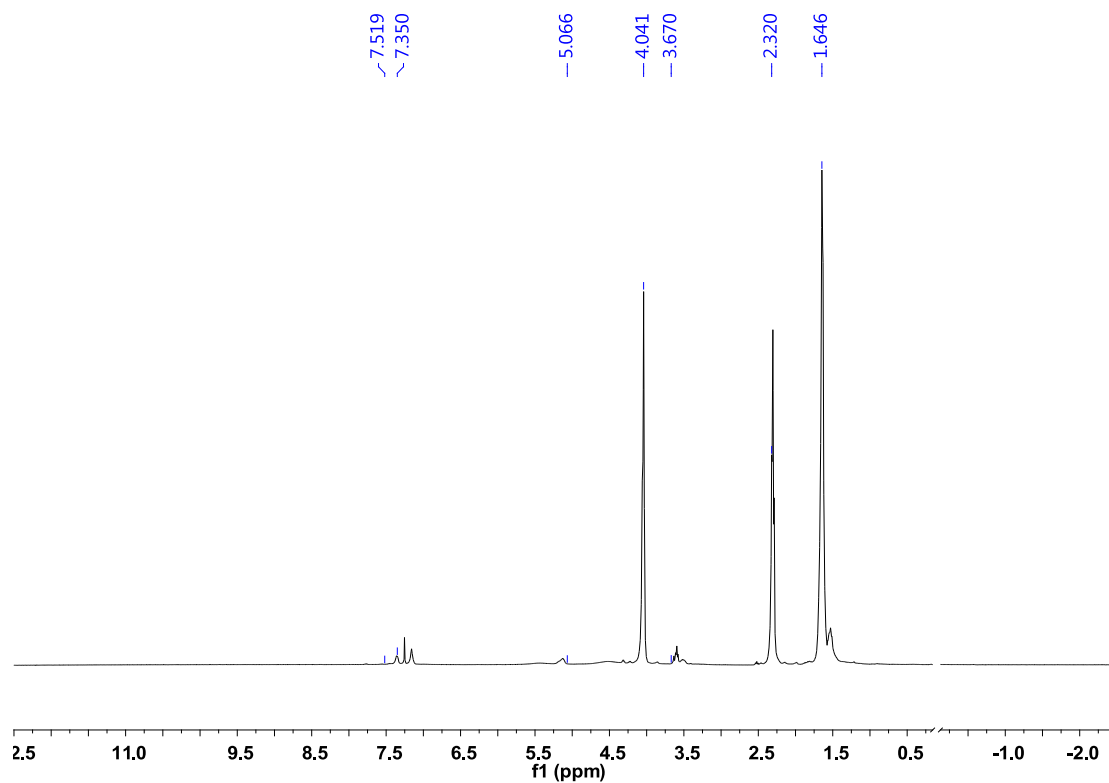

Figure 112. ^{1}H NMR spectrum of PVL (run 1 table 23).
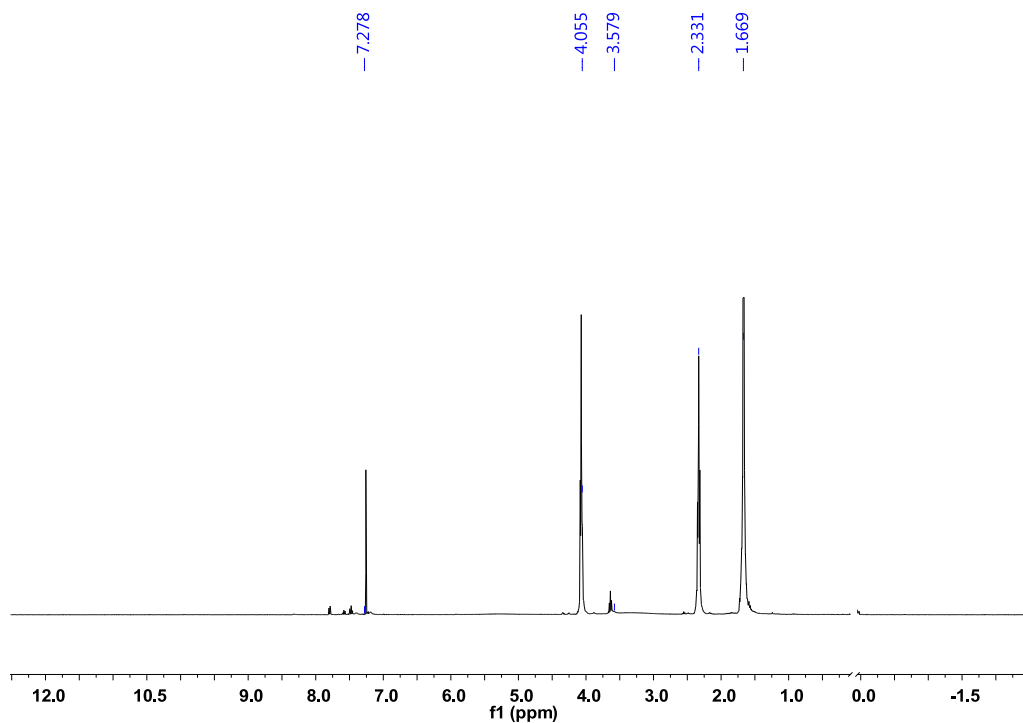
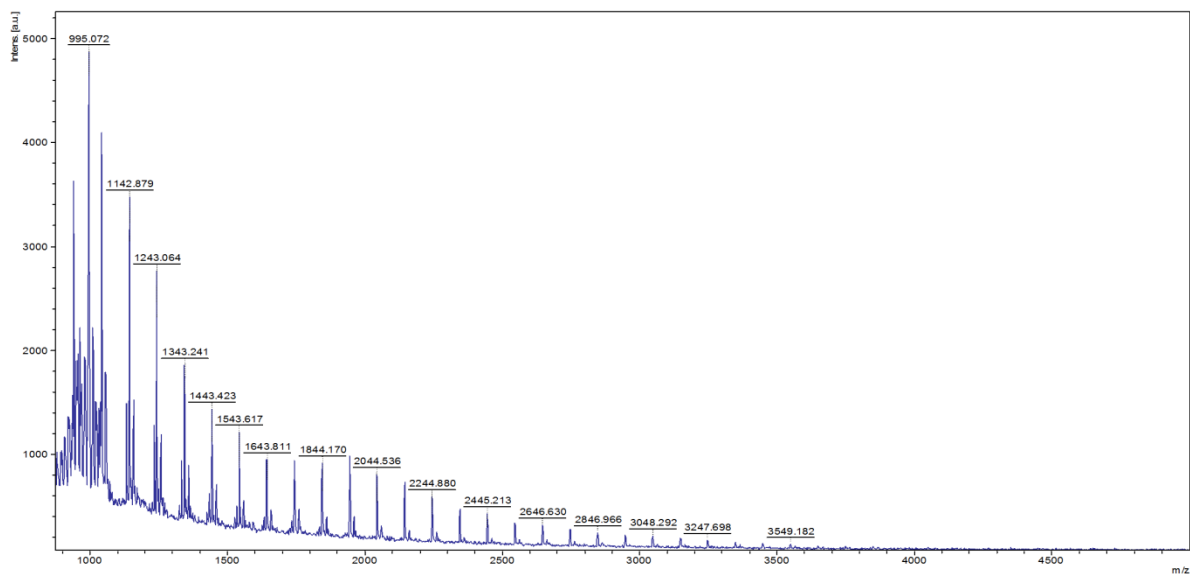**Figure 113**. ^{1}H NMR spectrum of PVL (run 8 table 23).

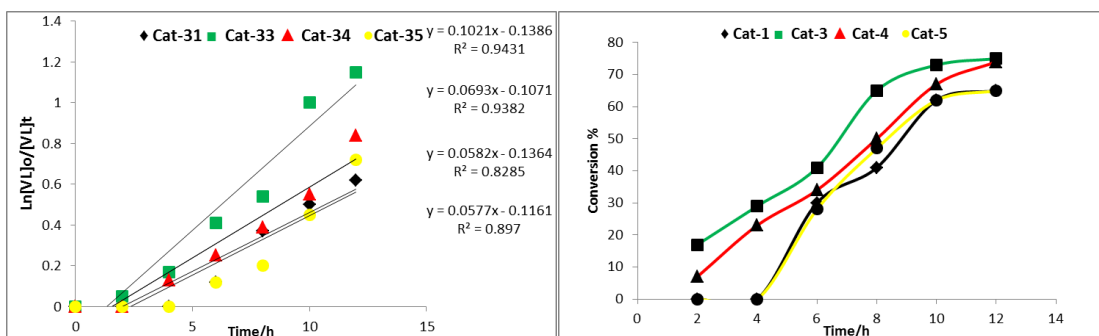**Figure 114**. MALDI-ToF spectrum of PVL (run 7, table 23).

Figure 115. Left: Plot of $\ln[\delta\text{-VL}]_o/[\delta\text{-VL}]_t$ *vs* time using **31** and **33** - **35**; Right: Relationship between conversion and time of ROP of δ-VL using **31** and **33** - **35**.

Finally, the attempted co-polymerization of ε-CL and *r*-LA was attempted (and the reverse addition), but this resulted in only the homo-polymerization and isolation of PCL.

4. Conclusion

In conclusion, the use of the acids $2,2'\text{-Ph}_2\text{C(X)(CO}_2\text{H)}$, where X = OH, NH$_2$, in combination with lithium *tert*-butoxide or phenoxide results in the formation of multi-metallic assemblies incorporating a variety of structural motifs such as chains, open cubes, capsules and ladders based on Li-O repeat units. For the ring opening polymerization (ROP) of ε-caprolactone (ε-CL), *rac*-lactide (*rac*-LA) and δ-valerolactone (δ-VL), all complexes except **32** were active, requiring in the case of **31**, the presence of BnOH. The polymerizations afforded polylactides with molecular weights much lower than the calculated values, but with relatively narrow molecular weight distributions (< 2.0). Kinetic studies indicated the rate order **33** > **34** > **35** > **31**, and a first order dependence on the monomer concentration as well as an induction period (slow activation). Tentative structure active relationships are proposed such as the presence of O-*t*Bu and/or THF ligation being beneficial *versus* acetonitrile being detrimental.

5. Refernces

[1] (a) C. K. Williams, *Chem. Soc. Rev.*, **2007**, 36, 1573. (b) A. Arbaoui and C. Redshaw, *Polym. Chem.*, **2010**, 1, 801. (c) W. Alkarekshi, A. P. Armitage, O. Boyron, C. J. Davies, M. Govere, A. Gregory, K. Singh and G. A. Solan, *Organometallics*, **2013**, 32, 249 and references therein. (d) Y. Liu, W. -S. Dong, J. -Y. Liu and Y. -S. Li, *Dalton Trans.*, **2014**, 43, 2244.

[2] (a) C. Redshaw, M. R. J. Elsegood and K. E. Holmes, *Angew Chemie, Int. Ed.*, **2005**, 44, 1850. (b) C. Redshaw and M. R. J. Elsegood, *Angew Chemie, Int. Ed*. **2007**, 46, 7453.

[3] M. Braun, *Angew Chemie.*, **1996**, 108, 565; *Angew Chemie. Int. Ed.*, **1996**, 35, 519.

[4] A search of the CSD for the $Ph_2C(X)$ motif (X = O, NH) afforded 31 hits, the majority of which (80 %) were organic compounds; CSD system: F. H. Allen, *Acta Cryst.*, **2002**, B**58**, 380.

[5] A. K. Sutar, T. Maharana, S. Dutta, C. −T. Chen and C. −C. Lin, *Chem. Soc. Rev*. **2010**, 39, 1724.

[6] (a) B. −T. Ko and C. −C. Lin, *J. Am. Chem. Soc*., **2001**, 123, 7973. (b) M. H. Chisholm, C. −C. Lin, J. C. Gallucci and B. −T. Ko, *Dalton Trans.*, **2003**, 406. (c) C. −A. Huang and C. −T. Chen, *Dalton Trans.*, **2007**, 5561. (d) W. Clegg, M. G. Davidson, D. V. Graham, G. Griffen, M. D. Jones, A.R. Kennedy, C. T. O'Hara, L. Russo and C. M. Thomson, *Dalton Trans.*, **2008**, 1295. (e) Y. Huang, Y. –H. Tsai, W. –C. Hung, C. –S. Lin, W. Wang, J. –H. Huang, S. Dutta and C. –C. Lin, *Inorg. Chem.*, **2010**, 49, 9416. (f) W. –Y. Lu, M. –W. Hsiao, S. C. N. Hsu, W. –T. Peng, Y. –J. Chang, Y. –C. Tsou, T. –Y. Wu, Y. –C. Lai, Y. Chen and H. −Y. Chen, *Dalton Trans.*, **2012**, 41, 3659. (g) N. Ikpo, C. Hoffmann, L. N. Dawe and F. M. Kerton, *Dalton Trans.*, **2012**, *41*, 6651. (h) R.

K. Dean, A. M. Reckling, H. Chen, L. N. Dawe, C. M. Schneider and C. M. Kozak, *Dalton Trans*., **2013**, 42, 3504. (i) D. Alhashmialameer, N. Ikpo, J. Collins, L. N. Dawe, K. Hattenhauer and F. M. Kerton, *Dalton Trans*., **2015**, 44, 20216.

[7] As of 01.09.16, the price of benzilic acid is £13.50 for 100 g, whereas $2,2^{/}$ diphenylglycine costs £92.80 for 5 g (prices do not include VAT). Source SigmaAldrich.com.

[8] H. Nakajima, M. Yasuda and A. Baba, *Dalton Trans*., **2012**, 41, 6602.

Chapter 7

Ring opening polymerization of lactides and lactones by multimetallic alkyl zinc complexes derived from the acids Ph$_2$C(X)CO$_2$H (X = OH, NH$_2$)

1. Introduction

As a biocompatible metal, zinc is an attractive target for the development of initiators for the production of biodegradable polymers. The ligand set can also play a pivotal role in determining the catalytic behaviour of the ROP system. Chelating *N,O-* or *O,O-* ligand sets have shown great potential.[1] With this in mind, the use of acids containing the motif $Ph_2C(X)$, where X = OH, NH_2, which is known to impart crystallinity,[2] has been investigated. A search of the CSD revealed 33 hits, the majority of which were organic in nature; a chart of the non-organic structures is given in the (**Appendix chart 2**). Given that zinc complexes have also shown promise over the years as ROP pre-catalysts, [3] we have now turned our attention to alkylzinc complexes incorporating the $Ph_2C(X)$ motif. where X = OH, NH_2, i.e. benzilic acid (X = OH) and diphenylglycine (X = NH_2). Redshaw and co-workers have previously published a number of intriguing molecular structures derived from these acids and alkylzinc and aluminium reagents including tetra-, hexa- and octanuclear ring systems, [4] however the ROP capability of such systems was not examined. Herein the family of complexes available by employing zinc reagents where R = Me or a fluorinated aryl group (**Scheme 15**), has been extended, and assessed as to their ability to act as catalysts towards the ROP of ε-caprolactone (ε-CL), δ-valerolactone (δ-VL) and *rac*-lactide (*r*ac-LA); the co-polymerization of ε-CL with *r*ac-LA has also been studied.

R= Me (**36**), Et (**37**), C$_6$H$_4$CF$_3$-2 (**38**),
C$_6$H$_2$(F)$_3$-2,4,6 (**39**)

40, L = MeCN
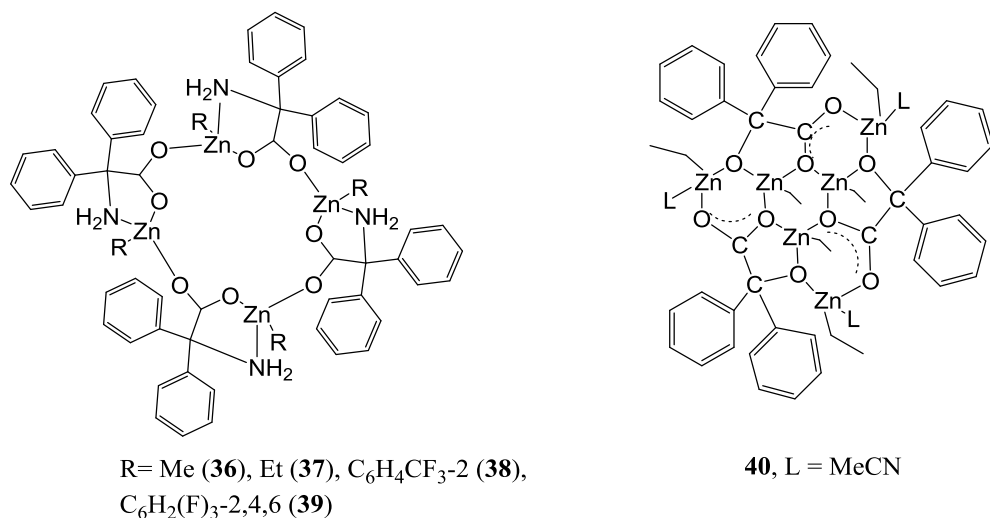
Scheme 15. Organozinc complexes **36** - **40** studied herein

2. Results and Discussion

2.1 Use of 2,2$'$-diphenylglycine (dpgH)

Using the procedure reported by Redshaw *et al*, [4b] we here reacted Me$_2$Zn (2.1 equiv.) was reacted with dpgH and following work-up, the resulting white solid was characterized via elemental analysis, IR spectroscopy with *v*NH stretches at 3345 and 3233 cm^{-1}, and by ^{1}H NMR spectroscopy with doublets at 3.02 and 5.79 ppm assigned to *exo* and *endo* NH$_2$ protons respectively. Single crystals for **36** suitable for X-ray diffraction were grown from a saturated solution of acetonitrile. The molecular structure is shown in (**Figure 116**) for an alternative view (**Appendix figure 158**), with selected bond lengths and angles. As for the ethyl derivative [EtZn(dpg)]$_4$ **37**, each zinc is four coordinate with a Ph$_2$C(NH$_2$)CO$_2$ ligand binding in *N,O* fashion, whilst the other oxygen of this ligand binds to an adjacent zinc. The result is a 16-membered ring adopting an up-down-up-down conformation, in which the carboxylates all bind in *anti/syn* fashion. One of the NH$_2$ groups is involved in an intramolecular H-bond to a neighbouring dpg carboxylate oxygen, whilst another forms an H-bond to an

182

acetonitrile. In terms of packing, there are two channels containing acetonitriles that run parallel to *b* and *c*.
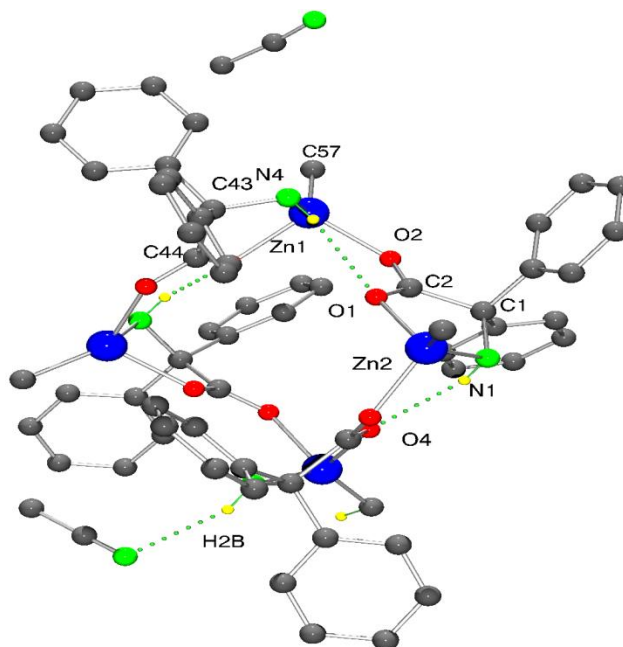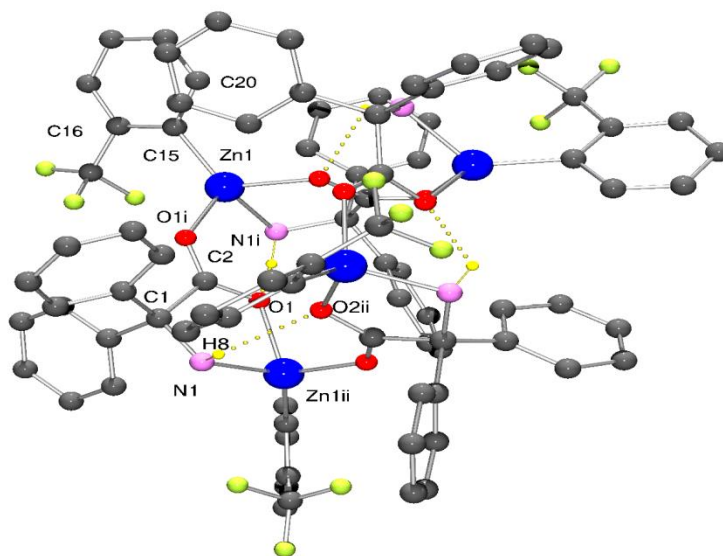

Figure 116. Molecular structure of **36**. Selected bond lengths (Å) and angles (°): Zn(1) – O(2) 2.017(2), Zn(1) – O(7) 2.056(3), Zn(1) – N(4) 2.090(3), Zn(1) – C(57) 1.958(4), Zn(2) – O(1) 2.090(3), Zn(2) – O(4) 2.029(3), Zn(2) – N(1) 2.083(3), Zn(2) – C(58) 1.937(5); Zn(1) – O(2) – C(2) 132.0(2), Zn(1) – O(7) – C(44) 117.1(2), Zn(1) – N(4) – C(43) 109.2(2), Zn(2) – O(1) – C(2) 115.7(2), Zn(2) – O(4) – C(16) 130.5(2), Zn(2) – N(1) – C(1) 110.4(2).

When the reagent [EtZnCl][5] was reacted with dpgH, the only crystalline material isolated following work-up was the known compound [$ZnCl_2(NCMe)_2$]. Although the structure has been previously reported, both the previous data collections were conducted at room temperature. [6] thus our structure of [$ZnCl_2(NCMe)_2$] is presented herein in the (**Appendix 159** and **160**), which reveals a layer structure.

Similar use of (2-$CF_3C_6H_4$)$_2$Zn led to the isolation of [(2-$CF_3C_6H_4$)Zn(dpg)]$_4$ (**38**) in good yield (68 %). The product was characterized by IR spectroscopy with *v*NH stretches at 3306, 3242 and 3172 cm^{-1}, and by ^{1}H NMR spectroscopy with

doublets at 3.02 and 5.79 ppm assigned to *exo* and *endo* NH_2 protons respectively. Crystals suitable for X-ray diffraction were grown from a saturated solution of acetonitrile at ambient temperature. The structure of **38**, shown in (**Figure 117)** for an alternative view **Appendix figure 161**, was crystallographically challenging in that it was both merohedrally twinned via the twin law 010 100 00-1 (major component 54(2) %), and racemically twinned (Flack parameter 0.472(2)). A structure was only possible after temporary 'de-twinning' of the reflection data in XPREP. The full data and the twin law were then used for the structure refinement.

One quarter of the Zn_4 is unique, and the zinc centres are arranged up, down, up, down with bar4 symmetry in the macrocycle. There is no solvent of crystallization; the packing is shown in (**Appendix figure 162.**)
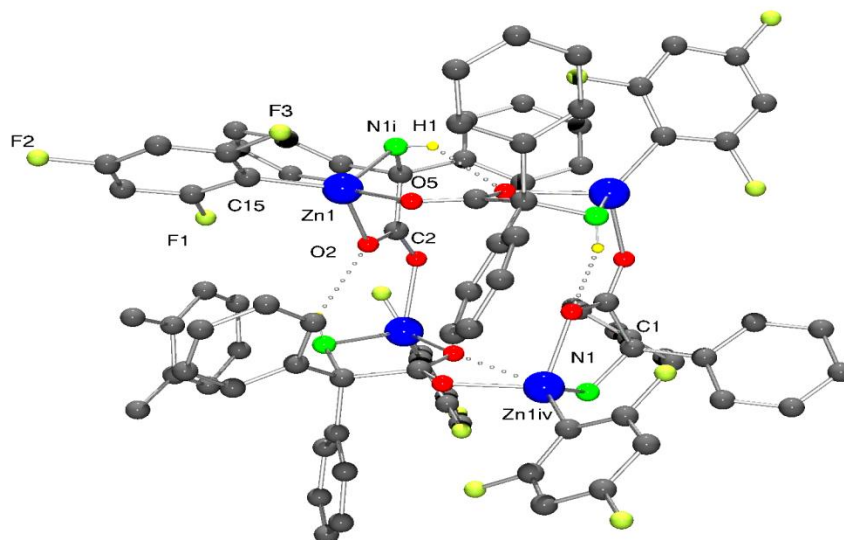

Figure 115. Molecular structure of **38**. Selected bond lengths (Å) and angles (°): Zn(1) – O(2) 1.993(7), Zn(1) – O(1$^/$) 2.049(6), Zn(1) – N(1^i) 2.091(8), Zn(1) – C(15) 1.966(10), Zn(1^{ii}) – O(1) 2.048(6), Zn(1^{ii}) – N(1) 2.091(8) Zn(1) – C(15) – C(16) 125.9(9), Zn(1) – C(15) – C(20) 118.5(8), Zn(1^{ii}) – O(1) – C(2) 116.6(6), Zn(1^{ii}) – N(1) – C(1) 109.7(5).

Extending the methodology to the use of $(2,4,6\text{-}F_3\text{-}C_6H_2)_2Zn$ led to the isolation of the complex $[(2,4,6\text{-}F_3\text{-}C_6H_2)Zn(dpg)]_4$ (**39**) in moderate yield (*ca*. 40 %), for which the IR spectrum contained νNH stretches at 3318 and 3172 cm^{-1}, and the ^{1}H NMR spectrum doublets at 3.43 and 5.38 ppm assigned to *exo* and *endo* NH$_2$ protons respectively. Single crystals were grown from a saturated solution of acetonitrile at ambient temperature. The molecular structure is shown in (**Figure 118)** for an alternative view (**Appendix figure 163)**, with selected bond lengths and angles given in the caption. The asymmetric unit comprises one quarter of $[(2,4,6\text{-}F_3\ C_6H_2)Zn(dpg)]_4 \cdot 4(C_7H_8) \cdot 1.59(H_2O)$ given the $\overline{4}$ symmetry. There was a significant residual electron density peak close to an aromatic ring H atom. This had no clear origin and made no chemical sense, but was modelled as a partial water molecule with *ca*. 40% occupancy with H atoms not located. One of the N*H* protons H-bonds to the Zn-bound O(1) carboxylate atom, while the other forms a C–H···π interaction to the toluene of crystallisation with the distance from the ring centroid to the H atom being 2.549 Å. The core structure is very similar to that in described in **36** above. In the packing of **39**, there are some weak intermolecular C–H···F interactions between $2,4,6\text{-}F_3\text{-}C_6H_2$ groups and $2,4,6\text{-}F_3\text{-}C_6H_2$ groups and the toluene molecule

Figure 118. Molecular structure of **39**. Selected bond lengths (Å) and angles (°): Zn(1) – O(2) 2.008(2), Zn(1) – O(1^i) 2.0304(19), Zn(1) – N(1^i) 2.065(2), Zn(1) – C(15) 1.965(3); Zn(1) – O(2) – C(2) 124.62(18), Zn(1^{iv}) – N(1) – C(1) 111.26(16).

2.2 Use of benzilic acid

For comparative studies, the previously reported complex $[(ZnEt)_3(ZnL)_3(benz)_3]$

(**40**; L = MeCN) has also been prepared. [4b]

2.3 Molecular structure of tris(boron) intermediate

During the preparation of $(2\text{-}CF_3C_6H_4)_2Zn$, we isolated and structurally

characterized the acetonitrile solvate of $(2\text{-}CF_3C_6H_4)_3B(NCMe)$. This

intermediate was prepared using a modification of the synthesis of $B(C_6F_5)_3$

reported by Lancaster,[7] however we limited the scale of this preparation (< 5 g)

and conducted it behind a safety shield given the precedent for explosions when

using halogeno(trifluoromethyl)benzenes for Grignard synthesis.[8] We note that

Ashley and coworkers have employed i-PrMgCl for metal halogen exchange with

1-bromo-3,5-bis(trifluoromethyl)benzene, which was subsequently reacted with

$BF_3.OEt_2$ to afford tris[3,5-bis(trifluoromethyl)phenyl]borane.[9]

The molecular structure of $(2\text{-}CF_3C_6H_4)_3B(NCMe)$ is shown in (**Figure 119)** with

selected bond lengths and angles given in the caption. The three phenyl groups

are twisted by X, Y and Z °, forming a propeller-like orientation. The acetonitrile

free complex has previously been characterized, which possessed near C_3

symmetry and twist angles of 45.6, 49.3 and 52.9 °, reflecting the increased space

available around the 3-ccordinate B centre. [10]
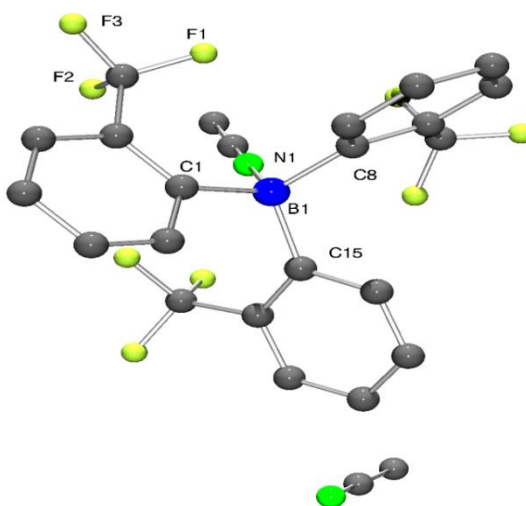
Figure 119. Molecular structure of $(2\text{-}CF_3C_6H_4)_3B(NCMe)\cdot MeCN$. Selected bond
lengths (Å) and angles (°): B(1) – N(1) 1.5857(17), B(1) – C(1) 1.6507(19), B(1) – C(8)
1.6450(19), B(1) – C(15) 1.6434(19); N(1) – B(1) – C(1) 107.58(10), N(1) – B(1) – C(8)
106.65(10), N(1) – B(1) – C(15) 108.31(10).

3. Ring opening polymerization

3.1 Homopolymerization of ε-caprolactone, rac-lactide and δ-valerolactone.

Complexes **36** – **40** have been screened for their ability to ring open polymerize (ROP) ε-caprolactone, *rac*-lactide or δ-valerolactone in the absence of benzyl alcohol (BnOH) at 110 $^{\circ}$C. Compound **39** was used to optimize the polymerization conditions and the results are summarized in (**Table 24**). The observations results suggested that the best results could be obtained when using a molar ratio for [monomer]: [**4**] of 150:1 for ε-CL or 100:1 for *rac*-LA and δ-VL at a temperature of 110 $^{\circ}$C over 1 h for ε-CL or 12 h or 24 h for *rac*-LA and δ-VL, respectively. Under these conditions, each of **36** – **40** was screened for the ROP of ε-CL, *rac*-LA and δ-VL; the resulted are presented in (**Table 25**).

Table 24. Optimum condition screening for the ROP of ε-CL, *rac*-LA and δ-VL using **39**.

Run	Monomer	[Monomer]:[Cat]:[OH]	Time/h	Temp/°C	Conv^a (%)	$M_n{}^b{}_{\times10^3,GPC}$	$M_{n,Cal}{}^c$	PDI^d
1	ε-CL	125:1:0	1	110	91	11400	12980	1.40
2	ε-CL	250:1:0	1	110	78	15000	22260	1.38
3	ε-CL	375:1:0	1	110	88	20800	37670	1.41
4	ε-CL	500:1:0	1	110	91	33700	51930	1.68
5	ε-CL	625:1:0	1	110	85	43800	60640	1.43
6	ε-CL	750:1:0	1	110	89	56200	76190	1.51
7	ε-CL	250:1:0	3	80	69	8590	19700	1.21
8	ε-CL	250:1:0	3	60	22	3850	6280	1.09
9	ε-CL	250:1:0	3	25	---	---	---	---
10	ε-CL	250:1:1	1	110	67	2580	11580	1.10
11	*r*-LA	50:1:0	12	110	74	3370	5330	1.19
12	*r*-LA	100:1:0	12	110	67	6150	9660	1.23
13	*r*-LA	150:1:0	12	110	61	9670	13190	1.27
14	*r*-LA	200:1:0	12	110	65	13000	18740	1.51
15	*r*-LA	250:1:0	12	110	60	15400	21620	1.37
16	*r*-LA	300:1:0	12	110	64	22900	27670	1.40
17	*r*-LA	150:1:0	12	80	19	1460	4110	1.09
18	δ-VL	50:1:0	24	110	42	860	2400	1.04
19	δ-VL	100:1:0	24	110	58	2670	3850	1.13
20	δ-VL	150:1:0	24	110	41	3210	6200	1.23
21	δ-VL	200:1:0	24	110	31	4750	7812	1.08
22	δ-VL	250:1:0	24	110	51	5800	15420	1.25
23	δ-VL	300:1:0	24	110	60	8820	21170	1.12

^{a} Determined by ^{1}H NMR spectroscopy. ^{b} M_n from GPC. ^{b} Calculated from ([Monomer]$_0$/[Cat]$_0$) × conv.(%) × Monomer molecular weight. ^{d} From GPC

Table 25. ROP screening using **36 – 40**.

Run	Cat	Monomer	[Monomer]:Cat:BnOH	Time	Conv^a (%)	M_n^b,GPC	$M_{n,Cal}^c$	PDI^d
1	**36**	ε-CL	150:1:0	1	74	9580	12670	1.37
2	**37**	ε-CL	150:1:0	1	82	10600	14040	1.31
3	**38**	ε-CL	150:1:0	1	90	12840	15400	1.40
4	**39**	ε-CL	150:1:0	1	92	12900	15750	1.31
5	**40**	ε-CL	150:1:0	1	84	10800	14380	1.10
6	**36**	r-LA	100:1:0	12	55	4550	7930	1.88
7	**37**	r-LA	100:1:0	12	57	5010	8220	1.25
8	**38**	r-LA	150:1:0	12	66	7030	14270	1.51
9	**39**	r-LA	100:1:0	12	67	6150	9660	1.23
10	**40**	r-LA	100:1:0	12	61	5970	8790	1.27
11	**36**	δ-VL	100:1:0	24	42	1300	4240	2.12
12	**37**	δ-VL	100:1:0	24	50	1810	5040	2.18
13	**38**	δ-VL	100:1:0	24	54	2810	5440	1.14
14	**39**	δ-VL	100:1:0	24	58	2670	5850	1.13
15	**40**	δ-VL	100:1:0	24	51	1740	5140	1.73

^{a} Determined by ^{1}H NMR spectroscopy.^{b} M_n GPC values corrected considering Mark-Houwink factors (0.56 poly(ε-caprolactone), 0.58 (polylactide)) from polystyrene standards in THF.^{c} Calculated from ([Monomer]$_0$/[cat]$_0$) x conv.(%) x Monomer molecular weight. ^{d}From GPC

3.1.1 For ε-CL

The relationship between the monomer to catalysts mole ratios and the number of average molecular weight values for **39** (**Figures 120)** is near linear indicating that this is a living polymerization process, polydispersity in the range 1.10 to 1.40 indicate that the process was well controlled. The activity associated with the complexes bearing a fluorinated aryl group, namely **38** and **39** was higher than those possessing an alkyl group (complexes **36**, **37** and **40**); observed molecular weights (M_n) followed the same trend. Nomura and coworkers have previously noted enhanced catalytic performances when employing fluorinated imino substituents in phenoxyimine aluminium catalysts for the ROP of ε-CL.[11] Furthermore, a first-order dependence on the ε-CL concentration was observed for the polymerization rate for the ROP of ε-CL (**Figure 121,** left). From the K$_{obs}$ values, it is evident that the catalytic activity follows the order **39** > **38** > **36**,

again suggesting that the presence of the fluorinated aryl group led to an improvement in the catalytic performance. Also, the relationship between conversion and time for the polymerization of ε-CL is presented (**Figure 121, right**). From the ^{1}H and ^{13}C NMR spectra (**Figures 122** and **123**) of the PCL indicated that the end groups were CH_2OH and ONa, and there was no evidence for cyclic PCL. The MALDI-TOF spectrum (**Figure 124)** of the PCL revealed peaks separated by 114 mass units also, there was evidence of a second, albeit minor, population.
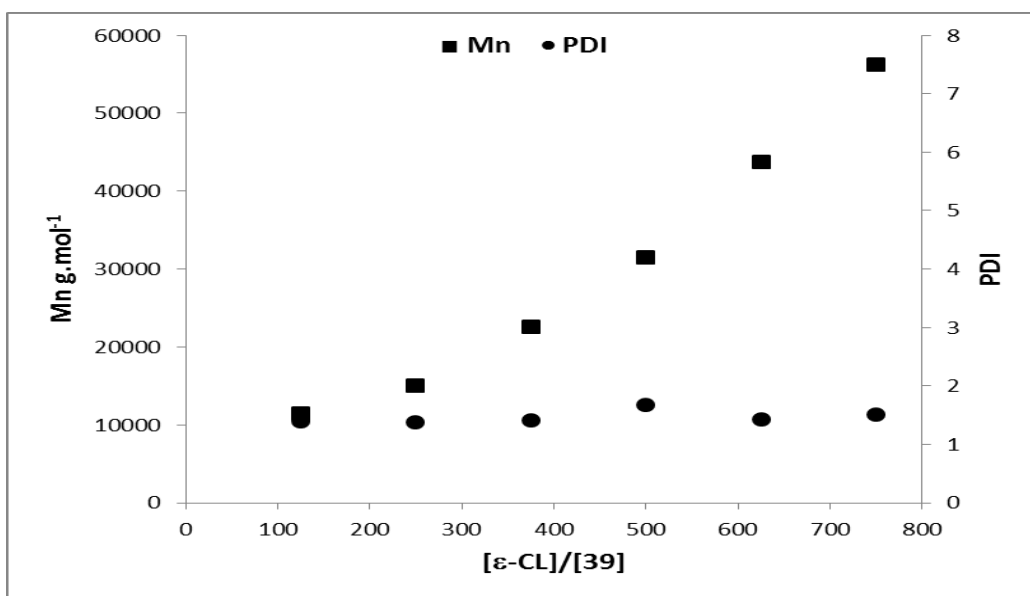
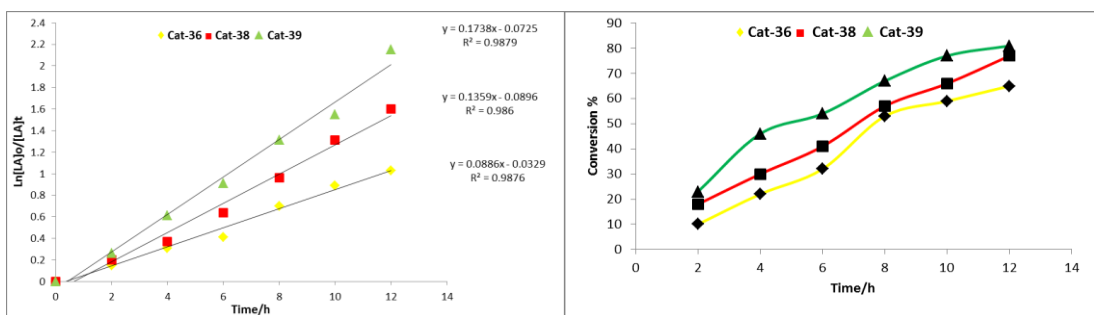**Figure 120.** Relationship between [CL]/[**39**] and the number of average molecular weight and PDI of the polymer.
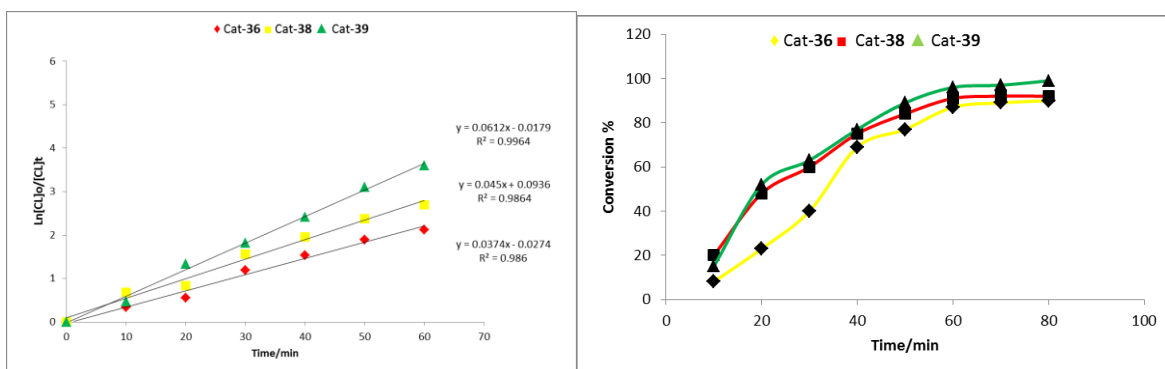
Figure 121. Left: Plot of ln[CL]$_o$/[CL]$_t$ *vs* time using complex **36, 37** and **39**; Right : Relationship between conversion and time for the polymerization of CL.
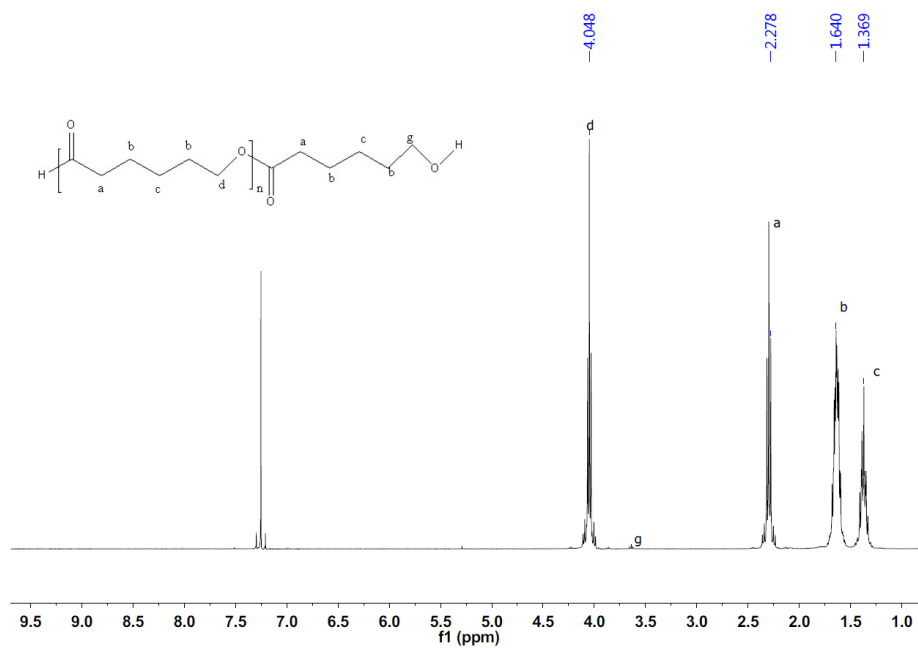

Figure 122. ^{1}H NMR spectrum of polycaprolactone (run 1 table 25).
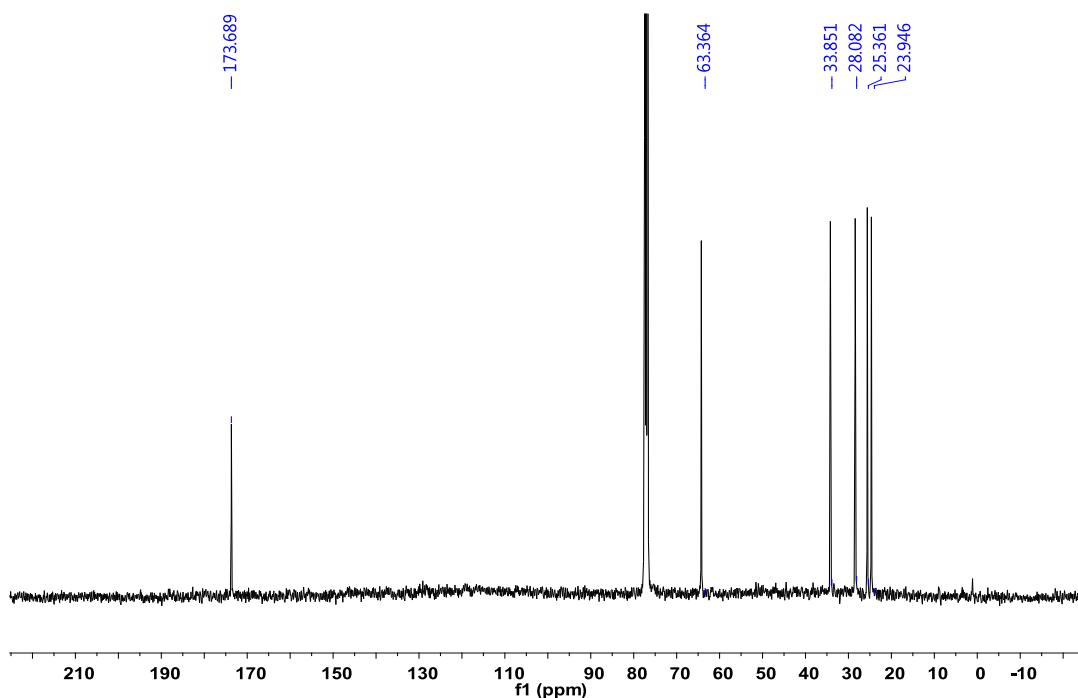
Fig. 123. ^{13}C NMR spectrum of polycaprolactone (run 1 table 25) obtained using **36**.
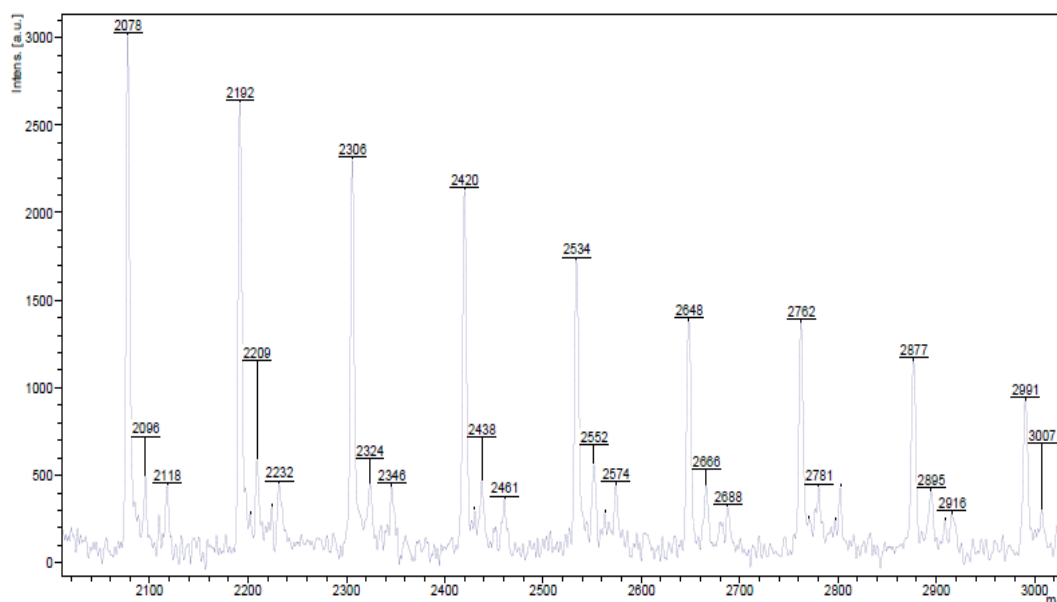
Figure 124. MALDI-ToF spectrum of PCL (run 8, table 24) obtained using **39**.

3.1.2 For rac-LA

Screening of **36 – 40** (**Table 25.** runs 6 -10) indicated that the complexes bearing the fluorinated aryl groups again performed better than those bearing the alkyl groups at zinc. According to the entries (**Table 24,** runs 11-15), there is a linear

193

relationship between M_n values and [*rac*-Lactide]/[**39**] (**Figures 125**) with PDI [1.19 − 1.51] that suggest a living polymerization process and some degree of control. The plot shown in (**Figure 126**, left) reveals a first order dependence on [*r*ac-LA], whilst the K_{obs} values indicated the activity order **39** > **38** > **36**. (**Figure 126**, right) revealed monomer conversion reached to 50% after 6 hours. The ^{1}H NMR and ^{13}C NMR spectra of the PLA (**Figures 127** and **128**) are consistent with non-cyclic products. The MALDI-TOF spectrum of the polylactide (**Figure 129**) contained a series of peaks separated by half a lactide unit (72.0). Homonuclear decoupled and 2D *J*-resolved ^{1}H NMR spectra of the resulting polymers revealed that these systems gave atactic PLA (**Figures 130** - **133**).
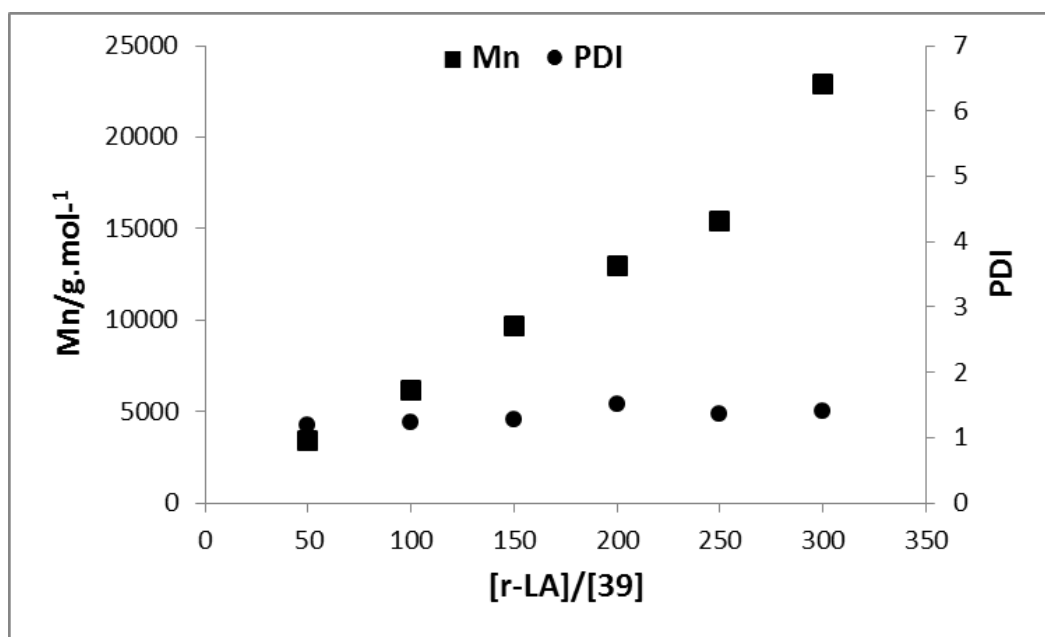
Figure 125. Relationship between [*rac*-Lactide]/[**39**] and the number of average molecular weight and PDI of the polymer.

Figure 126. Left: Plot of ln[*r*ac-LA]$_o$/[*r*ac-LA]$_t$ *vs* time using **36**, **38** and **39**; Right: Relationship between conversion and time of polymerization.
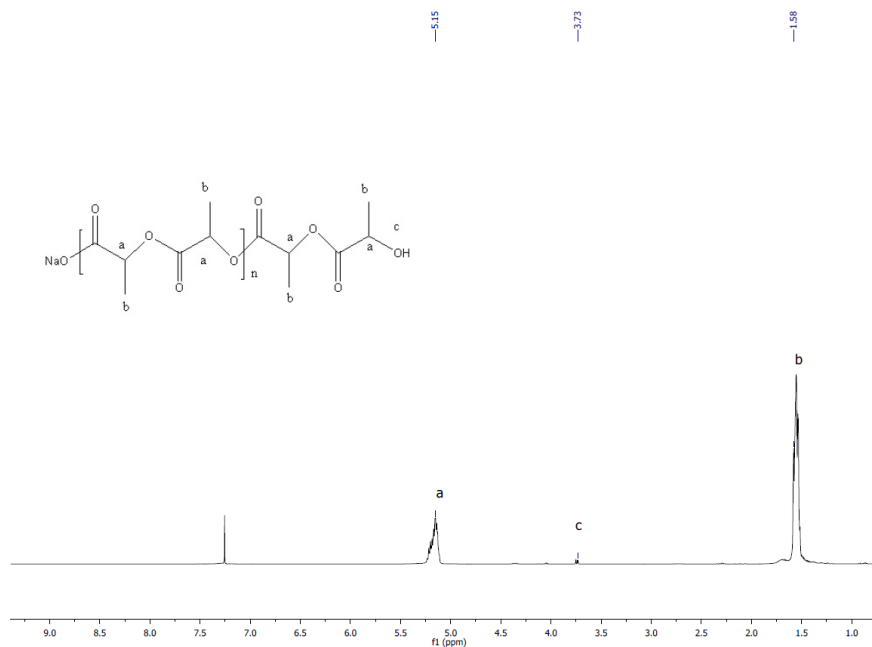
Figure 127. ^{1}H NMR spectrum of polylactide (run 6 table 25).
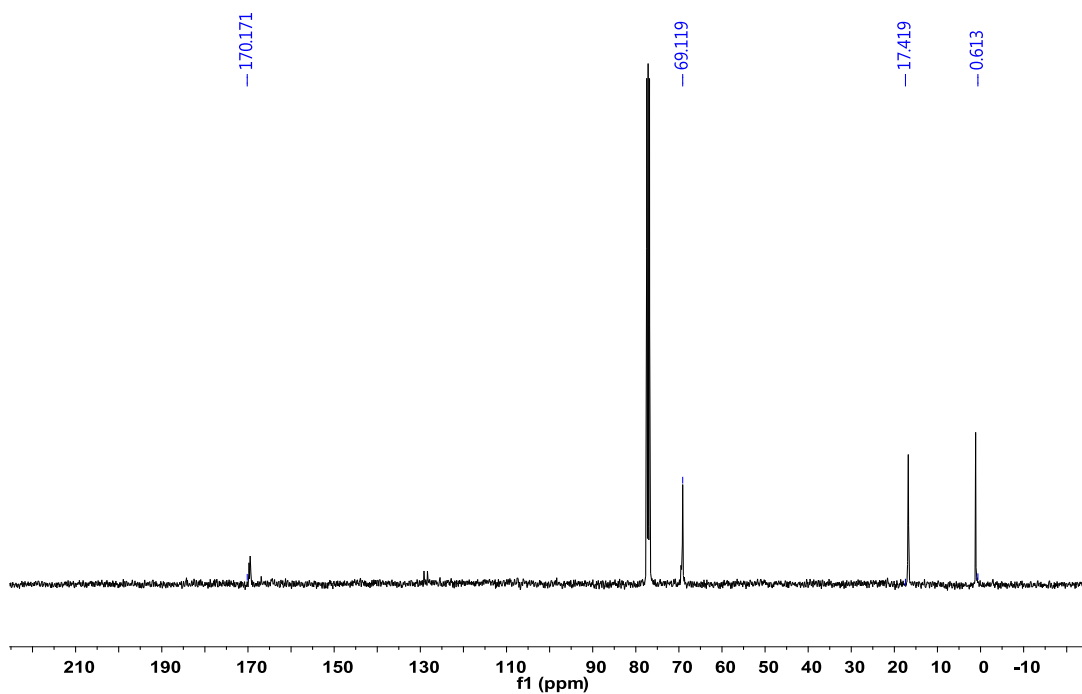
Figure 128. ^{13}C NMR spectrum of polylactide (run 6 table 25).
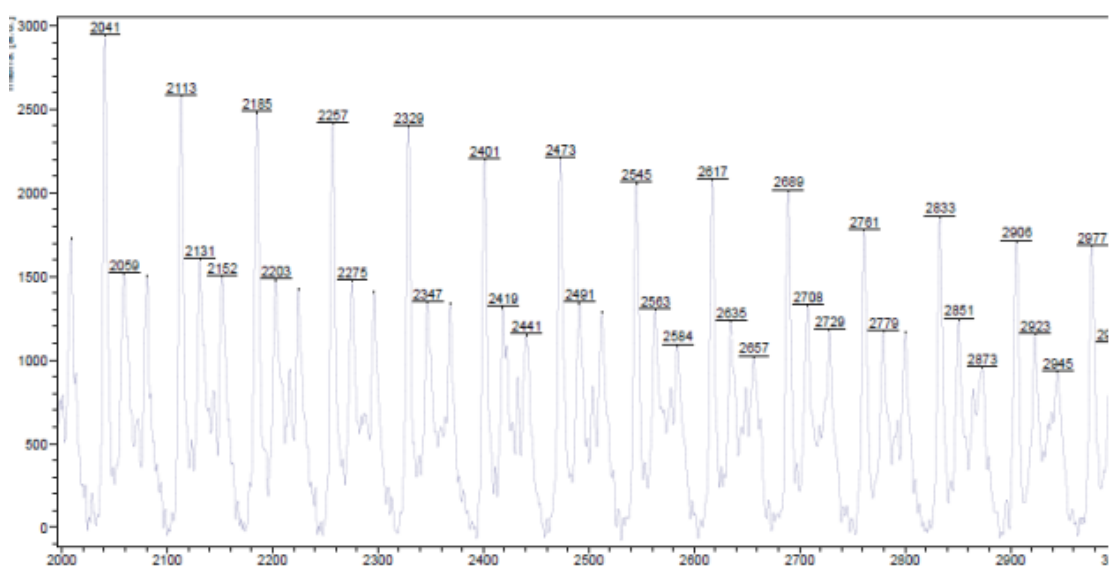
Figure **129**. MALDI-ToF spectrum of poly(*rac*-LA) (run 6, table 125).
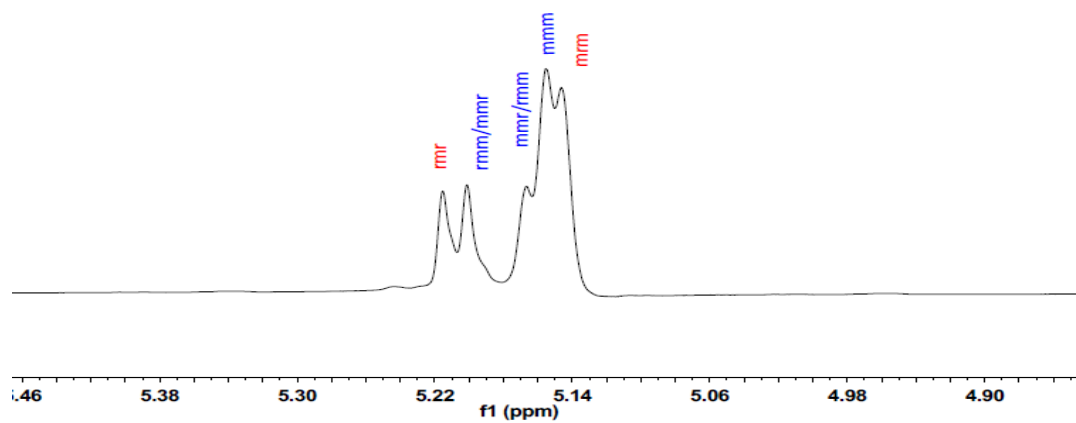
Figure 130. Homonuclear decoupled ^{1}H NMR spectrum of of poly($r$ac-LA), (run 6, table 25).
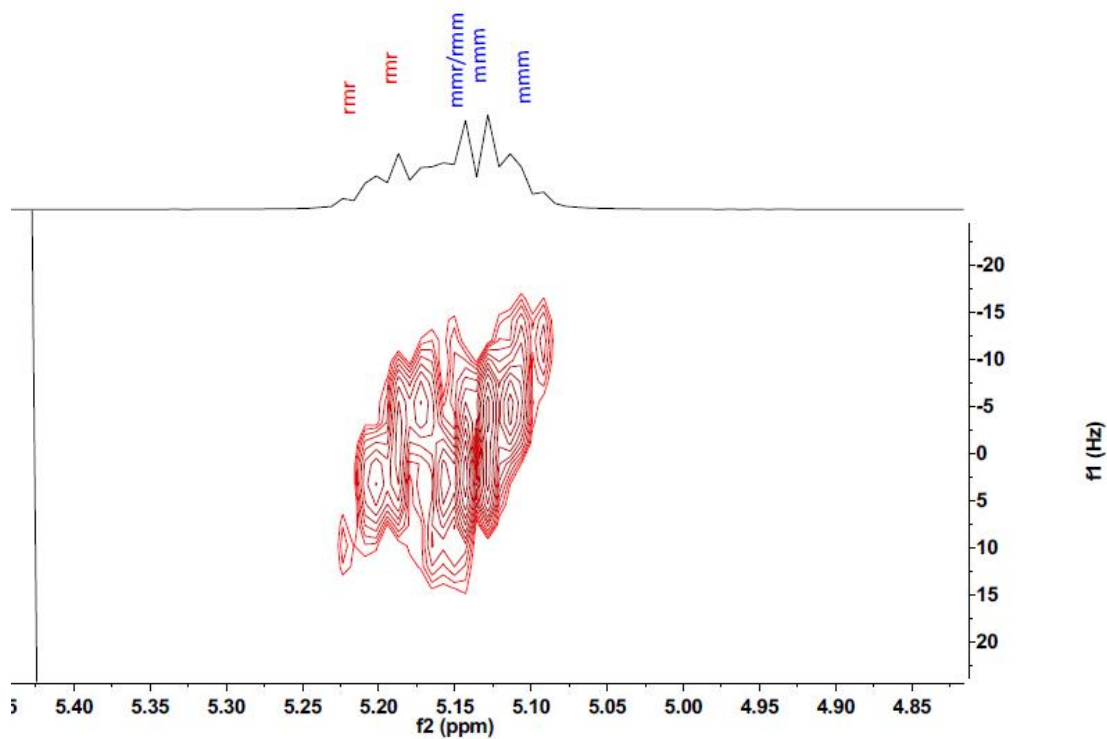
Figure 131. 2D J-resolved ^{1}H NMR spectrum of poly(rac-LA) (run 6, table 25).
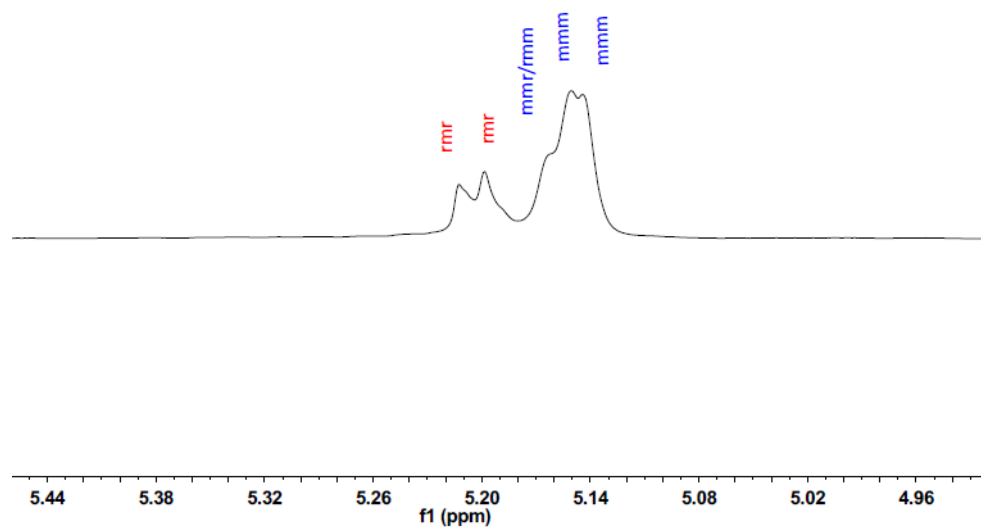
Figure 132. Homonuclear decoupled ^{1}H NMR spectrum of of poly(*rac*-LA), (run 8, table 25).
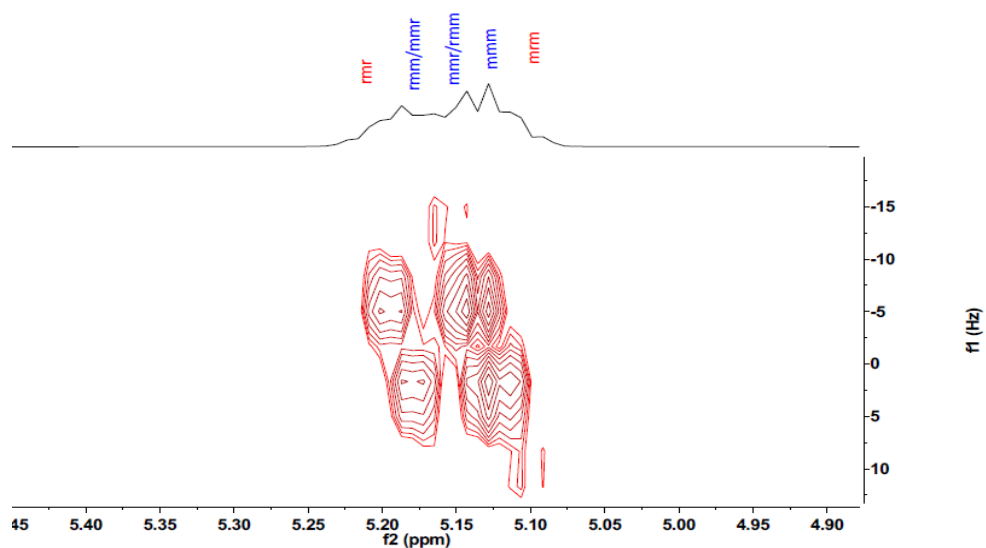
Figure 133. 2D J-resolved ^{1}H NMR spectrum of poly(*rac*-LA) (run 8, table 25).

3.1.3 For δ-VL

The ROP of δ-valerolactone catalyzed by complexes **36** - **40** was also investigated; the results are presented in (**Table 25)** (runs 11 − 15). As for both the other monomers screened herein, high conversions and polymer molecular

198

weights were achieved when using the systems bearing the fluorinated aryl groups at zinc. Systems **38** and **39** also exhibited better controlled (PDIs 1.13 and 1.14) than the other systems employed for the ROP of δ-valerolactone. The plot of [δ-VL]/[**39**] versus M_n values (**Figure 134**) that suggest there is a living polymerization process and some degree of control. From the ^{1}H NMR spectra of the PVL (**Figure 135**), peak at 3.62 revealed the presence of CH$_2$OH end group. In general, it was evident that the ROP of δ-VL required more robust conditions than were required for ε-CL, which is consistent with the thermodynamic parameters for these lactones.
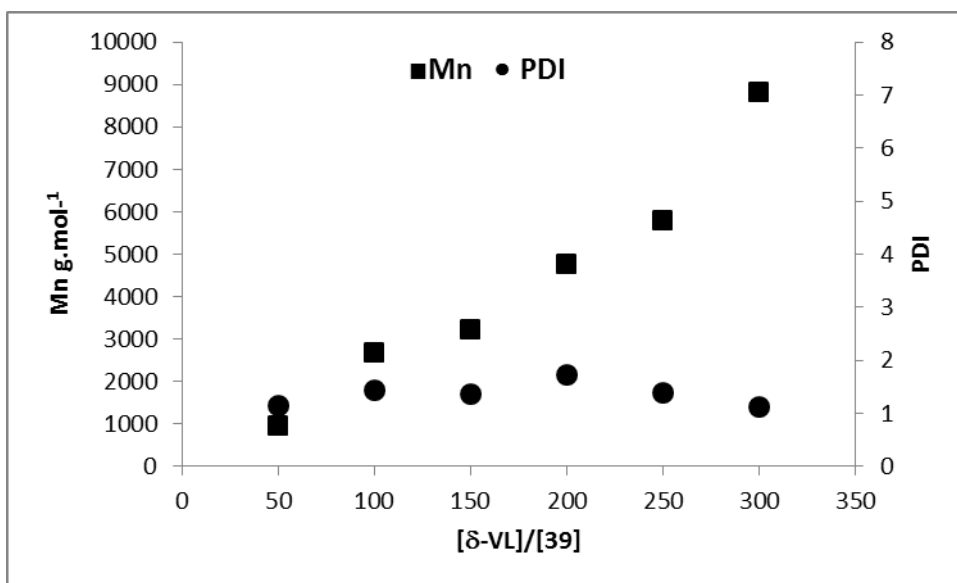
Figure 134. Relationship between [δ-valerolactone]/[**39**] and the number of average molecular weight and PDI of the polymer.
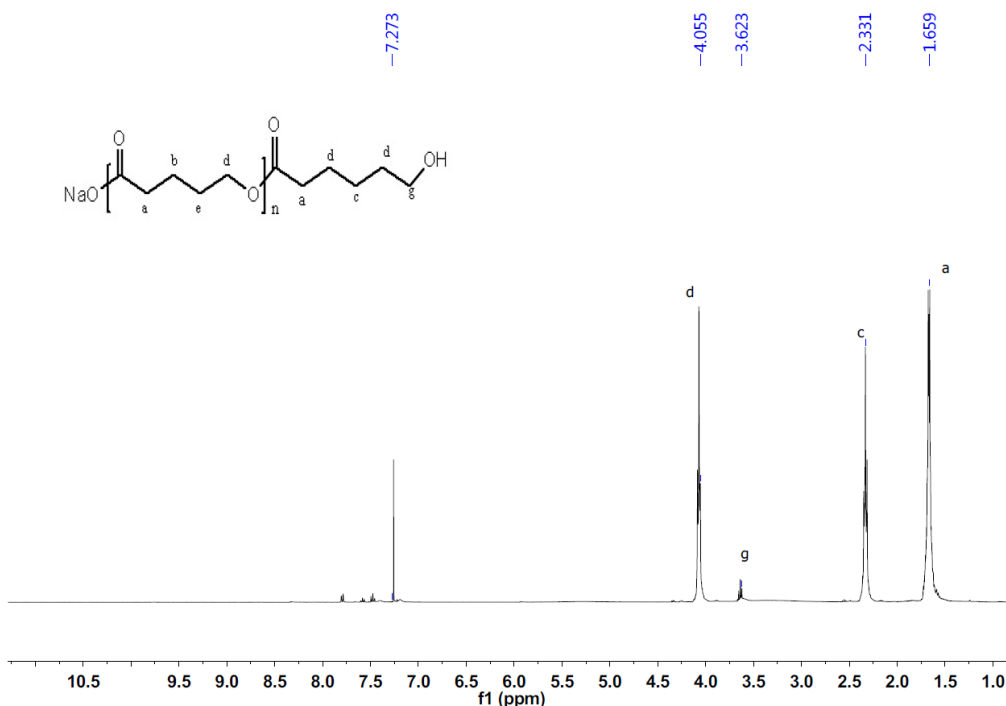
Figure 135. ^{1}H NMR spectrum of PVL (run 11 table 25).

3.2 Co-polymerization of ε-caprolactone and rac-lactide.

The co-polymerization of ε-CL with *rac*-LA was studied using complexes **36** to **40** at 110 ^{o}C, and the results are summarized in (**Table 26**). Yields of the co-polymers were in the range 58 − 77 %, however unlike for the homopolymerizations, there was no obvious advantage in using the fluorinated systems in terms of activity, though they afforded slightly higher polylactide content as observed by ^{1}H NMR spectra, (**Figure 136**). The ^{13}C NMR spectra of the co-polymers (**Figure 137**) exhibited both carbonyl signals at 169 and 174 ppm due to the polycaprolactone and polylactide components, respectively. Thermal analysis (by DSC) of the co-polymers revealed (**Figure 138**) two peaks at about 51.72 ^{o}C and 160.71 ^{o}C. The reverse addition of monomers resulted in little or no polymerization.

200

Table 26. Synthesis of diblock co-polymers from cyclic ester monomers (ε-CL+ *r*-LA).

Run[a]	Cat	CL:LA[b]	Yield	M_n[c]	PDI[d]
1	**36**	62:38	65	5310	1.09
2	**37**	60:40	72	2900	1.12
3	**38**	53:47	77	5160	1.19
4	**39**	55:45	58	2210	1.25
5	**40**	56:44	69	3590	1.08
6[e]	**39**	---	---	---	---

[a] Optimum conditions: 1h ε-CL 110 °C/12h *r*-LA 110 °C, (150 [ε-CL]: 150 [*r*-LA]: [cat]). [b] Ratio of CL to LA observed in the co-polymer by ^{1}H NMR spectroscopy. [c] M_n values were determined by GPC in THF *vs* PS standards and were corrected with a Mark–Houwink factor ($M_{n, GPC} \times 0.56 \times$ % PCL + $M_{n,GPC} \times 0.58 \times$ % P *r*-LA). [d] PDI were determined by GPC. [e] Reverse addition (*ie r*-LA added first).
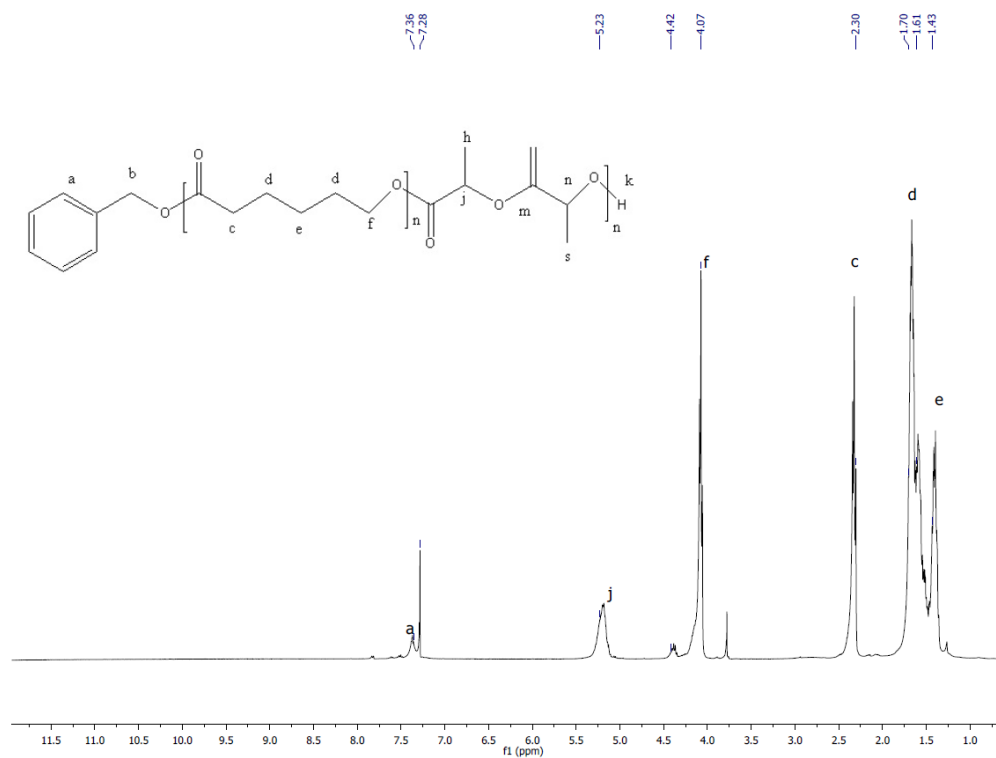
Figure 136. ^{1}H NMR spectrum of copolymer PCL+ poly(*rac*-LA), (run 1, table 25).
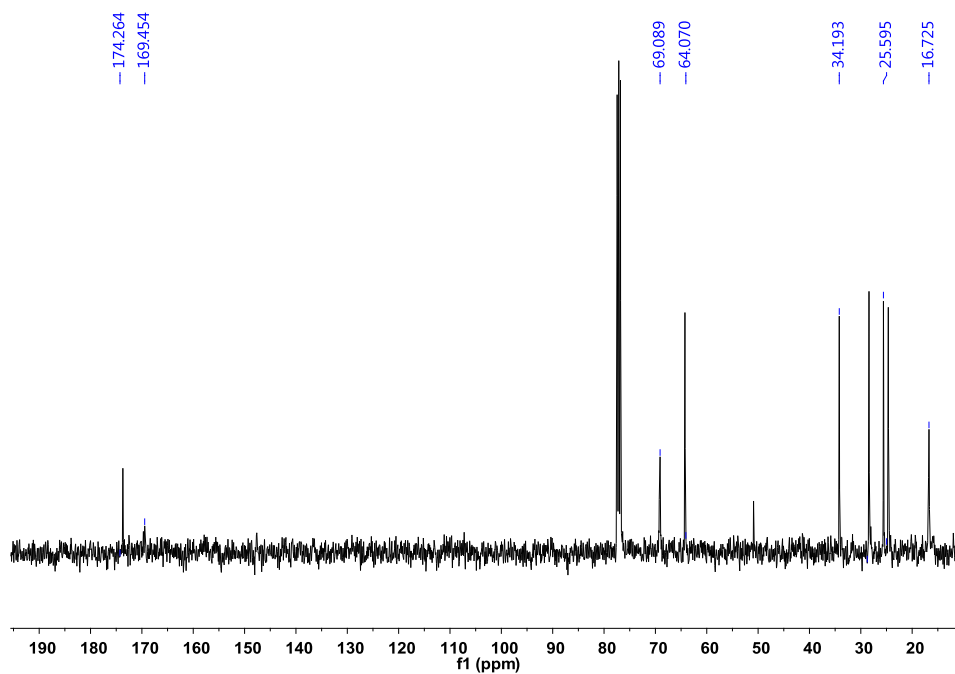
Figure 137. ^{13}C NMR spectrum of co-polymer PCL+ PLA, (run 7, table 26).
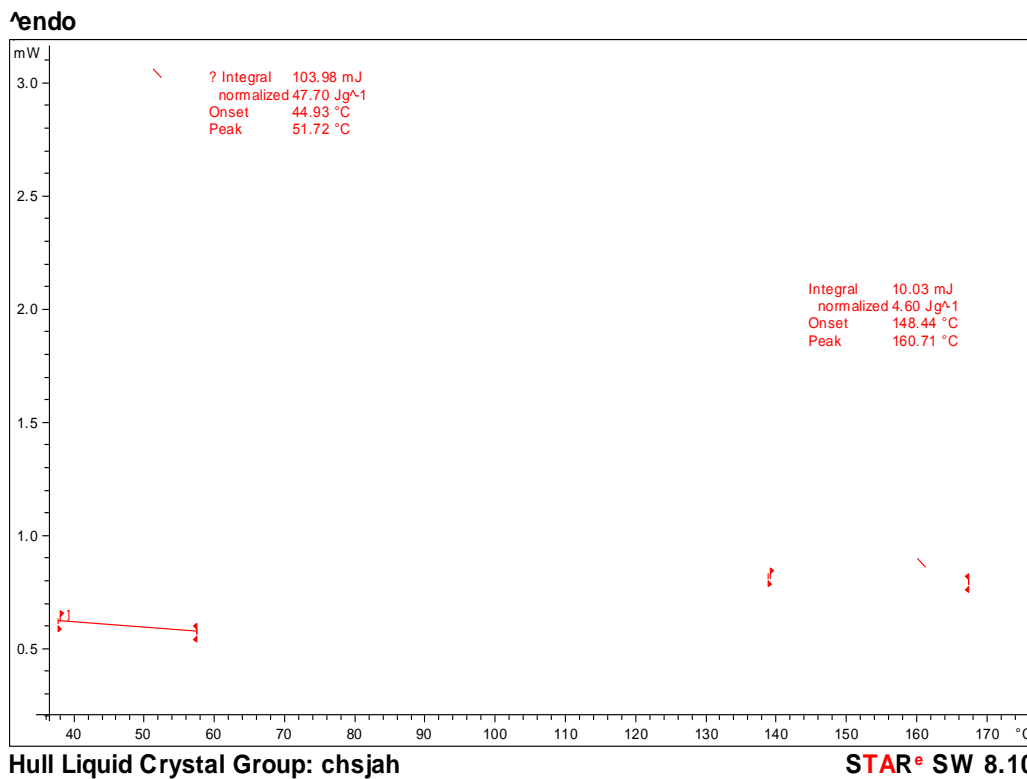
Figure 138. DSC plot of co-polymer from ε-CL and *rac*-LA, (run 2, table 26).

4. Conclusion

In conclusion, a series of alkylzinc complexes of formula [RZn(dpg)]$_4$, where R = Me (**36**), Et (**37**), 2-CF$_3$C$_6$H$_4$ (**38**), 2,4,6-F$_3$C$_6$H$_2$ (**39**) and dpg is derived from Ph$_2$C(NH$_2$)CO$_2$H (dpgH) have been synthesized. In each complex, the core structure is very similar with the zinc macrocycle adopting an up, down, up, down conformation. Complexes **36** – **39** and the known benzylic acid (benzH) derived complex [(ZnEt)$_3$(ZnL)$_3$(benz)$_3$] (**40**) were found to be active for the ROP of ε-Cl, *rac*-LA and δ-VL, with or without benzyl alcohol present. Complexes **38** and **39** bearing fluorinated aryls at zinc were found to afford the highest activities. All complexes were also capable of affording copolymers via sequential addition of the monomers ε-Cl and *rac*-LA.

5- References

[1] (a) R. E. Drumright, P. R. Gruber and D. E. Henton, *Adv. Mater.*, **2000**, 12, 1841.

(b) M. A. Woodruff and D. W. Hutmacher, *Prog. Polym., Sci.*, **2010**, 35, 1217. (c) A. L.Sisson, D. Ekinci and A. Lendlein, *Polymer*, **2013**, 54, 4333.

[2] F. H. Allen, *Acta Cryst.*, **2002**, B58, 380.

[3] C. K. Williams, L. E. Breyfogle, S. K. Choi, W. Nam, V. G. Young, M. A. Hillmyer and W. B. Tolman, *J. Am. Chem. Soc.*, **2003**, 125, 11350.

[4] (a) C. Redshaw, M. R. J. Elsegood and K. E. Holmes *Angew. Chem. Int. Ed.*, **2005**, 44, 1884. (b) C. Redshaw and M. R. J. Elsegood, *Angew. Chem. Int. Ed.*, **2007**, 46, 7453.

[5] A. Guerrero, D. L. Hughes and M. Bochmann, *Organometallics,* **2006**, 25, 1525.

[6] (a) I.V. Isakov and Z.V. Zvonkova, Nauk SSSR (Russ.) *Proc. Nat. Acad. Sci. USSR*, **1962**, 145, 808. (b) V.K. Bel'sky, N.R. Stetsova. B.M. Balychev, P.A.Storozhenko, L.V. Ivankina, and A.I. Gobumov, *Inorg. Chim. Acta*, **1989**, 164, 211.

[7] S. J. Lancaster, *ChemSpider,* **2003**, 215.

[8] N. A. Yakelis and R. G. Bergman, *Organometallics*, **2005**, 24, 3579.

[9] T. J. Herrington, A. J. W. Thom, A. J. P. White and A. E. Ashley, *Dalton Trans.*, **2012**, 41, 9019.

[10] S. Toyota, M. Asakura, M. Ōki and F. Toda, *Bull. Chem. Soc. Jpn.*, **2000**, 73, 2357.

[11] N. Iwasa, S. Katao, J. Liu, M. Fujiki, Y. Furukawa and K. Nomura, *Organometallics*, **2009**, 28, 2179.

Chapter 8

Experimental section

1. General

All manipulations were carried out under an atmosphere of dry nitrogen using conventional Schlenk and cannula techniques or in a conventional nitrogen-filled glove box. Diethyl ether, tetrahydrofuran, hexane and toluene were refluxed over sodium and benzophenone. Dichloromethane and acetonitrile were refluxed over calcium hydride. All solvents were distilled and degassed prior to use. Deuterated solvents were dried over phosphorous pentoxide. IR spectra (Nujol mulls, KBr windows) were recorded on a Nicolet Avatar 360 FT IR or a Nicolet iS5 FT IR spectrometer. Mass spectrometry data were recorded by the EPSRC National Mass Spectrometry Service Centre at Swansea University or by staff at the University of Hull. Elemental analyses were performed by the elemental analysis service at London Metropolitan University or by staff at the University of Hull.

^{1}H, ^{13}C, ^{13}P (reference H_3PO_4 in D_2O $\delta_P = 0$ ppm), ^{19}F(reference $CFCl_3$ $\delta_F = 0$ ppm) and ^{11}B(15% BF_3Et_2O in CDCl3 $\delta_B = 0$ ppm) NMR spectra were performed at room temperature on a JNM LA-400 MHz spectrometer, JEOL, or a JNM ECP-400 MHz spectrometer, JEOL. The ^{51}V NMR spectra were calibrated against an external $VOCl_3/CDCl_3$ reference. The ^{7}Li NMR spectra were calibrated against an external $LiCl/D_2O$ reference. Gel permeation chromatography (GPC) measurements were performed using a Viscotek, 270

DUAL DETOCTOR. Polymer melting points were determined using a TA Instruments DSC 822E/200RO.

Crystal data (**Chapter 2**) were collected on a Rigaku Saturn 724+ CCD diffractometer using synchrotron radiation at DLS beam line I19 for L_1H_4, using the same instrument but with sealed tube MoKα radiation for $L_2H_4 \cdot 2MeCN$, **1**$\cdot$6MeCN, **2**$\cdot$3½MeCN$\cdot$0.614toluene, and **4**$\cdot$3½MeCN, and a Stoe IPDS diffractometer for **3**$\cdot$5MeCN and **4**$\cdot$5MeCN. Data were corrected for L^p effects and for absorption, based on repeated and symmetry equivalent reflections and solved by direct methods or a dual-space method (SHELXS-2013/SHELXT).[1][2] Structures were refined by full matrix least squares on F^2.[3] H atoms were included in a riding model except for H(1), H(3) and H(4) in L2H4, and H(7) and H(8) in **4**$\cdot$3½MeCN for which coordinates were refined. Hydrogen atom U_{iso} values were constrained to be 120% of that of the carrier atom except for methyl and hydroxyl-H (150%). Several structures exhibited two-fold disorder in tert-butyl groups and/or solvent molecules where restraints were applied to geometry and anisotropic displacement parameters. For **4**$\cdot$5MeCN, the crystal examined was a non-merohedral twin. The second twin component was identified on the diffractometer and both components integrated and used for refinement of the crystal structure. In this structure one MeCN of crystallization per unit cell was refined as a diffuse area of electron density by the Platon Squeeze procedure17 and three MeCNs per asymmetric unit were refined at half weight. In **3**$\cdot$5MeCN, four MeCNs per unit cell were refined using the Squeeze procedure.

X-ray diffraction data (**Chapter 3)** For **5** were collected using synchrotron radiation at Daresbury Laboratory, Station 9.8, using silcon 111 monochromated radiation and a Bruker 1K CCD detector. X-ray diffraction data for **6** and **12** were collected using a Stoe & Cie GmbH, Darmstadt, Germany. Diffraction data for **7** and **8**·6MeCN were collected on a Bruker AXS GmbH, Karlsruhe, Germany. Diffraction data for **10**·2C$_6$H$_{14}$ and **11**·6MeCN were collected on a Rigaku Corp., Tokyo, Japan. All data collections except that for **5** utilised monochromated Mo-Kα radiation and ω-scans. Standard procedures were employed for the integration and processing of the data. Crystals were coated in a thin film of perfluoropolyether oil and mounted at the tip of a glass fibre (MiTeGen mount for **10**·2C6H14 and **11**·6MeCN) located on a goniometer. All data sets were collected from crystals at low temperature using an Oxford Cryosystems, Long Hanborough, Oxfordshire, UK. Crystal structures were solved using routine automatic direct methods implemented within SHELXS-97,[4] or iterative charge-flipping methods (SHELXT).[5] Completion of structures was achieved by performing least squares refinement against all unique $F2$ values using SHELXL-2014.[6] All non-H atoms were refined with anisotropic displacement parameters. Hydrogen atoms were placed using a riding model except for H(3) in **8**·6MeCN for which the coordinates were freely refined. The Platon SQUEEZE routine was used to model regions of disordered hexane solvent of crystallisation (2 molecules per complex) in **10**·2C$_6$H$_{14}$ and MeCN (2.5 per complex) in **11**·6MeCN.[7] CCDC 1425489-1425495 contain the supplementary crystallographic data for this paper:

Single crystal diffraction data (**Chapter 4**) were collected by the UK National Crystallography Service using a Rigaku FR-E+ diffractometer. This operates with a SuperBright rotating anode X-ray generator and high flux optics. This is designed to deal with the most challenging samples sent to the service. Despite the high flux, the crystal of **13** examined was found to scatter X-rays very poorly and little appreciable diffraction was observed beyond ~1.1 Å. It was possible to solve the structure using this data and routine refinements of a structural model were possible. It was possible to use anisotropic displacement parameters for all non-hydrogen atoms and the refinement was stable with no unusual features. Although the crystal examined was weakly scattering the solution is sound and it gives extremely useful chemical information. The data for **14**, although weak, are more routine and standard procedures were applied in structure solution. Structures were solved using Direct Methods implemented within SHELXS-2013 and refined within SHELXL-2014.[4]

(**Chapter 5**) Structures were solved using automated direct methods within SHELXS-86 or intrinsic phasing within SHELXT.[4] Structures were refined by full-matrix least squares refinement within SHELXL-2014 using all unique data.[5], [8] Hydrogen atoms were placed using a riding model. Where data were sufficiently good, methyl group orientations were refined. Many of the structures displayed disorder in the position of methyl groups or in solvent of crystallisation. This disorder was modelled using standard techniques.

Diffraction data were collected on a range of different CCD diffractometers and were corrected for absorption and Lp effects using multi-scan methods.[9] The

details are presented in (**Appendix table 28**). For **24** the crystal examined was twinned. The structure was refined using all observed reflections within SHELXL using the HKLF5 formalism. Samples of **L⁹**H(dpa) and **L⁹**H(dpg) were collected at different temperatures from samples made in the same way. In each case the structure determination was repeated using a second crystal to confirm the correctness of the crystal structure at that temperature. Diffraction data for **28** were collected using synchrotron radiation at Daresbury Laboratory Station 9.8. For **29**: The structure was refined as a two-component twin using the HKLF5 protocol as above for **24**. The two domains were related by a 178.8° rotation about the real and direct [010] direction. Two out of three H atoms on CH_3^+ group at C(5) are disordered. In the difference electron density map, one clear peak is seen with a peak height of *ca.* 0.9 e$Å^{-3}$ which is refined fully occupied as H(5A). There are also *ca.* four smaller peaks of between 0.4-0.6 e$Å^{-3}$ which are refined in pairs as the other CH_3^+ H atoms. A similar pattern of electron density peaks and partial H-atom disorder was observed in **28**.

Diffraction data for (**Chapter 6**) were collected on CCD area detector diffractometers using a rotating anode X-ray source for **31**·2THF, **31**$^{/}$, **33**, **34**, and **35**, and synchrotron radiation for **32**·2MeCN·THF.[10] Full details are presented in (**Appendix table 28**). Data were corrected for absorption and Lp effects. Structures were solved by direct or iterative methods and refined by full-matrix least squares on F^2. [5],[11] The bound THF molecule in **31′** is disordered in two different orientations in the ratio 67.6:32.4(5). This was handled using standard procedures. There was disorder in the position of one benzilate anion (centred on C(58)) in **32**·2MeCN·THF. The different orientations (ratio

73.09:26.91(17)) are related by rotating the molecule to interchange the positions of carboxylate and alkoxy moieties. It was possible to model this complicated disorder with standard procedures. There is disorder present in each of the unique parts of the asymmetric unit in **35**. One phenyl ring, C(9)-C(14) adopts two different positions in the ratio 52.6:47.4(9). Similarly the rings C(33)-C(38) and C(39)-C(44) display orientational disorder with the major components 55.1(11) % and 56.6(10) % occupied respectively.

Diffraction data for (**Chapter 7**) were collected on a Bruker APEX 2 CCD diffractometer and were corrected for absorption and Lp effects. [3],[5],[11] Further details are provided in (**Appendix table 28**). Structures were solved by direct methods {charge flipping for **39**·4(C_7H_8)·1.59(H_2O)} and refined by full matrix least squares methods. N–H distances were restrained for structures **36**·2MeCN and **39**·4(C_7H_8)·1.59(H_2O). The structure **38** was refined as merohedrally twinned via the twin law 010 100 00–1 (major component 54(2) %), and racemically twinned (Flack parameter 0.472(2)). A structure solution was only possible after temporary 'de-twinning' of the reflection data. The full data and the twin law were then used for the structure refinement. For **39**·4(C_7H_8)·1.59(H_2O) the toluene lies on a symmetry element and the methyl group was 50/50 disordered over two positions as a result. There was also a significant residual electron density peak close to an aromatic ring H atom. This was modelled as a partial water molecule with 39.7(9)% occupancy with H atoms not located.

2. Synthesis of known compounds

The ligands L^1H_4, L^1H_4, L^4H_2, L^5H_3, L^7H, $L^{10}H$ were synthesized following the reported literature method.[12-16] The precursor [Nb(O)Cl$_3$(NCMe)$_2$] and L^{11} were prepared via (Me$_3$Si)$_2$O.[17,18] The complexes **12**, **18**, **19**, **20**, **27, 37** and **40** were

prepared as described in the literatures.[15,16][19-20] Pro-ligand (L^3H_2) was purchased commercially and dried *in-vacuo* prior to use.

3. Synthesis of Nb and Ta tetraphenolate complexes

*3.1 Synthesis of {[NbCl$_3$(NCMe)]$_2$(μ-p-L^1)}·6MeCN (**1**·6MeCN)*
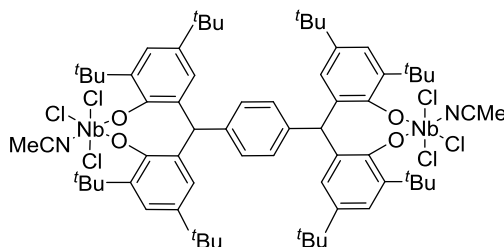
α, α, α′, α′-Tetra (3,5-di-*tert*-butyl-2-hydroxyphenyl)-*p*-xylene L^1H_4 (1.66 g, 1.80 mmol) was dissolved in toluene (40 mL). $NbCl_5$ (1.00 g, 3.70 mmol) was added as a solid and the system was refluxed for 12 h. The volatiles were removed *in vacuo*, and the residue was extracted into warm acetonitrile (30 mL); prolonged standing at 0 °C gave orange plates of the compound **1.** Yield(2.46 g, 83.00%). MS (positive nanospray in CH_2Cl_2–MeCN):1364.5 (M − Cl), 1323.5 (M − Cl − MeCN), 1211.6 (M − 3Cl −2MeCN), 1176.2 (M − 3Cl − 2MeCN). Found: C, 59.06; H, 6.63; N 0.77. $C_{68}H_{92}Cl_6N_2O_4Nb_2$ (sample dried in vacuo for 12 h; − 7MeCN) requires C, 58.33; H, 6.60; N, 1.03%. IR (Nujol, KBr,cm^{-1}): 2308w, 2286w, 1645w, 1568w, 1303w, 1235m, 1171bs,1118s, 1087m, 1019w, 1009w, 904m, 886s, 829m, 815s, 721s, 639w, 559m, 545m, 479w, 446w. ^{1}H NMR (acetone-d$_6$): δ =7.20–6.78 (overlapping m, 12H, aryl*H*), 6.07 (s, 2H, C*H*), 2.05 (s, 6H, C*H$_3$*CN), 1.38 (s, 36H, C(C*H$_3$*)$_3$), 1.15 (s, 36H, C(C*H$_3$*)$_3$).

3.2 Synthesis of {[NbCl$_2$(OEt)(NCMe)]$_2$(μ -p-L^1)}•3½MeCN•0.614toluene (2•3½MeCN•0.614toluene)
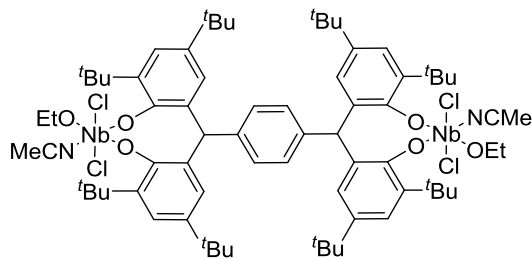
To NbCl$_5$ (0.59 g, 2.18 mmol) in toluene (20 mL) at -78 ^{o}C was added ethanol (5 ml) and the solution was stirred for 5 min., following which α,α,α′,α′-tetra(3,5-di-*tert*-butyl-2-hydroxyphenyl)-*p*-xylene (1.00 g, 1.08 mmol) in toluene (10 mL) was added and the mixture was then stirred for 48 h at ambient temperature. After the volatiles were removed *in-vacuo*, the residue was extracted into acetonitrile (20 ml) or dichloromethane (20 mL) and on prolonged standing (1 − 2 days) at ambient temperature, red prisms of **2** formed. Yield (1.84 g, 63.00%). MS (positive nanospray in CH$_2$Cl$_2$/MeCN): 1333 (M − EtOH − MeCN). IR (Nujol, KBr, cm^{-1}): 2312w, 2290w, 1626w, 1598w, 1570w, 1506w, 1405m, 1362s, 1292m, 1256m, 1230s, 1198s, 1154m, 1104s, 1094s, 1054s, 1020s, 974w, 916s, 880s, 862s, 816w, 799m, 776m, 761m, 659m, 645w, 615w, 594w, 556m, 464m, 453m. Found: C, 57.55,* despite repeated attempts sample gave unsatisfactory C values; H, 7.58; N, 0.59. C$_{70}$H$_{99}$Cl$_4$N$_2$O$_6$Nb$_2$ (sample dried in vacuo for 12h; - 4.5 MeCN- 0.614 toluene) requires C, 61.00; H, 7.24; N, 1.02 %. ^{1}H NMR (CDCl$_3$): δ = 7.31 − 7.15 (overlapping m, 15H, aryl$H$ + 0.614C$_6$H$_5$CH$_3$), 5.04 (bm, 4H, OCH_2 + CH), 4.15 (bm, 2H, OCH_2), 2.33 (0.614C$_6$H$_5$CH_3), 1.98 (bs, 10.5H, 3.5CH_3CN), 1.45 (s, 36H, C(CH_3)$_3$), 1.22 (s, 36H, C(CH_3)$_3$), 1.20 (m, 3H, OCH$_2$CH_3), 1.15 (m, 3H, OCH$_2$CH_3).

3. 3 Synthesis of {[TaCl₂(OEt)(NCMe)]₂(μ-p-L¹)}·5MeCN (3·5MeCN)

$$3.\ 3\ Synthesis\ of\ \{[TaCl_2(OEt)(NCMe)]_2(\mu\text{-}p\text{-}L^1)\}\cdot5MeCN\ (\textbf{3}\cdot5MeCN)$$

As for **2**, but using TaCl₅ (0.78 g, 2.18 mmol) and L¹H₄ (1.00 g, 1.08 mmol) affording **3** as yellow crystals. Yield (1.38 g, 75.00%). Found: C, 55.06; H, 7.03; N, 0.34. C₇₂H₁₀₂Cl₄N₂O₄Ta₂ (sample dried *in vacuo* for 12 h; - 6.5MeCN) requires C, 54.03; H, 6.41; N, 0.46 %. IR (Nujol, KBr, cm⁻¹): 2334w, 2286w, 1676w, 1573w, 1296s, 1256s, 1238s, 1154s, 1111s, 1073s, 1020s, 971w, 917w, 889m, 810w, 761s, 721s, 658w, 582w, 553m, 444w. MS (solvated with CH₂Cl₂ and diluted with MeCN for positive nano-electrospray technique): ᵐ/_z 1404 [MH − 3Cl − OEt − MeCN)]⁺. ¹HNMR (acetone-d₆): δ = 7.26–6.74 (overlapping m, 12H, aryl*H*), 6.07 (s, 2H, C*H*), 3.54 (m, 4H, OC*H₂*), 1.30 (s, 36H, C(C*H₃*)₃), 1.22 (m, 3H, OCH₂C*H₃*), 1.15 (s, 36H, C(C*H₃*)₃),1.11 (m, 3H, OCH₂C*H₃*). MeCN obscured by solvent.

3. 3 Synthesis of {[TaCl₂(OEt)(NCMe)]₂(μ-p-L¹)}·5MeCN (3·5MeCN)

$3.\ 3\ \textit{Synthesis of } \{[TaCl_2(OEt)(NCMe)]_2(\mu\text{-}p\text{-}L^1)\}\cdot5MeCN\ (\mathbf{3}\cdot5MeCN)$

As for **2**, but using $TaCl_5$ (0.78 g, 2.18 mmol) and L^1H_4 (1.00 g, 1.08 mmol) affording **3** as yellow crystals. Yield (1.38 g, 75.00%). Found: C, 55.06; H, 7.03; N, 0.34. $C_{72}H_{102}Cl_4N_2O_4Ta_2$ (sample dried *in vacuo* for 12 h; - 6.5MeCN) requires C, 54.03; H, 6.41; N, 0.46 %. IR (Nujol, KBr, cm⁻¹): 2334w, 2286w, 1676w, 1573w, 1296s, 1256s, 1238s, 1154s, 1111s, 1073s, 1020s, 971w, 917w, 889m, 810w, 761s, 721s, 658w, 582w, 553m, 444w. MS (solvated with CH_2Cl_2 and diluted with MeCN for positive nano-electrospray technique): $^m/_z$ 1404 [MH − 3Cl − OEt − MeCN)]⁺. ¹HNMR (acetone-d₆): δ = 7.26–6.74 (overlapping m, 12H, aryl*H*), 6.07 (s, 2H, C*H*), 3.54 (m, 4H, OC*H₂*), 1.30 (s, 36H, C(C*H₃*)₃), 1.22 (m, 3H, OCH₂C*H₃*), 1.15 (s, 36H, C(C*H₃*)₃),1.11 (m, 3H, OCH₂C*H₃*). MeCN obscured by solvent.

3. 4- Synthesis of {[Nb(NCMe)Cl(m-L₂H₂)₂]}·3½MeCN (4·3½MeCN) and {[Nb(NCMe)Cl(m-L₂H₂)₂]}·5MeCN (4·5MeCN).
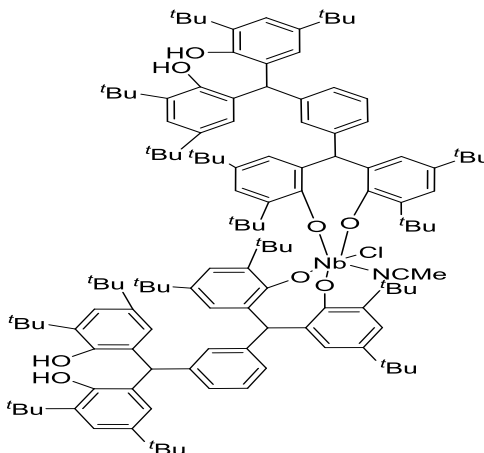
α,α,α′,α′-Tetra (3,5-di-*tert*-butyl-2-hydroxyphenyl)-*m*-xylene (L^2H_4, 4.10 g, 4.44 mmol) and $[Nb(O)Cl_3(NCMe)_3]$ (2.61 g, 8.78 mmol) were refluxed in toluene (40 mL) for 12 h. On cooling to room temperature, volatiles were removed *in-vacuo*, and the residue was extracted into warm (30 mL) acetonitrile. Prolonged standing (2 days) at 0 ^{o}C afforded orange prisms of **4.** Yield (2.46 g, 52.00 %). Found: C, 76.41; H, 8.91; N, 3.01. $C_{130}H_{179}ClNO_8Nb$·3½MeCN requires C, 76.32; H, 8.86; N, 2.92 %. MS (positive nanospray in CH_2Cl_2/MeCN): 1937 (MH – Cl – MeCN), 1919 (M – Cl – MeCN – OH), 1902 (M – Cl – MeCN – 2OH), 1885 (M – Cl – MeCN – 3OH), (M – Cl – MeCN – 4OH). IR (Nujol, KBr, cm^{-1}): 3545w, 3523w, 3428w, 2295w, 2261w, 1651w, 1600w, 1391m, 1377m, 1323w, 1291m, 1260s, 1212s, 1190s, 1153w, 1121m, 1022m, 970w, 913m, 885s, 859m, 799s, 770w, 753w, 719m, 708w, 669w, 645w, 560w, 468w, 451w. ^{1}H NMR (C_6D_6): δ =7.65–6.80 (6×m, 12H, aryl*H*), 5.45 (s, 2H, C*H*), 4.91 (s, 4H, O*H*), 2.18 (bs, 6H, C*H₃*CN), 1.51 (s, 36H, C(C*H₃*)₃), 1.23 (s, 36H, C(C*H₃*)₃).

4. Synthesis of Mo complexes.

4.1 Synthesis of [Mo(NAr)$_2$L^{3}Me] (5)
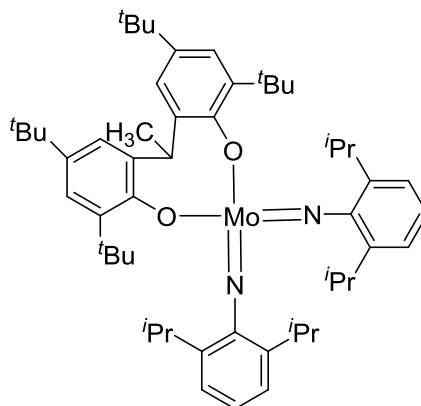
A mixture of [Mo(N-2, 6 di-isopropyl)$_2$(O*t*-Bu)$_2$] (0.94 g, 1.59 mmol) and L^{3}H$_2$ (0.70 g, 1.59 mmol) were stirred in diethyl ether (*ca* 20 mL) for 1 h. The volatiles were removed under reduced pressure and the residue taken-up in diethyl ether (*ca* 20 mL). This cycle was repeated three times before the residue was extracted with hot heptane (*ca* 30 mL). Yellow prisms of the product were deposited on cooling to room temperature. Yield (0.62 g, 44.00 %). Further crops can be obtained from the mother-liquor; overall yield 70.00 %. Found: C, 72.89; H, 9.00; N, 3.09. MoN$_2$O$_2$C$_{54}$H$_{78}$ requires C, 73.40; H, 8.98; N, 3.29. IR: 2369w, 1587w, 1322m, 1262s, 1221s, 1153m, 1130s, 1105s, 1020s, 982m, 932w, 901w, 882w, 827s, 752s, 730m, 691w, 630w, 608w, 578m. 537w, 455w. ^{1}H NMR (CDCl$_3$, 400 MHz): δ 7.64 (d, 2H, aryl*H*, ^{3}J$_{HH}$ = 2.4 Hz), 7.17-6.66 (several m, 8H, aryl*H*), 5.16 (q, 1H, J$_{HH}$ = 6.8 Hz, C*H*), 3.72 (sept, 2H, J$_{HH}$ = 6.8 Hz, C*H*(CH$_3$)$_2$), 2.75 (sept(br), 2H, J$_{HH}$ = 6.8 Hz, C*H*(CH$_3$)$_2$), 1.66 (d, 3H, J$_{HH}$ = 6.8 Hz, C*H$_3$*), 1.28 (s, 18H, C(C*H$_3$*)$_3$), 1.24 (d, 12H, J$_{HH}$ = 7.2 Hz, CH(C*H$_3$*)$_2$), 1.19 (s, 18H, C(C*H$_3$*)$_3$), 0.3 (d, 12H, J$_{HH}$ = 6.8 Hz, CH(C*H$_3$*)$_2$).

4.2 Synthesis of [Mo(NAr)₂L⁴] (6)
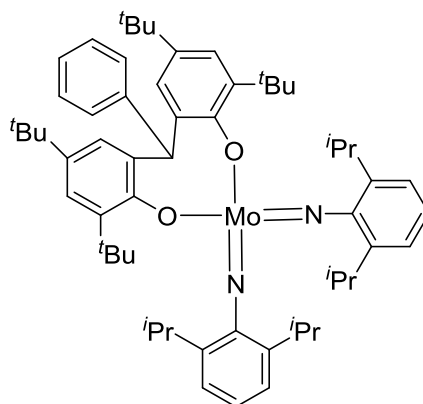
The compounds [Mo(NC$_6$H$_3$*i*-Pr$_2$-2,6)$_2$(O*t*-Bu)$_2$] (1.00 g, 1.60 mmol) and L^{4}H$_2$ (0.84 g, 1.60 mmol) in pentane (30 mL) were refluxed for 12 h. On cooling to room temperature, the volatiles were removed under reduced pressure and the residue was taken up in CH$_2$Cl$_2$ (20 mL). Orange-yellow prisms of the product were deposited upon standing at room temperature (2 days). Yield (0.85 g, 47.00%). Further crops of **6** can be obtained on concentrating and cooling of the mother liquor, overall yield *ca* 70 %. Found: C, 75.02; H, 8.50; N, 2.95, requires C, 74.97; H, 8.53; N, 2.96 %. IR: 2350w, 1567w, 1323m, 1262s, 1221s, 1152m, 1120s, 1100s, 1036s, 979m, 933w, 910w, 882w, 828s, 756s, 749m, 705w, 664w, 607w, 574m. M.S. (EI$^+$): 945 (M$^+$). ^{1}H NMR (C$_6$D$_6$, 400 MHz): δ 7.83 (d, 2H, J$_{HH}$ = 2.4 Hz, aryl*H*), 7.43-6.78 (several m, 8H, aryl*H*), 4.89 (s, 1H, C*H*), 4.07 (sept, 2H, J$_{HH}$ = 6.8 Hz, C*H*(CH$_3$)$_2$), 3.20 (sept(br), 2H, C*H*(CH$_3$)$_2$, 1.46 (s, 18H, C(CH$_3$)$_3$), 1.15 (d, 12H, J$_{HH}$ = 6.8 Hz, C*H*(CH$_3$)$_2$), 1.33(s, 18H, C(CH$_3$)$_3$), 0.65 (d, 12H, J$_{HH}$ = 6.8 Hz, CH(CH$_3$)$_2$).

*4.3- Synthesis of [Mo(Nt-Bu)(μ-NC$_6$F$_5$)(L^3)]$_2$ (**7**)*
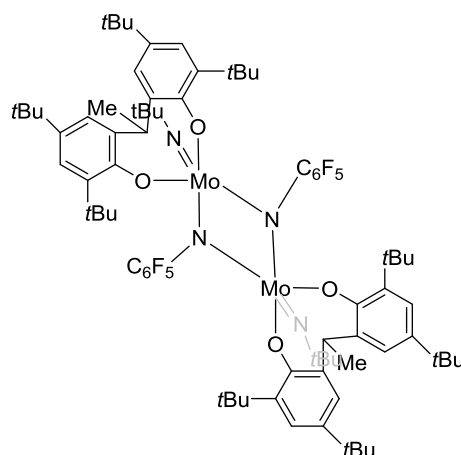
As for **5**, but using [Mo(NC$_6$F$_5$)(Nt-Bu)Cl$_2$(dme)] (1.00 g, 2.02 mmol), LiOt-Bu (0.33 g, 4.12 mmol) and 2,2'-CH$_3$CH[4,6-(t-Bu)$_2$C$_6$H$_2$OH]$_2$ (0.89 g, 2.03 mmol). Extraction into acetonitrile or dichloromethane and standing at ambient temperature for 2 days afforded **7** as yellow/orange prisms. Yield (0.42g, 35.00%). Found: C, 59.59; H, 6.73; N, 3.31. C$_{80}$H$_{106}$F$_{10}$Mo$_2$N$_4$O$_4$·½CH$_2$Cl$_2$ requires C, 59.97; H, 6.69; N, 3.48. IR: 1506s, 1495s, 1485vs, 1406w, 1374w, 1361w, 1311w, 1293w, 1261m, 1243m, 1217s, 1185m, 1164m, 1150m, 1127m, 1101m, 1023s, 991s, 904w, 876w, 860w, 831m, 802m, 765w, 760m, 750m, 727m, 692w, 663w, 634w, 600m, 574s. ^{19}F NMR (C$_6$D$_6$): δ -163.25 (m, 4F, *o-F*), -165.82 (m, 4F, *m-F*), -174.58 (m, 2F, *p-F*). M.S. (Electrospray): 1387.5 (M$^+$ - C$_6$F$_5$NH$_2$), 1241 (M$^+$ - C$_6$F$_5$NH$_2$ – 2t-BuNH$_2$). ^{1}H NMR (CDCl$_3$): δ 7.26 - 6.99 (4x m, 8H, aryl$H$), 4.45 (q, 2H, J$_{HH}$ = 5.4 Hz, CH), 1.69 (d, 3H, J$_{HH}$ = 5.4 Hz, CH_3), 1.36 (s, 36H, C(CH_3)$_3$), 1.30 (s, 36H, C(CH_3)$_3$), 0.07 (s, 18H, imido C(CH_3)$_3$).

4.4 Synthesis of [Mo(NC$_6$H$_3$i-Pr$_2$-2,6)(NCMe)(μ-O)L^{5}H]$_2$ (8)
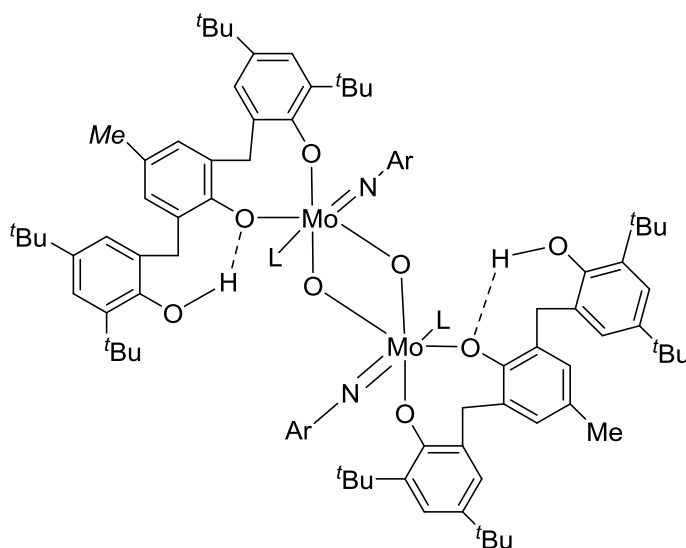
As for **5**, but using [Mo(NC$_6$H$_3$*i*-Pr$_2$-2,6)$_2$(O*t*-Bu)$_2$] (1.00 g, 1.6 mmol) and L^{5}H$_3$ (0.87g, 1.6 mmol). The product was crystallized from a saturated acetonitrile solution on prolonged standing at -20 $^\circ$C. Yield (1.13 g, 71.00%). Found: C, 69.33; H, 8.08; N, 3.45. C$_{102}$ H$_{140}$ Mo$_2$ N$_4$ O$_8$ (sample dried *in-vacuo* − 5MeCN) requires C, 70.05; H, 8.08; N, 3.93. IR: 2726w, 2681w, 1658w, 1570w, 1463s, 1377s, 1306w, 1261s, 1232w, 1201w, 1093bs, 1020bs, 920w, 876w, 859w, 800s, 721w, 660w, 617w. M.S. (MALDI): 1505.7 (M$^+$ - 7MeCN − ArNH$_2$ − H$_2$O). ^{1}H NMR (CDCl$_3$): δ 8.04 − 6.64 (overlapping m, 18H, aryl*H*), 5.45 (bm, 4H, C*H*$_2$), 3.86 (br s, 4H, C*H*$_2$), 2.74 (br sept, 4H, C*H*(CH$_3$)$_2$), 2.23 (s, 6H, C*H*$_3$), 2.01(s, 6H, C*H*$_3$CN), 1.42 (s, 36H, C(C*H*$_3$)$_3$), 1.27 (overlapping signals, 60H, C(C*H*$_3$)$_3$ + CH(C*H*$_3$)$_2$); O*H* not observed.

*4.5. Synthesis of {[Mo(NC$_6$H$_3$i-Pr$_2$-2,6)]$_2$(μ-L^1)} (**9**)*
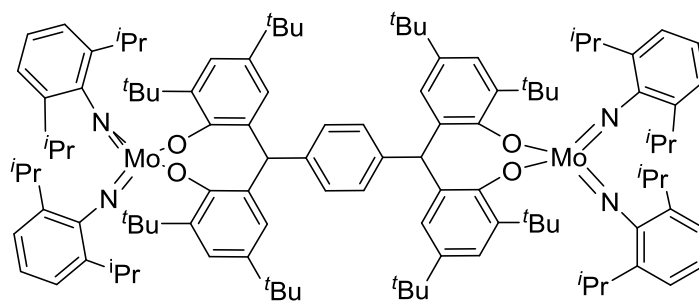
To the compounds [Mo(NC$_6$H$_3$i-Pr$_2$-2,6)$_2$(Ot-Bu)$_2$] (0.84 g, 2.18 mmol) and L^{1}H$_4$ (1.00 g, 1.09 mmol) was added diethyl ether (30 mL). After stirring for 10 mins, the volatiles were removed *in-vacuo*, and the process was repeated three times. The residue was then extracted into acetonitrile solution on prolonged standing at -20 °C. Yield (0.79 g, 40.00 %). Found: C, 73.78; H, 9.06; N, 2.79 %. C$_{112}$ H$_{154}$ Mo$_2$ N$_4$ O$_4$ requires C, 74.12; H, 8.49; N, 3.09 %. IR: 2725w, 2359w, 2340w, 1620w, 1568w, 1461s, 1377s, 1324w, 1261w, 1221m, 1152w, 1099m, 1021w, 933w, 909s, 871s, 799s, 753w, 742w, 722w. M.S. (MALDI): 1012 (MH$^+$ - 3 NC$_6$H$_3$i-Pr$_2$-2,6 – Mo). ^{1}H NMR (C$_6$D$_6$, 400 MHz): δ 7.80 - 6.89 (several m, 24H, aryl*H*), 5.50 (s, 1H, C*H*), 4.90 (s, 1H, C*H*), 2.64 (sept, 8H, J$_{HH}$ = 6.8 Hz C*H*(CH$_3$)$_2$), 1.51 (s, 38H, C(C*H$_3$*)$_3$), 1.21 (s, 38H, C(C*H$_3$*)$_3$), 1.15 (d, 24H, J$_{HH}$ = 6.8 Hz, CH(C*H$_3$*)$_2$), 1.13 (d, 24H, J$_{HH}$ = 6.8 Hz, CH(C*H$_3$*)$_2$).

*4.6 Synthesis of {[Mo(NC₆H₃i-Pr₂-2,6))]₂(μ-L²)} (**10**)*
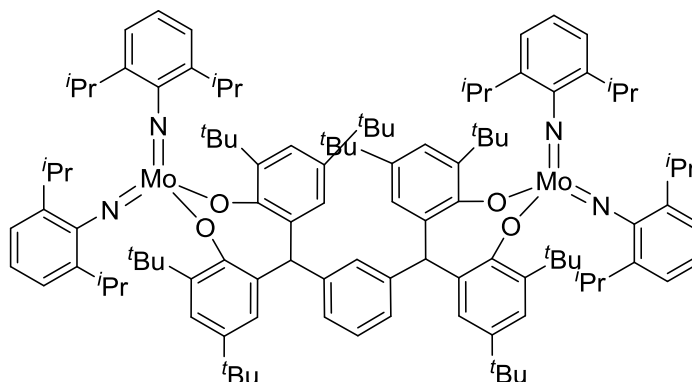
As for **9**, but using [Mo(NC₆H₃*i*-Pr₂-2,6))₂(O*t*-Bu)₂] (1.26 g, 3.27 mmol) and L²H₄ (1.50 g, 1.63 mmol). Yellow prisms of the product **10** were deposited on cooling to room temperature. Yield (1.40 g, 47.70%). Further crops can be obtained from the mother-liquor; overall yield 70.00 %. Found: C, 73.94; H, 8.51; N, 2.88 %. $C_{112}H_{154}Mo_2N_4O_4$ requires C, 74.12; H, 8.49; N, 3.09 %. IR: 2345w, 1541w, 1321w, 1281w, 1220m, 1139m, 1053w, 981m, 930s, 903s, 852s, 760w, 747m. M.S. (Electrospray): 1152 (M⁺ - 3ArNH₂ – 2*t*-Bu). ¹H NMR (CDCl₃, 400 MHz): δ 7.31 - 6.63 (several m, 24H, aryl*H*), 5.56 (s, 1H, C*H*), 4.71 (s, 1H, C*H*), 2.95 (sept, 8H, J_HH 6.6 Hz C*H*(CH₃)₂), 1.35 (s, 38H, C(C*H₃*)₃), 1.28 (d, 24H, J_HH = 6.6 Hz, CH(C*H₃*)₂), 1.26 (d, 24H, J_HH = 6.6 Hz, CH(C*H₃*)₂), 1.14 (s, 38H, C(C*H₃*)₃).

4.7 Synthesis of {[Mo(NC₆F₅)(Ot-Bu)₂]₂(μ-L¹)}·6MeCN (11·6MeCN).
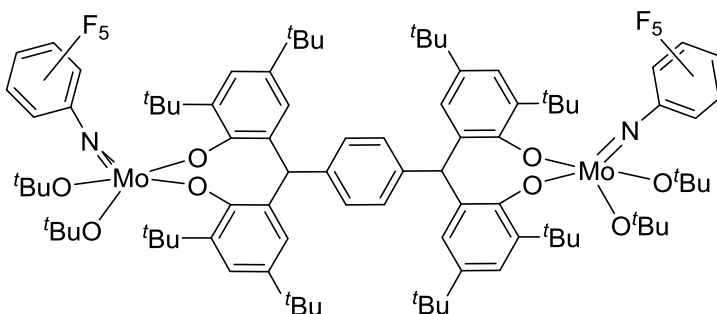
As for **9**, but using [Mo(NC$_6$F$_5$)$_2$(Ot-Bu)$_2$] (1.32 g, 2.18 mmol) with L^{1}H$_4$ (1.00 g,1.09 mmol) affording **11** as orange colored prisms. Yield (1.23 g, 56.00 %). On recrystallization from acetonitrile or dichloromethane. Found: C, 57.18; H, 6.40; N, 1.68. C$_{92}$H$_{122}$Mo$_2$F$_{10}$N$_2$O$_8$ ·2½CH$_2$Cl$_2$ requires C, 57.40; H, 6.47; N, 1.42 %. IR: 2726w, 2360w, 2341w, 1590w, 1571w, 1463s, 1377s, 1324w, 1261s, 1236w, 1214w, 1199w, 1150w, 1102m, 1021m, 958w, 914w, 870m, 760w, 721m. ^{19}F NMR (C$_6$D$_6$): δ -163.29 (m, 4F, o-F), -165.82 (m, 4F, m-F), -172.83 (m, 2F, p-F). M.S. (Electrospray): 1583 (M$^+$ - C$_6$F$_5$NH$_2$), 1509 (M$^+$ - C$_6$F$_5$NH$_2$ – t-BuOH), 1435 (M$^+$ - C$_6$F$_5$NH$_2$ – 2t-BuOH), 1361 (M$^+$ - C$_6$F$_5$NH$_2$ – 3t-BuOH), 1287 (M$^+$ - C$_6$F$_5$NH$_2$ – 4t-BuOH). ^{1}H NMR (CDCl$_3$): δ 7.26 – 6.45 (overlapping m, 12H, aryl$H$), 5.61 (s, 1H, CH), 4.72 (s, 1H, CH), 1.41 (s, 36H, C(CH_3)$_3$), 1.36 (s, 18H, CO(CH_3)$_3$), 1.14 (s, 18H, CO(CH_3)$_3$), 1.09 (s, 36H, C(CH_3)$_3$).

5. Synthesis of Venadium di, tri- and tetra-phenolate complexes

5.1 Synthesis of [VO(Ot-Bu)L^3] (13)
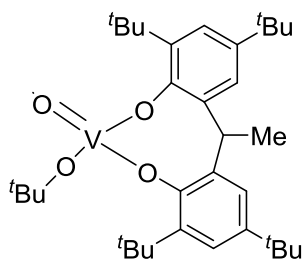
L^{3}H$_2$ (2.0 g, 4.58 mmol) and [VO(Ot-Bu)$_3$] (1.32 g, 4.61 mmol) were heated unfer reflux in toluene (30 mL) for 12 h. Upon cooling, volatiles were removed *in-vacuo*, and the product extracted using warm acetonitrile 30 mL. Upon standing overnight for 12 h at 0 °C, red/brown prisms formed. Yield (1.96 g, 76.00 %). IR (cm^{-1}): 3487w, 1567w, 1417m, 1361s, 1292s, 1240w, 1229w,

1214w, 1199w, 1190w, 1155m, 1125m, 1108s, 1013s, 1003s, 978m, 876w, 845w, 799s, 767w, 722m, 636w. Found: C, 70.69; H 9.35. $C_{34}H_{53}VO_4$ requires C, 70.81; H, 9.26 %. ^{51}V NMR (CDCl$_3$, 298 K): -482.4 ($w_{1/2}$ = 63 Hz). ^1H NMR (CDCl$_3$, 400 MHz): δ: 7.51 – 7.16 (overlapping m, 4H, aryl*H*), 5.08 (q, 1H, J$_{HH}$ 8.0 Hz, C*H*$_{bridge}$), 1.71 (s, 9H, C(C*H$_3$*)$_3$), 1.58 (d, 3H J$_{HH}$ 8.0 Hz, C*H*$_{3\ bridge}$), 1.42 (s, 18H, C(C*H$_3$*)$_3$), 1.33 (s, 18H, C(C*H$_3$*)$_3$).

*5. 2 Synthesis of {L^1[VO(i-PrO)]$_2$}·2CH$_2$Cl$_2$ (**14**·2CH$_2$Cl$_2$).*
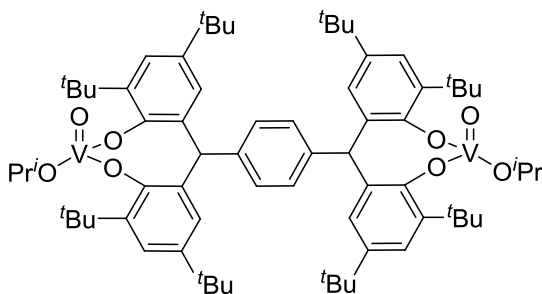
L^{1}H$_4$ (4.1 g, 4.44 mmol) and [VO(*i*-PrO)$_3$] (2.10 mL, 8.90 mmol) were heated under reflux in toluene (30 mL) for 12 h. On cooling, volatiles were removed *in-vacuo* and the residue was extracted into dichloromethane (30 mL). Prolonged standing at 0 °C afforded **14** as a brown solid. Yield (4.32 g, 83.00%). $C_{70}H_{100}V_2O_8$·¾CH$_2$Cl$_2$ (sample dried *in-vacuo* for 2 h) requires C 68.80, H, 8.28. Found C, 68.66, H 8.29 %. MS (solid, ASAP technique): *m/z* 1171.5 [M]$^+$, 1111.6 [M-O*i*Pr]$^+$, 1069.5 [M-O*i*Pr-*i*Pr]$^+$. IR: 1572w, 1408w, 1260s, 1225w, 1189w, 1149w, 1093bs, 1019bs, 873w, 862w, 799s, 722w, 663w, 601w. ^{51}V NMR (CDCl$_3$) δ = -449.7 ($w_{1/2}$ = 688 Hz). ^1H NMR (CDCl$_3$): δ = 7.38 – 7.14 (overlapping m, 8H, aryl*H*), 6.77 (s, 4H, aryl*H*), 6.33 (s, 2H, C*H*), 5.64 (sept, ^{3}J$_{HH}$ 4.0 Hz, 2H, C*H*Me$_2$), 5.29 (s, 4H, C*H$_2$*Cl$_2$), 1.61 (d, ^{3}J$_{HH}$ 4.0 Hz, 12H, CH(C*H$_3$*)$_2$), 1.44 (s, 36H, C(C*H$_3$*)$_3$), 1.23 (s, 36H, C(C*H$_3$*)$_3$).

*5. 3 Synthesis of {L²[VO(Oi-Pr)]₂}·2CH₂Cl₂ (**15·2CH₂Cl₂**)*
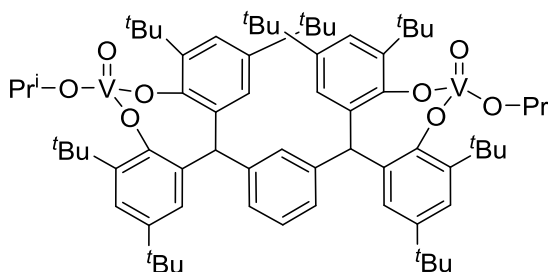
As for **16**, but using $L^{3m}H_4$ (4.1 g, 4.4 mmol) and [VO(*i*-PrO)₃] (2.10 mL, 8.90

mmol) affording **15** as a brown solid. Yield (3.87 g, 66.00 %). Crystals suitable

for X-ray diffraction were obtained on cooling (-20 $^{\circ}$C) of a saturated

dichloromethane solution. $C_{70}H_{98}V_2O_8 \cdot \frac{1}{2}CH_2Cl_2$ (sample dried *in-vacuo* for 12 h)

requires C 68.93, H, 8.07. Found C, 68.66, H 8.29 %. MS (solid, APCI): 1170.6

$[MH]^+$, 1111.5 $[MH - OiPr]^+$, 1068.5 $[MH - Oi\text{-}Pr - i\text{-}Pr]^{2+}$. IR: 1598m, 1568w,

1406m, 1376s, 1361s, 1325m, 1290m, 1263s, 1237m, 1222s, 1196m, 1104bs,

1005bs, 981bs, 928w, 911m, 860m, 844s, 810m, 797m, 780m,769s, 740m, 722m,

698w, 669m, 648w, 607m. ^{51}V NMR (CDCl₃): δ = -449.9 ($w_{1/2}$ = 688 Hz). ^{1}H

NMR (CDCl₃): δ = 7.25 − 7.14 (overlapping m, 6H, aryl*H*), 6.78 (m, 2H, aryl*H*),

6.62 (s, 2H, aryl*H*), 6.27 (s, 2H, C*H*), 5.62 (sept, 2H, $^3J_{HH}$ 4.0 Hz, C*H*Me₂), 5.29

(s, 4H, CH₂Cl₂), 1.61 (d, 12H, $^3J_{HH}$ 4.0 Hz, CH*Me₂*), 1.40 (s, 36H, C(C*H₃*)₃), 1.17

(s, 36H, C(C*H₃*)₃).
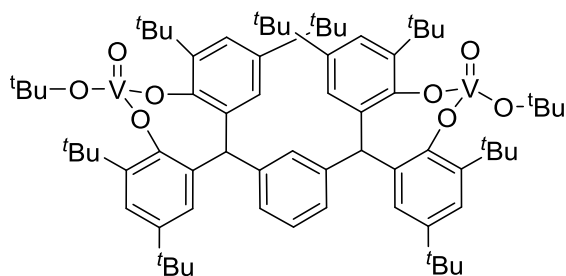
As for **16**, but using [VO(*t*-BuO)$_3$] (3.20 g, 8.90 mmol) and *m*-L^{2}H$_4$ (4.1 g, 4.40 mmol) were heated under reflux in toluene (30 mL) for 12 h. On cooling, the volatiles were removed *in-vacuo*, and the residue was extracted into acetonitrile (30 ml). Concentration (to *ca* 15 ml) and cooling (-78 ^{o}C) afforded **16** as a brown solid. Yield (4.22 g, 70.00 %). C$_{72}$H$_{104}$V$_2$O$_8$·2CH$_2$Cl$_2$ requires C 64.90, H, 7.95. Found C 64.82, H 8.02 %. MS (solid, APCI): 1069.3 [M − O*t*Bu - *t*Bu]$^{2+}$. IR: 1570w, 1301w, 1261s, 1202w, 1189w, 1154w, 1091bs, 1018s, 915w, 880w, 862w, 799s, 722m, 661w, 645w. ^{51}V NMR (CDCl$_3$) δ = -468.9 ($w_{1/2}$ = 652 Hz). ^{1}H NMR (CDCl$_3$, sample dried *in-vacuo* for 12 h) δ: 7.33 - 7.13 (3x m, 8H, aryl*H*), 6.73 (s, 4H, aryl*H*), 6.30 (s, 2H, C*H*), 5.29 (s, 4H, C*H*$_2$Cl$_2$), 1.69 (s, 18H, OC(C*H*$_3$)$_3$), 1.43 (s, 36H, C(C*H*$_3$)$_3$), 1.27 (s, 36H, C(C*H*$_3$)$_3$).

5. 5 Synthesis of {[V(NCMe)(Np-MeC$_6$H$_4$)Cl]$_2$(μ-p-L^1)} 17·MeCN
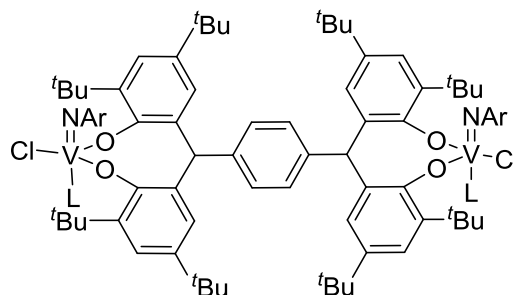
p-L^{1}H$_4$ (1.00 g, 1.08 mmol) and [V(N*p*-MeC$_6$H$_4$)Cl$_3$] (0.60 g, 2.29 mmol) were stirred in THF (30 mL) for 5 min., then Et$_3$N (0.63 mL, 4.55 mmol) was added and the mixture was left to stir for 12 h. Following removal of volatiles *in-vacuo*, the residue was extracted in MeCN (30 ml) and on prolonged standing (1 - 2 days) at ambient temperature, small prisms of **17** formed. Yield (1.09 g, 69.00 %). C$_{78}$H$_{100}$N$_2$Cl$_2$V$_2$O$_4$ (sample dried *in-vacuo* for 12 h, -2MeCN) requires C, 71.92, H, 7.74, N, 2.15 %. Found C 71.34, H 8.23, N 1.71 %. MS (solid, APCI): 1302 [M − 2MeCN]$^+$, 1266 [M − 2MeCN − Cl]$^+$. IR: 2336w, 2309w, 2277w, 2251w, 1627w,1586w, 1526w, 1504m, 1320m, 1320w, 1289m, 1260s, 1224m, 1200m, 1166w, 1106s, 1018s, 909w, 873w, 835m, 806s, 793m, 750w, 723w, 703w, 665m, 643w, 625w, 591m, 571w, 553w, 510w, 490s, 473w, 464w, 415m. ^{51}V NMR (CDCl$_3$) δ = -218.9 ($w_{1/2}$ = 1074 Hz). ^{1}H NMR (CDCl$_3$): δ = 7.40 − 7.01 (5x m, 20H, aryl*H* + imidoaryl*H*), 5.83 (s, 2H, C*H*), 2.22 (s, 6H, *CH$_3$*CN), 2.16 (s, 6H, C*H$_3$*C$_6$H$_4$), 1.59 (s, 36H, C(C*H$_3$*)$_3$), 1.29 (s, 36H, C(C*H$_3$*)$_3$).

6. Synthesis of schiff base ligands and organoaluminium complexes

6.1 Synthesis of Ph,MeCHN=CH(3,5-t-Bu$_2$C$_6$H$_2$-OH-2) L^{8}H
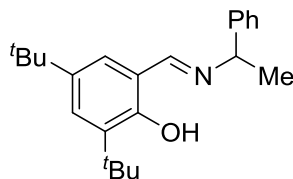
 To a solution of 3,5-di-*tert*-butylsalicylaldehyde (2.34 g, 10.0 mmol) with a few drops of glacial acetic acid in anhydrous ethanol (15 mL) under argon at 50 °C was added a solution of α-methylbenzylamine (1.21 g, 10.0 mmol) in anhydrous ethanol (15 mL) over a period of 30 min with stirring. The mixture was then refluxed for an additional 6 h. Upon cooling to ambient temperature, the volatiles were removed under vacuo, and the residue was recrystallized from ethanol at −20 °C to give **L^{8}H** as a yellow powder. Yield (3.2 g, 95.00%). Elemental analysis calculated for C$_{23}$H$_{31}$NO: C, 81.85; H, 9.26; N, 4.15. Found: C, 81.67; H, 9.33; N, 4.27%. IR (nujol null, KBr): 3441m, 2967s, 2868m, 2358w, 1626s, 1585w, 1464 w, 1452w, 1438w, 1383m, 1360m, 1343w, 1322w, 1270m, 1248s, 1207m, 1174s, 1135w, 1115w, 1075m, 1029w, 976m, 906w, 880w, 824m, 773m, 759s, 730w, 700s, 644w, 631w, 594w, 541m, 499w. MS (ESI, positive mode): 338.4 MH$^+$. ^{1}H NMR (400 MHz, CDCl$_3$): δ 13.68 (s, 1 H, O*H*), 8.43 (s, 1 H, C*H*=N), 7.40 - 7.33 (m, 5 H, aryl-*H*), 7.28 - 7.26 (m, 1 H, aryl-*H*), 7.86 (d,1 H, *J* = 2.4 Hz, Ar-*H*), 4.56 - 4.52 (m, 1 H, C*H*(CH$_3$)), 1.65 (d, 3 H *J* = 6.4 Hz, CH(C*H*$_3$)), 1.46 (s, 9 H, C(C*H*$_3$)$_3$), 1.30 (s, 9 H, C(C*H*$_3$)$_3$).

6.2 Synthesis of Ph$_2$CHN=CH(3,5-t-Bu$_2$C$_6$H$_2$-OH-2) L^{9}H
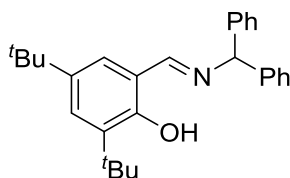
By using the procedure described above for synthesis of **L^{8}H**, the ligand **L^{9}H** was obtained by the reaction of 3,5-di-*tert*-butylsalicylaldehyde (2.34 g, 10.0 mmol) with benzhydrylamine (1.83 g, 10.0 mmol) as a yellow powder. Yield (1.10g 92.00%). Elemental analysis calculated for C$_{28}$H$_{33}$NO: C, 84.17; H, 8.32; N, 3.51. Found: C, 84.35; H, 8.43; N, 3.47%. IR (nujol mull, KBr, cm^{-1}): 3435m, 3060w, 3029w, 2956w, 2868w, 2361w, 1631s, 1586w, 1493w, 1455m, 1386m, 1357m, 1342w, 1322w, 1269m, 1246s, 1204m, 1171s, 1133w, 1089m, 1050s, 1028s, 980w, 916w, 880w, 846w, 827m, 800w, 766m, 746m, 733w, 703s, 644w, 620w, 612w, 561w, 538w, 509w, 468w. MS (ESI, positive mode): 400.2 MH$^+$. ^{1}H NMR (400 MHz, CDCl$_3$) δ: 13.74 (s, 1 H, O*H*), 8.41 (s, 1 H, C*H*=N), 7.32 (d, 1H, *J* = 2.4 Hz, aryl-*H*), 7.28 - 7.23 (m, 8 H, aryl-*H*), 7.19 - 7.15 (m, 2 H, aryl-*H*), 7.01 (d,1H, *J* = 2.4 Hz, aryl-*H*), 5.52 (s, 1 H, C*H*(Ph)$_2$), 1.38 (s, 9 H, C(C*H*$_3$)$_3$), 1.21 (s, 9 H, C(C*H*$_3$)$_3$).

6.3 Synthesis of Ph$_2$CHN=CH$_2$(3,5-t-Bu$_2$C$_6$H$_2$-OH-2) L^{9}H via dpg

2,2$^/$-Diphenylglycine (1.13 g, 5.00 mmol) and 2-hydroxy-3,5-di-*tert*-butylsalicylaldehyde (1.17 g, 5.00 mmol) were refluxed in ethanol for 3 days using a Dean-Stark condenser. Following removal of the ethanol, the residue was triturated with methanol (50 mL), filtered and dried. Yield (1.26 g, 63.00%). C$_{28}$H$_{33}$NO·⅔MeOH requires C 81.82, H 8.54, N 3.33 %. Found: C 81.96, H 8.65,

N 3.34%. IR (nujol mull, KBr, cm^{-1}): 3432bs, 1629s, 1603m, 1577w, 1477s, 1446s, 1393m, 1361m, 1297w, 1260s, 1236m, 1203m, 1163m, 1078w, 1025m, 947w, 875m, 780w, 758m, 726w, 686s, 672w, 646w, 592w, 539w, 454w. MS (ES, positive mode): 400.4 MH^{+}. ^{1}H NMR (400 MHz, CDCl$_3$) δ: 13.84 (s, 1 H, OH), 8.52 (s, 1 H, CH=N), 7.42 (d, 1 H, J = 2.4 Hz, aryl-H), 7.37 - 7.34 (m, 8 H, aryl-H), 7.29 - 7.26 (m, 2 H, Ar-H), 7.26 (d, 1 H, J = 2.4 Hz, Ar-H), 5.63 (s, 1 H, CH(Ph)$_2$), 1.49 (s, 9 H, C(CH_3)$_3$), 1.32 (s, 9 H, C(CH_3)$_3$).

6.4 Synthesis of [i-PrCHN=CH(3,5-t-Bu$_2$C$_6$H$_2$-O-2)AlEt$_2$] (21)
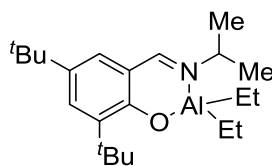
A solution of AlEt$_3$ (1.9 mL, 3.0 mmol, 2 M in toluene) was added at room temperature to a solution of *i*-PrCHN=CH(3,5-*t*-Bu$_2$C$_6$H$_2$-OH-2) **L^{7}H** (0.74 g, 2.7 mmol) in toluene (25 mL) over a period of 30 min with stirring. Then the mixture was refluxed for an additional 12 h. Upon cooling to room temperature, the volatiles were removed under vacuo, and the residue was recrystallized from acetonitrile to give **21** as a yellow solid. Yield (0.53 g, 55.00%). Elemental analysis calculated for C$_{22}$H$_{38}$AlNO: C, 73.50; H, 10.65; N, 3.90. Found: C, 73.33; H, 10.35; N, 3.73%. IR (nujol mull, KBr, cm^{-1}): 3730w, 2959s, 2871m, 1629s, 1553m, 1470m, 1445m, 1422m, 1385m, 1361m, 1318w, 1276m, 1258m, 1238w, 1203w, 1179m, 1163w, 1118s, 1058w, 1025w, 977w, 955w, 855m, 785m, 754w, 716w, 647w, 526w, 411w. MS (ES, positive mode): 359.2 M. ^{1}H NMR (400 MHz, CDCl$_3$): δ: 8.12 (s, 1 H, CH=N), 7.42 (d, 1 H, J = 2.0 Hz, aryl-H), 6.90 (d, 1 H, J = 2.0 Hz, aryl-H), 3.72 - 3.65 (m, 1 H, CH(CH$_3$)$_2$), 1.37 (d, 6

H, J = 3.2 Hz, -CH(CH_3)$_2$), 1.34 (s, 9 H, -C(CH_3)$_3$), 1.21 (s, 9 H, C(CH_3)$_3$), 0.94 -

0.90 (m, 6 H, Al(CH$_2$CH_3)$_2$), −0.07 - (−0.22) (m, 4 H, Al(CH_2CH$_3$)$_2$).

6.5 Synthesis of [Me,PhCHN=CH(3,5-t-Bu$_2$C$_6$H$_2$-O-2)AlMe$_2$] (22)
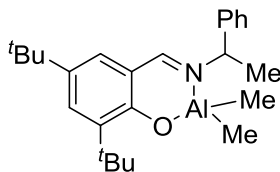
A solution of AlMe$_3$ (1.6 mL, 2.5 mmol, in toluene 1.6 M) was added at room

temperature to a solution of Ph, MeCHN=CH(3,5-*t*-Bu$_2$C$_6$H$_2$-OH-2) **L^{8}H** (0.77 g

2.3 mmol) in hexane (25 mL). The resulting yellow solution was stirred for 12 h.

The solution was filtered and concentrated, affording **22** a yellow solid. Yield

(0.60 g, 66.00%). Elemental analysis calculated for C$_{25}$H$_{36}$AlNO: C, 76.30; H,

9.22; N, 3.56. Found: C, 76.25; H, 9.31; N, 3.40%. IR (nujol mull, KBr, cm^{-1}):

3429s, 3064w, 3037w, 2960s, 2866m, 2358w, 2335w, 1616s, 1553m, 1543m,

1469m, 1454m, 1439m, 1414m, 1391m, 1355m, 1322s, 1299w, 1275w, 1254s,

1237w, 1200m, 1178s, 1138w, 1085m, 1058w, 1029w, 990w, 932w, 910w,

880w, 855s, 816w, 782m, 763s, 702s, 674s, 613w, 596w, 537m, 490w, 410w.

MS (ESI): $^m/_z$ 378.6 [M − Me]$^+$, 363.6 [M − 2Me]$^+$. ^{1}H NMR (400 MHz, CDCl$_3$)

δ: 8.11 (s, 1 H, CH=N), 7.49 - 7.36 (m, 5 H, aryl-H), 7.18 (s, 1 H, aryl-H), 6.90

(s, 1 H, aryl-H), 4.93 - 4.92 (m, 1 H, CH(CH$_3$)), 1.78 - 1.76 (d, 3 H, J = 4.0 Hz,

CH(CH_3)), 1.39 (s, 9 H, C(CH_3)$_3$), 1.27 (s, 9 H, C(CH_3)$_3$), −0.79 (s, 3 H, AlCH_3),

−0.93 (s, 3 H, AlCH_3).

*6.6 Synthesis of [Me,PhCHN=CH(3,5-tBu₂C₆H₂-O-2)AlEt₂] (**23**)*
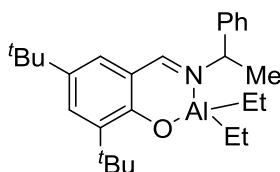
As for **21**, but using Me,PhCHN=CH(3,5-t-Bu$_2$C$_6$H$_2$-OH-2) **L^{8}H** (0.77 g, 2.30 mmol) and AlEt$_3$ (1.6 mL, 2.50 mmol, 1.6 M in toluene) affording **23** as a yellow solid. Yield (0.6 g, 66.00%). Elemental analysis calculated for C$_{27}$H$_{40}$AlNO: C, 76.92; H, 9.56; N, 3.32. Found: C, 76.65; H, 9.33; N, 3.28%. IR (nujol mull, KBr, cm^{-1}): 3423w, 2954s, 2866w, 1627s, 1559m, 1473m, 1444w, 1422m, 1388w, 1361w, 1277m, 1258m, 1236w, 1202m, 1176s, 1134w, 1120w, 1081w, 1056w, 1034w, 982w, 910w, 874w, 852m, 787w, 758m, 715w, 699w, 605w, 524w. MS (ESI): $^m/_z$ 392 [M − Et]$^+$, 363 [M − 2Et]$^+$. ^{1}H NMR (400 MHz, CDCl$_3$) δ: 8.12 (s, 1 H, C*H*=N), 7.49 (d, *J* = 2.0 Hz, 1 H, aryl-*H*), 7.42-7.34 (s, 5 H, aryl-*H*), 6.88 (d, 1 H, *J* = 2.0 Hz, aryl-*H*), 4.56 - 4.51 (m, 1 H, C*H*(CH$_3$)), 1.78 (d, 3 H, *J* = 7.0 Hz, CH(C*H*$_3$)), 1.40 (s, 9 H, CH(C*H*$_3$)), 1.26 (s, 9 H, CH(C*H*$_3$)), 0.97 - 0.85 (m, 6 H, Al(CH$_2$C*H*$_3$)$_2$), −0.72 - (−0.31) (m, 4 H, Al(C*H*$_2$CH$_3$)$_2$).

*6.7 Synthesis of [Ph₂CHN=CH(3,5-t-Bu₂C₆H₂-O-2)AlMe₂] (**24**)*
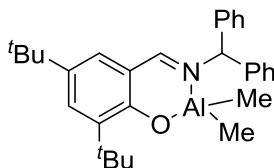
As for **21**, but using Ph$_2$CHN=CH(3,5-t-Bu$_2$C$_6$H$_2$-OH-2) **L^{9}H** (1.00 g, 2.50 mmol) and AlMe$_3$ (1.70 mL, 2.70 mmol, in toluene 1.6 M) afforded **24** as yellow crystals. Single crystals suitable for X-ray analysis were grown from a saturated hexane solution. The solution was filtered and concentrated, affording **24** as a yellow crystalline solid. Yield (0.90 g, 79.00%). Elemental analysis calculated for

$C_{30}H_{38}AlNO$: C, 79.09; H, 8.41; N, 3.07. Found: C, 79.19; H, 8.28; N, 3.20%. IR (nujol mull, KBr, cm^{-1}): 3428w, 2965s, 2866w, 1616s, 1561w, 1543s, 1469s, 1441m, 1424s, 1389m, 1362m, 1344w, 1318s, 1275w, 1258s,1241w, 1199w, 1183s, 1164m, 1148m, 1134m, 1026w, 995m, 965w, 924w, 887m, 855s, 807w, 784m, 760s, 708w, 677s, 641w, 602m, 552m, 491m, 410w. MS (ESI): $^{m}/_{z}$ 423.6 [M -2Me]$^{+}$. ^{1}H NMR (400 MHz, CDCl$_3$) δ: 8.00 (s, 1 H, CH=N), 7.52 (d, 1 H, J = 2.6 Hz, aryl-H), 7.42 - 7.32 (m, 6 H, aryl-H), 7.23 - 7.18 (m, 4 H, aryl-H), 6.81 (d, 1 H, J = 2.5 Hz, aryl-H), 6.23 (s, 1 H, CHPh$_2$), 1.40 (s, 9 H, C(CH_3)$_3$), 1.26 (s, 9 H, C(CH_3)$_3$), −0.96 (s, 3 H, AlCH_3), −0.97 (s, 3 H, AlCH_3). For [Ph$_2$CHNCH$_2$(3,5-t-Bu$_2$C$_6$H$_2$-OH-2)AlMe$_2$] (**26**): Yield *ca*. 10 %. ^{1}H NMR (C$_6$D$_6$, 400 MHz) δ: 7.31 - 6.40 (6× m, 12H, aryl-H), 4.09 (s, 2H, CH_2), 1.42 (s, 9 H, C(CH_3)$_3$), 1.13 (s, 9 H, C(CH_3)$_3$), −0.97 (s, 6 H, AlCH_3). ^{13}C NMR (C$_6$D$_6$): −10.01 (AlCH_3).

6.8 Synthesis of [Ph$_2$CHN=CH(3,5-t-Bu$_2$C$_6$H$_2$-O-2)AlEt$_2$] (25)
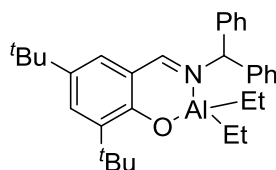
As for **24**, but using Ph$_2$CHN=CH(3,5-t-Bu$_2$C$_6$H$_2$-OH-2) **L^{9}H** (1.00 g, 2.50 mmol) and AlEt$_3$ (1.35 mL, 2.75 mmol, 2 M in toluene) affording **25** as a yellow solid. Yield (0.76 g, 63.00%). Elemental analysis calculated for $C_{32}H_{42}AlNO$: C, 79.46; H, 8.75; N, 2.90. Found: C, 79.25; H, 8.33; N, 2.67%. IR (nujol mull, KBr, cm^{-1}): 3694w, 3428w, 2954s, 2855w, 1616s, 1556w, 1543m, 1493w, 1463w, 1417w, 1392m, 1359w, 1329w, 1280w, 1254w, 1232w, 1198w, 1174m, 1004m, 988w, 916w, 879w, 852w, 784w, 757w, 730w, 699s, 640m, 538w. MS calculated

for **25** ($^m/_z$): 483.31 (100.0%), 484.31 (35.5%), 485.31 (6.1%). Found MS (ESI): $^m/_z$ 423.7 [M – Et]$^+$. ^{1}H NMR (400 MHz, CDCl$_3$) δ: 7.99 (s, 1 H, C*H*=N), 7.51 (d, *J* = 2.8 Hz, 1 H, aryl-*H*), 7.39 - 7.35 (m, 6 H, aryl-*H*), 7.22 - 7.20 (m, 4 H, aryl-*H*), 6.78 (d,1H, *J* = 2.8 Hz, aryl-*H*), 6.20 (s, 1 H, C*H*Ph$_2$), 1.41 (s, 9 H, C(C*H$_3$*)$_3$), 1.25 (s, 9 H, C(C*H$_3$*)$_3$), 0.87 - 0.83 (m, 6H, Al(CH$_2$C*H$_3$*)$_2$), –0.23 - –0.36 (m, 4 H, Al(C*H$_2$*CH$_3$)$_2$).

6.9 Synthesis of {Ph$_2$PC$_6$H$_4$N[(Me$_2$Al)$_2$μ-CH$_3$](μ-Me$_2$Al)} (28)
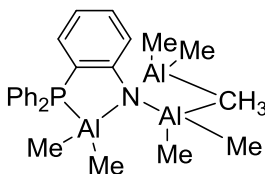
To 1-NH$_2$,2-PPh$_2$C$_6$H$_4$ (1.50 g, 5.41 mmol) in toluene (20 mL) was added Me$_3$Al (5.41 mL, 2.0 M, 10.8 mmol) and the system was refluxed for 12 h. On cooling, the volatiles were removed *in vacuo*, and the residue was extracted into warm MeCN (20 mL). Prolonged standing (2 - 3 days) at ambient temperature afforded small white prisms of **28**. Yield (1.12 g, 56.00%). Elemental analysis calculated for C$_{25}$H$_{35}$Al$_3$NP·0.87MeCN·0.39toluene: C, 66.43; H, 7.64; N, 4.2 %. Found: C, 66.39; H, 7.64; N, 4.92%. IR (nujol mull, KBr, cm^{-1}): 2940m, 2923s, 2853s, 2725w, 2671w, 1610m, 1586w, 1457s, 1377s, 1301m, 1260m, 1182w, 1157w, 1089m, 1068m, 1026m, 891w, 801m, 743m, 722m, 695s, 548w, 505w, 492w, 474w. MS (ES, positive mode): $^m/_z$ 389 [M – Al(CH$_3$)$_3$]. ^{1}H NMR (CDCl$_3$) δ: 7.36 - 7.34 (m, 2H, C$_6$*H$_2$*), 7.32-7.28 (m, 10H, *Ph*P), 6.78–6.66 (m, 2H, C$_6$*H$_2$*), 2.33(s, H, *toluene*), 2.26 (bs, 3H, Al-*CH$_3$*-Al), 2.00(s,3H, *MeCN* –0.81(bs, 18H, *CH$_3$*-Al). ^{31}P NMR (CDCl$_3$) δ: –19.80.

6.10 Synthesis of {Ph₂N[(Me₂Al)₂ μ-Me]} (29)
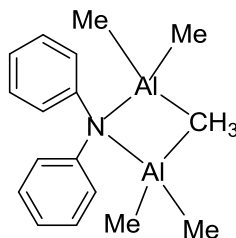
To Ph$_2$NH (0.84 g, 5.0 mmol) in toluene (30 mL) was added Me$_3$Al (5.0 mL, 2 M, 10.0 mmol), and the system was refluxed for 12 h. On cooling, the volatiles were removed *in-vacuo*, and the residue was extracted into warm acetonitrile (30 ml). Cooling to 0 °C afforded colourless prisms of **29**. Yield (0.92 g, 62.50%). X-ray quality crystals were obtained from MeCN. C$_{17}$H$_{25}$Al$_2$N·⅓MeCN requires C 68.22, H 8.35, N 5.98 %. Found: C 68.76, H 8.35, N 6.00%. IR (nujol mull, cm^{-1}): 3414w, 3192w, 2953s, 2922s, 2852s, 2727w, 2670w, 1936w, 1876w, 1788w, 1594s, 1520s, 1493s, 1415s, 1376s, 1339w, 1310m, 1261m, 1201s, 1079s, 1029s, 1005w, 917m, 846s, 801s, 746m, 694s, 608m, 570m, 524m, 503m, 482w, 479m. MS (ES, positive mode): 225.6 M$^+$ −Al(CH$_3$)$_3$. ^{1}H NMR (400 MHz, CD$_3$CN) δ: 7.17 - 6.77 (m, 10H, aryl-*H*), 2.17 (s, 1H, N-*H*), 1.94 (s, 3H, Al-*CH$_3$*-Al), −0.87 (s, 6H, Al*CH$_3$*), −0.96 (s, 6H, Al*CH$_3$*).

6.11 Synthesis of [Ph₂CHNH(μ-Me₂Al)]₂·MeCN (30·MeCN)
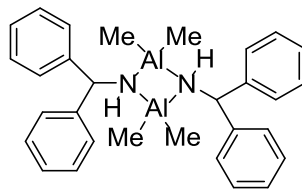
As for **28**, but using Ph$_2$CHNH$_2$ (0.91 g, 5.0 mmol) and Me$_3$Al (2.5 mL, 2.0 M, 5.0 mmol) affording **30** as colourless needles. Yield (1.12 g, 47.20%). C$_{30}$H$_{36}$Al$_2$N$_2$ requires C 75.29, H 7.58, N 5.89%. Found: C 74.68, H 8.20, N 5.72 %. IR (nujol mull, KBr, cm^{-1}): 3286m, 2925s, 2857s, 2726w, 2672w, 1967w, 1946w, 1799w, 1622m, 1539w, 1494s, 1453s, 1377s, 1316m, 1259m, 1187s, 1080s, 1039s, 1017s, 916m, 874s, 819s, 758m, 742m, 697s, 594m, 570m, 509m, 499m, 479m, 451w. MS (ES, positive mode): MH$^+$ 479, [MH$^+$ + MeCN] 519. ^{1}H NMR (400 MHz,CDCl$_3$) δ: 7.40 - 7.15 (m, 20H, aryl-*H*), 5.10 (s, 1H, C*H*(Ph)$_2$), 5.07(s, 1H, C*H*(Ph)$_2$), 2.17 (s, 1H, N-*H*), 2.14 (s, 1H, N-*H*), 1.98 (s,3H, *Me*CN), − 0.97(s, 6H, AlC*H₃*), 1.02(s, 6H, AlC*H₃*).

7. Synthesis of lithium complexes

7.1 Synthesis of [Li(benz)(THF)]₂ (31·2THF)
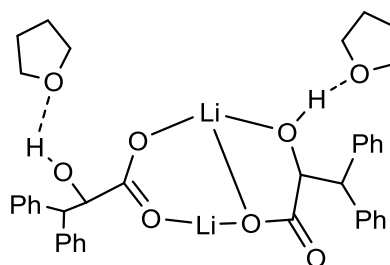
A solution of lithium *tert*-butoxide (4.38 mL, 4.38 mmol, 1 M in THF) was added at room temperature to a solution of benzylic acid (1.00 g 4.38 mmol) in tetrahydrofuran (30 mL). The resulting solution was stirred for 12 h, volatiles were removed *in-vacuo*, and the residue was extracted into warm THF (30 mL).

Prolonged standing at 0 °C afforded colourless crystals of **31**. Yield (1.70 g, 63.00%). Further stirring of the product in MeCN (30 ml) for 10 mins, afforded the polymorph **31′**. Elemental analysis calculated for $C_{28}H_{22}Li_2O_6 \cdot 2THF$: C, 70.54; H, 6.20 %. Found: C, 70.37; H, 6.42 %. IR (nujol null, KBr): 3590w, 2954bs, 2726w, 1631m, 1490s, 1377s, 1312w, 1261w, 1202w, 1180w, 1157w, 1093m, 1063m, 1051w, 1032w, 968w, 9941w, 915w, 801w, 770s, 756w, 722m, 696w, 672w, 625w, 595w, 520m, 502w, 460w, 430m. MS (ES, positive mode): $^m/_z$ 595.1 [$MH^+ - H_2O$], 445.6 [$-C_6H_6 - THF$], 367.7 [$-C_6H_6$]. ^1H NMR ($DMSO_d^6$) δ: 7.25 - 7.18 (3 × m, 20H, C_6H_5), 6.31 (s, 2H, *OH*), 3.60 (t, 8H, J_{HH} = 6.4 Hz, *CH₂*), 1.75 (m, 8H, *CH₂*). ^7Li NMR ($DMSO_d^6$) δ 2.02.

*7.2 Synthesis of [Li₇(benz)₇(MeCN)] (**32**·2MeCN·THF)*
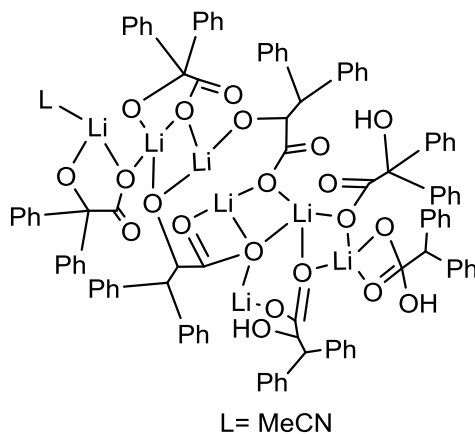
L= MeCN

A solution of lithium *tert*-butoxide (8.76 mL, 8.76 mmol, 1 M in THF) was added at room temperature to a solution of benzylic acid (1.00 g, 4.38 mmol) in tetrahydrofuran (30 mL). The resulting solution was stirred for 12 h, volatiles were removed *in-vacuo*, and the residue was extracted into refluxing (30 mL) acetonitrile (10 mins reflux). Prolonged standing at ambient temperature afforded white crystals of **32**. Yield (0.85 g, 77.00 %). Elemental analysis calculated for $C_{103}H_{93}Li_7N_3O_{22}$: C, 69.76; H, 5.24; N, 2.37

%. Found: C, 69.67; H, 5.61; N, 2.33 %. IR (nujol null, KBr): 3549m, 3454w, 3408w, 3053w, 2954s, 2922s, 2725w, 2671w, 2304w, 2271w, 2248w, 1960w, 1888 w, 1817w, 1667w, 1656s, 1625s, 1599s, 1490w, 1462s, 1377s, 1338w, 1302s, 1262s, 1214w, 1182w, 1161m, 1056m, 1045s, 1027s, 1002m, 967m, 944w, 935w, 917w, 908w, 891w, 844w, 804w, 759m, 743m, 756m, 722m, 696s, 601s, 512m, 470w, 412w. MS (ES, positive mode): $^{m}/_{z}$ 1740 [MH$^+$ – MeCN – 3H$_2$O]. ^{1}H NMR (DMSO$_d^6$) δ: 7.58 – 7.12 (3 × m, 70H, C$_6$$H_5$), 6.22 (s, 2H, O$H$), 3.64 (t, 4H, J_{HH} = 6.4 Hz, CH_2), 2.08 (s, 9H, CH_3CN), 1.77 (m, 4H, CH_2). ^{7}Li NMR (DMSO$_d^6$) δ 2.52.

7.3 Synthesis of {Li$_8$(Ot-Bu)$_2$[(benz)](OCPh$_2$CO$_2$CPh$_2$CO$_2$t-Bu)$_2$(THF)$_4$} (33)
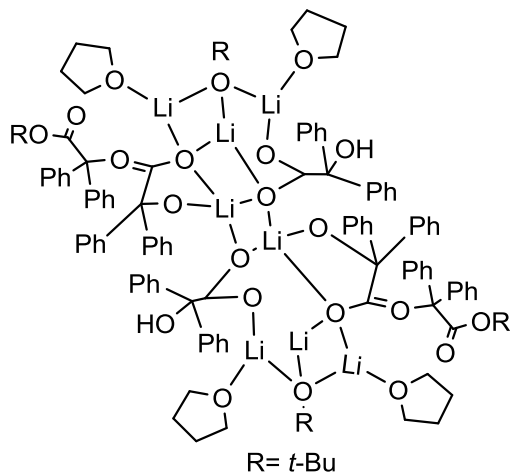
R= *t*-Bu

A solution of lithium *tert*-butoxide (8.76 mL, 8.76 mmol, 1 M in THF) was added at room temperature to a solution of benzilic acid (1.00 g 4.38 mmol) in tetrahydrofuran (30 mL). The resulting solution was stirred for 12 h, then filtered to afford colourless crystals of **33.** Yield (0.96 g, 71.00%). Elemental analysis calculated for Elemental analysis calculated for C$_{116}$H$_{128}$Li$_8$O$_{22}$: C, 72.13; H, 6.63 %. Found: C, 71.06; H, 6.16%. IR (nujol null, KBr): 3296w, 2954s, 2923s, 2853s, 2725w, 2671w, 1634w, 1458s, 1377s, 1305w, 1260s, 1201w, 1154w, 1063m,

1051w, 1024s, 968w, 941m, 916w, 891w, 846w, 799w, 771m, 756m, 722m, 696s, 594w, 490w. MS (ES, positive mode): $^m/_z$ 1645.6 [M −2tBuOH −THF − tBu], 1411.6 [−3C_6H_6], 367.7 [−C_6H_6]. ^{1}H NMR (DMSO$_d^6$) δ: 8.46 (s, 2H, *OH*), 7.47 - 7.06 (3 × m, 60H, aryl*H*), 3.41 (t, 16H, $^3J_{HH}$ = 6.6 Hz, *CH$_2$*), 2.50(m, 16H, *CH$_2$*), 1.12 (s, 36H, C*(CH$_3$)$_3$*). ^{7}Li NMR (DMSO$_d^6$) δ 2.83.

7.4 Synthesis of [Li$_6$(Ot-Bu)$_2$(dpg)$_2$(THF)$_2$] (34)
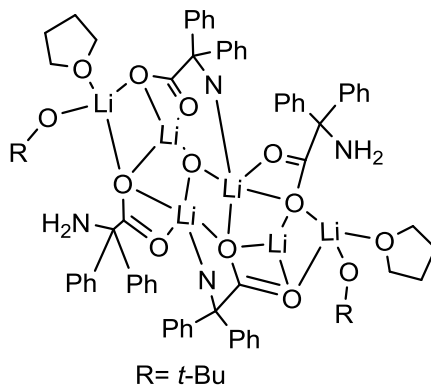
R= t-Bu

A solution of lithium *tert*-butoxide (8.80 mL, 8.80 mmol, 1 M in THF) was added at room temperature to a solution of 2,2$^/$-diphenylglycine (1.00 g 4.40 mmol) in tetrahydrofuran (30 mL). The resulting solution was stirred for 12 h, then filtered to afford colourless crystals of **34**. Yield (0.96 g, 71.00 %). Elemental analysis calculated for $C_{72}H_{82}Li_6N_4O_{12}$: C, 69.84; H, 6.62; N, 4.53 %. Found: C, 69.23; H, 6.71; N, 4.84 %. IR (nujol null, KBr): 3358m, 3296m, 3159w, 2954s, 2923s, 2853s, 2725w, 2671w, 2359w, 1955 w, 1885w, 1602s, 1462s, 1377s, 1305w, 1260s, 1203s, 1169w, 1078m, 1033w, 1006s, 971w, 933m, 918w, 898w, 847w, 793s, 766m, 734m, 722m, 698s, 670w, 626w, 585w, 494w, 433w, 425w. MS (ES, positive mode): $^m/_z$ 1220 [MH$^+$ −NH$_3$]. ^{1}H NMR (CDCl$_3$) δ: 7.64 - 6.78 (m, 40H, aryl*H*), 3.56 (t, 8H, J_{HH} = 6.4 Hz , *CH$_2$*), 2.10 (s, 8H, N*H$_2$*), 1.40 (m, 8 *CH$_2$*), 1.04 (s, 18H, C(C*H$_3$*)$_2$). ^{7}Li NMR (DMSO$_d^6$) δ 2.76.

*7.5 Synthesis of [Li$_8$(PhO)$_4$(dpg)$_4$(MeCN)$_4$] (**35**).*

L= MeCN
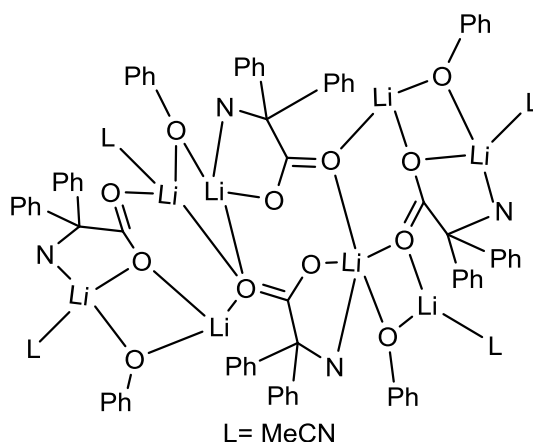
A solution of lithium phenoxide (8.80 mL, 8.80 mmol, 1 M in THF) was added at room temperature to a solution of diphenylglycine (1.00 g 4.40 mmol) in tetrahydrofuran (30 mL). The resulting solution was stirred for 12 h, volatiles were removed *in-vacuo*, and the residue was extracted into warm (30 ml) acetonitrile. Prolonged standing at 0 $^{\rm o}$C afforded white crystals of **35**. Yield (0.70 g, 54.00%). Elemental analysis calculated for C$_{88}$H$_{80}$Li$_8$N$_8$O$_{12}$·2THF: C, 70.19; H, 5.84; N, 6.82 %. Found: C, 69.72; H, 5.39; N, 6.49 %. IR (nujol null, KBr): 3583m, 3454w, 2955w, 2890s, 2854s, 2725m, 2671w, 2349w, 2299w, 2299w, 1939w, 1590s, 1462s, 1377s, 1300w, 1260s, 1214w, 1092w, 1019w, 875w, 799s, 722m, 703w, 660w, 619w, 553w, 512w, 470w. MS (ES, positive mode): $^{\rm m}/_{\rm z}$ 1220 [M −4PhOH −2MeCN]. ^{1}H NMR (CDCl$_3$) δ: 7.18 - 7.00 (m, 36H, aryl*H*), 6.63-6.57 (m, 24H, aryl*H*), 4.07 (s, 8H, N*H$_2$*), 3.30 (t, 8H, C*H$_2$*) 1.71 (s, 12H, C*H$_3$*CN), 1.47 (m, 8H, C*H$_2$*). ^{7}Li NMR (DMSO$_{\rm d}^6$) δ 2.34.

8. Synthesis of zinc complexes

*8.1 Synthesis of [MeZn(dpg)]₄·2MeCN (**36**·2MeCN)*
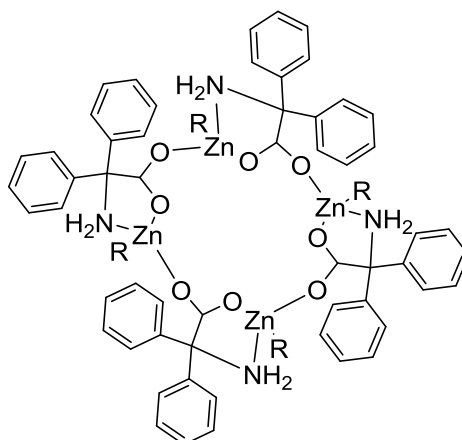
R= Me

A solution of dimethylzinc (9.25 mL, 9.25 mmol, 1 M in toluene) was added at room temperature to a solution of diphenylglycine (1.00 g 4.40 mmol) in toluene (30 mL). The resulting solution was heated under reflux for 12h, volatiles were removed *in-vacuo*, and the residue was extracted into warm acetonitrile (30ml). Prolonged standing at 0 °C afforded white crystals of **36**. Yield (0.98 g, 68.10%). Elemental analysis calculated for $C_{60}H_{60}N_4O_8Zn_4·2(C_2H_3N)$: C, 58.68; H, 5.04; N, 6.44 %. Found: C, 58.67; H, 4.91; N, 6.58%. IR (nujol null, KBr): 3345m, 3233bw, 2955s, 2923s, 2853s, 2358w, 1659w, 1644m, 1602s, 1491w, 1460s, 1378s, 1260s, 1211w, 1152w, 1135 w, 1108w, 1079m, 1042m, 1022s, 945m, 808s, 769m, 730m, 701s, 730m, 671m, 636w, 624w, 615m, 571w, 535w, 500w, 473w. MS (ES, positive mode): $^m/_z$ 1036 [M - Ph₂C(NH₂)CO₂H -3Me], 971 [M-Ph₂C(NH₂)CO₂H- ZnMe-2Me], 744[M-2Ph₂C(NH₂)CO₂H- ZnMe- 2Me], 517 [M-3Ph₂C(NH₂)CO₂H- ZnMe- 2Me]. ¹H NMR (CDCl₃, 400 MHz) δ: 7.02 – 7.60 (3x m, 40H, aryl*H*), 5.79 (d, 4H, J =10.8, *endo*-N*H₂*), 3.02 (d, 4H, J = 10.8, exo-N*H₂*), 2.35 (s, 6H, *CH₃*CN), 0.22 (s, 6H, Zn-C*H₃*), 0.07 (s, 6H, Zn-C*H₃*).

8.2 Synthesis of [(2-CF3C6H4)Zn(dpg)]4 (38)
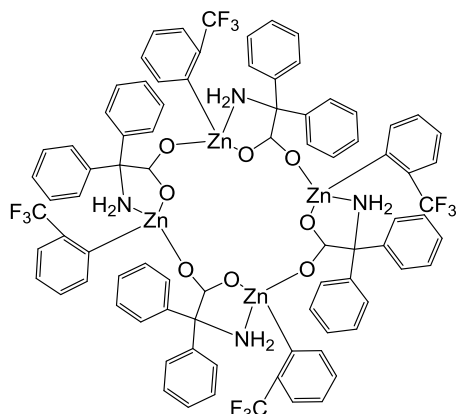
As for **36**, but using $(2\text{-}CF_3C_6H_4)_2Zn$ (3.28 g, 9.24 mmol) and diphenylglycine (1.00 g, 4.40 mmol). Prolonged standing at 0 °C afforded white crystals of **38**. Yield (1.14 g, 59.00%). Elemental analysis calculated for $C_{84}H_{56}F_{12}N_4O_8Zn_4$ ·0.2(C_2H_3N): C, 57.70; H, 3.22; N, 3.35 %. Found: C, 57.91; H, 3.28; N, 3.31 %. IR (nujol null, KBr): 3306 w, 3242bw, 3175w, 1661s, 1644s, 1608w, 1493w, 1343s, 1262s, 1195w, 1160w, 1131m, 1090m, 1079s, 1051m, 1040m, 1026s, 803s, 773w, 760w, 744w, 731w, 694s, 673w, 615s. MS (ES, positive mode): $^m/_z$ 1519 [M–$Ph_2C(NH_2)CO_2H$], 1373 [M–$Ph_2C(NH_2)CO_2H$–Ar-CF_3]. ^1H NMR (CDCl$_3$, 400 MHz) δ: 7.57 – 7.02 (4x m, 56H, aryl*H*), 5.79 (d, 4H, $^2J_{HH}$=10.7 Hz, *endo*-N*H*$_2$), 3.02 (d, 4H, $^2J_{HH}$=10.7 Hz, *exo*-N*H*$_2$), 2.35 (s, 0.6H, C*H*$_3$CN). ^{19}F NMR (dmso$_{d6}$) δ: - 61.09.

8.3 Synthesis of [(2,4,6-F)$_3$C$_6$H$_2$)Zn(dpg)]$_4$·1.59(H$_2$O) (39·1.59H$_2$O)
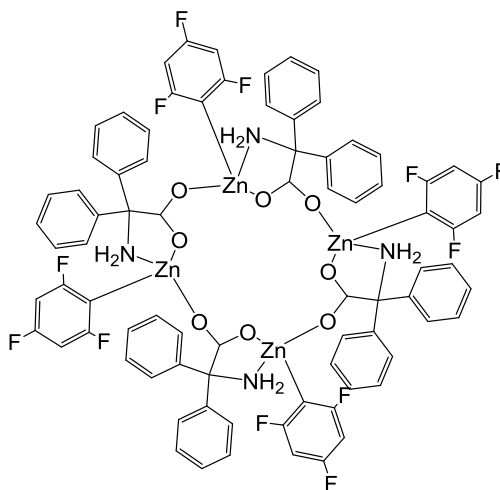
As for **36**, but using (2,4,6-FC$_6$H$_2$)$_2$Zn (3.03g 9.24 mmol) and diphenylglycine (1.00 g 4.40 mmol). Prolonged standing at 0 ^{o}C afforded **39**. Yield (1.14g, 54.00 %). Elemental analysis calculated for C$_{94}$H$_{72}$F$_{12}$N$_4$O$_8$Zn$_4$·1.59(H$_2$O): C, 59.25; H, 3.78; N, 2.95 %. Found: C, 58.92; H, 3.70; N, 3.28 %. IR (nujol null, KBr, cm^{-1}): 3318s, 3172w, 2725w, 1660m, 1605s, 1587m, 1460s, 1377s, 1305w, 1260m, 1148m, 1101m, 1042w, 1022m, 990m, 839w, 802m, 774m, 743m, 728m, 698m, 631w, 609w, 512w, 472w. MS (ES, positive mode): $^m/_z$ 867.1 [M - 2H$_2$O]; ^{1}H NMR (CDCl$_3$, 400 MHz) δ: 7.46 – 7.12 (4x m, 48H, aryl*H*), 5.38 (d, 4H, ^{2}J$_{HH}$=11.2 Hz, *endo*-N*H*$_2$), 3.43 (d, 4H, ^{2}J$_{HH}$=11.2 Hz, *exo*-N*H*$_2$), 2.35 (s, 6H, 2*CH$_3$*CN). ^{19}F NMR (dmso$_{d6}$) δ: -83.91 (s, 4F, *o-F*), -84.37 (s, 4F, *o-F*), -107.29 (s, 1F, *p-F*), -112.81 (s, 2F, *p-F*), -114.78 (s, 1F, *p-F*).

8.4 Synthesis of (2-CF$_3$C$_6$H$_4$)$_3$B·MeCN.
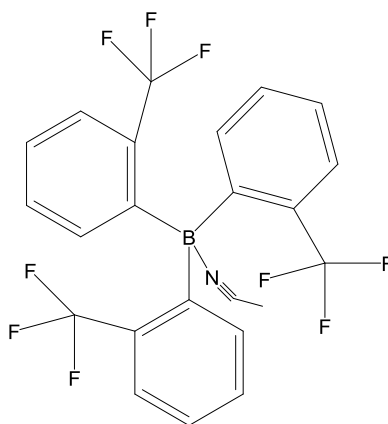
2-Bromobenzotrifluoride (5.60 mL, 0.041 mol) was slowly added to Mg (1.00 g, 0.041 mol) turnings in diethyl ether (150 mL) at 0 ^{o}C and the system was stirred for 2 h. The Grignard solution was then added to BF$_3$.Et$_2$O (1.60 mL, 0.013 mol) in toluene (100 mL) at 0 ^{o}C, and the system was slowly allowed to warm to ambient temperature. The diethyl ether was then removed *in vacuo*, and the system was heated to 100 ^{o}C on a water bath for 1 h. Following removal of volatiles, the residue was extracted into hexane (150 mL). Removal of the hexane and crystallization from acetonitrile (80 mL) afforded (2-CF$_3$C$_6$H$_4$)$_3$B·MeCN. Yield (4.6g, 79.80%). IR (nujol null, KBr, cm^{-1}): 2922 b, 2345w, 2341w, 1954w, 1661m, 1596m, 1462s, 1376s, 1313s, 1258m, 1164m, 1142m, 1060w, 1032m, 999m, 899s, 801m, 771m, 669m, 655w, 645w, 616w, 581w, 497w, 441w. MS (ES, positive mode): $^m/_z$ 446 [M − MeCN], 300 [M–MeCN −Ar-CF$_3$]. ^{1}HNMR (CDCl$_3$, 400 MHz) δ: 7.72 − 7.22 (4x m, 12H, aryl*H*), 1.99 (s, 3H, C*H$_3$*CN). ^{11}B NMR (CDCl$_3$, 400 MHz) δ: 70.13(bs). ^{19}F NMR (CDCl$_3$) δ: - 55.48.

Ring opening polymerization.

Typical polymerization procedures in the presence of one equivalent of benzyl alcohol (Table 4, run 1) are as follows. A toluene solution of **22** (0.010 mmol, 1.0 mL toluene) and BnOH (0.010 mmol) were added into a Schlenk tube in the glove-box at room temperature. The solution was stirred for 5 min, and then ε-caprolactone (2.5 mmol) along with 1.5 mL toluene(or lactide) was added to the solution. The reaction mixture was then placed into an oil bath pre-heated to the required temperature, and the solution was stirred for the prescribed time. The polymerization mixture was then quenched by addition of an excess of glacial acetic acid (0.2 mL) into the solution, and the resultant solution was then poured into methanol (200 mL). The resultant polymer was then collected on filter paper and was dried *in* vacuo.

9. Refernces

[1] G. M. Sheldrick, *Acta Crystallogr., Sect. A: Fundam. Crystallogr.*, **2008**, 64, 112.

[2] G. M. Sheldrick, *Acta Crystallogr., Sect. A: Fundam. Crystallogr.*, **2015**, 71, 3.

[3] G. M. Sheldrick, *Acta Crystallogr., Sect. C: Cryst. Struct.Commun.*, **2015**, 71, 3.

[4] G. M. Sheldrick, *Acta Crystallogr.*, **2008**, A64, 112.

[5] G.M. Sheldrick, *Acta Cryst.*, **2015**, A71, 3.

[6] P. Van der Sluis, A. L. Spek, BYPASS: An effective method for the refinement of crystal structures containing disordered solvent regions. *Acta Crystallogr. A,* **1990**, *A46*, 194.

[7] G.M. Sheldrick, SHELXTL user manual, version 6.10. Bruker AXS Inc., Madison, WI, USA, **2000**.

[8] SMART (2001), SAINT (2001 & 2008), and APEX 2 (**2008**) software for CCD diffractometers. Bruker AXS Inc., Madison, USA.

[9] (a) APEX 2 & SAINT, and software for CCD diffractometers. (**2013**). Bruker AXS Inc., Madison, USA. (b) Agilent (2013). CrysAlis PRO. Agilent Technologies, Yarnton, Oxfordshire, England. (c) Rigaku (2012) CrystalClear-SM Expert. Rigaku, The Woodlands, TX, USA.

[10] L. Palatinus and G. Chapuis, *J. Appl. Cryst.* **2007**, 40, 786.

[11] L. H. Tang, E. P. Wasserman, D. R. Neithamer, R. D. Krystosek, Y. Cheng, P. C. Price, Y. Y. He and T. J. Emge, *Macromolecules*, **2008**, 41, 7306.

[12] A. G. Maestri and S.N. Brown, *Inorg. Chem.* **2004**, *43*, 6995–7004.

[13] C. Redshaw and S. M. Humphrey, *Polyhedron* **2006**, *25*, 1946.

[14] P. A. Cameron, V. C. Gibson, C. Redshaw, J. A. Segal, M. D. Bruce, A. J. P. White and D. J. Williams, *Dalton Trans*. **1999**, 1883.

[15] S. Milione, F. Grisi, R. Centore and A. Tuzi, *Eur. J. Inorg. Chem*. **2008**, 5532.

 [16**]** V. C. Gibson, T. P. Kee and A. Shaw, *Polyhedron*, **1988**, **7**, 2217.

[17] M. K. Cooper, J. M. Downes, P. A. Duckworth, M. C. Kerby, R. J. Powell and M. D. Soucek, *Inorg. Synth*. **1989**, **25**, 129.

 [18] P. W. Dyer, V. C. Gibson, J. A. K. Howard, B. Whittle, C. Wilson and C. Four. *J. Chem. Soc. Chem. Commun*., **1992**, 1666.

[19] A. Arbaoui, D. Homden, C. Redshaw, J. A. Wright, S. H. Dale and M. R. J. Elsegood, *Dalton Trans*., **2009**, 8911.

[20] C. Redshaw and M. R. J. Elsegood, *Angew. Chem. Int. Ed*. **2007**, *46*, 7453.

Chapter 9

Appendix
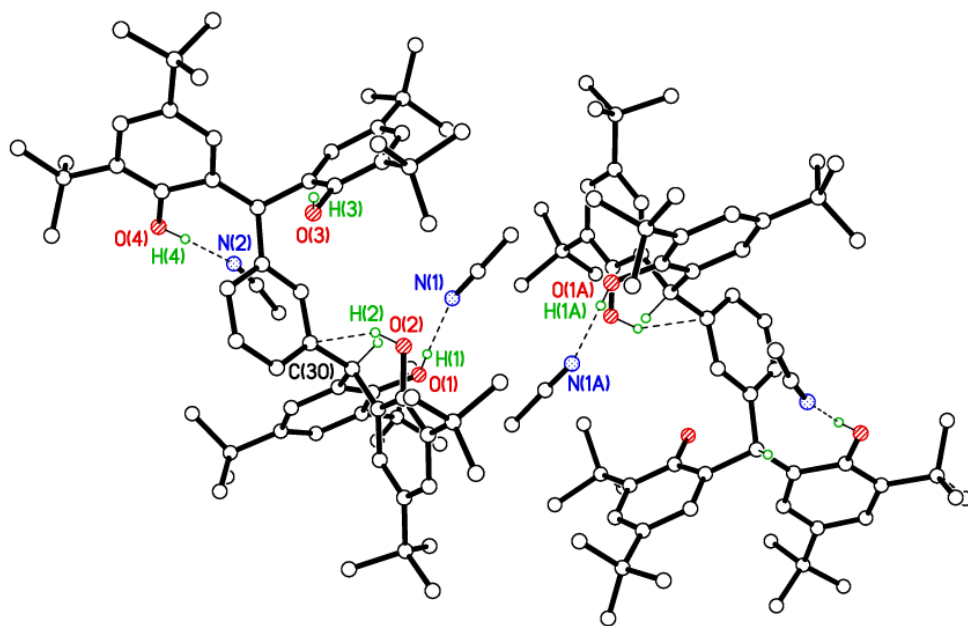
Figure 139. Molecules of $L^2H_4 \cdot 2MeCN$ form centrosymmetric pairs encapsulating pairs of symmetry-related acetonitrile molecules.
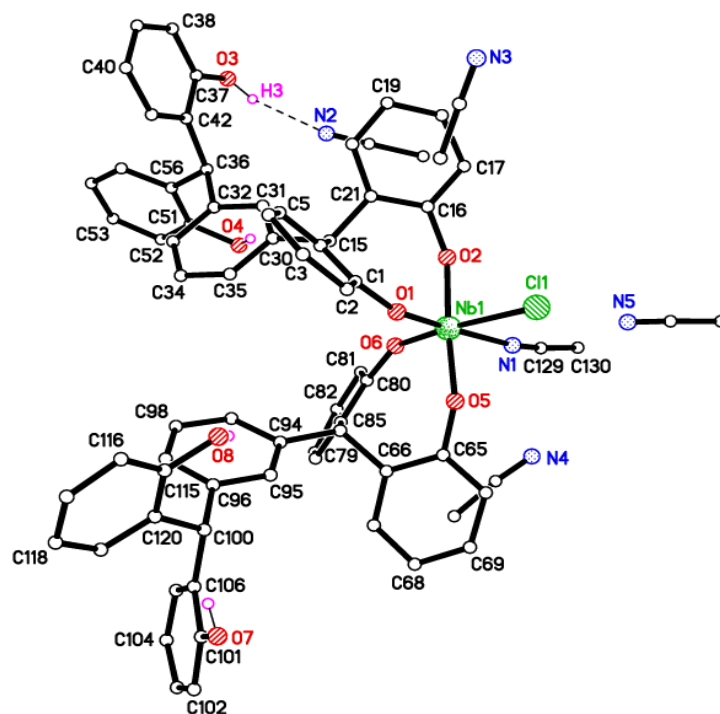
Figure 140. Molecular structure of **4.**5MeCN. Hydrogen atoms except O*H*, and tBu groups have been removed for clarity.
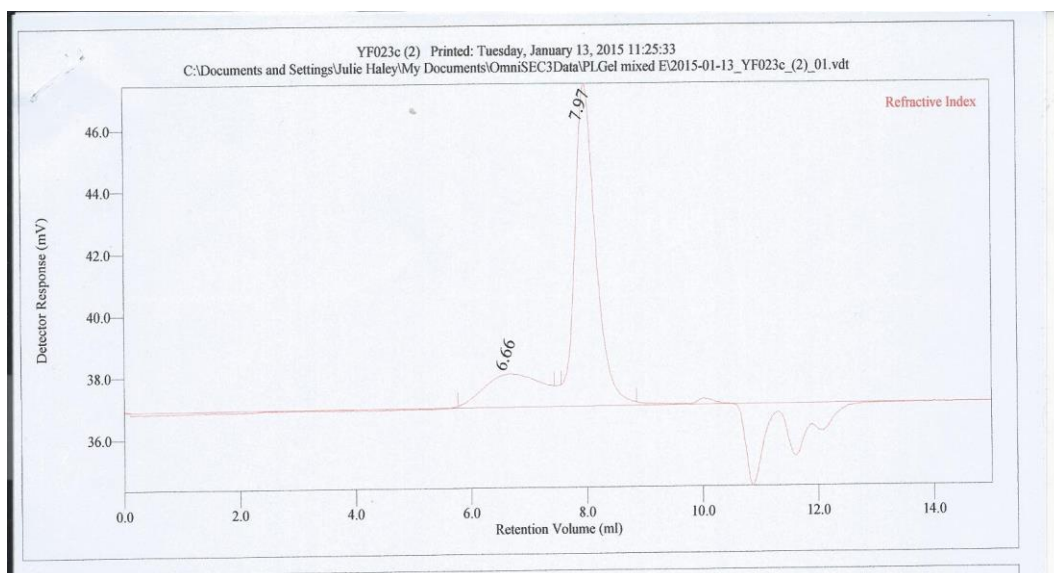
Figure. 141. Bimodal distribution of products using $\{[NbCl_2(OEt)(NCMe)]_2(\mu\text{-}p\text{-}L^1)\}\cdot3\tfrac{1}{2}MeCN\cdot0.614$toluene (table 2) .
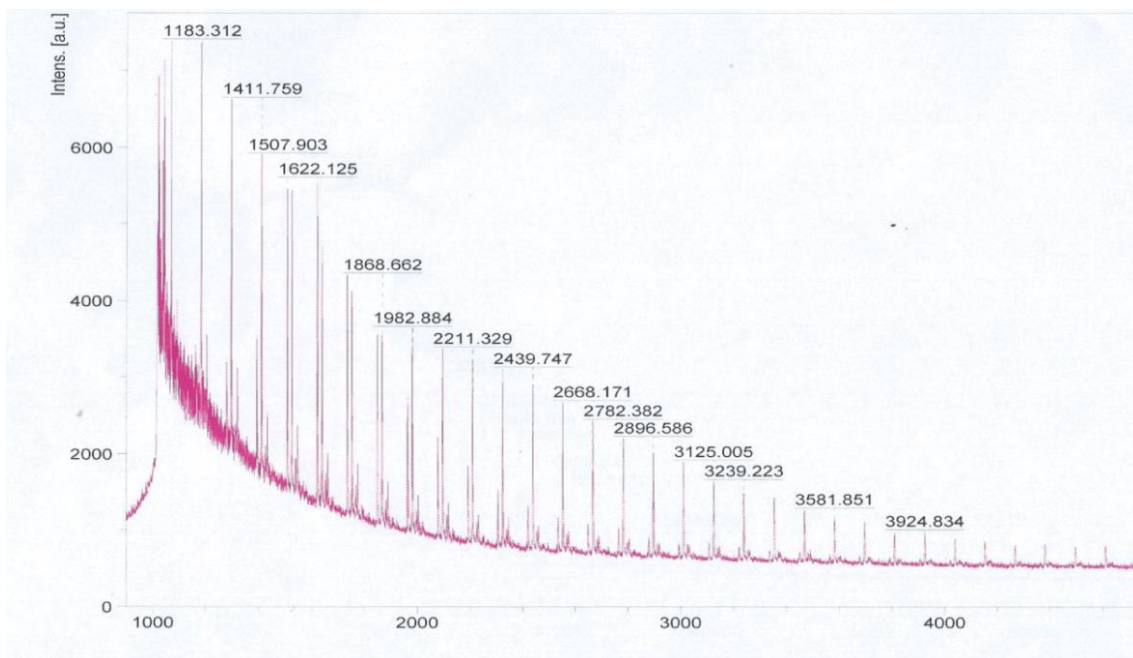
Figure 142. MALDI-ToF spectrum of PCL (run 3, table 6*).*
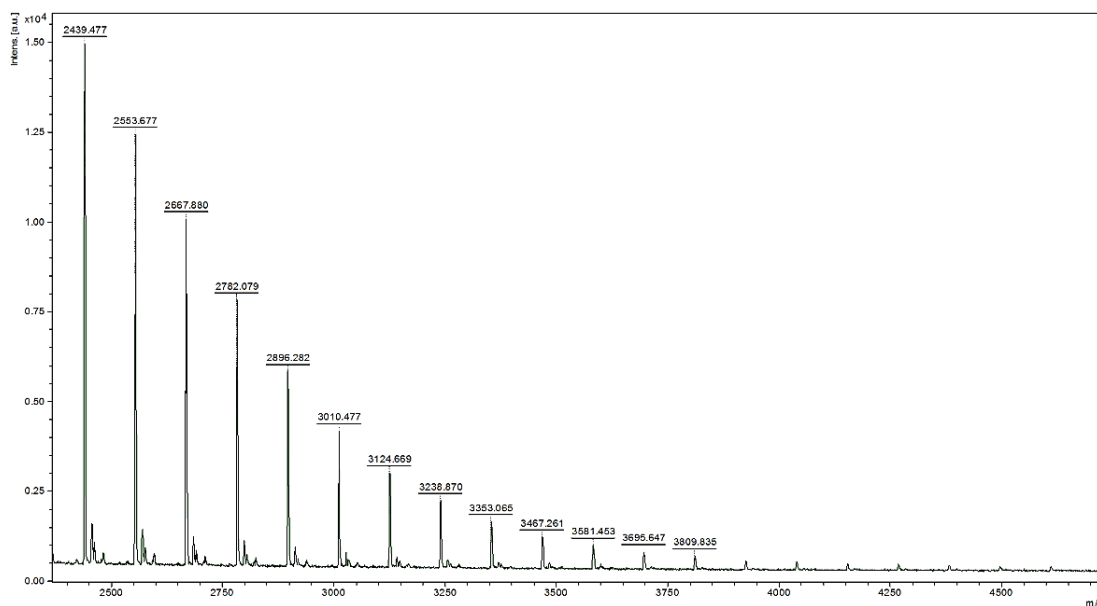
Figure 143. MALDI-ToF spectrum of PCL (run 21, table 6).
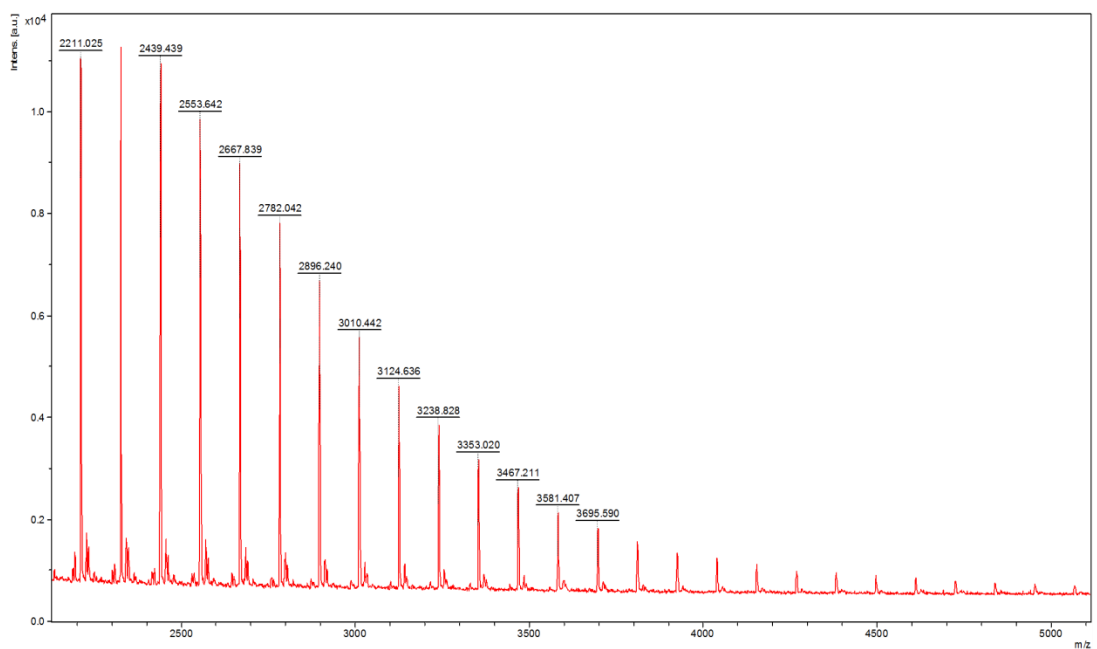
Figure 144. MALDI-ToF spectrum of PCL (run 33, table 6).
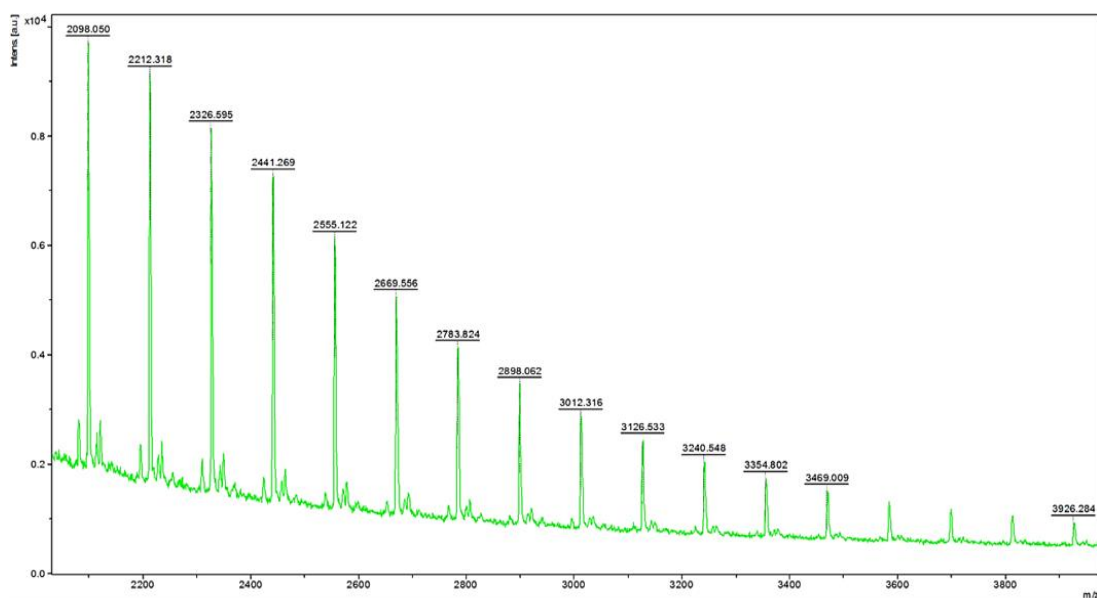
Figure 145. MALDI-ToF spectrum of PCL (no solvent run 1, table 7).
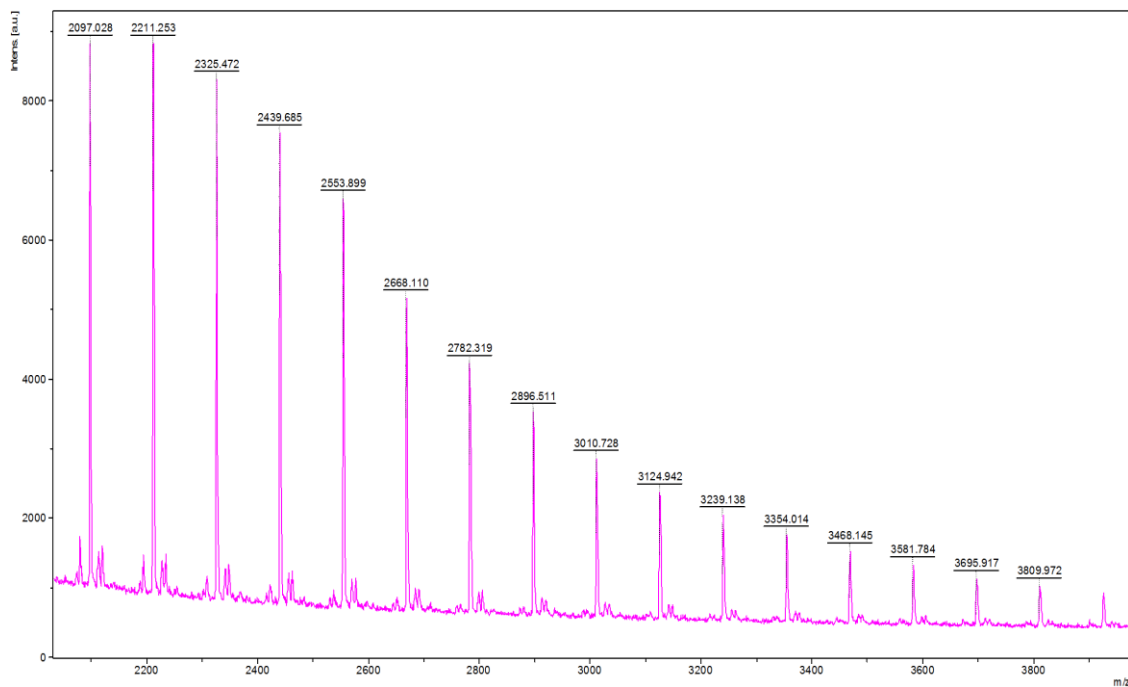
Figure 146. MALDI-ToF spectrum of PCL (run 8, table 7).
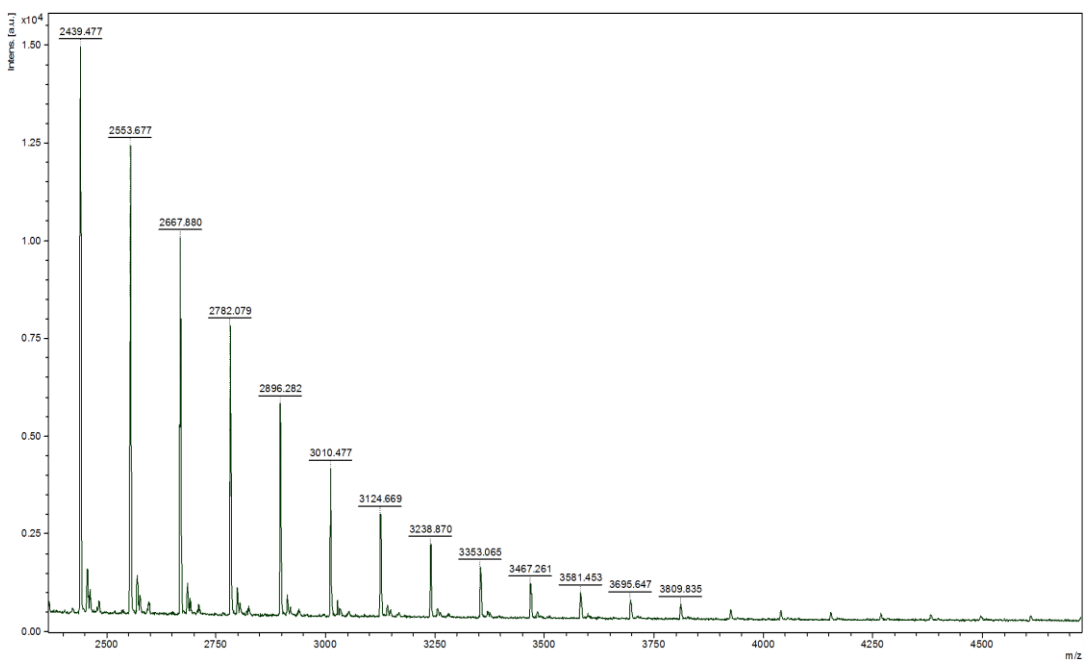
Figure 147. MALDI-ToF spectrum of PLA (run 10, table 8).
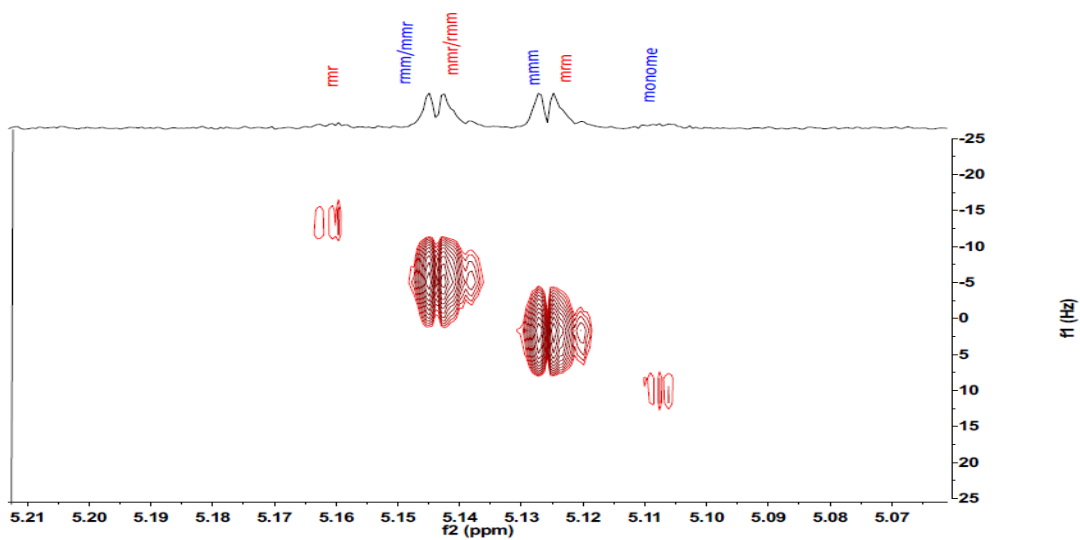
Figure 148. 2D J-resolved ^{1}H NMR spectrum of PLA (run 6, table 9).
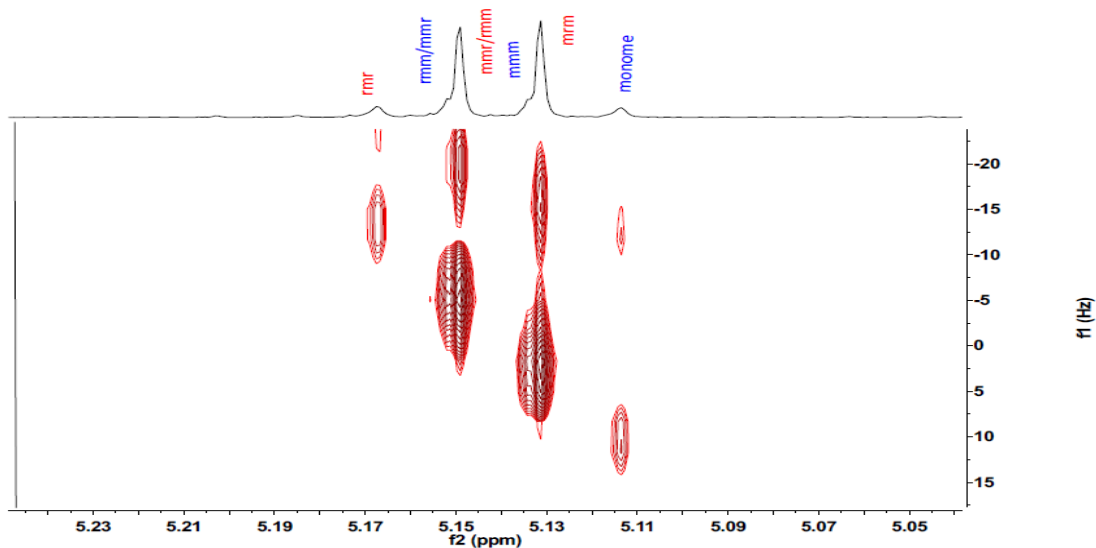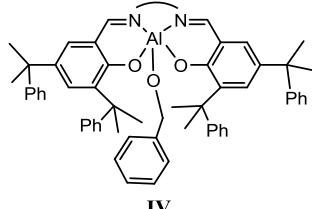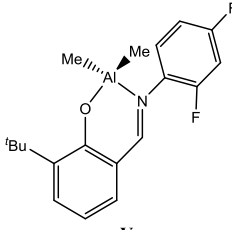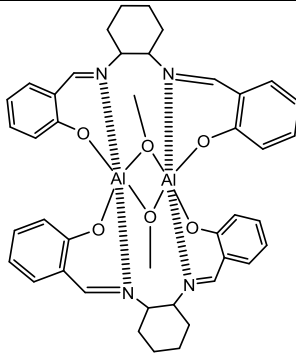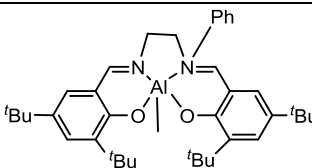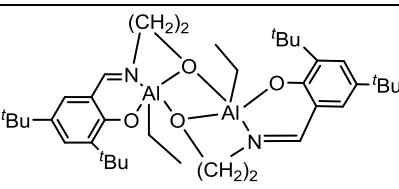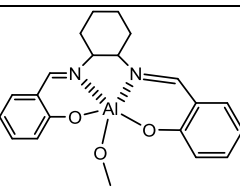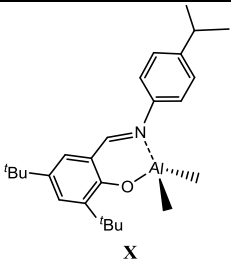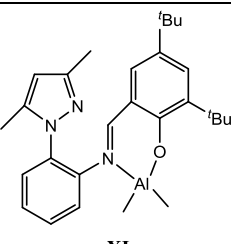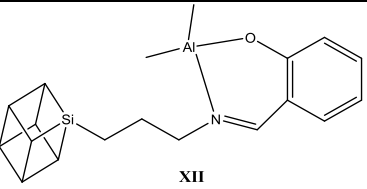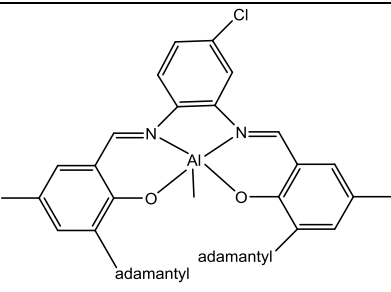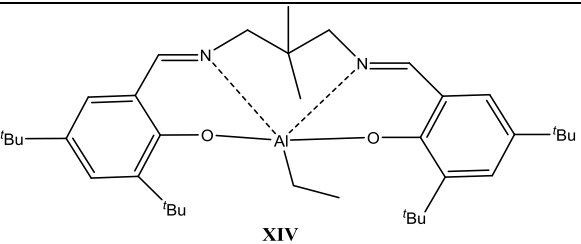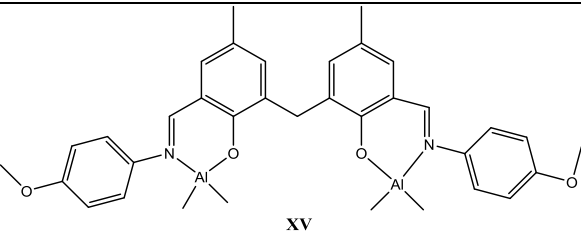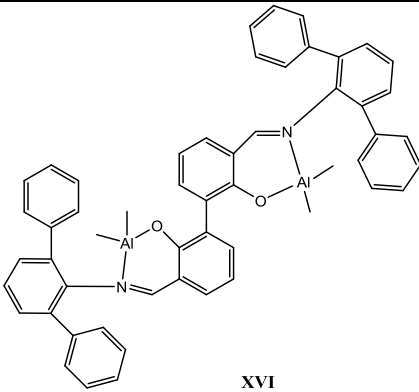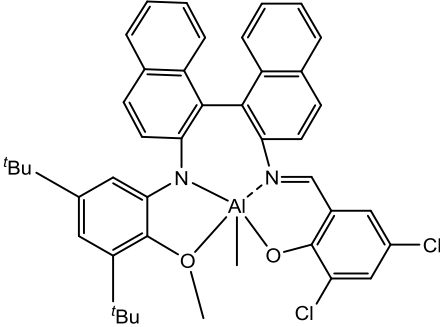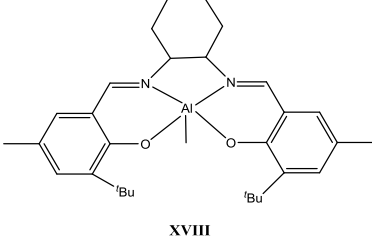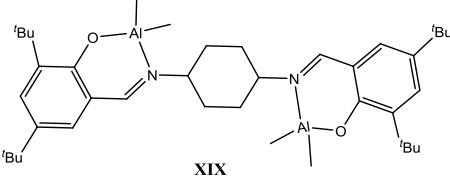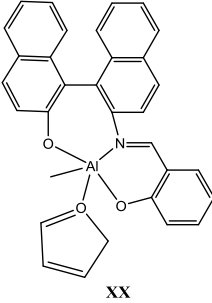
Figure 149. 2D J-resolved ^{1}H NMR spectrum of PLA (run 20, table 9).
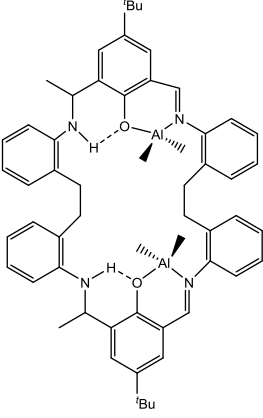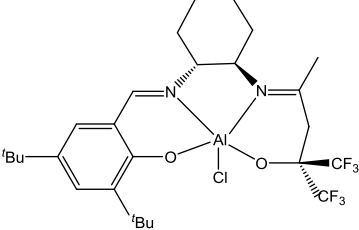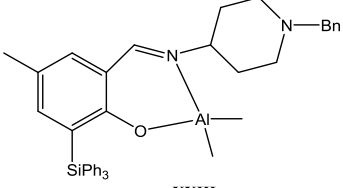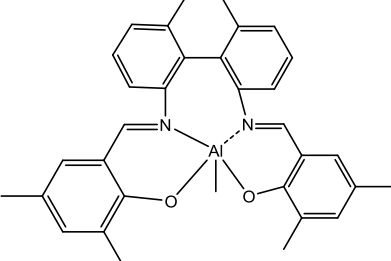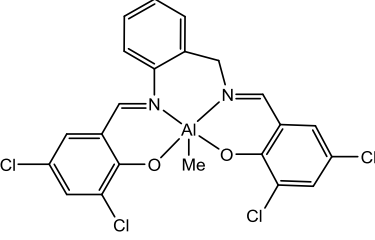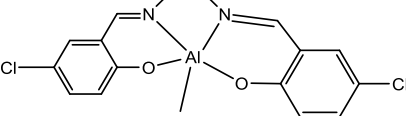
Table 27. List of aluminium phenoxyimine catalysts employed in ROP of cyclic esters.

Ref.	Structure	Monomer	Conditions and results
3a	**I**	*rac*-LA	80 ^{o}C, time = 2h [M]:[Cat]:[OH] = 100:1:2 Conv. 99 % M_{nGPC} = 5250, PDI = 1.16
3b	**II**	*rac*-LA	30 ^{o}C, reaction time=32h [M]:[Cat]:[OH]=100:1:1 Conv. 90 % M_{nGPC} =23700, PDI= 1.11
3c	**III**	ε-CL	60 ^{o}C, time = 30 min [M]:[Cat]:[OH] = 250:1:1 Yield 99 % M_{nGPC} = 56000, PDI = 1.64
		δ-VL	60 ^{o}C, time = 30 min [M]:[Cat]:[OH] =250:1:1 Yield 90 % M_{nGPC} = 25400, PDI = 1.39
		rac-LA	80 ^{o}C, time = 24 h [M]:[Cat]:[OH] = 100:1:1 Yield 94 % M_{nGPC} = 21300, PDI = 1.30

3d	 **IV**	*rac*-LA	70 °C, time =12 h [M]:[Cat]:[OH] = 100:1:0 Conv. 94 % M_{nGPC} = 21 000 (12 200), PDI = 1.07
3e	 **V**	ε-CL	50 °C, time = 4 h [M]:[Cat]:[OH] = 250:1:1 Conv. 97 % M_{nGPC} = 39400, PDI = 1.48
3f	 **VI**	δ-VL ε-CL	100 °C, time = 15 h [M]:[Cat]:[OH] = 100:1:0 Conv. >91 % M_{nGPC} = 4900, PDI = 1.63 100 °C, time = 5 h [M]:[Cat]:[OH] = 50:1:0 Conv. >95 % M_{nGPC} = 5200, PDI = 1.28
3g	 **VII**	*rac*-LA	100 °C, time = 24 h [M]:[Cat]:[OH] = 100:1:1 Conv. 99 % M_{nGPC} =12050, PDI = 1.27
3h	 **VIII**	*rac*-LA	70 °C, time = 15 h [M]:[Cat]:[OH] = 50:1:0 Conv. 64 % M_{nGPC} = 6987, PDI = 1.04
3f	 **IX**	ε-CL	100 °C, time = 6 h [M]:[Cat]:[OH] = 100:1:0 Conv. >95 % M_{nGPC} =11400, PDI = 1.65

3i	**X**	*rac*-LA	100 °C, time = 48 h [M]:[Cat]:[OH] = 250:1:1 Yield 100 % $M_{n\text{GPC}}$ = 29600, PDI = 1.38
3j	**XI**	ε-CL	110 °C, time = 80 min [M]:[Cat]:[OH] = 200:1:0 Conv. 96.1 % $M_{n\text{GPC}}$ =109000, PDI = 1.03
		rac-LA	Inactive
3k	**XII**	*rac*-LA	80 °C, time = 24 h [M]:[Cat]:[OH] =100:1:1 Conv. 99 % $M_{n\text{GPC}}$ = 13850, PDI = 1.36
3l	**XIII**	*rac*-LA	70 °C, time = 24 h [M]:[Cat]:[OH] =100:1:1 Conv. 99 % $M_{n\text{GPC}}$ = 23100, PDI = 1.19
3m	**XIV**	*rac*-LA	70 °C, time = 24 h [M]:[Cat]:[OH] = 100:1:2 Conv. 95 % $M_{n\text{GPC}}$ = 25700, PDI = 1.05
3n	**XV**	*rac*-LA	70 °C, time =18 h [M]:[Cat]:[OH] = 122:1:1 Conv. 95 % $M_{n\text{GPC}}$ = 7100, PDI = 1.20

3o	\n\n**XVI**	*rac*-LA	70 °C, time = 20 min\n[M]:[Cat]:[OH] = 250:1:1\nConv. 100 %\n$M_{nGPC}$ = 59100, PDI = 1.24
3p		*rac*-LA	70 °C, time = 45 h\n[M]:[Cat]:[OH] = 100:1:1\nConv. 85 %\n$M_{nGPC}$ = 21300, PDI= 1.08
3q	\n\n**XVIII**	ε-CL	50 °C, time = 24 h\n$M_{nNMR}$= 2700
3r	\n\n**XIX**	*rac*-LA	130 °C, time = 24 h\n[M]:[Cat]:[OH] = 100:1:4\nConv. 99 %\n$M_{nGPC}$ = 5400, PDI = 1.24
3s	\n\n**XX**	*rac*-LA	70 °C, time = 48 h\n[M]:[Cat]:[OH] = 250:1:1\nConv. 100 %\n$M_{nGPC}$ = 35200, PDI = 1.12

3t	**XXI**	ε-CL	25 °C, time = 12 h [M]:[Cat]:[OH] = 500:1:1 Conv. 99 % M_{nGPC} = 49500, PDI = 1.70
3u	**XXII**	*rac*-LA	80 °C, time = 72 h [M]:[Cat]:[OH] = 100:1:0 Conv. 80 % M_{nGPC} = 10400, PDI = 1.18
3v	**XXIII**	*rac*-LA	110 °C, time = 21 h [M]:[Cat]:[OH] = 500:1:5 Conv. 85 % M_{nSEC} = 11800, PDI = 1.09
3w	**XXIV**	*rac*-LA	110 °C, time = 72 h [M]:[Cat]:[OH]=100:1:0 Conv. 96 % M_{nGPC} = 30900, PDI = 2.06
3x	**XXV**	*rac*-LA	70 °C, time: reaction quenched at conversion > 90% [M]:[Cat]:[OH]=50:1:1 Conv. 90 % M_{nGPC} = 9320, PDI = 1.13
3y	**XXVI**	*rac*-LA	110 °C, time =120 h [M]:[Cat]:[OH] =100:1:1 Conv. 70 % M_{nGPC} =12200, PDI = 1.10
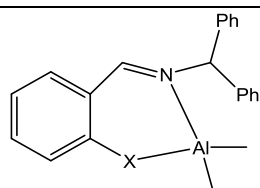
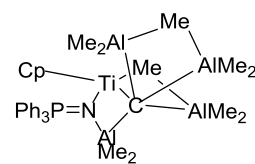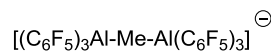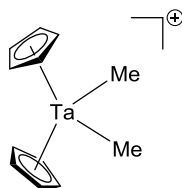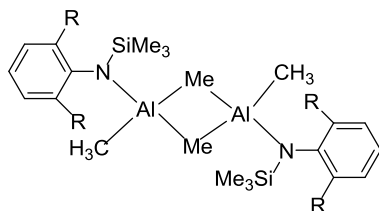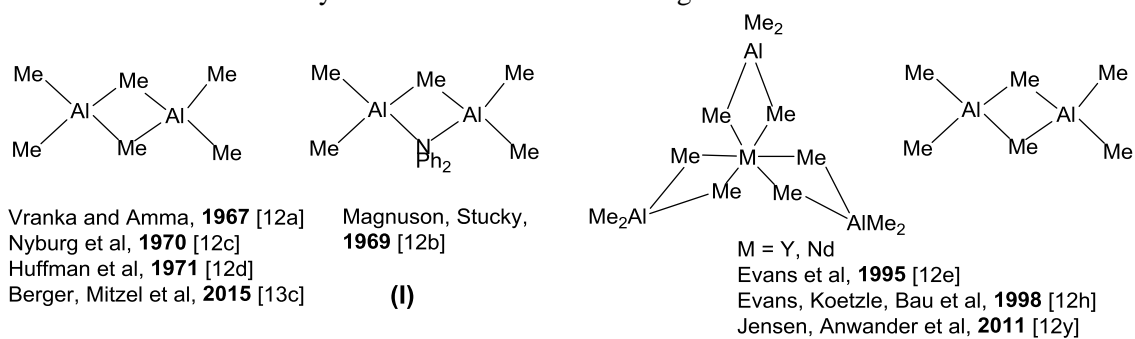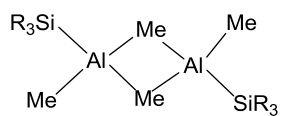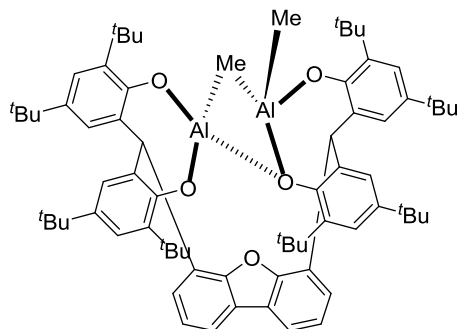| 3z | **XXVII** | *L*-LA | X=O
70 °C,Time =230 min
[M]:[Cat]:[OH] =100:1:2
Conv. 92 %
M_{nGPC}=4900, PDI = 1.04
X=S
70 °C, Time = 80 min
[M]:[Cat]:[OH] =100:1:2
Conv. 90 %
M_{nGPC}=5900, PDI = 1.07 |
| | | ε-CL | X=O
r.t, Time = 360 min
[M]:[Cat]:[OH] = 100:1:2
Conv. 89 %
M_{nGPC} = 3100, PDI = 1.08
X=S
r.t, Time = 80 min
[M]:[Cat]:[OH] =100:1:2
Conv. 92 %
M_{nGPC} = 3300, PDI = 1.05 |
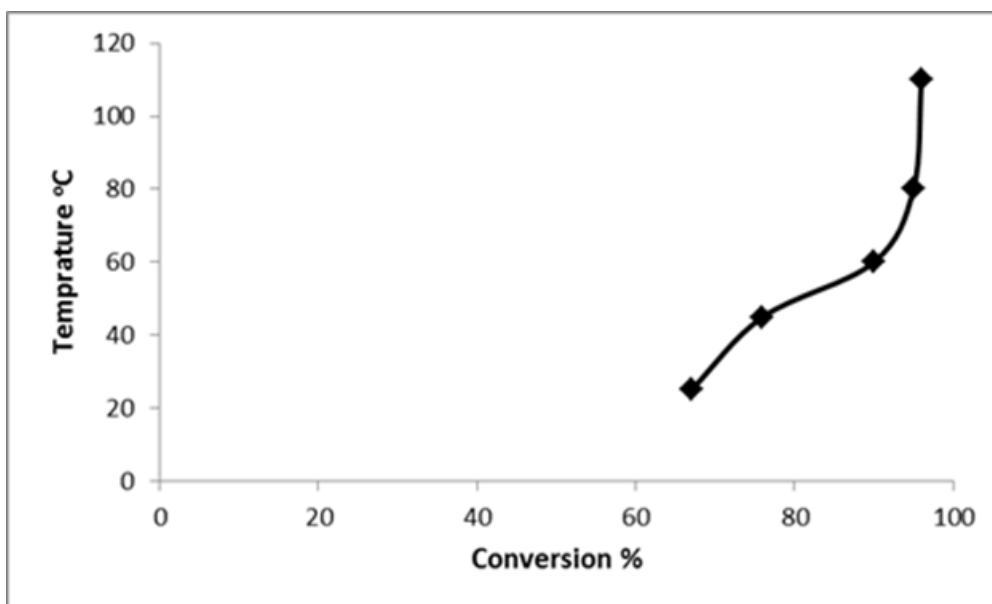
Figure 150. Plot of temperature *versus* monomer conversion for ROP of ε-CL by **24**/BnO

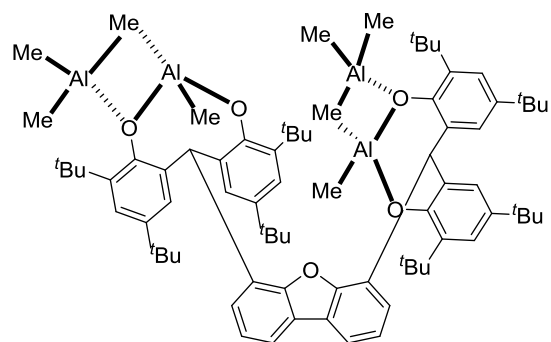**Chart 1.** List of structurally characterized Al-Me-Al bridges.

Vranka and Amma, **1967** [12a]
Nyburg et al, **1970** [12c]
Huffman et al, **1971** [12d]
Berger, Mitzel et al, **2015** [13c]

Magnuson, Stucky,
1969 [12b]

(I)

M = Y, Nd
Evans et al, **1995** [12e]
Evans, Koetzle, Bau et al, **1998** [12h]
Jensen, Anwander et al, **2011** [12y]

R = ^{i}Pr
Roesky et al, **1997** [12f]

R = ^{i}Pr
Jordan et al, **1998** [12i]

R = Me
Roesky et al, **1998** [12g]

Scott et al,
2000 [12o]

Chen et al, **2000** [12m]

Winter et al, **2000** [12l]

$[(C_6F_5)_3Al\text{-}Me\text{-}Al(C_6F_5)_3]$

Chen, Abboud, **2000** [12n]

Stephan et al, **2000** [12k]
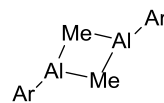Stephan et al, **2001** [12p]
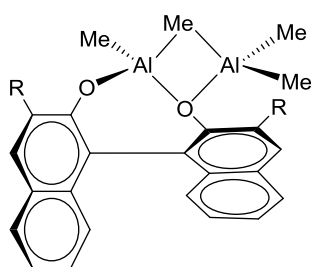
259

R= SiMe$_3$
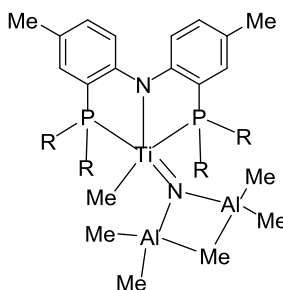Weidlein et al, **2000** [12j]

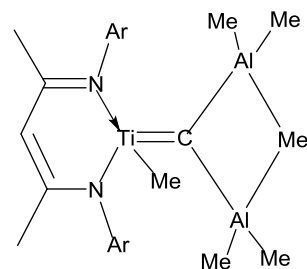Scott et al, **2002** [12q]

Scott et al, **2002 [**12q]

Ar = C$_6$F$_5$
Cowley, Jones et al, **2003** [12r]

R = SiPh$_3$
Rothwell et al, **2003** [12s]

R = ^{i}Pr
Mindiola et al, **2007** [12t]

Ar = 2,6-^{i}Pr$_2$C$_6$H$_3$
Roesky et al, **2008** [12u]
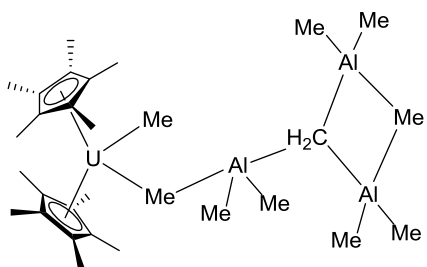
Anwander, Evans et al, **2009** [12v]
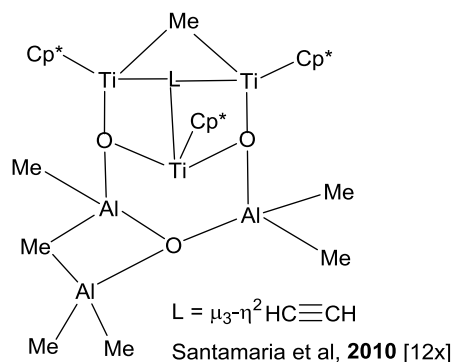
L = μ_3-η^2HC≡CH
Santamaria et al, **2010** [12x]
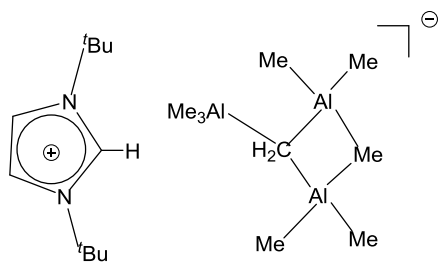
Dagorne et al, **2010** [12w]
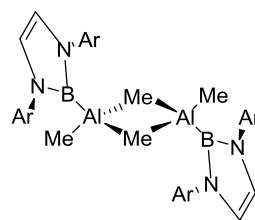
Ar = 2,6-(*i*Pr)$_2$C$_6$H$_3$
Anwander et al, **2012** [12z]
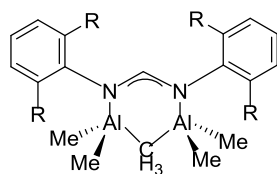
R = Et, *i*Pr
Deacon, Junk, Anwander et al, **2013** [13a]
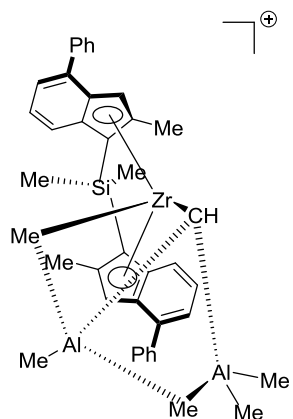
Carpentier, Kirillov et al, **2015** [13b]
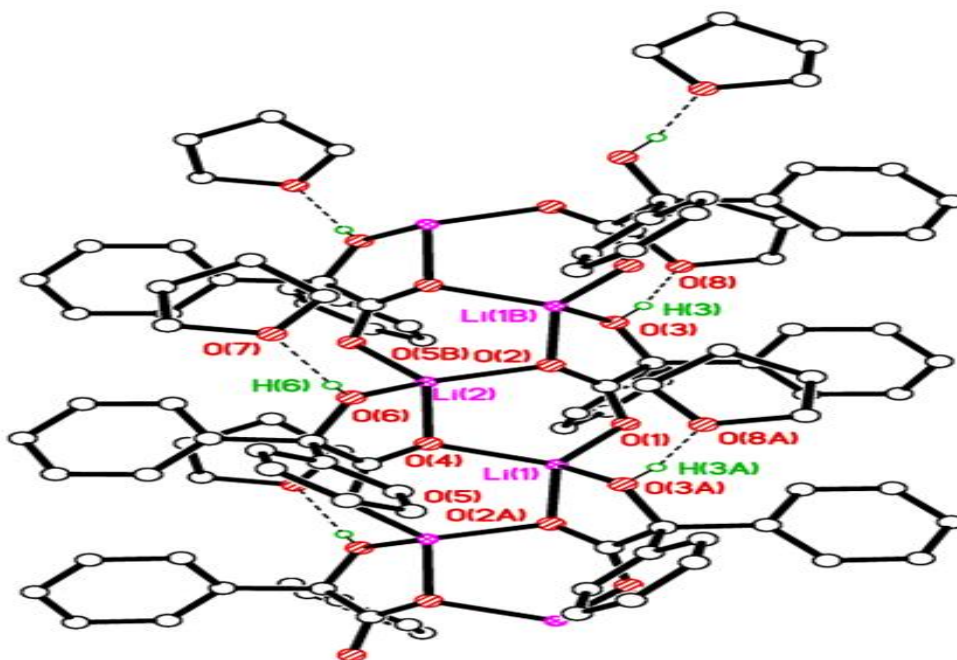
Figure 151. Chains of **31** parallel to the crystallographic *a* direction.
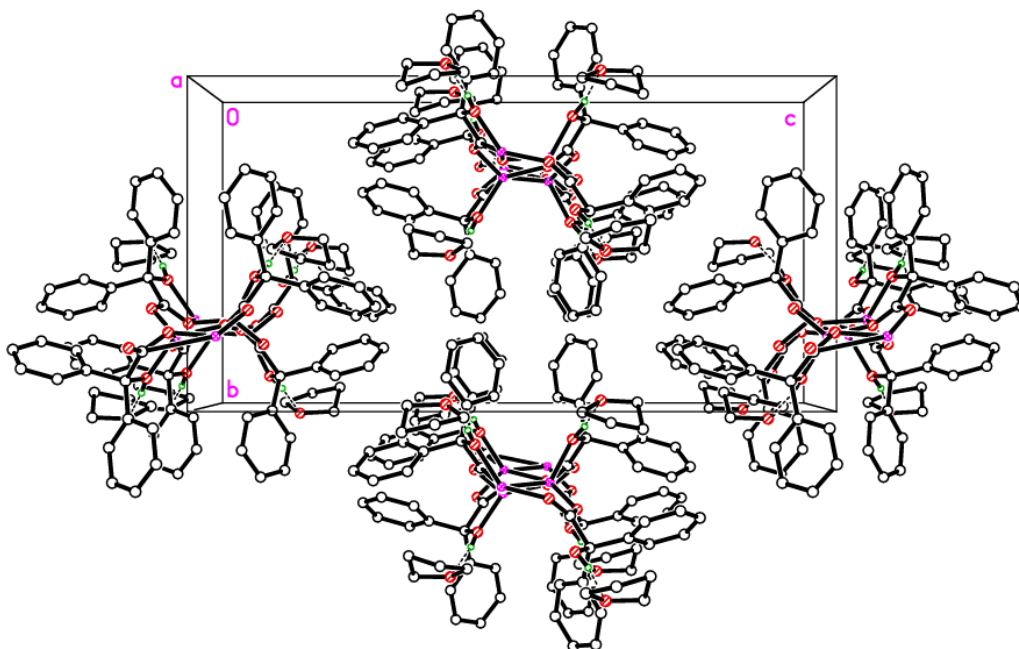
Figure 152. Packing of **31**
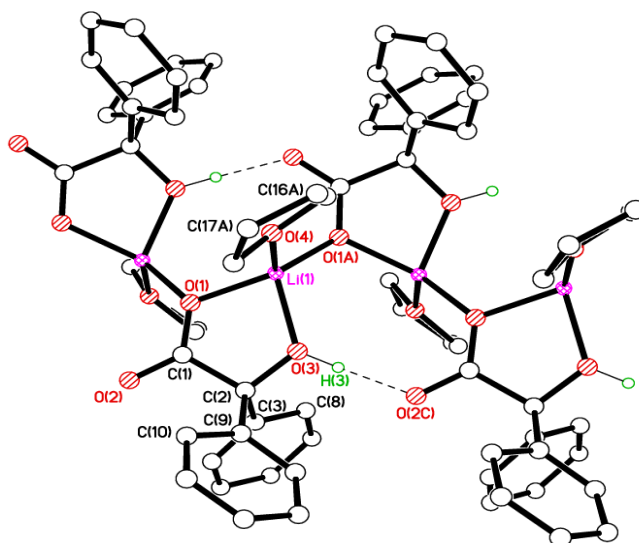
Figure 153. Coordination about Li(1) in **31**′ and H-bonds supporting the chain structure. Selected bond lengths (Å) and angles (°): Li(1)–O(1) 1.926(4), Li(1)–O(1A) 1.900(3), Li(1)–O(3) 1.917(3), Li(1)–O(4) 1.962(4); O(1)–Li(1)–O(1A) 134.88(19), O(1)–Li(1)–O(3) 82.99(13), O(3)–Li(1)–O(4) 109.95(17).
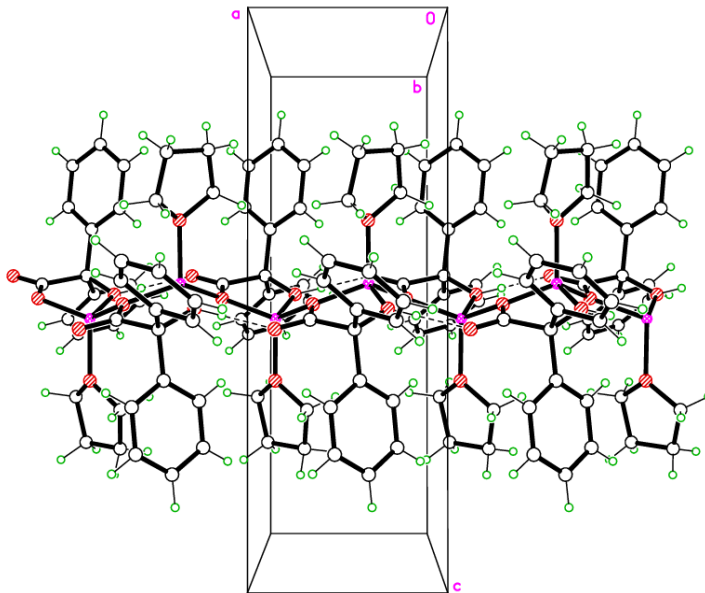
Figure 154. Chains in **31**′ which are all aligned along *a*, are arranged in a square grid in the *bc* plane. Between the chains there are no classic hydrogen bonds but there is evidence for C−H···π interactions between the benz ligands and THF. This view is orthogonal to that in figure 2 above.
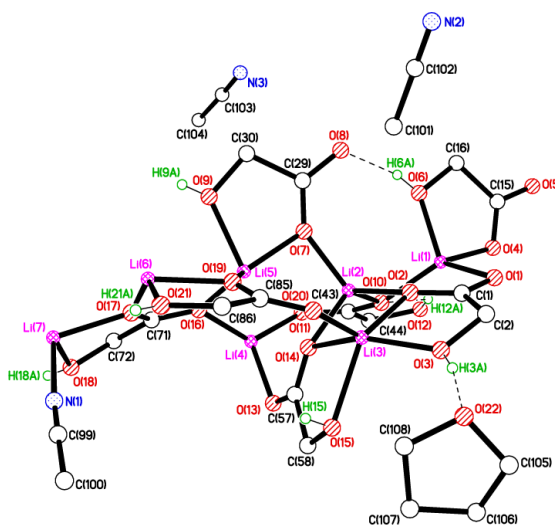
Figure 155. Alternative view of complex **32**.
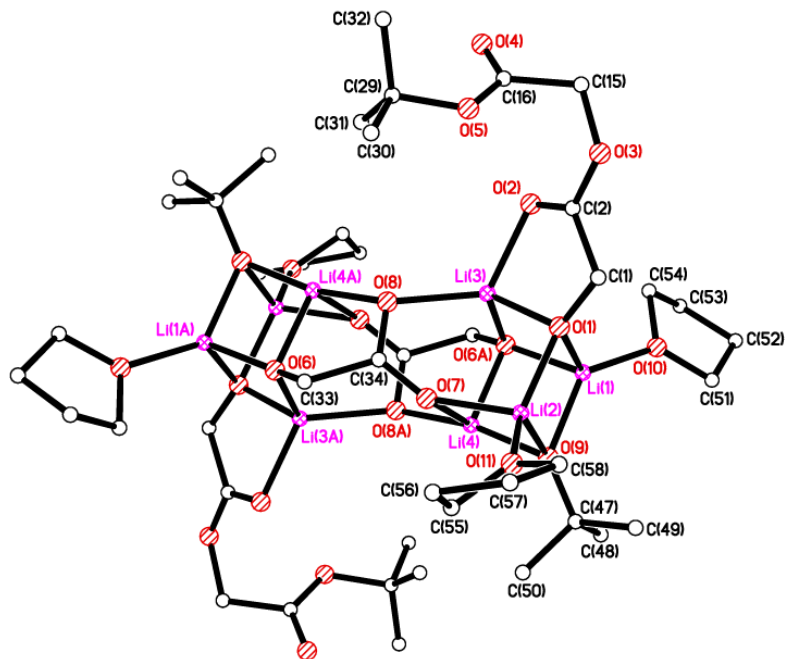
Figure 156. Alternative view of complex **33**.
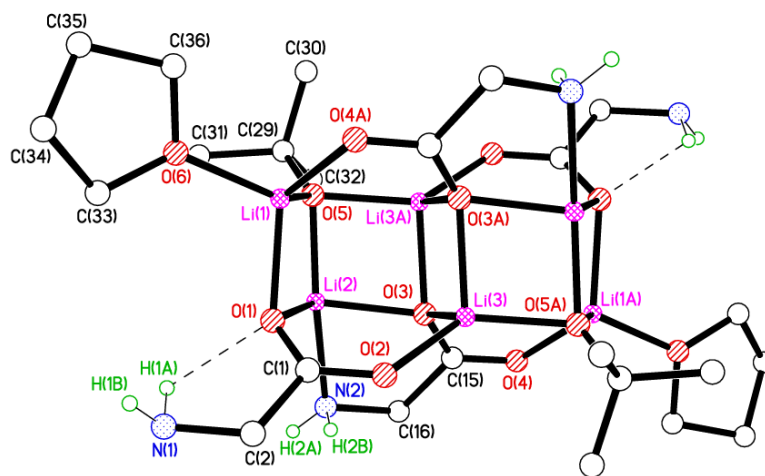
Figure 157. Alternative view of complex **34**.

Chart 2. Previously reported metal/main group complexes derived from 2,2′-diphenylglycine.

Redshaw 1997

Gibson 1997

Redshaw 2007

Redshaw 2011 (M= Cu, Zn)

Redshaw 2009

Redshaw 2005

Redshaw 2005

Powell, Roesky 2013
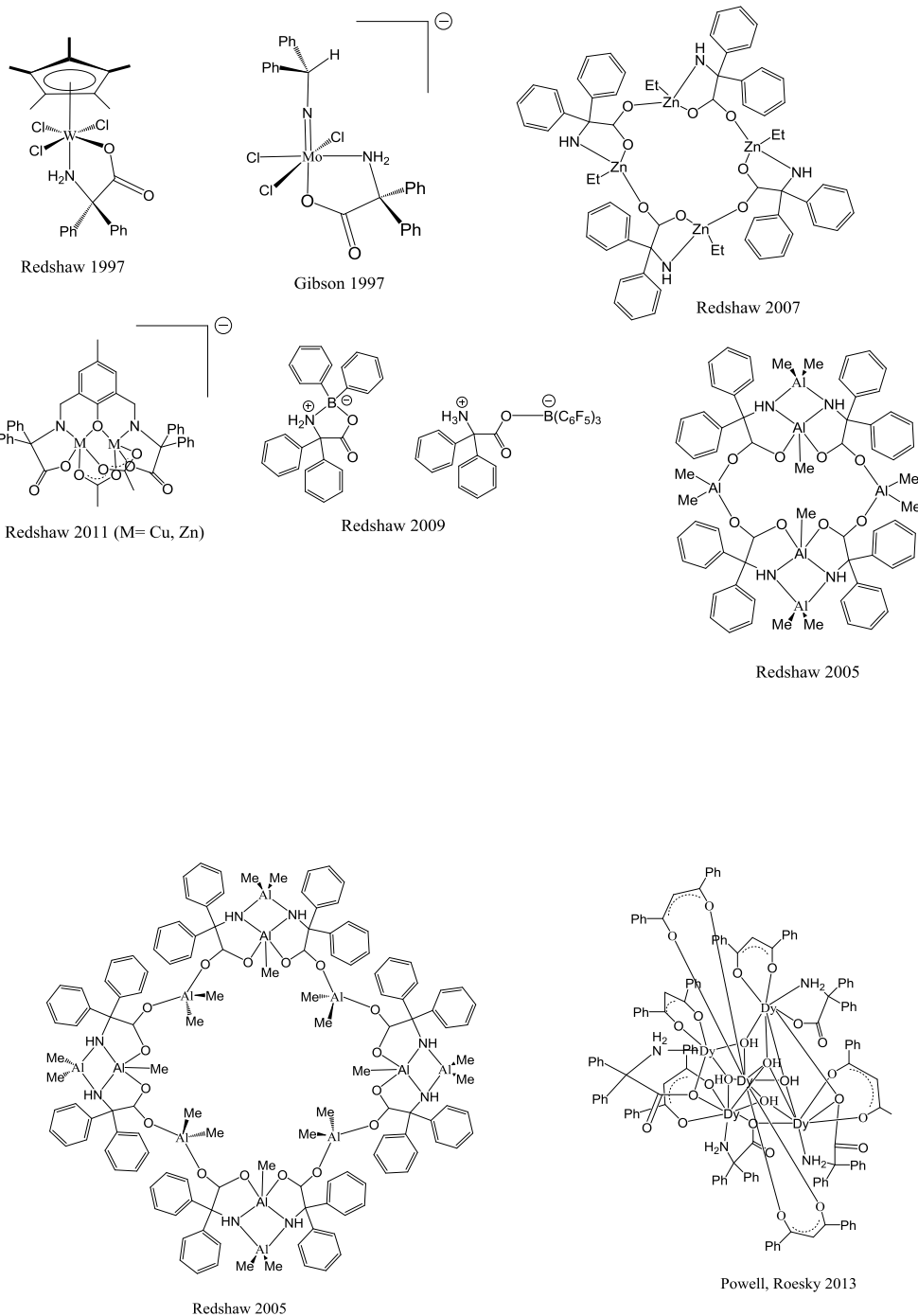
Figure 158. Alternative view of **36**.
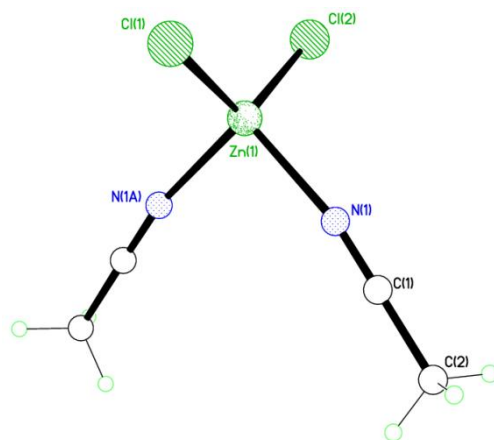
Figure 159. View of $[ZnCl_2(NCMe)_2]$
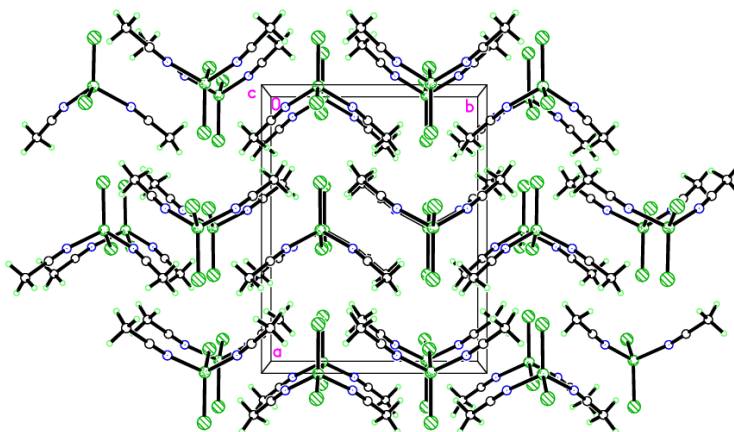
Figure 160. Layered structure in [ZnCl$_2$(NCMe)$_2$]
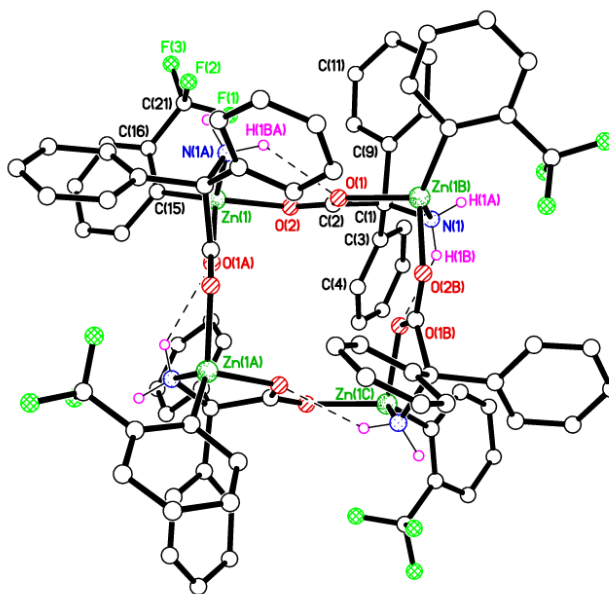
Figure 161. Alternative view of **38**.
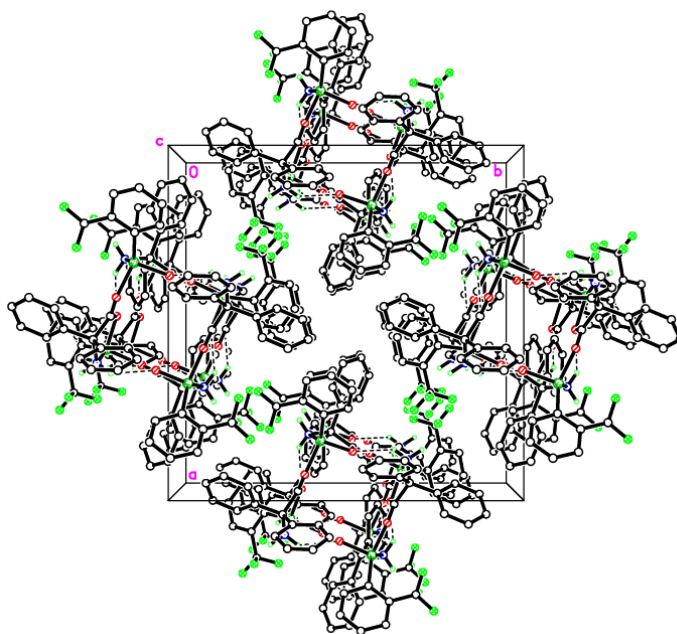
Figure 162. Packing diagram of **38**.
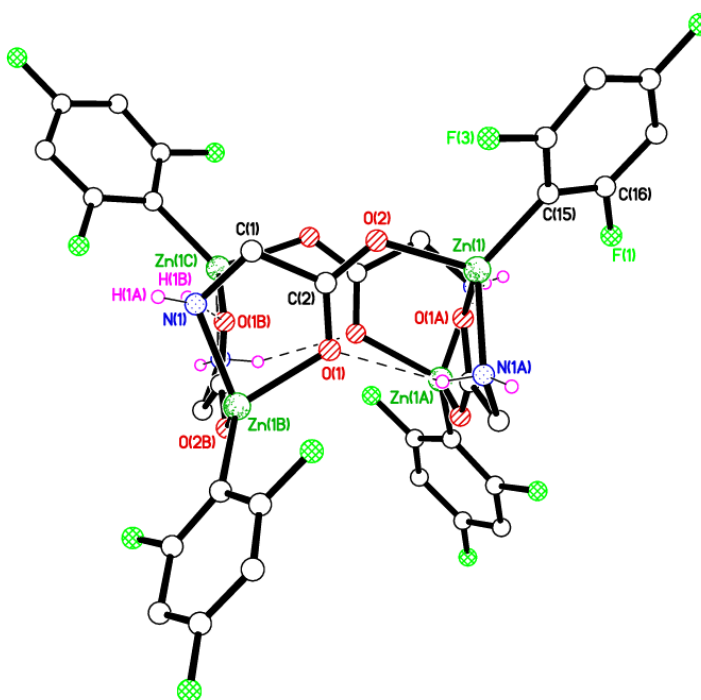
Figure 163. Alternative view of **39**.

Table 28. Crystallographic data for the ligands and complexes reported in this study.

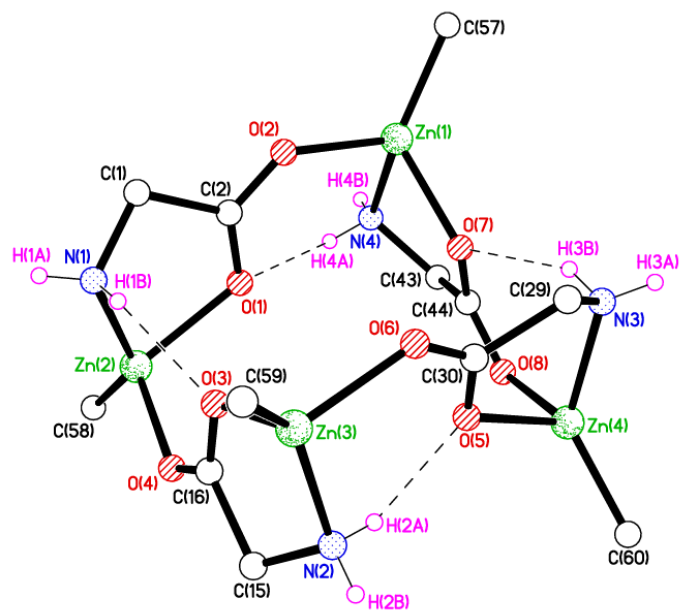| Compound	L^1H_4	$L^2H_4\cdot2MeCN$	$1\cdot6MeCN$	$2\cdot3\frac{1}{2}MeCN\cdot0.614toluene$
Formula	$C_{64}H_{90}O_4$	$C_{64}H_{90}O_4\cdot2(C_2H_3N)$	$C_{68}H_{92}Cl_6N_2Nb_2O_4\cdot6(C_2H_3N)$	$C_{72}H_{102}Cl_4N_2O_6Nb_2\cdot3\frac{1}{2}(C_2H_3N)\cdot0.614(C_7H_8)$
Formula weight	923.35	1005.46	1646.27	1619.45
Crystal system	Triclinic	Triclinic	Triclinic	Triclinic
Space group	$P\bar{1}$	$P\bar{1}$	$P\bar{1}$	$P\bar{1}$
a (Å)	11.778(11)	14.643(1)	10.8601(8)	12.6086(9)
b (Å)	15.190(15)	15.4125(11)	12.1510(9)	16.8197(12)
c (Å)	18.55(2)	16.1202(11)	17.9452(13)	21.7135(15)
α (°)	68.19(3)	75.412(12)	72.153(13)	89.714(2)
β (°)	83.42(5)	69.309(11)	79.492(15)	86.846(2)
γ (°)	69.19(4)	73.026(12)	77.185(14)	73.006(2)
V (Å^3)	2880(5)	3209.9(5)	2181.2(4)	4396.8(5)
Z	2	2	1	2
Temperature (K)	100(2)	100(2)	100(2)	100(2)
Wavelength (Å)	0.6889	0.71073	0.71073	0.71073
Calculated density (g.cm^{-3})	1.065	1.040	1.253	1.223
Absorption coefficient (mm^{-1})	0.06	0.06	0.50	0.43
Transmission factors (min./max.)	0.532 and 1.000	0.113 and 1.000	0.614 and 1.000	0.746 and 1.000
Crystal size (mm^3)	0.10 x 0.02 x 0.01	0.09 x 0.04 x 0.01	$0.05 \times 0.04 \times 0.01$	$0.17 \times 0.07 \times 0.06$
θ(max) (°)	22.5	22.5	25.0	27.6
Reflections measured	32266	21642	20034	77150
Unique reflections	8221	8056	7527	20127
R_{int}	0.179	0.216	0.094	0.051
Reflections with $F^2 > 2\sigma(F^2)$	4391	3030	4629	17091
Number of parameters	651	728	546	1054
R_1 [$F^2 > 2\sigma(F^2)$]	0.116	0.146	0.077	0.057
wR_2 (all data)	0.313	0.484	0.207	0.169
GOOF, S	1.10	1.03	1.05	1.02
Largest difference peak and hole (e Å^{-3})	0.34 and −0.27	1.17 and −0.32	1.36 and −0.96	1.22 and −1.68

Compound	3·5MeCN	4·3½MeCN	4·5MeCN
Formula	$C_{72}H_{102}Cl_4N_2O_6Ta_2 \cdot 5(C_2H_3N)$	$C_{130}H_{179}ClNNbO_8 \cdot 3½(C_2H_3N)$	$C_{130}H_{179}ClNNbO_8 \cdot 5(C_2H_3N)$
Formula weight	1800.52	2155.78	2217.36
Crystal system	Triclinic	monoclinic	triclinic
Space group	$P\bar{1}$	$P2_1/c$	$P\bar{1}$
Unit cell dimensions			
a (Å)	12.6367(8)	30.358(2)	17.5553(17)
b (Å)	16.8848(11)	17.6674(12)	19.1574(15)
c (Å)	21.6085(14)	24.5131(17)	22.552(3)
α (°)	87.781(5)	90	74.926(8)
β (°)	87.412(5)	93.6385(17)	81.846(9)
γ (°)	73.944(5)	90	73.063(7)
V (Å^3)	4424.5(5)	13121.0(15)	6988.0(12)
Z	2	4	2
Temperature (K)	150(2)	100(2)	150(2)
Wavelength (Å)	0.71073	0.71073	0.71073
Calculated density (g.cm^{-3})	1.351	1.091	1.054
Absorption coefficient (mm^{-1})	2.64	0.17	0.16
Transmission factors (min./max.)	0.412 and 0.624	0.699 and 1.000	0.796 and 1.000
Crystal size (mm^3)	$0.35 \times 0.35 \times 0.20$	0.08 x 0.06 x 0.06	$0.30 \times 0.25 \times 0.20$
θ(max) (°)	25.5	25.0	19.8
Reflections measured	93502	69292	25016
Unique reflections	40462	22952	12529
R_{int}	0.039	0.072	0.138
Reflections with $F^2 > 2\sigma(F^2)$	26933	13966	3851
Number of parameters	862	1529	1396
R_1 [$F^2 > 2\sigma(F^2)$]	0.082	0.072	0.082
wR_2 (all data)	0.226	0.183	0.238
GOOF, S	0.94	1.06	0.79
Largest difference peak and hole (e Å^{-3})	2.48 and −2.77	0.89 and −0.90	0.50 and −0.30

Compound	5	6·CH$_2$Cl$_2$	7	8·6MeCN
Formula	C$_{54}$H$_{78}$MoN$_2$O$_2$	C$_{59}$H$_{80}$MoN$_2$O$_2$·CH$_2$Cl$_2$	C$_{80}$H$_{106}$F$_{10}$Mo$_2$N$_4$O$_4$	C$_{102}$H$_{140}$Mo$_2$N$_4$O$_8$·6(C$_2$H$_3$N)
Formula weight	883.12	1030.11	1569.56	1988.37
Crystal system	Triclinic	Triclinic	Monoclinic	Triclinic
Space group	P1	p -1	$P2_1/n$	P-1
a (Å)	10.0435(8)	11.7691(7)	14.2727(8)	13.0178(8)
b (Å)	10.3143(8)	14.1045(9)	15.4944(8)	13.4853(8)
c (Å)	12.8862(11)	18.0657(12)	18.0242(10)	16.9177(10)
α (°)	74.5019(14)	83.543(5)	-	106.1133(10)
β (°)	87.3130(14)	81.066(5)	98.4505(10)	96.4972(10)
γ (°)	78.6415(14)	74.829(5)	-	92.7062(10)
V (Å^3)	1261.15(18)	2851.1(3)	3942.7(4)	2825.3(3)
Z	1	2	2	1
Temperature (K)	150(2)	150(2)	150(2)	150(2)
Wavelength (Å)	0.6861	0.71073	0.71073	0.71073
Calculated density (g·cm^{-3})	1.163	1.200	1.322	1.169
Absorption coefficient (mm^{-1})	0.27	0.37	0.39	0.28
Transmission factors (min./max.)	0.960 and 0.995	0.912 and 0.857	0.958 and 0.985	0.936 and 0.970
Crystal size (mm^3)	0.15 × 0.12 × 0.02	0.50 × 0.45 × 0.45	0.11 × 0.07 × 0.04	0.24 × 0.15 × 0.11
θ (max) (°)	29.2	29.3	28.9	
Reflections measured	13007	30297	24317	25167
Unique reflections	11751	15207	9273	13076
R_{int}	0.031	0.0572	0.048	0.027
Reflections with $F^2 > 2\sigma(F^2)$	11618	11245	6286	10128
Number of parameters	554	615	498	659
R_1 ($F^2 > 2\sigma(F^2)$)	0.038	0.042	0.044	0.043
wR_2 (all data)	0.094	0.102	0.110	0.107
GOOF, S	1.01	0.91	1.03	1.03
Largest difference peak and hole (e Å^{-3})	0.75 and −0.49	1.11 and −1.31	0.46 and −0.46	0.70 and −0.54

Compound	10·2C$_6$H$_{14}$	11·6MeCN	12
Formula	C$_{112}$H$_{154}$Mo$_2$N$_4$O$_4$·2(C$_6$H$_{14}$)	C$_{92}$H$_{122}$F$_{10}$Mo$_2$N$_2$O$_8$·6(C$_2$H$_3$N)	C$_{28}$H$_{44}$Cl$_2$MoN$_2$O$_2$
Formula weight	1984.61	2012.11	607.49
Crystal system	Monoclinic	Triclinic	Triclinic
Space group	$C2/c$	$P\bar{1}$	$P\bar{1}$
a (Å)	40.815(3)	18.7522(10)	10.0491(10)
b (Å)	17.0938(11)	22.6704(12)	10.6022(11)
c (Å)	16.3488(11)	25.8469(18)	15.6133(19)
α (°)	90	79.933(6)	92.902(9)
β (°)	94.8200(10)	81.162(6)	90.577(9)
γ (°)	90	81.434(6)	112.932(8)
V (Å^3)	11365.9(13)	10605.9(11)	1529.2(3)
Z	4	4	2
Temperature (K)	100(2)	100(2)	150(2)
Wavelength (Å)	0.71073	0.71073	0.71073
Calculated density (g·cm^{-3})	1.160	1.260	1.319
Absorption coefficient (mm^{-1})	0.27	0.31	0.63
Transmission factors (min./max.)	1.000 and 0.634	0.976 and 0.994	0.981 and 0.855
Crystal size (mm^3)	0.18 × 0.09 × 0.04	0.08 × 0.05 × 0.02	0.40 × 0.38 × 0.06
θ(max) (°)	27.5	25.0	26.4
Reflections measured	67463	101749	11706
Unique reflections	12964	36898	6145
R_{int}	0.0710	0.182	0.0965
Reflections with $F^2 > 2\sigma(F^2)$	9692	14715	3429
Number of parameters	566	2420	326
R_1 ($F^2 > 2\sigma(F^2)$)	0.044	0.084	0.063
wR_2 (all data)	0.126	0.212	0.156
GOOF, S	1.02	0.86	0.89
Largest difference peak and hole (e Å^{-3})	0.67 and −0.47	0.88 and −2.06	0.55 and −0.95

Compound	**13**	**14**	**15·2CH$_2$Cl$_2$**
Formula	C$_{34}$H$_{53}$O$_2$V	C$_{70}$H$_{100}$O$_8$V$_2$	C$_{70}$H$_{100}$O$_8$V$_2$·2(CH$_2$Cl$_2$)
Formula weight	576.70	1171.37	1339.21
Crystal system	Monoclinic	Monoclinic	Orthorhombic
Space group	*P2$_1$/c*	*P2$_1$/c*	*P*bca
a (Å)	13.886(8)	10.967(4)	11.0268(7)
b (Å)	23.550(14)	10.344(3)	19.1028(13)
c (Å)	10.938(7)	27.9706(10)	70.103(5)
α (°)			90
β (°)	110.492(8)	92.329(6)	90
γ (°)			90
V (Å^3)	3351(4)	3170.4(15)	14766.7(17)
Z	4	2	8
Temperature (K)	150(2)	100(2)	100(2)
Wavelength (Å)	0.71075	0.71075	0.71075
Calculated density (g.cm^{-3})	1.143	1.227	1.205
Absorption coefficient (mm^{-1})	0.329	0.349	0.448
Transmission factors (min./max.)	0.502 and 1.000	0.600 and 1.000	0.682 and 1.000
Crystal size (mm)	0.06× 0.01 × 0.01	0.09 × 0.03 × 0.01	0.27 × 0.10 × 0.02
θ(max) (°)	25.171	25.095	27.507
Reflections measured	37155	17727	91884
Unique reflections	5977	5568	16405
R$_{int}$	0.3338	0.1786	0.0794
Reflections with $F^2 > 2\sigma(F^2)$	2250	2591	11323
Number of parameters	368	372	763
R_1 [$F^2 > 2\sigma(F^2)$]	0.0922	0.0987	0.0723
wR_2 (all data)	0.2193	0.2427	0.2255
GOOF, *S*	1.016	1.058	1.043
Largest difference peak and hole (e Å^{-3})	0.323 and –0.321	0.585 and –0.489	0.624 and -1.154

Compound	**16**·2CH$_2$Cl$_2$	**16**·3CH$_2$Cl$_2$	**17**·2MeCN
Formula	C$_{72}$H$_{104}$O$_8$V$_2$.2(CH$_2$Cl$_2$)	C$_{71}$H$_{102}$O$_8$V$_2$· 3(CH$_2$Cl$_2$)	C$_{82}$H$_{106}$Cl$_2$N$_4$O$_4$V$_2$·2MeCN
Formula weight	1369.28	1440.18	1466.59
Crystal system	Monoclinic	Monoclinic	Monoclinic
Space group	*P*2$_1$/*n*	*P*2$_1$/*n*	*P*2$_1$/*n*
a (Å)	21.4616(15)	21.479(15)	10.6773(7)
b (Å)	14.3723(10)	14.382(9)	18.5913(13)
c (Å)	25.6780(18)	25.952(18)	21.2520(15)
α (º)			90
β (º)	104.267(1)	103.682(7)	96.0750(10)
γ (º)			90
V (Å^3)	7676.2(9)	7789(9)	4194.9(5)
Z	4	4	2
Temperature (K)	100	100	100(2)
Wavelength (Å)	0.71073	0.6889	0.71073
Calculated density (g.cm^{-3})	1.185	1.228	1.161
Absorption coefficient (mm^{-1})	0.43	0.46	0.337
Transmission factors (min./max.)	0.678 and 1.000	0.947 and 0.982	0.754 and 1.000
Crystal size (mm)	0.10 × 0.07 × 0.02	0.12 × 0.05 × 0.04	0.20 × 0.03 × 0.03
θ(max) (°)	27.5	22.5	27.609
Reflections measured	91396	50369	14230
Unique reflections	17489	11066	14230
R$_{int}$	0.073	0.196	0.0798
Reflections with $F^2 > 2\sigma(F^2)$	13364	6500	12276
Number of parameters	794	889	453
R_1 [$F^2 > 2\sigma(F^2)$]	0.054	0.128	0.0736
wR_2 (all data)	0.162	0.370	0.1911
GOOF, *S*	1.04	1.03	1.109
Largest difference peak and hole (e Å^{-3})	0.86 and −0.41	0.78 and −0.67	0.808 and -0.535

Compound	L^9Hdpa	L^9Hdpg	24	26
Formula	$C_{28}H_{33}NO$	$C_{28}H_{33}NO$	$C_{30}H_{38}AlNO$	$C_{30}H_{38}AlNO$
Formula weight	399.55	399.55	455.59	455.59
Crystal system	Triclinic	Monoclinic	Monoclinic	Triclinic
Space group	$P\bar{1}$	$P2_1/c$	$P2_1$	$P\bar{1}$
Unit cell dimensions				
a (Å)	10.0491(4)	19.264(5)	12.019(7)	10.4155(6)
b (Å)	11.8421(5)	5.9804(7)	9.329(2)	12.2889(7)
c (Å)	22.5152(9)	22.048(3)	12.761(6)	22.1595(13)
α (°)	86.153(3)	90	90	78.099(2)
β (°)	88.412(3)	111.594(15)	111.22(5)	80.513(2)
γ (°)	67.738(4)	90	90	80.731(2)
V (Å^3)	2474.05(19)	2361.8(8)	1333.8(11)	2713.5(3)
Z	4	4	2	4
Temperature (K)	293(2)	150(2)	150(2)	160(2)
Wavelength (Å)	0.71073	0.71073	0.71073	0.71073
Calculated density (g.cm^{-3})	1.073	1.124	1.134	1.115
Absorption coefficient (mm^{-1})	0.064	0.067	0.097	0.10
Transmission factors (min./max.)	0.716/1.000	0.955/0.979	0.977/0.986	0.936/0.978
Crystal size (mm^3)	$0.7 \times 0.4 \times 0.2$	$0.45 \times 0.25 \times 0.05$	$0.28 \times 0.20 \times 0.19$	$.70 \times 0.52 \times 0.23$
θ(max) (°)	29.226	25.235	25.331	28.865
Reflections measured	32360	8827	7484	20453
Unique reflections	11750	4231	7484	12306
R_{int}	0.0319	0.0620	0.1661	0.0183
Reflections with $F^2 > 2\sigma(F^2)$	6867	2051	3692	10043
Number of parameters	548	280	287	611
R_1 [$F^2 > 2\sigma(F^2)$]	0.0762	0.0494	0.1195	0.0464
wR_2 (all data)	0.2324	0.1135	0.3432	0.1186
GOOF, S	1.042	0.804	1.007	1.019
Largest difference peak and hole (e Å^{-3})	0.673 and −0.468	0.237 and −0.316	0.719 and −0.427	).363 and −0.275

Compound	**28**	**29**	**30·MeCN**
Formula	$C_{25}H_{35}Al_3NP$	$C_{17}H_{25}Al_2N$	$C_{32}H_{39}Al_2N_3$
Formula weight	461.45	297.34	519.62
Crystal system	Triclinic	Monoclinic	Triclinic
Space group	$P\bar{1}$	$P2_1/n$	$P\bar{1}$
Unit cell dimensions			
a (Å)	8.7689(14)	12.9996(3)	11.13092(14)
b (Å)	12.714(2)	9.1655(2)	11.31747(15)
c (Å)	12.722(2)	14.6167(2)	14.07252(15)
α (°)	79.822(2)	90	104.6534(10)
β (°)	77.110(2)	91.416(2)	108.3655(11)
γ (°)	75.776(2)	90	105.3906(11)
V (Å^3)	1329.0(4)	1741.02(6)	1508.40(3)
Z	2	4	2
Temperature (K)	150(2)	100(2)	100(2)
Wavelength (Å)	0.6861	0.71073	0.71075
Calculated density (g.cm^{-3})	1.153	1.134	1.144
Absorption coefficient (mm^{-1})	0.193	0.158	0.12
Transmission factors (min./max.)	0.977/0.996	0.475/1.000	0.872/1.000
Crystal size (mm^3)	$0.12 \times 0.08 \times 0.02$	$0.24 \times 0.19 \times 0.10$	$0.19 \times 0.15 \times 0.10$
θ(max) (°)	29.349	27.483	27.482
Reflections measured	8760	25639	39175
Unique reflections	6934	6880	6903
R_{int}	0.0274	0.0136	0.0224
Reflections with $F^2 > 2\sigma(F^2)$	4786	6178	6628
Number of parameters	293	202	347
R_1 [$F^2 > 2\sigma(F^2)$]	0.0478	0.0700	0.0366
wR_2 (all data)	0.1339	0.2052	0.0958
GOOF, S	1.014	1.059	1.024
Largest difference peak and hole (e Å^{-3})	0.525 and –0.320	0.769 and –0.302	0.388 and –0.317

Compound	**31**·2C$_4$H$_8$O	**31**$^{/}$	**32**·2MeCN·THF	**33**
Formula	C$_{28}$H$_{22}$Li$_2$O$_6$·2C$_4$H$_8$O	C$_{18}$H$_{19}$LiO$_4$	C$_{108}$H$_{94}$Li$_7$N$_3$O$_{22}$	C$_{116}$H$_{128}$Li$_8$O$_{22}$
Formula weight	611.8	306.27	1834.44	1929.70
Crystal system	Orthorhombic,	Orthorhombic	Monoclinic	Triclinic
Space group	*Pna*2$_1$	*P*2$_1$2$_1$2$_1$	*P*2$_1$/*n*	*P* $\bar{1}$
Unit cell dimensions				
a (Å)	10.099(2)	5.8603(12)	14.9367(10)	13.402(5)
b (Å)	12.685(3)	16.286(4)	27.942(2)	13.466(4)
c (Å)	24.611(6)	17.064(4)	23.4063(16)	17.306(8)
α (°)	90	90	90	68.55(3)
β (°)	90	90	105.2360(10)	75.65(4)
γ (°)	90	90	90	64.93(4)
V (Å^3)	3152.8(19)	1628.6(6)	9425.5(11)	2617(2)
Z	4	4	4	1
Temperature (K)	100 K	100(2)	100(2)	100(2)
Wavelength (Å)	0.71073	0.71075	0.6889	0.71073
Calculated density (g.cm^{-3})	1.283	1.249	1.293	1.224
Absorption coefficient (mm^{-1})	0.09	0.09	0.09	0.08
Transmission factors (min./max.)	0.982and 0.997	0.984 and 0.996	0.776 and 1.000	0.740 and 1.000
Crystal size (mm^3)	0.70 × 0.07 × 0.03	0.19× 0.17 × 0.04	0.20 × 0.04 × 0.03	0.13× 0.09 × 0.03
θ(max) (°)	30.2	30.1	27.6	25.0
Reflections measured	21169	12859	90603	22115
Unique reflections	7745	4342	21513	9154
R$_{int}$	0.036	0.021	0.077	0.078
Reflections with *F*^{2} > 2σ(*F*^{2})	7140	4342	90603	6016
Number of parameters	421	215	1248	664
R$_1$ [*F*^{2} > 2σ(*F*^{2})]	0.053	0.044	0.053	0.046
wR$_2$ (all data)	0.105	0.099	0.130	0.268
GOOF, *S*	1.07	1.04	1.03	1.146
Largest difference peak and hole (e Å^{-3})	0.24 and –0.25	0.33 and –0.33	0.42 and –0.41	0.32 and –0.36

Compound	34	35	36·2MeCN	38
Formula	$C_{72}H_{82}Li_6N_4O_{12}$	$C_{88}H_{80}Li_8N_8O_{12}$	$C_{60}H_{60}N_4O_8Zn_4·2(C_2H_3N)$	$C_{84}H_{56}F_{12}N_4O_8Zn_4$
Formula weight	1237.06	1497.12	1308.70	1746.87
Crystal system	Triclinic	Tetragonal	Monoclinic	Tetragonal
Space group	$P\,\bar{1}$	$P\,\bar{4}$	$P2_1/n$	$I\,\bar{4}$
Unit cell dimensions				
a (Å)	11.5582(17)	16.1256(7)	15.021(2)	18.401(5)
b (Å)	12.9469(19)	16.1256(7)	16.504(3)	
c (Å)	13.1142(19)	15.3363(9)	25.151(4)	11.347(3)
α (°)	118.444(8)	90	96.420(2)	90
β (°)	101.424(7)	90	6196.0(17)	3842(2)
γ (°)	92.831(7)	90	4	2
V (Å^3)	1667.7(4)	3988.0(4)	150(2)	150(2)
Z	1	2	0.71073	0.71073
Temperature (K)	100(2)	100(2)	1.403	1.510
Wavelength (Å)	0.71073	0.71073	1.59	1.32
Calculated density (g.cm^{-3})	1.232	1.247	0.535 and 0.763	0.504 and 0.890
Absorption Coefficient t(mm^{-1})	0.08	0.08	$0.45 \times 0.43 \times 0.18$	$0.60 \times 0.11 \times 0.09$
Transmission factors (min./max.)	0.986 and 0.998	0.63629 and 1.000	27.5	26.5
Crystal size (mm^3)	$0.18 \times 0.05 \times 0.20$	$0.04 \times 0.03 \times 0.02$	56708	16703
θ(max) (°)	25.00	26.145	14215	3988
Reflections measured	13706	16772	0.062	0.064
Unique reflections	5859	7856	10644	3856
R_{int}	0.134	0.068	769	256
Reflections with $F^2 > 2\sigma(F^2)$	3464	16772	0.053	0.055
Number of parameters	439	494	0.138	0.133
R_1 [$F^2 > 2\sigma(F^2)$]	0.098	0.091	1.07	1.11
wR_2 (all data)	0.245	0.239	1.08 and −0.89	1.54 and −1.13
GOOF, S	0.991	1.022		
Largest difference peak and hole (e Å^{-3})	0.29 and −0.30	0.49 and −0.40		

Compound	**39**	(2-CF$_3$C$_6$H$_4$)$_3$B·MeCN	ZnCl$_2$(NCMe)$_2$
Formula	C$_{66}$H$_{40}$F$_{12}$N$_4$O$_8$Zn$_4$·4(C$_7$H$_8$)·1.59 H$_2$O	C$_{23}$H$_{15}$BF$_9$N·C$_2$H$_3$N	C$_4$H$_6$Cl$_2$N$_2$Zn
Formula weight	1903.68	528.22	218.38
Crystal system	Tetragonal	monoclinic	Orthorhombic
Space group	$I\overline{4}$	$P2_1/c$	$Pnma$
Unit cell dimensions			
a (Å)	13.5944(5)	9.3027(5)	12.7113(11)
b (Å)		18.1466(10)	9.9296(8)
c (Å)	22.3469(9)	14.1566(8)	6.5812(6)
β (°)		94.8366(10)	
V (Å^3)	4129.9(3)	2381.3(2)	830.67(12)
Z	2	4	4
Temperature (K)	150(2)	150(2)	150(2)
Wavelength (Å)	0.71073	0.71073	0.71073
Calculated density (g.cm^{-3})	1.531	1.473	1.746
Absorption coefficient (mm^{-1})	1.24	0.14	3.52
Transmission factors (min./max.)	0.637 and 0.808	0.911 and 0.966	0.154 and 0.401
Crystal size (mm^3)	0.40 × 0.36 × 0.18	0.70 × 0.45 × 0.26	0.75 x 0.36 x 0.26
θ(max) (°)	30.6	30.0	31.7
Reflections measured	24843	27132	9419
Unique reflections	6188	6939	1440
R_{int}	0.026	0.040	0.027
Reflections with $F^2 > 2\sigma(F^2)$	5685	4851	1284
Number of parameters	291	336	48
R_1 [$F^2 > 2\sigma(F^2)$]	0.032	0.043	0.020
wR_2 (all data)	0.082	0.105	0.055
GOOF, S	1.04	1.05	1.04
Largest difference peak and hole (e Å^{-3})	0.60 and –0.39	0.33 and –0.21	0.36 and -0.30